Enantioselective Liquid-Liquid Extraction

in

Centrifugal Contactor Separators

Boelo Schuur

This Research Project was financially supported by DSM and Schering-Plough through the Separation Technology Program of the Netherlands Scientific Organisation (NWO).

RIJKSUNIVERSITEIT GRONINGEN

Enantioselective Liquid-Liquid Extraction in Centrifugal Contactor Separators

Proefschrift

ter verkrijging van het doctoraat in de
Wiskunde en Natuurwetenschappen
aan de Rijksuniversiteit Groningen
op gezag van de
Rector Magnificus, dr. F. Zwarts,
in het openbaar te verdedigen op
maandag 24 november 2008
om 14.45 uur

door

Boelo Schuur
geboren op 3 maart 1978
te Veendam

Promotores:	Prof. dr. ir. H. J. Heeres
	Prof. dr. J.G. de Vries
	Prof. dr. B. L. Feringa

Beoordelingscommmissie:	Prof. dr. ir. A.B. de Haan
	Prof. dr. ir. G. F. Versteeg
	Prof. ir. G. J. Harmsen

ISBN 978-90-367-3625-1
ISBN 978-90-367-3626-8 (electronic version)

Goa mor op zuik,
goa zulf mor op zuik.

(Jan Glas)

opgedragen aan Dorothee en Quentin

Contents

Summary 13

Samenvatting 19

Chapter 1 25

Introduction

General introduction 25
1.1 Chirality 25
1.2 Strategies towards enantiopure compounds 27
1.3 ELLE 31
1.3.1 Recognition principle 32
1.3.2 Enantioselective Liquid-Liquid Extraction Chemistry 33
1.3.2.1 Separations of racemic amino acid(s) (derivatives) by ELLE 35
1.3.2.2 Separations of Racemic Amino Alcohols and amines by ELLE 42
1.3.2.3 Racemate Separations of Aromatic Acids and other substrate classes by ELLE 45
1.3.2.4 Racemate separations by extraction with supercritical CO_2 51
1.4 Liquid-Liquid Extraction equipment 52
1.4.1 Selection of equipment 52
1.4.2 CCS equipment 53
1.5 Modeling extraction processes 54

1.5.1 Single stage equilibrium extraction 58
1.5.2 Multistage equilibrium extraction 63
1.5.3 Dynamic extraction processes 66
1.6 Aim of thesis 73
1.7 Nomenclature 75
1.8 References 76

Chapter 2 87

Equilibrium Studies on Enantioselective Liquid-Liquid Amino Acid Extraction using a Cinchona Alkaloid Extractant

2.1 Introduction 89
2.2 Experimental 90
2.3 Theory and reactive extraction modeling 92
2.4 Results and discussion 95
2.5 Conclusions 107
2.6 Nomenclature 107
2.7 References 108

Chapter 3 **111**

Enantioselective Equilibrium Liquid-Liquid Extraction of R,S-Phenylglycinol using a Bis Naphtyl Phosphoric Acid derivative as extractant

3.1 Introduction 113
3.2 Experimental 114
3.3 Theory 116
3.4 Results and discussion 120
3.5 Optimization of single equilibrium stage performance 125
3.6 Conclusions 129
3.7 Nomenclature 129
3.8 References 130

Chapter 4 **133**

Determination of the interfacial area of a continuous integrated mixer/separator (CINC) using a chemical reaction method

4.1 Introduction 135
4.2 Experimental 137
4.3 Theory 139
4.4 Physico-Chemical parameters 142
4.5 Results and discussion 144
4.6 Conclusions 152
4.7 Nomenclature 152
4.8 References 154

Chapter 5 **157**

Hydrodynamics in a Centrifugal Contactor Separator; Studies on Residence Time Distribution, Phase behavior and Drop Size Distribution

5.1 Introduction 159
5.2 Experimental 160
5.3 Theory and reactive extraction modeling 163
5.4 Results and Discussion 165
5.5 Conclusions 180
5.6 Nomenclature 180
5.7 References 182

Chapter 6 **185**

Continuous Chiral Separation of Amino Acid Derivatives by Enantioselective Liquid-Liquid Extraction in Centrifugal Contactor Separators

6.1 Introduction 187
6.2 Results and Discussion 189
6.3 Conclusions and outlook 196
6.4 Experimental 197
6.5 Nomenclature 198
6.6 References 199

Chapter 7 **201**

Experimental and modeling studies on the enantioseparation of 3,5-dinitrobenzoyl-(R),(S)-leucine by liquid-liquid extraction in a cascade of continuous centrifugal separators

7.1 Introduction 203
7.2 Multi-stage equilibrium ELLE model 205
7.3 Experimental methods 209
7.4 Results and discussion 211
7.5 Cascade optimization by equilibrium stage modeling 214
7.6 Maximizing the $A_{R,S}$ output 219
7.7 Conclusions 220
7.8 Nomenclature 220
7.9 References 222

List of Scientific Contributions by Boelo Schuur **225**

Dankwoord **228**

Summary:

Chiral objects do not have an internal mirror plane. A simple example of a chiral object is a (winking) smiley, see Figure S1. If the smiley winks (right) it cannot be superimposed on its mirror image and it is said to be chiral. On the other hand, when the smiley does not wink, it is achiral (left).

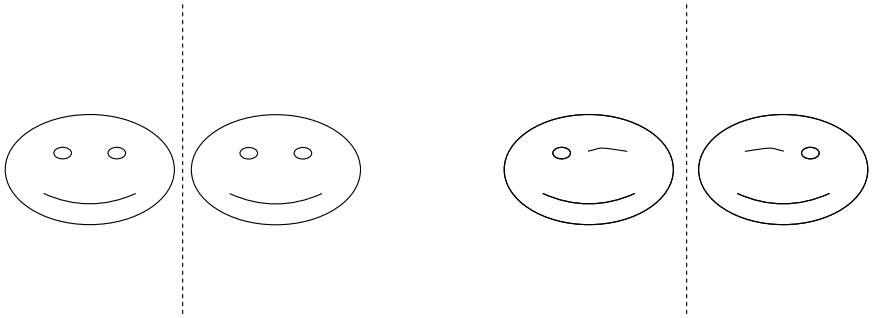

Figuur S1. Left: achiral smiley. Right: chiral winking smiley.

In chemistry, chirality is an important feature. When a molecule is chiral, the biological activity of the two different mirror images (enantiomers) may differ to a great extent. The consequences may be dramatic. For example, (*S*),(*S*)-ethambutol is the active ingredient in a drug against tuberculosis, whereas one of the other enatntiomers ((*R*),(*R*)-ethambutol) causes blindness. Another example is (S)-ketamine. (*S*)-ketamine is an anaestatic, while (*R*)-ketamine is a hallucinogen. Thus, the administration of these (and other) drugs in an enantiopure form to the patients is essential.

Several technologies have been developed for the production of single enantiomers. Racemic production followed by separation is the most common. However, the existing technologies have limitations. This in combination with the rapid increase in the demand for enantiopure compounds has stimulated research and development on alternatives. This thesis describes research on enantioselective liquid-liquid extraction (ELLE), a very promising but not yet commercialized technology. The objective of the research is to demonstrate the use of ELLE in a continuous mode in a bench scale unit. For this purpose, compact centrifugal contactor separators (CCS) were used. Two attractive ELLE-systems for further studies were investigated in batch and the results are described in Chapters 2 and 3. Important characteristics of CCS-equipment were investigated (Chapters

4 and 5) and one of het ELLE-systems was investigated in detail in the continuous CCS-equipment (Chapters 6 and 7).

In ELLE the mixture of enantiomers to be separated is dissolved in a liquid, which is usually water. This solution is called the feed. The feed is contacted with a second, immiscible liquid, usually an organic solvent, containing an extractant (host). The host is chiral and has a high affinity for only one of the solutes. By this selective reaction, one of the guests is extracted to a higher extent to the organic phase than the other, leading to an enantiomeric excess of this enantiomer in the extract phase. A schematic representation of the principles of ELLE is given in Figure S2.

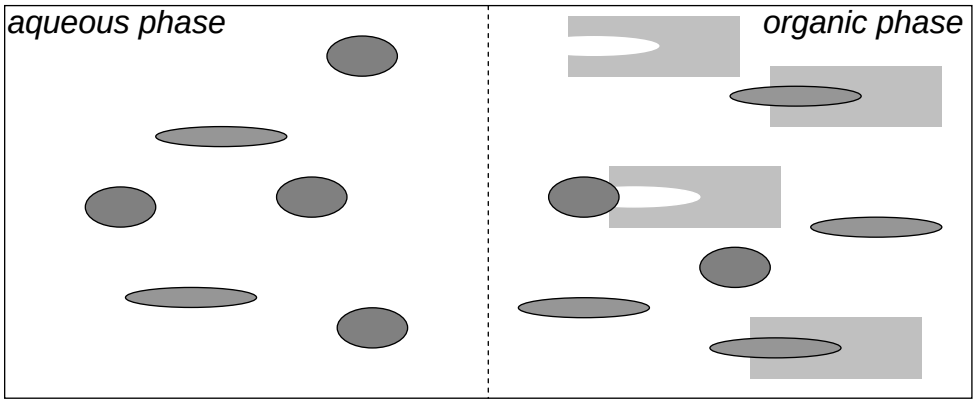

Figure S2. Schematic representation of ELLE. Symbolen: : (*S*)-enantiomer, : (*R*)-enantiomer, : extractant.

High selectivity for the binding between the host and one of the solutes is thus essential. However, it is also important that the interaction between host and solute is reversible. If the reaction between host and guest is irreversible, the host cannot be recycled, leading to unacceptable high manufacturing costs. The host should also be poorly or preferably insoluble in the water phase to avoid losses to the water phase. Finally, versatility is also highly desirable, meaning that a single host is capable of separating a family of compound classes and not only a single component with high selectivity.

In Chapters 2 and 3 research on the equilibrium extraction of an amino acid derivative (3,5-dinitrobenzoyl-(*R*),(*S*)-leucine, DNB-R,S-leu) and an aminoalcohol ((*R*),(*S*)-phenylglycinol, $PGL_{R,S}$) is discussed. For the chiral separation of DNB-R,S-leu a chiral cinchona alkaloid extractant (C) was selected from literature. The host (P) for the extraction of $PGL_{R,S}$ was developed by Bas Verkuijl in the group of Prof. dr. Feringa (University of

Groningen) and consists of a chiral phosphoric acid derivative. Experimental extraction studies were performed in batch and the results could be described well with equilibrium extraction models incorporating homogeneous organic phase complexation of host and guests. For both systems complete separation of the enantiomers could not be achieved in a single equilibrium stage. Multistage countercurrent processing was proposed to increase both the yield and enantioselectivity.

A schematic representation of a multistage countercurrent process is depicted in Figure S3. One of the enantiomers is preferentially extracted into the extract phase in the stages 1 - N by reaction with the chiral host. The other enantiomer leaves the system in the raffinate stream. The extract stream with enantiomer-host complex is transferred to a back-extraction section (stages 1 - M) where the enantiomer is recovered. The host is recycled to the extraction unit.

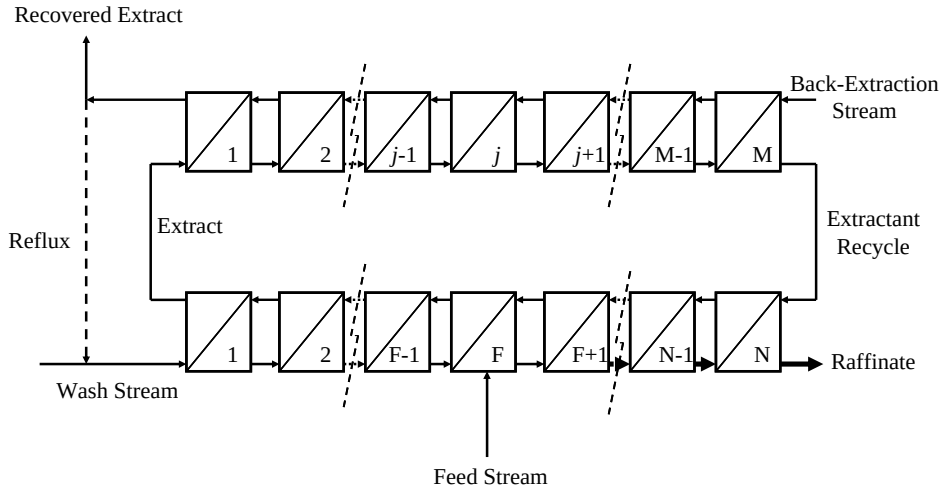

Figure S3. Countercurrent multistage extraction and back-extraction process.

A multistage countercurrent model was developed for the ELLE of DNB-R,S-leu and used to optimization the chiral separation in terms of yield and enantiopurity.

CINC V02 Centrifugal Contactor Separators (CCS) have been used for the continuous chiral extractions. In this equipment, two immiscible liquids are intensely mixed, leading to exchange of components between the two phases and subsequently separated again. Figure S4 shows a schematic representation (left) and a photograph (right) of the device.

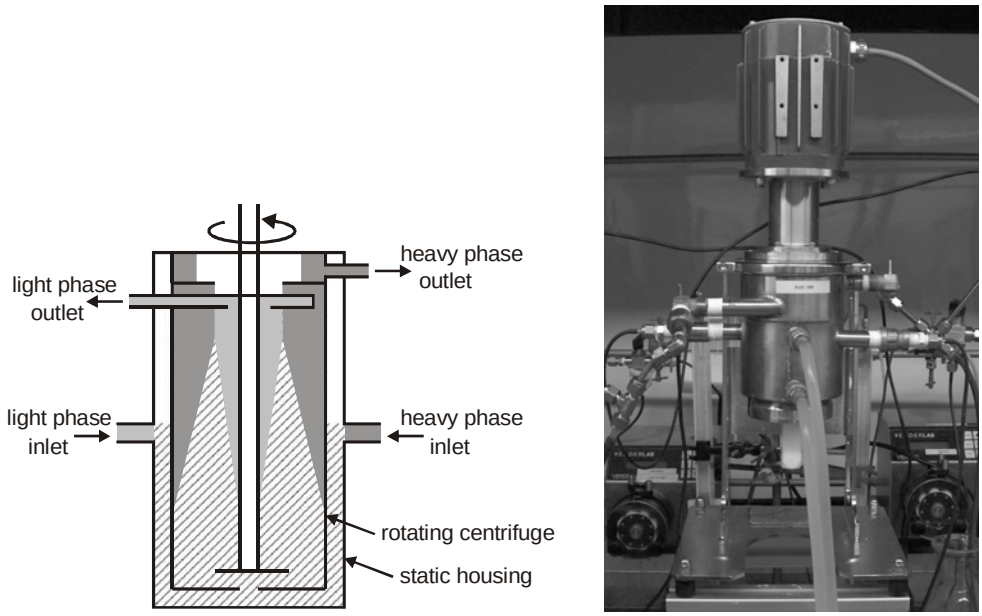

Figure S4. Schematic representation (left) and a photograph of the CCS (right). Dark grey areas in the schematic representation represent the heavy liquid, light grey the light liquid, and the hatched area the dispersion.

Both liquids enter at the sides of the cylindrically shaped device into a tight space between the static wall and the rotating centrifuge. Due to the speed of rotation and the short distance between the static and rotating walls, the liquids are intensely mixed. The dispersion is then transferred to the centrifuge through a hole in the bottom, where the large centrifugal forces cause efficient phase separation. This fast phase separation allows the use of a small centrifuge, making the equipment very compact in size. The unit operations mixing and separation are thus combined in a single device, making it a good example of what is known as process intensification.

Although the use of the CCS for separation purposes has already been known since the late 1960's, still not much is known about important characteristics of the device like the total interfacial area between two immiscible liquids, the size of the droplets in the system, which of the phases is continuous and which is disperse, and the macro mixing behavior of both phases. An in-depth exploration was performed to gain insights in these features and the results are given in Chapters 4 and 5. This information is of importance for modeling of processes taking place in the CCS.

The use of the CCS for continuous ELLE of DNB-R,S-leu is reported in Chapter 6. It is shown that the CCS acts as a single equilibrium stage. The possibility of recycling the host was also demonstrated by using a back-extraction step in a single CCS. Essentially quantitative recovery was possible by an extraction with an aqueous pH 9 stream.

The use of a cascade of 7 CCS devices for the enantioselective separation of DNB-R-S-leu including a back-extraction step is given in Chapter 7. The optimum cascade configuration was initially modeled using an equilibrium approach. With this configuration, the production of one of the enantiomers with an *ee* of 98% and a yield of 55% was proven experimentally. Good agreement between the experimental data and the model was also observed. With the validated model available, it was shown that full separation (*ee* > 99%) of DNB-R,S-leu in DNB-R-leu and DNB-S-leu should be possible when using a cascade of at least 11 stages. The model also predicts that the separation of 17.7 kg DNB-R,S-leu per week in the individual enantiomers is achievable with only 60g of host.

The research project has demonstrated that it is possible to perform ELLE in a continuous mode using the very compact CCS-equipment. One of the advantages of the CCS devices is that they can be used as bench scale devices for research and development purposes as well as for kilogram scale production. Good insights have been obtained in the characteristics of the CCS equipment, which may be of use not only for ELLE but also for other CCS applications

Samenvatting:

Chirale voorwerpen hebben geen intern spiegelvlak, terwijl a-chirale voorwerpen dat wel hebben. Een eenvoudig voorbeeld van chiraliteit is een al dan niet knipogende smiley. Wanneer een niet knipogende smiley gespiegeld wordt, is het spiegelbeeld identiek aan het origineel. In het geval van een knipogend smiley is dat niet het geval en is de smiley chiraal. Dit is weergegeven in Figuur S1.

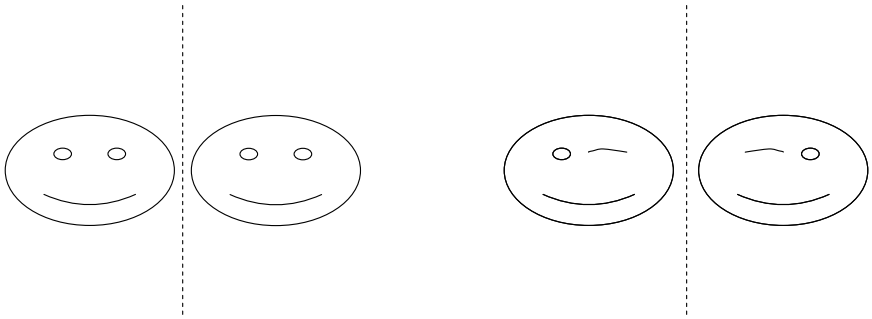

Figuur S1. Links: a-chirale smiley. Rechts: chiraal knipogend smiley.

In de chemie speelt chiraliteit een belangrijke rol. Wanneer een molecuul chiraal is, kan het voorkomen dat de biologische activiteit van de twee verschillende spiegelbeeld-isomeren (enantiomeren) verschilt. De gevolgen van deze verschillende activiteit kunnen dramatische vormen aannemen. Zo is (*S*),(*S*)-ethambutol een medicijn tegen tuberculose, terwijl het spiegelbeeld (*R*),(*R*)-ethambutol blindheid veroorzaakt. Een ander voorbeeld is (S)-ketamine. (*S*)-ketamine wordt gebruikt om patiënten onder narcose te brengen, terwijl (*R*)-ketamine hallucinerend werkt. Het is dus essentieel om (*S*),(*S*)-ethambutol en (*S*)-ketamine enantiozuiver toe te dienen aan patiënten.

Er zijn diverse manieren om enantiomeren zuiver te verkrijgen, waarvan het racemisch (als een mengsel) produceren en daarna scheiden van de enantiomeren het meest toegepast wordt. Omdat de vraag naar nieuwe enantiozuivere verbindingen snel toeneemt en de mogelijkheden van bestaande technieken gelimiteerd is, bestaat er grote behoefte aan nieuwe methodes om enantiomeren te scheiden. In dit proefschrift wordt een onderzoek naar een veelbelovende, maar nog nooit commercieel toegepaste techniek beschreven: enantioselectieve vloeistof-vloeistof extractie (EVVE). Het onderzoek is met name gericht op het aantonen van de mogelijkheid om EVVE in een continu proces uit te voeren. Hiertoe zijn een tweetal EVVE-processen op evenwicht onderzocht (hoofdstukken 2 en 3), is

onderzoek gedaan naar de apparaateigenschappen van de gebruikte CCS-apparatuur (hoofdstukken 4 en 5) en is één van de EVVE-processen continu uitgevoerd (hoofdstukken 6 en 7).

Bij EVVE wordt het mengsel van de te scheiden enantiomeren (het racemaat) opgelost in een vloeistof, meestal water. Deze oplossing wordt de voeding genoemd. De voeding wordt in contact gebracht met een tweede vloeistof die niet mengt met de eerste, meestal een organisch oplosmiddel. Hierdoor ontstaat een twee vloeistoffasen systeem, waar de opgeloste stoffen zich verdelen over de twee vloeistoffen. In het oplosmiddel is een extractant (gastheer) opgelost die kan reageren met de stoffen opgelost in de voeding (gasten). Voor EVVE is het essentieel dat de gastheer selectief reageert met één van de twee gasten. Door de chemische reactie wordt de voorkeurs-enantiomeer in hogere mate ge-extraheerd. Hierdoor ontstaat er van deze enantiomeer een overmaat in de extractiefase, terwijl de andere enantiomeer in overmaat aanwezig is in de voedingsfase. Figuur S2 is een schematische weergave van een EVVE systeem.

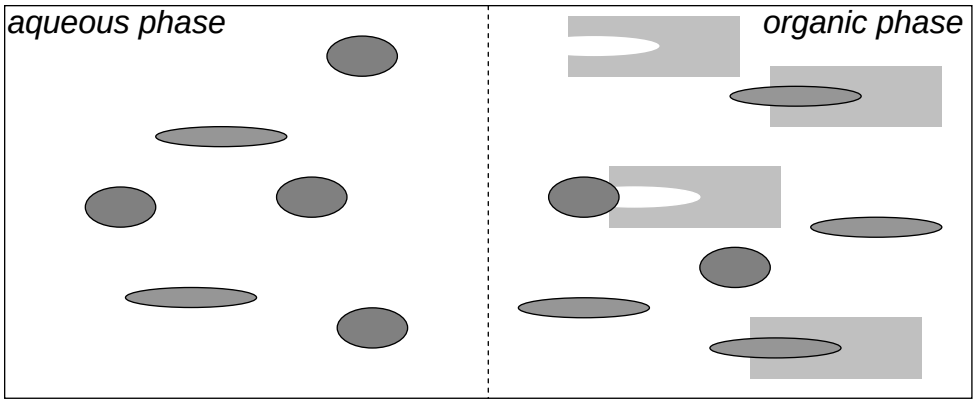

Figuur S2. Schematische weergave van EVVE. Symbolen: : (*S*)-enantiomeer, : (*R*)-enantiomeer, : extractant.

Naast selectiviteit is ook reversibiliteit een essentiële eigenschap waaraan de gastheer moet voldoen. Als de binding tussen gast en gastheer irreversibel is, kan de gastheer niet van de gast gescheiden en hergebruikt worden.. De hoge prijs van gastheren maakt hergebruik en dus reversibiliteit noodzakelijk. Om verlies van de gastheer tegen te gaan is het tevens van belang dat de oplosbaarheid van de gastheer in de voedingsfase minimaal is. Tenslotte is veelzijdigheid gewenst, hetgeen betekent dat met één gastheer een scala aan racematen

gescheiden kan worden. Zodoende kan de ontwikkelingstijd voor nieuwe processen verkort worden.

In de hoofdstukken 2 en 3 is onderzoek beschreven aan evenwichtsextracties van 3,5-dinitrobenzoyl-(*R*),(*S*)-leu (DNB-R,S-leu) en van (*R*),(*S*)-phenylglycinol ($PGL_{R,S}$). Voor DNB-R,S-leu werd een cinchona alkaloid extractant (C) uit de literatuur geselecteerd, de gastheer (P) voor extractie van $PGL_{R,S}$ werd ontwikkeld door Bas Verkuijl in de groep van Prof. dr. Feringa (RUG). Beide systemen waren goed te beschrijven met het homogene extractiemodel Een enkele extractie evenwichtsstap is niet voldoende voor een complete scheiding. Dit kan verbeterd worden door meerstapsprocessen toe te passen. Voor de EVVE van DNB-R,S-leu is een meerstapsproces onderzocht om de scheiding te optimaliseren.

In Figuur S3 is een schema van zo'n meerstaps tegenstroom proces afgebeeld. In de trappen 1 - N wordt één van de enantiomeren geëxtraheerd en overgedragen naar de "extract" stroom. De andere enantiomeer wordt niet geëxtraheerd ("raffinate"). De geextraheerde enantiomeer wordt in de back-extractie eenheid (trappen 1 - M) gescheiden van de gastheer. Deze kan dan hergebruikt worden.

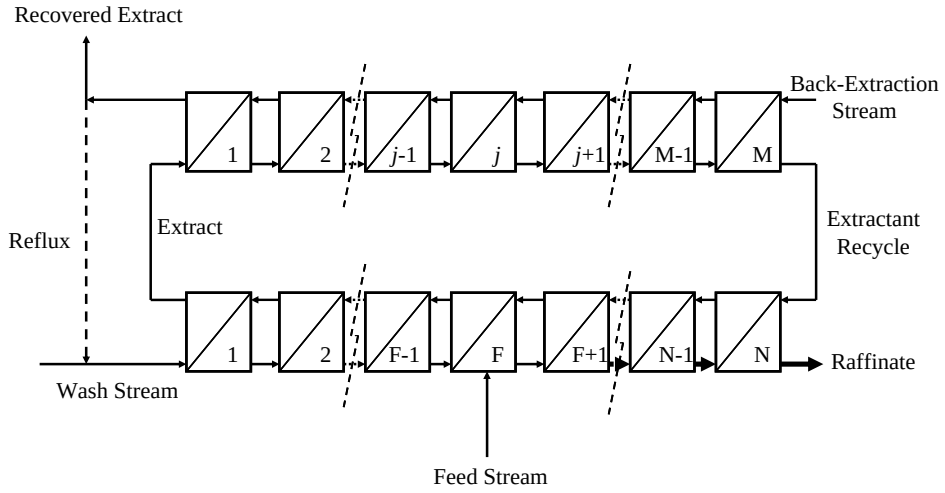

Figuur S3. Tegenstrooms meerstapsproces

In het onderzoek is EVVE uitgevoerd in compacte Continue Centrifugaal Scheiders (CCS) van het type CINC V02. In het apparaat worden twee onmengbare vloeistoffen achtereenvolgens intensief gedispergeerd waarbij overdracht van componenten plaatsvindt en weer gescheiden. Figuur S4 laat een schematische weergave en een foto zien.

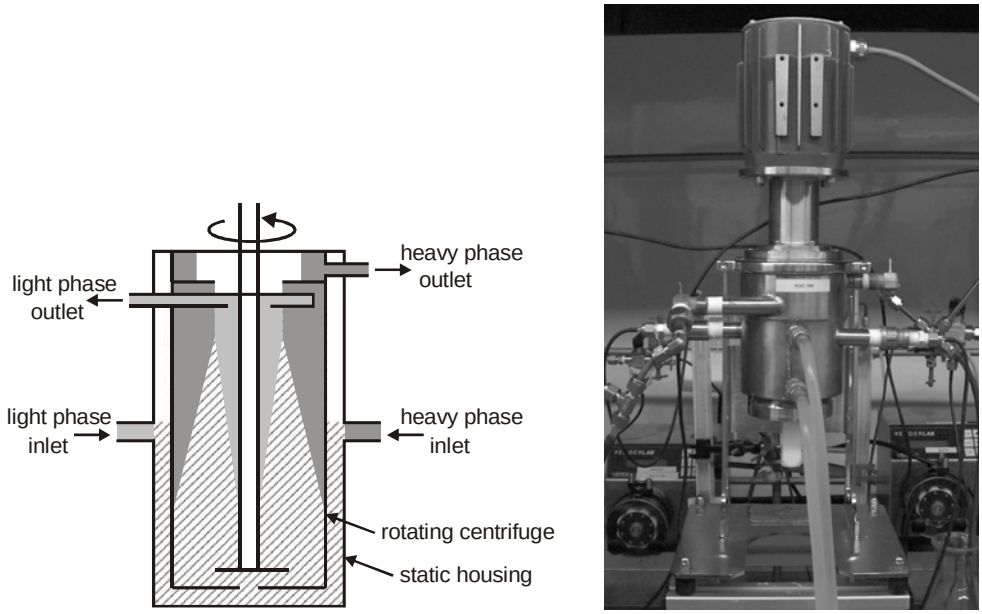

Figuur S4. Schematische weergave van de CCS (links) en foto (rechts). De zware vloeistof is donkergrijs weergegeven, de lichte vloeistof lichtgrijs en de dispersie gearceerd.

De beide vloeistoffen komen aan de zijkanten het cilindervormige apparaat binnen en komen dan in een smalle ruimte tussen de statische reactorwand en de roterende centrifuge. Door de snelle rotatie en de kleine afstand tussen de statische wand en de rotor worden de vloeistoffen intensief gedispergeerd. De dispersie wordt door een gat in de bodem de centrifuge binnengezogen. In de centrifuge vindt efficiënte scheiding plaats onder invloed van de grote centrifugaalkrachten. Op deze manier worden dus de functies mengen en scheiden in één apparaat gecombineerd, dit wordt ook wel proces intensificatie genoemd.

Hoewel gebruik van de CCS voor scheidingsdoeleinden al sinds het eind van de ’60-er jaren van de vorige eeuw bekend is, is er nog weinig bekend van karakteristieke apparaat eigenschappen zoals het totale interfasen oppervlak tussen de twee onmengbare vloeistoffen, de grootte van de druppels in het systeem, welk van de fasen in de dispersie de continue fase is en welke dispers en het macro-menggedrag van beide fasen. Onderzoek naar deze karakteristieken zijn beschreven in de hoofdstukken 4 en 5. Deze gegevens zijn belangrijk voor het modelleren van processen in de CCS, zoals gecombineerde chemische reacties en scheidingen. Het gebruik van de CCS voor EVVE is beschreven in hoofdstuk 6.

Tevens werd de reversibiliteit van de gast en gastheer binding aangetoond. Voor het terugwinnen (back-extractie) van de gastheer bleek een enkele CCS voldoende.

In hoofdstuk 7 is het gebruik van een cascade van 6 CCS-eenheden (geometrisch volume is 322 mL) met een enkele back-extractie-CCS experimenteel aangetoond voor de EVVE van DNB-R,S-leu. Alvorens te experimenteren werden de optimale instellingen bepaald met een evenwichtsmodel. Experimenteel werd met deze instellingen 98% *ee* bij 55% yield gehaald in goede overeenstemming met het model. Met het aldus gevalideerde model werd gedemonstreerd dat met een cascade van 11 trappen maximaal 17.7 kg DNB-R,S-leu per week gescheiden zou moeten kunnen worden met slechts 60 gram van de gastheer.

Het onderzoek heeft aangetoond dat met de zeer compacte CCS-apparatuur enantioselectieve extracties continu zijn uit te voeren. De kracht van de continue EVVE in CCS apparatuur is dat voor zowel initiële screening als kilogramschaal productie hetzelfde apparaat gebruikt kan worden. Tevens is er een goed inzicht verkregen in de eigenschappen van de CCS-apparatuur en zijn de evenwichtextractiemodellen voor een tweetal systemen opgesteld.

Chapter 1: Introduction

Enantioselective liquid-liquid extraction (ELLE) is a promising technology to separate the two enantiomers of a racemate using a chiral extractant. Although the technique is already known since the late 1960's[1-4], it has to the best of our knowledge not been applied on larger scale. A possible reason is the high costs associated with the use of chiral extractants. The liquid hold-up in traditional continuous extraction equipment is generally high and this leads to a large inventory of the often expensive chiral extractants in the process.
Centrifugal Contactor Separators (CCS)[5-7] are very compact continuous flow devices where dispersion of two immiscible liquids and subsequent separation are integrated. The devices are compact, flexible and combine a low liquid hold-up with high throughput rates. As such, the CCS seems ideal to bridge the gap between the typical ELLE laboratory experiments in batch to larger scale continuous operation. The aim of the work presented in this thesis is to demonstrate the potential of CCS equipment for enantioselective extraction.

In the introduction of this thesis the concept of chirality and chiral chemistry is introduced, and the need to develop efficient technology for the production of single enantiomers in the pharmaceutical, food and perfume industries is discussed[8,9]. Available methods to obtain enantiopure compounds are reviewed in section 1.2. Enantioselective liquid-liquid extraction is introduced in the third subsection. In here, the fundamentals of enantiomer discrimination are treated and available ELLE chemistry is reviewed. In the fourth subsection an introduction to LLE equipment is given, followed by a discussion on modeling of extraction processes. In the last subsection the scope and outline of the thesis are presented.

1.1 Chirality

Chirality is a symmetry property. Chiral shapes are not superimposable on their mirror-images. This concept is illustrated in Figure 1.1. The smiley on the left is perfectly symmetrical, superimposable on its mirror image and thus an achiral object. A winking smiley however, (Figure 1.1, right) cannot be superimposed on its own mirror image. Winking smileys are thus chiral objects. Chirality[10] is also observed in chemical substances containing asymmetric (chiral) centers, mostly in the form of asymmetric carbon atom(s). An asymmetric carbon atom has four different groups, and superimposing on its mirror-image is impossible.

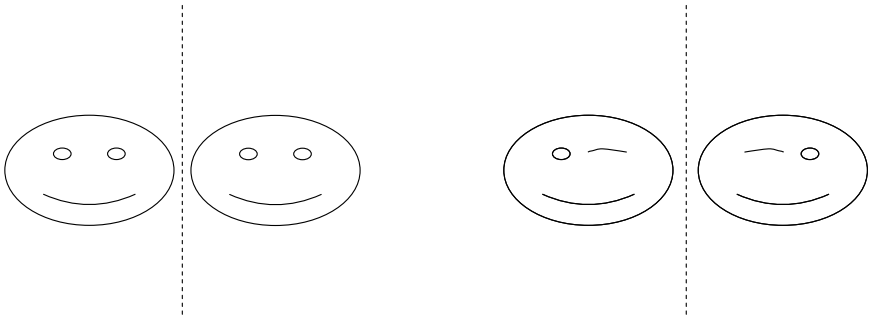

Figure 1.1. Achiral smileys on the left and chiral winking smileys on the right.

Alanine is an example of a relatively simple molecule containing an asymmetric carbon center. The two possible structures of alanine, depicted in Figure 1.2, are known as enantiomers[11].

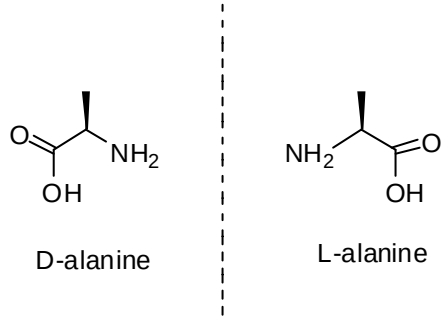

Figure 1.2. The two enantiomers of alanine.

Most physical properties of enantiomers are identical, an exception is the optical rotational behavior, a characteristic that was first discovered by Louis Pasteur[12] and is referred to as optical isomerism[11]. The chemical reactivity may differ.

Except for glycine, all naturally occurring amino acids are chiral. When bioactivity is pursued, for example in insecticides, herbicides and drugs, but also in food additives, flavors and fragrances[10,11], chirality plays an important role. The interactions of chiral bioactive species with the chiral biological receptor are often stereospecific[13], leading to different bioacitivity of the two enantiomers. Particularly for drugs this is a very serious

consequence of chirality. An illustrative example is the difference in bioactivity of the ketamine enantiomers (Figure 1.3)[14].

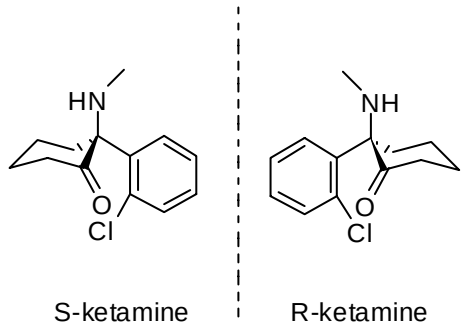

Figure 1.3. The two enantiomers of ketamine.

(*R*)-ketamine is hallucinogen whereas (*S*)-ketamine is an anaestatic. To avoid undesirable side effects of one of the enantiomers, there is a strong tendency in the pharmaceutical industry towards the production of enantiopure components[8]. The world wide sales of enantiopure drugs exceeded 159 billion US dollar in 2002 and the annual revenue growth shows double-digit figures[9].

1.2 Strategies towards enantiopure compounds

Three primary strategies towards the synthesis of enantiopure compounds[11,15,16] may be distinguished, see Figure 1.4. An overview of the various strategies with their advantages and drawbacks is given in Table 1.1. The chiral pool strategy uses chiral compounds from nature or products derived thereof (e.g. from fermentation processes). Examples of industrial fermentations are the productions of various acids[17], penicillin[18] and amino acids[19]. Usually the products obtained by this strategy are relatively cheap. Unfortunately, not all enantiopure precursors can be obtained from natural sources. When the chiral pool is no option, conversion of prochiral compounds into chiral compounds by asymmetric synthesis[20] is an attractive alternative. Asymmetric synthesis may either be realized by biocatalysis or by metal catalysis. In asymmetric catalysis, the activation energy of the favored reaction to the desired enantiomer is lowered to a larger extent by the chiral catalyst than the activation energy of the formation of the other enantiomer[21]. This is illustrated for the catalytic synthesis of S (the preferred enantiomer) and R from a racemic mixture of A

and B in Figure 1.5. The activation energy of the conversion of enantiomer B to product R is higher than the conversion of A to S.

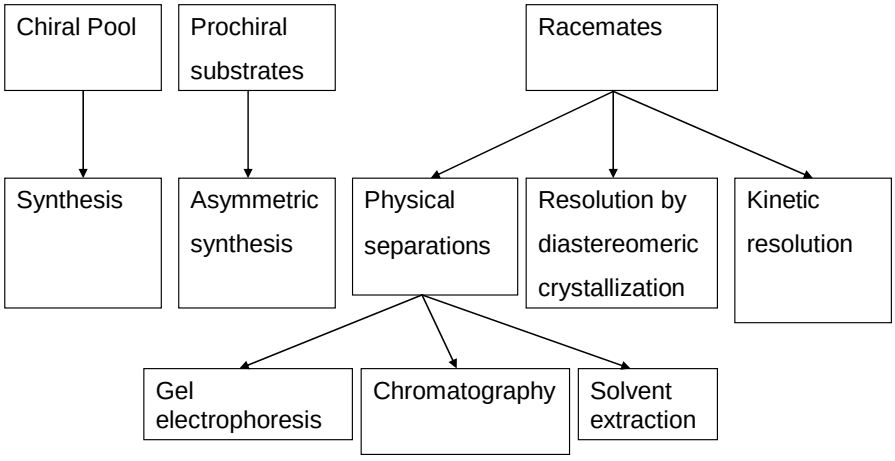

Figure 1.4. Synthetic strategies for enantiopure compounds[11].

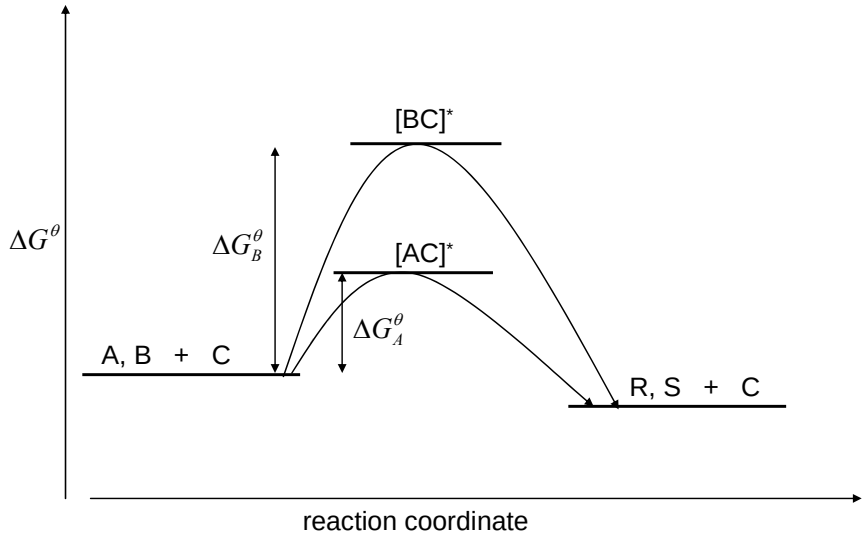

Figure 1.5. Catalytic conversion of a racemic mixture (A and B) to respectively S and R using a chiral catalyst.

Although the asymmetric catalysis is intrinsically very powerful, its practical use is seriously hampered by the long development times required to reach the stage of commercial production [22].

Enantiopure compounds may also be obtained by racemic synthesis followed by enantioseparation. This strategy is potentially much faster than asymmetric catalysis, as most racemic compounds are much easier to synthesize than the enantioselective variants. Separation of racemates on industrial scale is usually done using resolution by diastereomeric crystallization[23-26]. Here, the racemate is reacted with an enantiopure reactant to form a mixture of diastereomers. These may be separated easily due to differences in solubility. Although racemate separation by diastereomeric crystallization is the most abundant route towards enantiopure compounds, the main drawbacks are the low versatility and excessive solids handling[27]. An alternative is kinetic resolution[28]. Here, a bio- or metal catalyst is used to selectively convert one of the enantiomers into the product.

Several laboratory techniques have been investigated to separate racemates. Examples are chromatography[29] and capillary electrophoresis[30] and these have shown to be very practical on small scale[31-34]. Modifications of these techniques to allow for (semi)continuous preparative scale separations have been reported[35-37]. However, application of the techniques on a commercial scale appears complex and capital cost intensive[27]. Alternative are membrane-based approaches[38-41]. When using immobilized selectors in (liquid) membranes, the amount of selector needed can be reduced greatly. Limitations of this technology are the relatively low transport rates through the membranes and the risk of fouling.

In liquid-liquid extraction, diffusion and convection are the transport mechanisms, and high transport rates should be achievable[42]. Liquid-liquid extraction is a mature technology, which is advantageous when commercializing. The use of liquid-liquid extraction for enantioseparation is already known since the late 1960's[1-4]. ELLE is an attractive alternative for chromatography and resolution by crystallization. As far as we are aware, commercialization of ELLE has not been achieved to date. Most studies in the literature deal with exploratory chemistry research and only a few engineering studies have been reported[42-47].

Table 1.1 Overview of available techniques for enantiopure compounds.

Strategy	***Advantages***	***Limitations***
chiral pool	cheap	limited number of compounds available
asymmetric synthesis	only the desired enantiomer is produced, high atom efficiency	long and costly development; low versatility (e.g. for every product a new catalyst needs to be developed)
racemate resolution by diastereomeric crystallization	short development time; large scale approaches are common practice	undesired enantiomer is produced as waste; not always applicable; solids handling
kinetic resolution	high selectivities possible	technology not always applicable; undesired enantiomer is produced as waste
chromatographic and electrophoretical techniques	low selectivities still allow for high purity; practically all racemates can be separated with available selectors	high capital costs; complex processing in (semi) continuous mode; undesired enantiomer is produced as waste
membrane extraction processes	only small amount of host (selector) required	limited transport rate; risk of fouling; undesired enantiomer is produced as waste; limited number of enantioselective hosts available
liquid-liquid extraction	high transport rate; versatility (e.g. several racemates may be separated with the same host); easy to scale up;	moderate selectivity required to avoid excessive number of stages; no commercial examples; undesired enantiomer is produced as waste; limited number of enantioselective hosts available

1.3 Enantioselective liquid-liquid extraction

ELLE combines the concepts of solvent extraction[48,49] and enantiomeric recognition[50] in a single technique. The principle of ELLE with the extractant in the organic phase and the racemate to be resolved in the water phase is schematically displayed in Figure 1.6. The solute or guest transfers from the aqueous phase to the organic phase and interacts with an extractant or host in the organic phase. In this example, interaction of the host with the S-enantiomer is favored over interaction with the R-enantiomer. As a result, the organic phase while be enriched in the S-enantiomer and the aqueous phase in the R-enantiomer. The enantiomeric excess (*ee*) of the process is defined as:

$$ee = \frac{|[R]-[S]|}{[R]+[S]} \qquad (1.1)$$

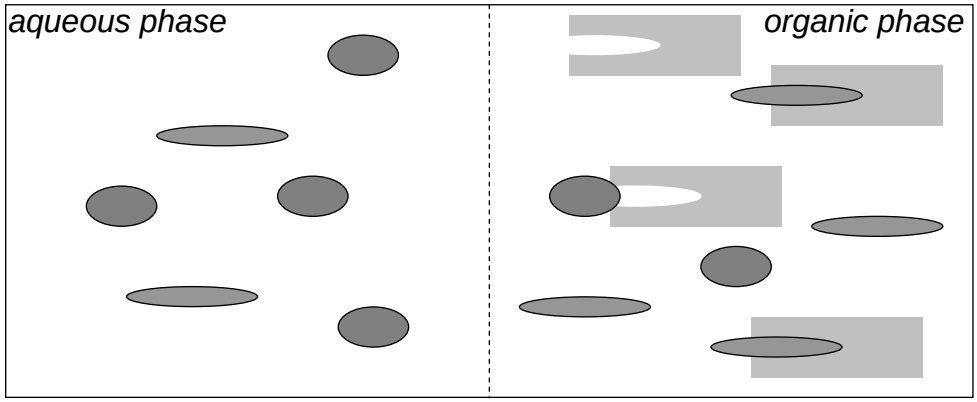

Figure 1.6. Enantiomeric recognition in a biphasic system. Symbols:  : S-enantiomer,  : R-enantiomer,  : host.

From a practical point of view, it is essential that the host remains in the organic phase. In case the host is soluble in the aqueous phase, additional procedures need to be developed for recovery of the host from the aqueous phase and this will limit the applicability. Thus for new systems, it is essential to design hosts that are essentially insoluble in the phase

containing the racemate to be separated. Good solubility of the host and the host-guest complexes in the extract phase and of the guest in the feed phase is desirable, to allow for concentrations much higher than the typically used 1mM in the literature. Another prerequisite is reversibility of the binding between the host and guest. Only then, the host may be recovered and re-used. A short introduction on the principle of enantiomeric recognition is given in the next subsection, followed by an overview of the host-guest systems reported in for liquid-liquid extraction systems.

1.3.1 Enantiomeric recognition

The principle of enantiomeric recognition is essential for enantioselective complexation and thus for ELLE. Without enantiomeric recognition, enantioselective processes are not possible. Complexes of the extractant with the enantiomers are formed as a result of intermolecular interactions[51]. These intermolecular interactions may comprise of hydrogen bonding, π-π, ion pairing, dipole stacking, Van der Waals interactions[50].

Nonbonding steric interactions are important for the enantioselectivity. In enantioselective complexations, at least three of the intermolecular interactions must be present[52]. Two of the interactions should be positive to fix the configuration of the complexation. The third interaction, the nonbonding steric interaction is different for both enantiomers. This two point fixation and difference in the third interaction is the basis for the enantiomeric recognition and is known as the three point rule[52]. The three point rule is illustrated in Figure 1.7.

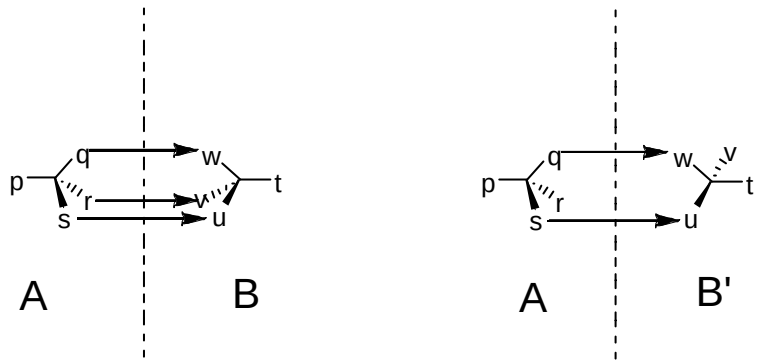

Figure 1.7. Illustration of the three point rule.

The interactions in the three-point rule form the enthalpic contribution to the free energy of formation of the complex, while interactions with the environment (i.e. solvent or other dissolved molecules) contribute entropically to the free energy of formation[53]. When the enthalpic contributions dominate over the entropic interactions, the enantiomeric recognition results in chiral discrimination[53].

For the least preferred enantiomer, complexation with the host is weaker due to a less favorable steric orientation. The equilibrium constant for complex formation is therefore smaller than that for the preferred enantiomer. This difference in equilibrium constants is a quantitative measure for the intrinsic selectivity of the host and expressed as:

$$\alpha_{\text{int}} = \frac{K_R}{K_S} \tag{1.2}$$

The intrinsic selectivity is related to the difference in Gibbs free energy of complex formation according to Eq. 1.3[54]:

$$\delta\Delta G = -RT \ln \alpha_{\text{int}} \tag{1.3}$$

1.3.2 Enantioselective Liquid-Liquid Extraction Chemistry

Molecular complexation with enantiomeric recognition has already been reported in the early 1970's by Nobel laureate Cram and coworkers[55]. Since then, a wide variety in hosts has been reported to separate racemates of different substance classes with LLE. In this subsection an overview of relevant developments in the chemistry of ELLE-systems is given, structured on substrate classes. An excellent overview of enantioselective extractants for separation of amines and amino alcohols was provided by Steensma *et al.*[27]. In this section, extractants for several classes of substrates are provided and the reported selectivities, a key property for ELLE-systems are considered and discussed. Selectivities may either be reported a the intrinsic selectivity, as defined in Eq. 1.2, or the operational selectivity. The latter is defined as:

$$\alpha_{op} = \frac{D_R}{D_S} \tag{1.4}$$

Here, D is the distribution of the enantiomers over the phases. The D for the R-enantiomer, D_R, is defined as:

$$D_R = \frac{[R]_{org}}{[R]_{aq}} \tag{1.5}$$

In case the selectivity was not reported in the original paper, the operational selectivity was calculated based on *ee*, yield or distribution data.
In the literature on ELLE two different types of extraction mechanism have been proposed, the homogeneous extraction model involving homogeneous reaction between host and guest and the interfacial reaction model. The two models are depicted in Figure 1.8. The main difference between the two models is the locus of the complexation reaction. The interfacial reaction model applies when the reaction takes place at the interface. This situation is likely to be valid when the guest is insoluble in the organic phase and the host is insoluble in the water phase. When either the host or guest is soluble in the other phase, homogeneous reactions are also possible. An extensive discussion on the differences between the two extraction models is provided in section 1.5.

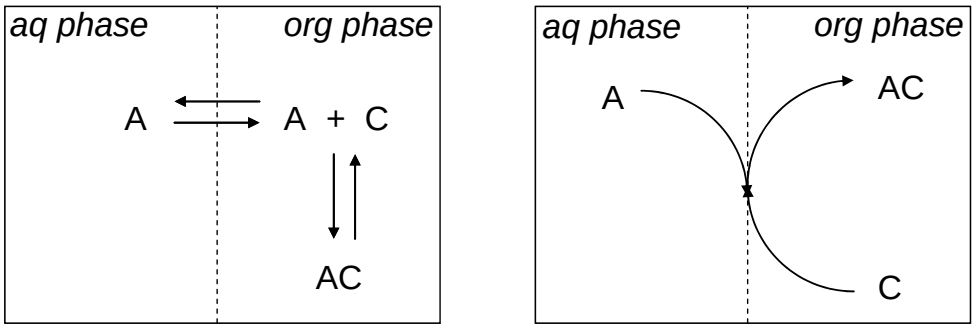

Figure 1.8. Homogeneous organic phase complexation mechanism (left) and interfacial complexation mechanism (right) of solute A with extractant C.

Inspection of the literature indicates that ELLE studies are nearly always performed in batch operation at room temperature or below (sometimes even below 0°C). Concentrations are typically in the order of 10^{-3} mol/L. Therefore, extraction conditions are not provided and discussed in this literature overview. The host should preferably be applicable for the separation of a number of substrate classes. In the following literature overview, versatility of the host is therefore also considered.

1.3.2.1 Separations of racemic amino acid(s) (derivatives) by ELLE

Enantiomeric recognition of amino acids and derivatives has a strong history, starting with Cram's chiral crown ether and dilocular (bearing 2 chiral moieties) extractants (Figure 1.9)[56-58].

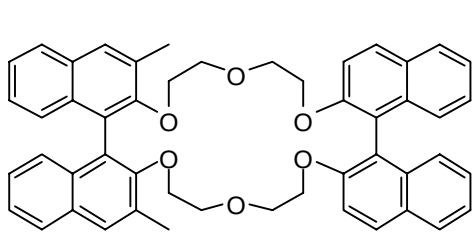

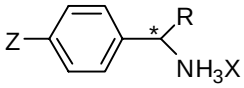

Z = H, OH
R = CH_3, CO_2CH_3
X = Br^-, Cl^-

Figure 1.9. Left: Cram's best dilocular host (α_{int} > 20 for several amino esters)[58], and right: examples of substrates investigated by Cram.

In the papers by Cram's group, the substrates are always assumed to be at least slightly soluble in the organic phase and very high homogeneous organic phase complexation equilibrium constants, defined as in Eq. 1.6, of up to several hundred thousand L/mol have been reported. C is the complexant, or host and R and S are the enantiomers. Intrinsic selectivities (Eq. 1.2) of up to 19.2 for amino acids[56], up to 12 for amine salts[57], and up to 31 for amino ester salts,[58] were observed.

$$K_{CR} = \frac{[CR]_{org}}{[C]_{org}[R]_{org}} \qquad K_{CS} = \frac{[CS]_{org}}{[C]_{org}[S]_{org}} \tag{1.6}$$

Enantioselective extractions of unprotected zwitterionic amino acids by crown ethers modified with a guanidinium group (Figure 1.10) were reported by the group of De Mendoza[59,60]. High *ee*'s of up to 79% were reported, these were however accompanied by low yields. The main disadvantages of the use of crown ethers are their demanding, multi-step synthesis and toxicity[61].

The enantioselective extraction of phenyl alanine (Phe, see Figure 1.10) has recently been studied by several groups[43,44,54,62,63]. Takeuchi *et al.* have described[64] the use of extractant Cu(II)-(N-decyl-(l)-hydroxyproline)$_2$ (Cu(II)-(C_{10}Hyp)$_2$, Fig. 1.11) for the

ELLE of Phe and various other amino acids. Intrinsic selectivities were observed for several amino acids ranging from 1.8-4.5, indicating that the extractant is versatile. using Cu(II)-(C_{12}Hyp)$_2$ and Cu(II)-(C_{12}Pro)$_2$. . Pickering and Chaudhuri[44,63] demonstrated the use of two different extractants (Cu(II)-(N-dodecyl-(l)-hydroxyproline)$_2$ (Cu(II)-(C_{12}Hyp)$_2$) and (S)-bis(phenylnaphto)-20-crown-6) for the ELLE of Phe. The selectivity using the Cu(II)-(C_{12}Hyp)$_2$ was in the range reported earlier by Takeuchi *et al.*[64], the crown ether showed a much better selectivity (α_{op} = 9.22).

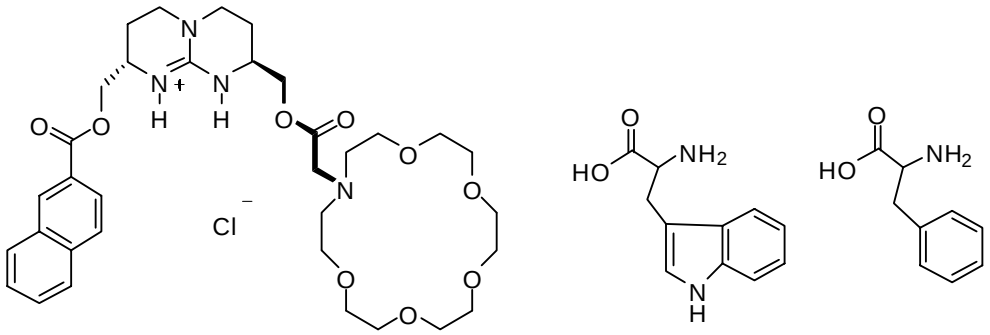

Figure 1.10. De Mendoza's guanidinium crown ether host and guests (tryptophan and phenyl alanine) [60].

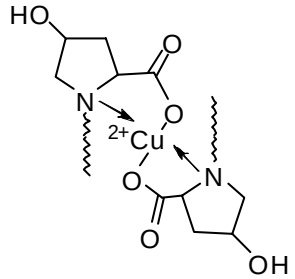

Figure 1.11. (Cu(II)-(N-decyl-(l)-hydroxyproline)$_2$[64]

Tan *et al.*[65,66] demonstrated the synergistic effects of chiral extractants with a-chiral co-extractants for Phe, Trp, and tyrosine (Tyr). Mixtures of tartaric acid derivatives and commercially available D2EHPA[65] and Aliquat 336[66] (see Figure 1.12) were applied. The highest observed operational enantioselectivity was about 4 for the system with

D2EHPA as co-extractant and Trp as substrate. Further optimization led to a selectivity of 5.3[67]. Lower selectivities were observed for Phe and Tyr.

Extractions of amino acid derivatives have been reported by several groups[68-73]. High selectivities (*ee* of up to over 90% at 70% overall yield), versatility and good reversibility were observed when using cinchona alkaloid type of extractants for the extraction of *N*-dinitrobenzoyl-substituted amino acids (Figure 1.13)[71].

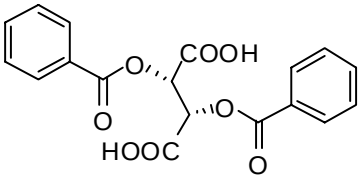

O,O'-dibenzoyl-(2R,3R)-tartaric acid

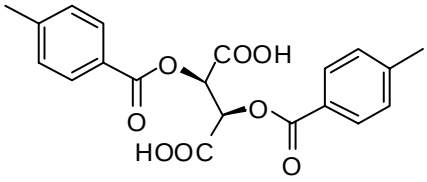

O,O'-dibenzoyl-(2S,3S)-4-toluoyl tartaric acid

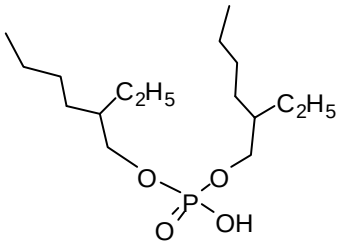

Di(2-ethylhexyl)phosphoric acid
(D2EHPA)

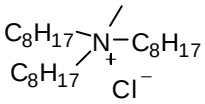

Trioctyl methyl ammonium chloride
(Aliquat 336)

Figure 1.12. Chiral tartaric acid derived extractants and co-extractants[66,67].

With a cobalt Salen extractant high aqueous raffinate *ee* (>90%) was observed for *N*-benzyl-substituted amino acids (Figure 1.14). As the yields were almost quantitative, the *ee* of the small portion remaining in the aqueous phase gives no accurate information on the selectivity and with the harsh conditions for recovery this extractant seems not so attractive[73].

Deoxyguanosine derivatives form aggregates by self-assembly (Figure 1.15). The intermolecular complexation of these aggregates with the guests is most likely to be highly reversible and selectivities up to 3 were reported for the potassium salts of 2,4-DNB-amino acids[68].

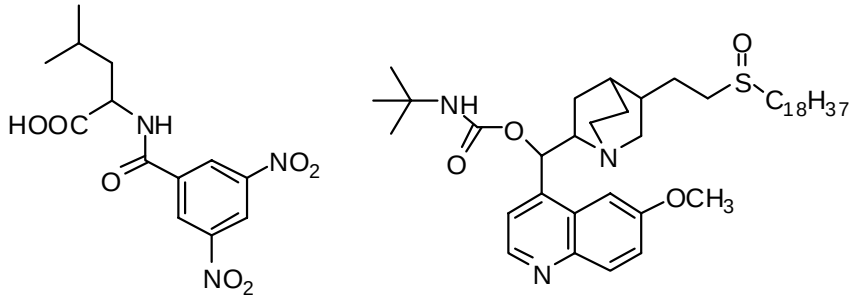

Figure 1.13. 3,5-DNB-R,S-leucine (left) and Cinchona alkaloid extractant (right)[71].

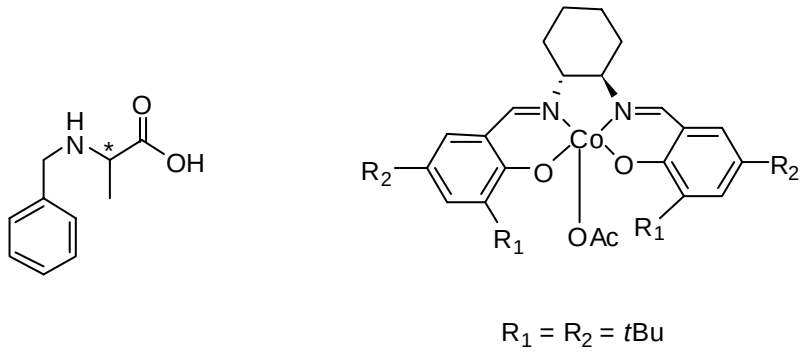

Figure 1.14. N-benzyl alanine (left) and Cobalt Salen extractant (right)[73].

The application of lipophilic lanthanide(III)tris(β-diketonate) complexes (Figure 1.16) for the ELLE of unprotected amino acids was demonstrated by Tsukube *et al.*[74,75] with reasonable *ee* (49%) and yield (14%).

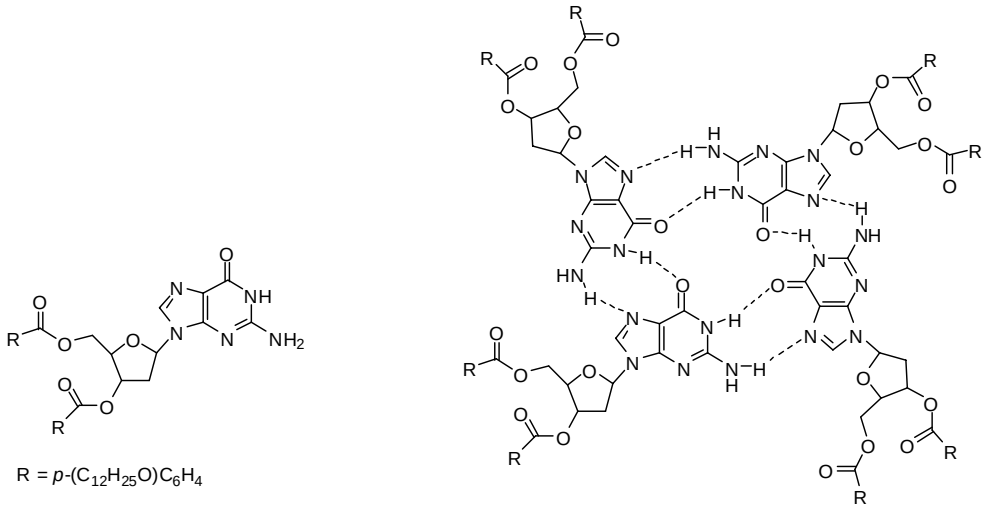

Figure 1.15. Deoxyguanosine derivative (left) and the G-quartet structure formed by self-assembly (right). The outside of the assembly is lipophilic, the inside hydrophilic[68].

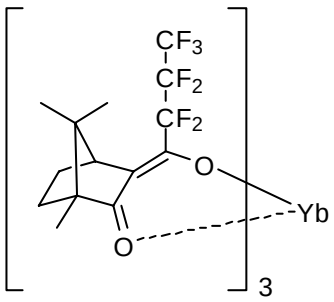

Figure 1.16. The best lanthanide(III) tris(β-diketonate) extractant for separation of racemic amino acids[75].

Table 1.2 Enantioselective extraction systems for amino acid and derivative in aqueous/organic biphasic systems.

substrate	***extractant(s)***	***organic solvent***	***enantio-selectivity***	***reference(s)***
amine salts,	crown ether	chloroform	1.5 - 1.9[a]	[57]
amino esters,			2.5 - 12[a]	[57]
amino acids			5.1 - 19.2[a]	[56]
amino esters	dilocular hosts	chloroform	< 31[a]	[58]
several amino	$Cu(II)C_{12}Hyp$	n-butanol	1.8 - 4.5[a]	[64]
acids	$Cu(II)C_{12}Pro$	n-pentanol		
		n-octanol		
Phe, Leu, Val,	$Cu(II)C_{12}Hyp$	decane/hexanol	1.1 - 2.1[b]	[43,46,54,63]
Pro	$Cu(II)C_{10}Hyp$	n-alcohols		
Trp, Phe, Tyr	tartaric acid derivatives and D2EHPA or Aliquat 336	n-octanol	1.4 - 5.3[b]	[65-67]
amino acid derivatives	deoxyguanosine derivatives	chloroform	1.02 - 3.03[b]	[68]
unprotected amino acids	Lanthanide(III) Tris(β-diketonate) complexes	dichloromethane	< 2.90[c]	[74,75]

[a]intrinsic enantioselectivity

[b]operational enantioselectivity

[c]In the reference, the extraction percentage is maldefined. The α_{op} was calculated assuming zero physical transport of phenylglycinol to the organic phase, which seems correct at the conditions applied, but is not generically true, see Chapter 3)

Mechanistic considerations for ELLE of amino acids and amino acid derivatives

As discussed in the introduction of this subsection and displayed in Figure 1.8, two different mechanisms of extraction have been proposed for ELLE. Here, a typical example is discussed to demonstrate the ambiguity in the ELLE literature. The example deals with ELLE of Phe by $Cu(II)\text{-}(C_{12}Hyp)_2$ or $Cu(II)\text{-}(C_{10}Hyp)_2$ (Fig 1.11). Takeuchi *et al.*[64] successfully described the process with homogeneous organic phase complexation. The use of this model was supported by work of Koska and Haynes[43], who showed that neutral (i.e. zero net charge) Phe partitions between both phases, and complexation is therefore likely

not limited only to the interface. Pickering and Chaudhuri[44,63] however, described the process with an interfacial anion exchange process (see Figure 1.17). For the extraction with Cu(II)-$(C_{12}Hyp)_2$ the interfacial equilibrium constant of complexation was defined as:

$$K_{eq}^{*} = \frac{[CuNPhe]_{org}[HN]_{org}}{[HPhe]_{aq}[CuN_2]_{org}} \tag{1.7}$$

The experimental trends described by both Koska and Haynes[43] and Pickering and Chaudhuri[44,63] indicate that the neutral form of Phe is reacting. The distribution ratio (Eq. 1.8) increased with increasing pH and approached the pI of 5.91[76]. This implies that the organic phase complexation mechanism is likely the most appropriate.

$$D_{Phe} = \frac{[Phe]_{org,all\ forms}}{[Phe]_{aq,all\ forms}} \tag{1.8}$$

Overdevest *et al.*[62], like Pickering and Chaudhuri[44] used the interfacial mechanism and included a Langmuir type of adsorption isotherm for modeling the enantioselective Phe extraction with an extractant anchored in a micelle. Also Pursell *et al.*[77] assumed interfacial anion exchange and found very good agreement between model prediction and (equilibrium) experiments.

It may thus be concluded, that although Phe is soluble in both phases, the interfacial reaction mechanism under some conditions predicts the experimental observations well.

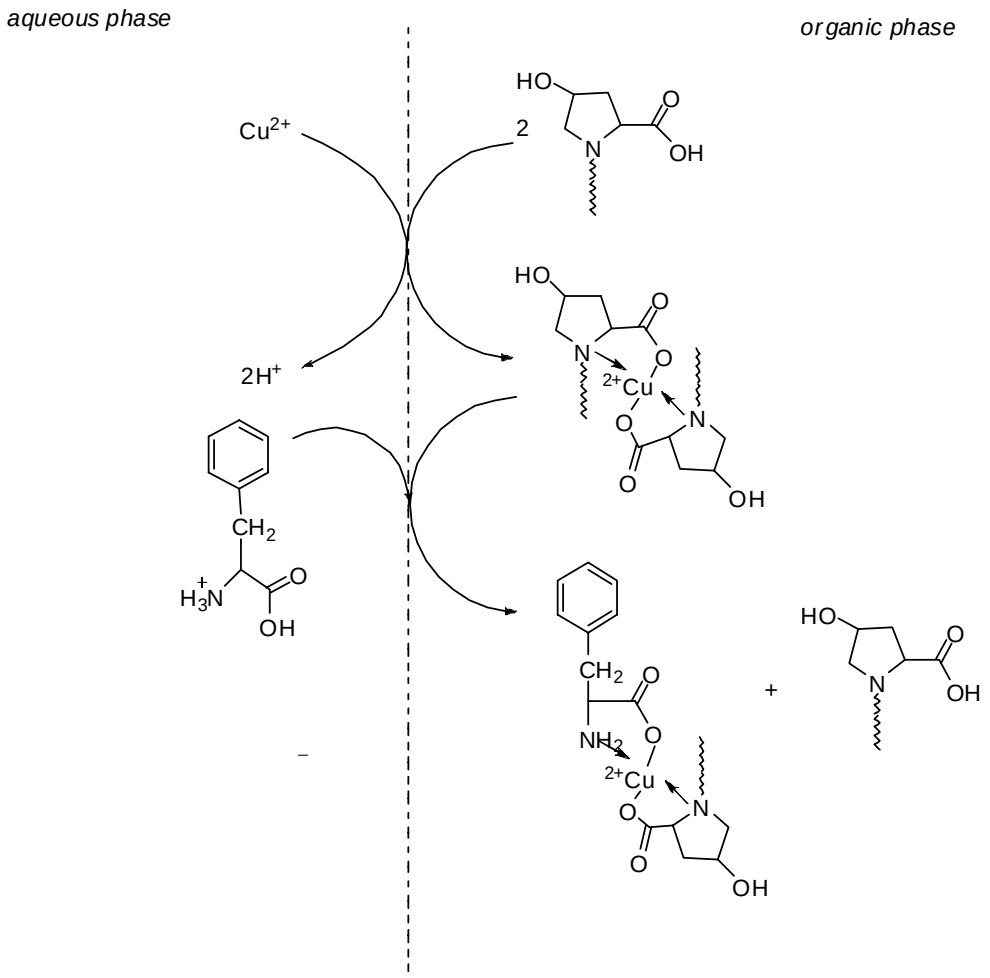

Figure 1.17. Interfacial complexation mechanism for protonated Phe with Cu(II)-(C_{12}Hyp)$_2$ proposed by Pickering and Chaudhuri[44].

1.3.2.2 Separations of Racemic Amino Alcohols and amines by ELLE

Naemura *et al.*[78,79] showed that chiral (azo)phenolic crown ethers in homogeneous organic solutions complexate enantioselectively with amines and amino alcohols. In a series of papers[27,45-47], Steensma *et al.* showed the potential of a large number of chiral selectors for ELLE[27]. They also applied the chiral azophenolic crown ether of Naemura *et al.* for enantioselective extraction of several amino alcohols and amines (Figure 1.18)[45] and have

provided good insights in the difficulties of modeling non-equilibrium (E)LLE processes[46]. Furthermore, an approach for multistage equilibrium modeling of ELLE processes was provided[47].
The enantioselectivity of up to 10 (for phenylglycinol) combined with good versatility and reversibility makes the crown ether a very promising extractant. A disadvantage of the crown ether is, however, the difficult multi step synthesis.

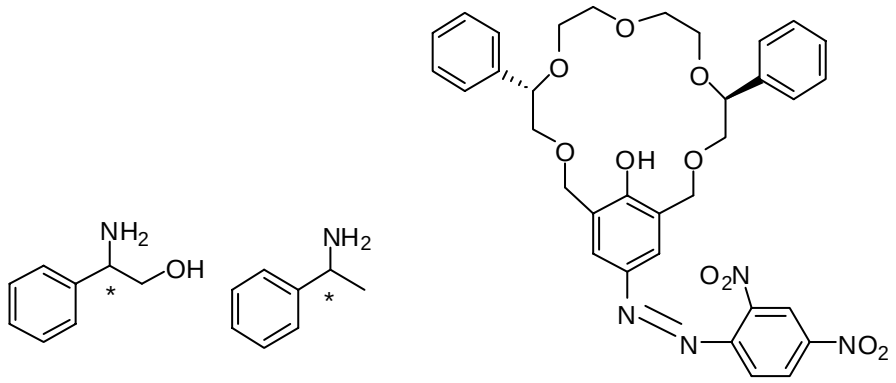

Figure 1.18. Substrates phenylglycinol (left), phenylethy amine (middle) and extractant Azophenolic crown ether (right)[45].

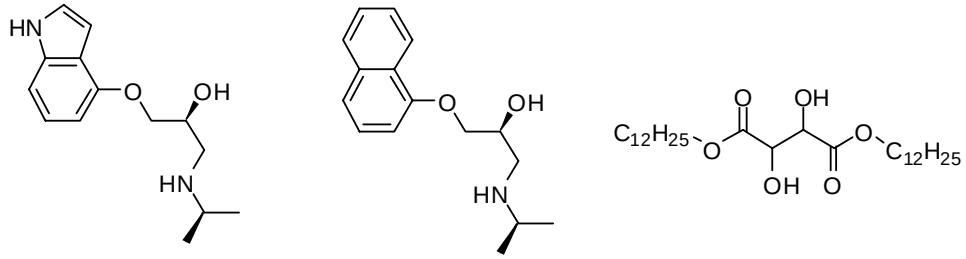

Figure 1.19. The amino alcohols pindolol (left) and propranolol (middle) and the extractant di(n-dodecyl)-tartrate (right).

Abe *et al.* reported the enantioselective extraction for interesting amino alcohols such as pindolol, propranolol, alprenolol and bucumolol (all β-blockers) using dialkyl L-tartrates in chloroform with boronic acid in the aqueous phase (Figure 1.19)[80] and the use of countercurrent extraction to improve the performance for propanolol[81]. The optimized

operational selectivity of the system was 2.71. Apparently, in the aqueous phase borate complexes were formed from boric acid and the amino alcohols. The formed complexes then transferred to the organic phase where enantioselective complexation with dialkyl L-tartrates caused leads to good extraction performance.

Viegas *et al.*[42] modeled the abovementioned system with propanolol/boric acid and di-*n*-dodecyltartrates in chloroform (Figure 1.19) . The system was modeled with an artificial neural network. The modeled intrinsic selectivity was 2.77, indicating that the operational selectivity achieved experimentally by Abe *et al.* (2.71)[81] was close to the intrinsic optimum of the system.

Prelog *et al.*[82] studied the extraction of the ammonium salts of several amino alcohols with tartaric acid esters in chlorinated (hydro)carbons. Selectivities of up to 1.73 were reported.

Very recently, Tang *et al.*[83] presented 2 promising extractants (Figure 1.20) for the extraction of amino alcohols containing binaphthyl moieties. High enantioselectivities for a range of amino alcohols in aqueous/organic biphasic systems with chloroform and benzene as organic phase were achieved. The best results were obtained for 2-amino-1-propanol (α_{int} =11) and 2-amino-1-butanol (α_{int} =15). Back-extraction of the host was achieved by performing a pH-shift.

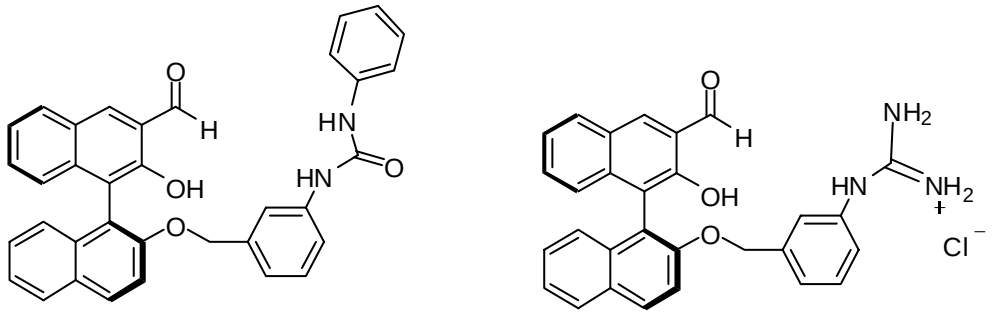

Figure 1.20. The binaphthyl extractants of Tang *et al.*[83].

Mechanistic considerations for ELLE of amino alcohols

Steensma *et al.* applied the homogeneous organic phase extraction model previously suggested by Takeuchi *et al.*[64] for extraction of amino acids for both the Cu(II)-$(C_{12}Hyp)_2$ and the crown ether extractant. In the case of the Cu(II)-$(C_{12}Hyp)_2$ the homogeneous organic phase complexation model was coupled with interfacial cation exchange for phase transfer of Cu^{2+}. Here, similar as for amino acids, the substrates partition between the liquid phases and the extraction mechanism is a function of the nature of the extractant. Homogeneous organic phase complexation was also the mechanism used by Viegas *et al.*

They measured physical partitioning of propanolol over the aqueous and chloroform phases.

Table 1.3 Enantioselective amino alcohol extraction systems in aqueous/organic biphasic systems

substrate	***extractant(s)***	***organic solvent***	***enantio-selectivity[a]***	***reference(s)***
several amino alcohols and amines	chiral crown ethers	various solvents	1.0 - 12[a]	[45-47,63,84]
several amino alcohols	tartaric acid derivatives	chloroform	1.5-2.9[a,b]	[42,80,81]
1,2-amino alcohols	binaphthyl containing extractants	chloroform, benzene	< 15[a]	[83]

[a]intrinsic enantioselectivity
[b]operational enantioselectivity

1.3.2.3 Racemate Separations of Aromatic Acids and other substrate classes by ELLE

Tartrate derivatives are very versatile extractants for amino alcohols or amino acids, see subsection 1.3.2.1. Chiral separation of racemic tartrate derivatives using ELLE has also been reported. Ohki *et al.*[85] studied the enantioselective extraction of di-*O*-benzoyl tartrate (DBT) by an extractant bearing a binaphthyl unit (Figure 1.21). It was convincingly demonstrated that the three point rule required for enantiorecognition is only obeyed when the dicationic form of the extractant is involved and the dianionic form of DBT.

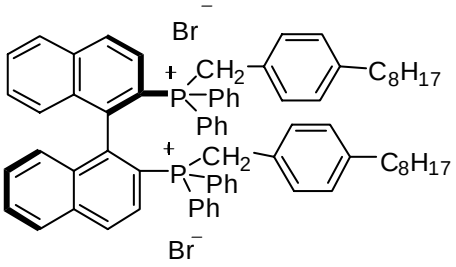

R-(-)-1,1'-binaphtyl-2,2'-diylbis[(*p*-octylbenzyl)diphenylphosphonium] dibromide

Figure 1.21. The binaphthyl based extractant reported by Ohki *et al.*[85].

The reported operational selectivity of this system is 1.36 at a substrate concentration of 5 mM and an extractant concentration 10 mM. Due to the highly hydrophobic character of the extractant and the highly hydrophilic character of the dianionic form of the DBT involved, this process is most likely an interfacial process. L-dipentyl tartrate was used as an organic phase extractant in combination with β-cyclodextrin (Figure 1.22) in the aqueous phase for the enantioselective extraction of mandelic acid from aqueous feeds (Figure 1.23) with an enantioselectivity of 2.1[86]. A similar approach was reported for α-cyclohexyl-mandelic acid (Figure 1.23), and for naproxen (Figure 1.23)[87]. Selectivities up to 2.49 were reported for these systems with the binary extractants mentioned above. Much lower but still reasonable selectivities of 1.46-1.85 were observed for the same substrates with a single extractant Cu(II)(C_{12}Pro)$_2$ in the organic phase[88].

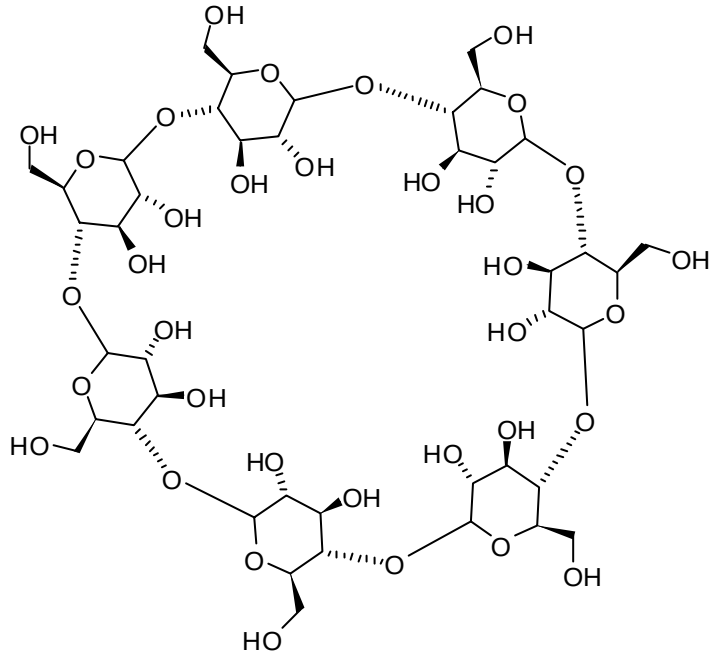

Figure 1.22. β-cyclodextrin, example of an aqueous chiral host.

ELLE of picrates using crown ethers has been reported by Colera *et al.*[89] and Nazarenko *et al.*[90] with selectivities up to 3. Picrates are salts or esters of picric acid (Figure 1.24, left) and known to be soluble in both the aqueous and organic phase[91].

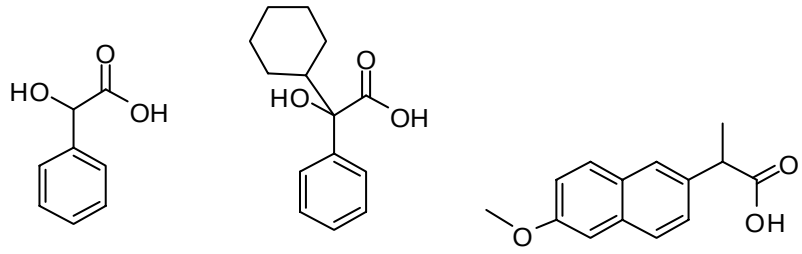

Figure 1.23. Mandelic acid[86] (left), α-cyclohexyl mandelic acid[87] (middle) and naproxen[87] (right).

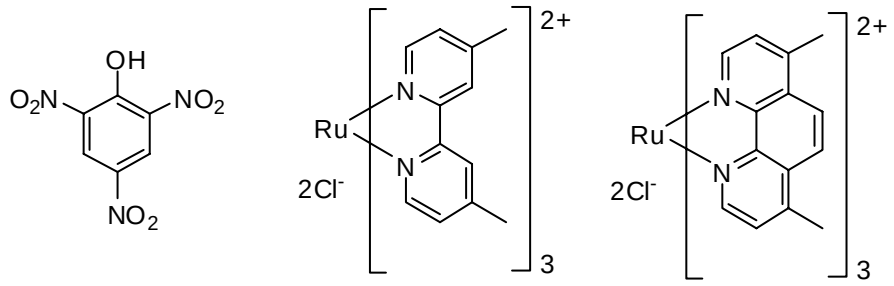

Figure 1.24. Structures of the picric acid (left), tris(4,4'-dimethylbipyridine)ruthenium dichloride (middle), and tris(4,7-dimethylphenanthroline)ruthenium dichloride (right).

Chiral Tris(diimine)ruthenium(II) complexes (Figure 1.24, middle and right) are interesting complexes because of their special photochemical[92] and biological[93] properties. The complexes can be used for the photo-activated cleavage of specific DNA[93] fragments and in photochemical molecular devices[92]. The enantiopure complexes are difficult to obtain. Lacour *et al.*[94] studied the use of ELLE for the separation of racemic complexes. Chiral lipophilic TRISPHAT anions (Figure 1.25) showed very high enantioselectivity for tris(diimine)ruthenium(II) complexes and values up to 49[94] were reported. Data on the reversibility of the complexation reaction and substrate versatility were not provided.

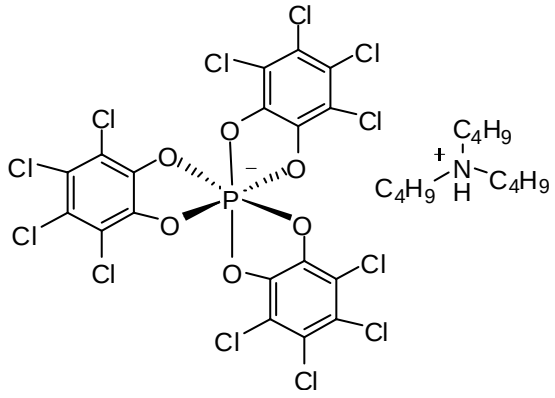

Figure 1.25. Molecular structure of the tri(n-butyl)ammonium TRISPHAT[94] extractant

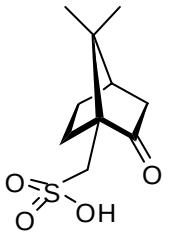

Figure 1.26. 1S-(+)-10- camphorsulfonic acid.

Tsurubou *et al.*[95,96] studied the separation of the cinchona alkaloid quinine/quinidine and cinchonine/cinchonidine (Figure 1.27). Several acetyl substituted amino acids and camphorsulfonic acid (Figure 1.26)[95,96] were used as chiral extractant. Using camphorsulfonic acid, a maximum enantioselectively of 1.21 was observed.

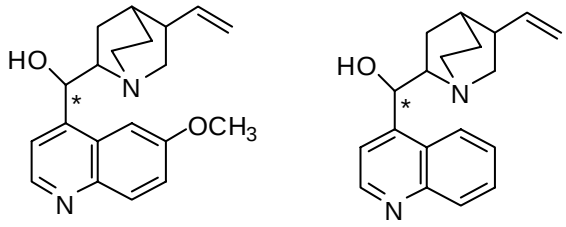

Figure 1.27. quinine/quinidine (left) and cinchonine/cinchonidine (right).

Table 1.4 Enantioselective extraction systems for aromatic acids and other classes in water/organic solvent biphasic systems

substrate	***extractant(s)***	***organic solvent***	***enantio-selectivity[a]***	***reference(s)***
Mandelic Acid	Cu(II)C_{12}Pro	butanol	1.46-1.85	[88]
Mandelic Acid, Naproxen ammonium salts of amino alcohols	β-cyclodextrin (aq) and tartaric acid derivatives (org)	pentanol, 1,2-dichloroethane	< 2.49	[86,87]
	tartaric acid esters	chlorinated (hydro)carbons	< 1.73	[82]
di-*O*-benzoyl tartrate	binaphthyl bearing diphosphonium salts	CCl_4 (50%)/ $ClCH_2CH_2Cl$ (50%)	< 1.36	[85]
cinchona alkaloids	acetyl substituted amino acids, D-10-camphorsulfonic acid	chloroform 1,2-dichloroethane	< 1.21	[95,96]
tris(diimine)-ruthenium(II) complexes	tri(n-butyl) ammonium-TRISPHAT	chloroform	5.5 - 42.5	[94]
ammonium picrates	chiral crown ethers, chiral pyridine-crown ethers	chloroform	< 3	[89,90]

[a]operational enantioselectivity

Mechanistic considerations for ELLE of cinchona alkaloids

The selectivity of camphorsulfonic acid for the enantioselective extraction of racemic pseudo-natural cinchona alkaloids (see previous paragraph) low (maximum 1.21). The extractant in its neutral form is soluble in both liquid phases. As a result, the reaction between host and guest may take place in both phases[97], and this is expected to lead to a reduction of the selectivity.

Kellner *et al.*[71] and Lindner and Lammerhöfer[98] describe the use of modified cinchona alkaloids for extraction of several dinitrobenzoyl substituted amino acids. The selectivity in those systems is much higher than reported here for the unmodified cinchona alkaloids. The reason for the difference in selectivity is most likely the difference in steric

hindrance. See Figure 1.28 for comparison of the unmodified and the modified cinchona alkaloids. The high selectivities of the modified cinchona alkaloid for DNB-substituted amino acids may thus be ascribed to this increased steric hindrance. Furthermore, possible partitioning between the phases is minimized by adding a long C_{18}-tail.

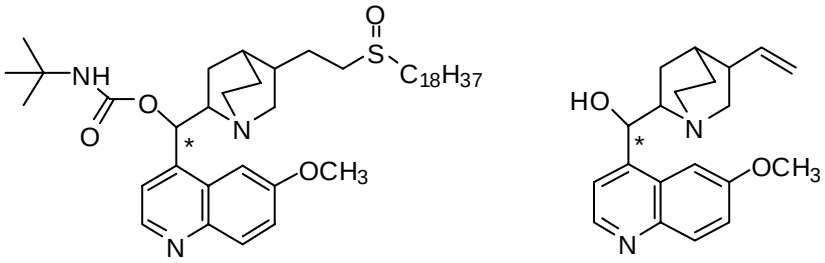

Figure 1.28. Comparison of the modified cinchona alkaloid (left)[71] with the natural version (right).

The high selectivities and versatility towards DNB-substituted amino acids make the modified cinchona alkaloids very interesting for further research. Various studies regarding conformational spaces[99-101] and enantioselective pathways[51,102] for (derivatized) cinchona alkaloids have been reported. As such, this system seems a perfect model system for chemical engineering studies on ELLE in a continuous mode.

1.3.2.4 Racemate separation by extraction with supercritical CO_2

A relative new technology for resolution of racemates is extraction with supercritical CO_2 (sCO_2)[103]. Several studies have shown high *ee*'s (up to 99%, typically around 60%) with good yields (typically about 30%) using ELLE with enantioselective extractants (mostly all described in previous categories) in the liquid (feed) phase and sCO_2 as extracting fluid[104-111]. With countercurrent equipment capable of handling (very) high pressures, this technology may be an interesting alternative for classical biphasic systems consisting of a water and organic phase.

1.4 Liquid-Liquid Extraction equipment

1.4.1 Selection of extraction equipment

A wide variety of liquid-liquid extractors is commercially available[48,112,113]. These may be categorized in column extractors (equipped with packed beds, rotating discs, sieve-plates (and pulsed flow), or reciprocating plates), mixer settlers and centrifugal extractors. Equipment selection is dependent on the process characteristics. Several authors have provided decision charts[114,115] and an example is displayed in Figure 1.29. Centrifugal extractors were developed for processes that require short residence times (e.g. in case of product instability), for emulsifying systems to improve separation and for systems with very small density differences between both phases[116-119].

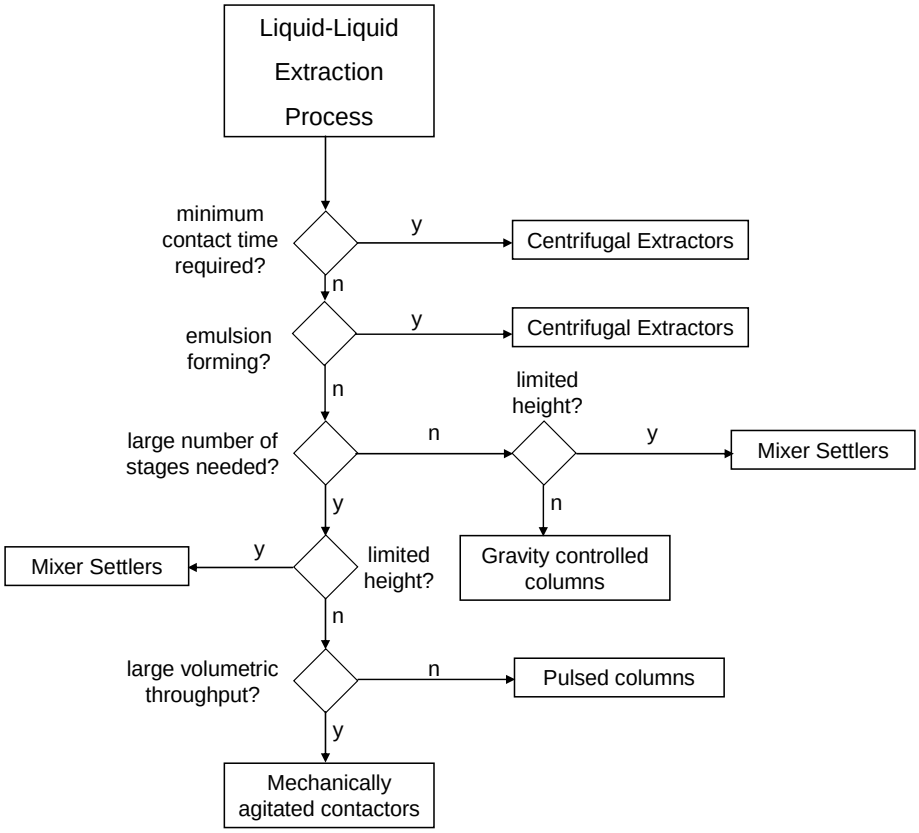

Figure 1.29. Selection chart for extraction equipment[115].

The centrifugal extractors described in the literature are mainly multistage continuous countercurrent operated extractors, such as the famous Podbielniak[120]. The use of these extractors is well established in the pharmaceutical industry[121].

1.4.2 Centrifugal Contactor Separators

In contrast to multistage centrifugal extractors single stage centrifugal equipment has received less attention. A typical example is the Annular Centrifugal Contactors[5,6], also known as a Centrifugal Contactor Separators (CCS)[122,123]. A representation of a typical CCS device, known as the CINC[7,124], is given in Figure 1.30. The CCS has originally been developed for processing nuclear waste[125]. A Chinese version of a CCS, closely resembling the CINC has been developed in parallel[126,127]. Besides for nuclear fuel processing, the use of CCS equipment has recently been reported for the extraction of L-Phe from the fermentation broth[128], for separation of ethylbenzene and octane with an ionic liquid extractant[129], and for the extraction of phenol from wastewater[130].

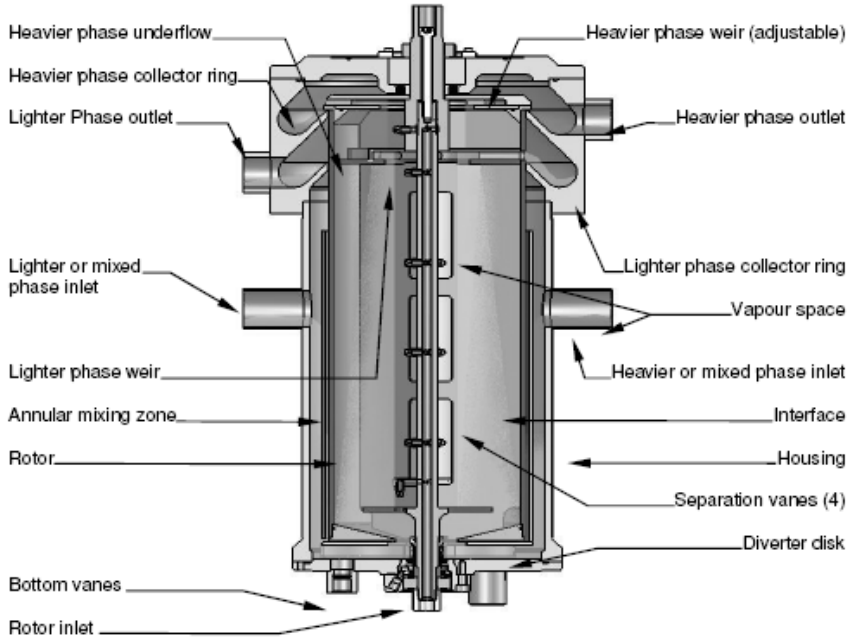

Figure 1.30. Cross-section of the CINC. Courtesy of Auxill Nederland B.V. With permission.

The CINC is basically a rotating centrifuge in a static house. The liquid(s) enter the CINC in the annular zone between the static wall and the rotating centrifuge, where intense mixing takes place. Next, they are transferred into the centrifuge where separation occurs by the centrifugal forces. A weir system allows collection of the individual phases. In a CCS device the unit operations mixing and separation are combined and as such the device is a good example of process intensification by integration [131,132]. A major aim of process intensification is reduction of plant size. In traditional extraction columns, operation is a compromise between efficient mixing and sufficient separation. When mixing is intensive, the drops are small resulting in difficult separation[133]. In the CCS equipment, the large centrifugal forces allows for a much smaller settling zone..

The CCS is well suited for ELLE. The equipment has a very low liquid hold-up, is easy to clean and is very compact. Due to the limited hold-up, losses are limited when changing feeds and this limits the use of precious, usually tailor made extractant[134]. The same reasoning also applies for expensive homogeneous catalysts. In our laboratory, application of the CCS for combined reaction and separation in a single device is pursued in parallel with ELLE[135].

Although engineering literature is available on CCS equipment, it is mainly concerned with flow instabilities[136] and design modifications[137-139]. Hardly any information is available on mixing behaviour, drop size distributions and residence time distributions. Only recently, computational fluid dynamics studies describing flow patterns in the annular zone have been reported[83,140,141]. Clearly detailed chemical engineering studies on equipment characteristics are required to aid the further development and optimization of ELLE and multiphase homogeneous catalysis.

1.5 Modeling enantioselective liquid-liquid extraction processes

Liquid-liquid extraction (LLE, also known as solvent extraction[48], or liquid extraction[49]) is a commonly applied separation technique in the fields of nuclear fuel reprocessing[142], hydrometallurgy[143], and in acid recovery[144-146]. The technology has gained extensive attention from both scientists and industry for many years[49,112,147-150]. Applying LLE for racemate separation is a relatively new variant. Evidently, the same basic principles for modeling LLE are also valid for ELLE. These principles are introduced here.

For optimization of existing LLE and the design of new processes, mathematical modeling is essential[151]. In general, modeling of multiphase fluid reactors requires knowledge on the kinetics and thermodynamics of the reactions, mixing patterns and the rate of transport through the interface[152]. Modeling is often performed on two levels, a

macroscopic reactor model with information of mixing of the phases and the hold-ups of the fluids in the reactor and a volume element model[153] to describe the overall rate of the reaction using both intrinsic kinetics and mass transfer rates [154]. The use of reactor- and volume element models is introduced here using a simple physical liquid-liquid extraction of component A. Figure 1.31 depicts a model for a stage in an extraction device. The reactor model is set up for the stage, the volume element is selected near the interface to describe mass transfer across the interface.

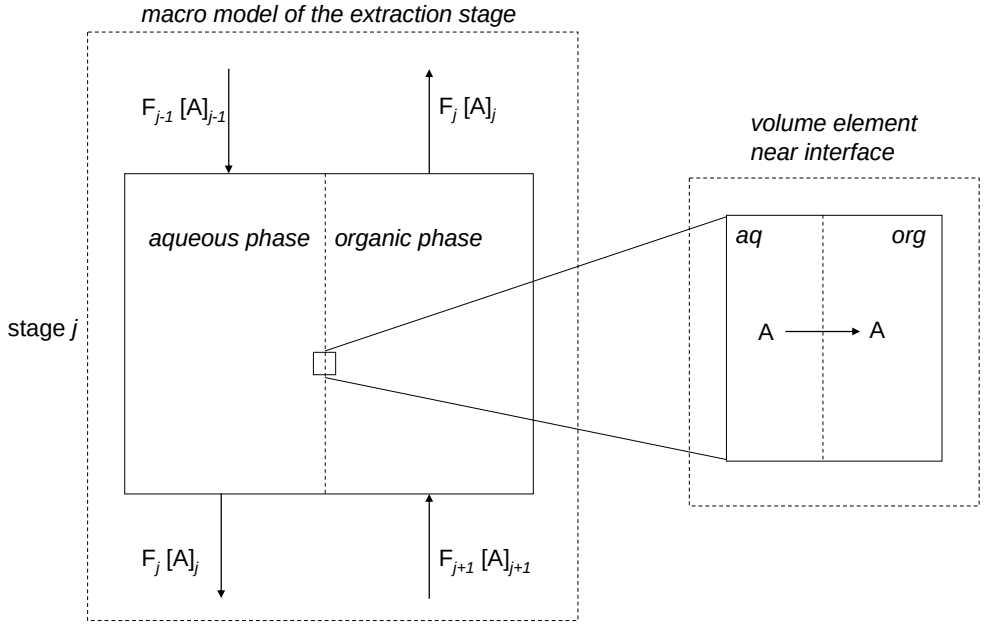

Figure 1.31. Reactor and volume element model for a stage in a LLE device for a physical extraction without reaction.

In the extraction stage depicted schematically in Figure 1.31 component A is transferred from the aqueous phase to the organic phase. The transport rate of A through the L-L interface is described by the volume element model. Numerous models have been developed for mass transfer through interfaces[155]. The most commonly used are the film model by Lewis and Whitman[156], the penetration model by Higbie[157] and the surface renewal model by Danckwerts[158]. The first is by far the simplest. In most cases, the model outcome for the three models is not significantly different[153]. Thus, we here applied the film model for describing the mass transfer process. The transport of A through the interface is quantified using a flux equation. The mechanism of transport to and from the

interface through the films is diffusion[159], and for simple systems as discussed here, Fick's law is applicable. The flux J_A of A through the interface is given by[153]:

$$J_{A,k} = -D_{A,k} \left. \frac{d[A]_k}{dx} \right|_{x=0} \qquad (k = aq, org) \tag{1.9}$$

By assuming that the steady state assumption is valid at the interface, the flux can be defined in terms of the bulk concentrations[153]:

$$J_A = \left(\frac{1}{k_{L,aq,A}} + \frac{1}{m_A k_{L,org,A}} \right)^{-1} \left([A]_{aq} - \frac{[A]_{org}}{m_A} \right) \tag{1.10}$$

Here $k_{L,k,A}$ is the mass transfer coefficient from A at side k, which is according to the film theory equal to:

$$k_{L,k,A} = \frac{D_{A,k}}{\delta_k} \tag{1.11}$$

The interfacial concentrations of A in both phases are related by the partitioning coefficient (Eq. 1.12) The partition coefficient is temperature dependent[160,161] and sometimes also concentration dependent[162].

$$m_A = \frac{[A]^*_{L2}}{[A]^*_{L1}} \tag{1.12}$$

The concentration profiles in the film layers are depicted schematically in Figure 1.32.

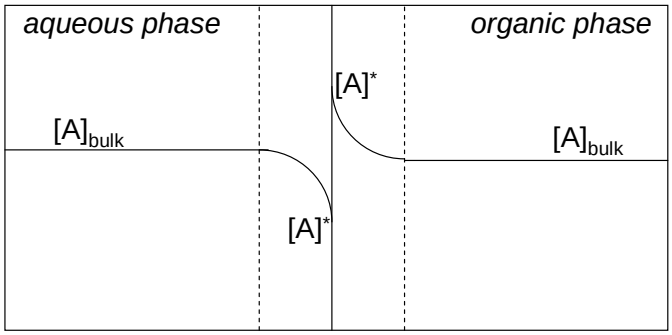

Figure 1.32. Concentration profile of A near the interface in dynamic physical extraction

The flux equation can be incorporated in the reactor model. In case both liquid phases are well mixed, the design equation for a continuous stirred tank may be applied. For the aqueous phase this reads:

$$V_{aq}\frac{d[A]_{aq}}{dt} = F_{aq,in}[A]_{aq,in} - F_{aq,out}[A]_{aq,out} - J_A A_{\text{int}} \qquad (1.13)$$

In case the mixing behavior is of the plug flow type, as is common in extraction columns [163], the concentrations are a function of the position in the column. In this case, the reactor model is given by:

$$V_{aq}\frac{d[A]_{aq}}{dt} = F_{aq,z}[A]_{aq,z} - F_{aq,(z+dz)}[A]_{aq,z+dz} - J_A A_{\text{int}} \qquad (1.14)$$

In case of intermediate mixing more complicated mixing models need to be applied (e.g. axial dispersion model, tanks in series model.

In case the contact time between the phases is much longer than the time needed for the system to reach chemical and physical equilibrium, the extraction process may be described by an equilibrium process and the time does not have to be taken into account in the models. Equilibrium modeling is less complicated than dynamic modeling and is therefore used extensively in (E)LLE[49]. Sometimes the equilibrium approach is used and an efficiency factor is included to compensate for non-equilibrium[130]:

$$\varepsilon = \frac{[A]_{aq,in} - [A]_{aq,out}}{[A]_{aq,in} - [A]_{aq,eq}} \qquad (1.15)$$

In the following subsections the modeling of single stage equilibrium extractions, multistage equilibrium extractions and dynamic extraction processes are discussed.

1.5.1 Single Stage Equilibrium Extraction

Extractions without chemical reaction (physical extraction)

In the most simple form of LLE a solute A in liquid 1 (L1) is transferred from L1 by contacting the solution with a second liquid (L2). Figure 1.33 schematically displays the physical extraction process.

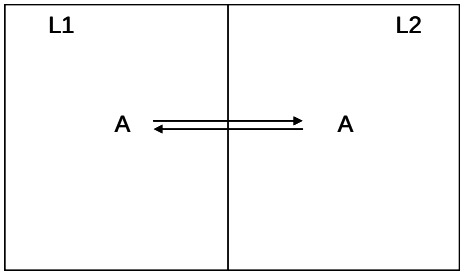

Figure 1.33. Extraction of A from L1 to L2.

Ternary systems like the one depicted in Figure 1.33 have been studied thoroughly[49], including thermodynamic studies and studies on activity coefficients as function of the composition and temperature. The current discussion will be limited to the ideal case where the solvents L1 and L2 are immiscible. In equilibrium the activity of species A in L1 equals the activity in L2 so that we can write:

$$a_{A,L1} = a_{A,L2} = \gamma_{A,L1}[A]_{L1} = \gamma_{A,L2}[A]_{L2} \qquad (1.16)$$

The activity coefficients $\gamma_{A,L1}$ and $\gamma_{A,L2}$ are not equal and as a result, the concentrations of A in both phases will not be equal at equilibrium. The equilibrium distribution of A over the phases L1 and L2 is defined as:

$$m_A = \frac{[A]_{L2}}{[A]_{L1}} \tag{1.17}$$

In this relation the property *m* is the partition coefficient of species A for the phases L1 and L2. The partition coefficient is temperature dependent[160,161] and sometimes also concentration dependent[162]. The extraction factor[49,164] for A is defined as:

$$Ef_A = \frac{V_{L2}}{V_{L1}} \frac{[A]_{L2}}{[A]_{L1}} \quad \text{or} \quad Ef_A = \frac{F_{L2}}{F_{L1}} \frac{[A]_{L2}}{[A]_{L1}} \tag{1.18}$$

Extraction with homogeneous reactions

The relations for extraction combined with homogeneous reactions are more complex than those derived for physical extraction only. For example, when L1 is an aqueous solution of weak acids A and B, the dissociation relations of the acids should be included, see Figure 1.34. The dissociation equilibrium for species A is given in Eq. 1.19.

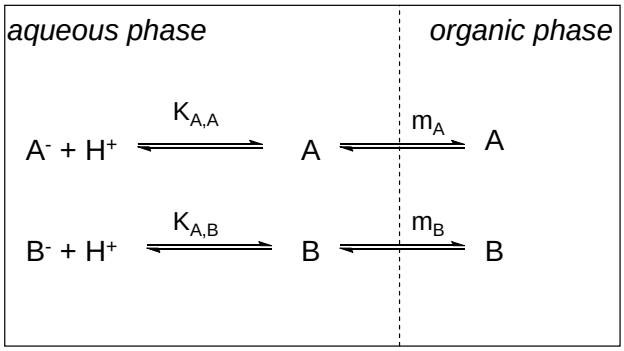

Figure 1.34. Equilibrium extraction of weak acids A and B.

$$K_{A,A} = \frac{\gamma_{A^-}[A^-]\gamma_{H^+}[H^+]}{\gamma_A[A]} \tag{1.19}$$

In practical systems, when the concentration range of A is sufficiently low, it may be assumed that γ_A is constant. When buffered solutions are used however, the ionic activity

coefficients should be included e.g. by applying a Debye-Hückel limiting law[165] as given in Eq. 1.20.

$$^{10}\log(\gamma_i) = \frac{-a\left|z_i^2\right|\sqrt{I}}{1+b\sqrt{I}} + \beta I \qquad (1.20)$$

Here a, b and β are system specific constants, depending on the ion-ion interactions, the ion diameter and ion-solvent interactions. For NaCl at 25°C: the parameters have the values 0.5115, 1.316 and 0, respectively[165]. I is the ionic strength:

$$I = \frac{1}{2}\sum_i z_i^2 c_i \qquad (1.21)$$

The organic-aqueous biphasic system at equilibrium as depicted in Figure 1.34 may be described by two dissociation equilibria and two partition relations. The distribution of species A over the two phases is defined by Eq. 1.22a, for species B a similar equation is valid.

$$D_A = \frac{[A]_{org}}{[A]_{aq} + [A^-]_{aq}} \qquad (1.22a)$$

In LLE it is common to apply an extractant in order to increase the distribution ratio of the desired species[146,147,150,166]. Figure 1.35 shows a system of two aqueous weak acids being contacted with an organic solution of extractant C. This is a typical example of a real LLE-system.

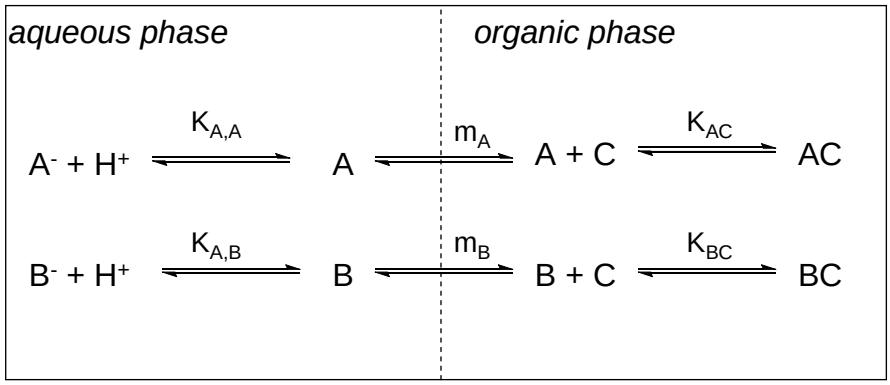

Figure 1.35. Example of a LLE-system with aqueous phase dissociation, partitioning over the phases and organic phase complexation.

The system of equilibrium relations is now extended with the complexation relations in the organic phase, for A defined as (see for comparison Eq. 1.6):

$$K_{AC} = \frac{[AC]_{org}}{[A]_{org}[C]_{org}} \tag{1.23}$$

Here, for simplicity only 1,1-stoichiometry is treated, but in acid extractions by tertiary amines, multiple complexes may be formed[167,168]. The system of equilibria then expands according to the number of different complexes present at equilibrium.

Due to complex formation of extractant C with the solutes A and B, the distribution of the solutes over the phases increases. The distribution of A over the two phases for a system containing an extractant is given by Eq. 1.22b:

$$D_A = \frac{[A]_{org} + [AC]_{org}}{[A]_{aq} + [A^-]_{aq}} \tag{1.22b}$$

A similar relation is valid for the distribution of species B over the phases. A measure for the selectivity is the separation factor[133] or operational selectivity[47] of the extraction system (see also Eq. 1.5):

$$\alpha_{op} = \frac{D_A}{D_B} \tag{1.24}$$

Enantioselective extraction with homogeneous reactions

The system as depicted in Figure 1.35 is a general example of a reactive extraction with homogeneous complexation in the organic phase and dissociation in the aqueous phase. A special case is chiral separation by ELLE. Chiral separation as depicted in Figure 1.35 requires a (chiral) enantioselective extractant C. Thus, when A and B in Figure 1.35 are enantiomers, the partition coefficient and dissociation (and/or protonation) constants are identical for both enantiomers and the difference in complexation constants induces the chiral separation.

For a process to become economically viable, several requirements need to be fulfilled. The extractant should be insoluble in the aqueous phase, have a high affinity for the enantiomers, but the complexation reaction should be reversible to be able to recycle the extractant. Furthermore, high solubility and chemical versatility is desired, meaning that multiple racemates of the same component class may be separated with a single extractant. In this way, development costs and time for new extractants may be avoided. A high selectivity is preferred, but in practice (operational) enantioselectivities are below 5 (see Table 1.2), and therefore multistage processes are required.

Enantioselective extraction with heterogeneous (interfacial) reactions

When the extractant is completely insoluble in the feed phase containing the racemate and vise versa the racemate is completely insoluble in the extract phase, the interface is the locus of reaction. This mechanism is typical for anion exchange extraction[169], depicted in Figure 1.36. Enantioselective extraction following this mechanism may be observed with ionic extractants such as quaternary ammonium salts, for example derived from cinchona alkaloids like quinine and quinidine. These have successfully been applied in chiral electrophoresis[170] and chiral phase transfer catalysis[171,172].

The difference with homogeneous extraction systems is a partition coefficient of zero for the extractant and racemate and interfacial instead of homogeneous complexation. As interfacial concentrations are in general unknown, the equilibrium relations are usually expressed in bulk concentrations using equilibrium relations between the bulk and interface. The set of equilibrium relations and mass balances describing the interfacial

process depicted in Figure 1.36 contains Eqs. 1.25, 1.19 and the three component mass balances.

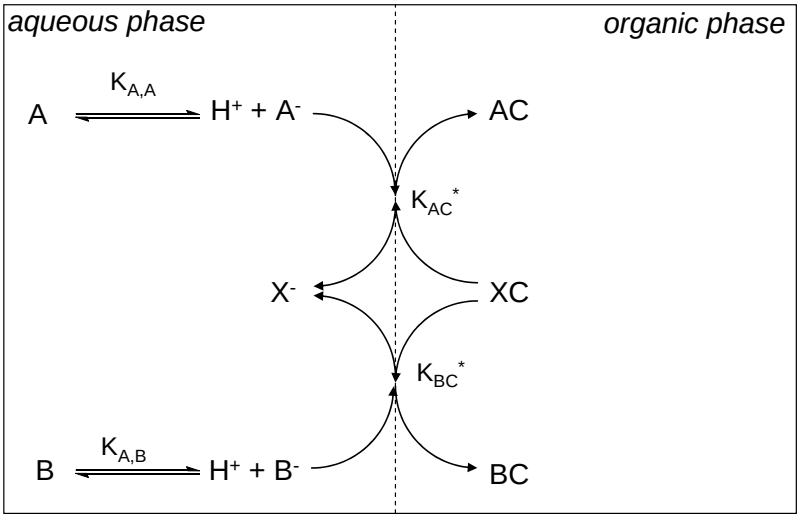

Figure 1.36. (Enantio)selective extraction through interfacial reaction (anion exchange)

The complexation of A and C at the interface is given by Eq. 1.25, a similar equation is valid for complexation of B and C.

$$K_{AC}^{*} = \frac{[X^-]_{aq}[AC]_{org}}{[A^-]_{aq}[C]_{org}} \tag{1.25}$$

The aqueous phase dissociation equilibrium of A was given by Eq. 1.19. A similar equation is valid for dissociation of B, when A and B are enantiomers, the constants $K_{A,A}$ and $K_{A,B}$ are identical.

1.5.2 Multistage Countercurrent Equilibrium Processes

The principle of a countercurrently operated multistage (E)LLE is illustrated in Figure 1.37. In this fractional extraction scheme for an ELLE process[173], two immiscible liquids flow

countercurrently through the cascade and the racemic feed enters near the centre of the cascade.

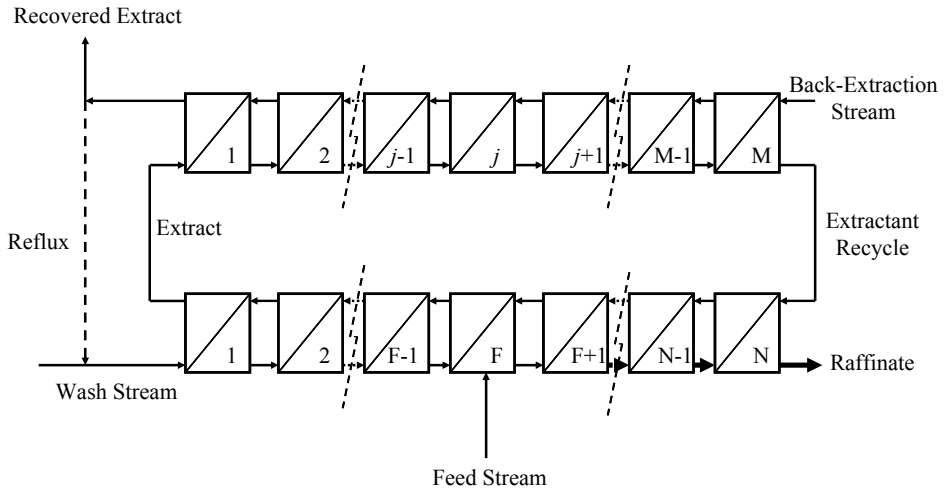

Figure 1.37. Multistage Fractional ELLE Process

In the strip section (stages F to N), one of the enantiomers is stripped from the feed stream and ends up in the extract stream. Typically part of the other enantiomer is co-extracted and needs to be washed out in the wash section (stages 1 to F-1) by applying a wash stream[47]. The extract is then transferred to a back-extraction unit, a cascade of M stages. This is again operated countercurrently, to back-extract the enantiomer from the extract. Typically, the back-extraction efficiency is improved by operating at elevated temperature[146,174] or a different pH[175] compared to the extraction cascade. The recovered extract stream may be recycled to the extraction unit for a new extraction cycle. Part of the back-extraction stream may be refluxed to the cascade in the wash-stream at the first stage[47]. Hereby the efficiency of the process can be improved, leading to possible reduction of the wash flow and the number of stages.

The Fenske equation[176], based on a full reflux process where the back-extraction stream is fully recycled, provides a reasonable estimate for the minimum number of equilibrium stages required for a certain separation. For separation of A and B in an A-rich extract stream and a B-rich raffinate, the Fenske equation is given in Eq. 1.26. The prediction of the minimum number of stages for various operational selectivities is given in Figure 1.38.

$$N_{\min} = \frac{\ln\left[\dfrac{x_{A,E}/\left(1-x_{A,E}\right)}{x_{A,R}/\left(1-x_{A,R}\right)}\right]}{\ln\left(\alpha_{op}\right)} \tag{1.26}$$

Here, the $x_{A,E}$ is the mole fraction of the solute in the extract that consists of A, i.e.

$$x_{A,E} = \frac{[A]_E}{[A]_E + [B]_E} \tag{1.27}$$

$x_{A,R}$ is defined similarly. For example, if the desired *ee* is 99% ($X_{A,E}$) and the operational selectivity is 2, the Fenske equation gives a minimum number of stages of 15.

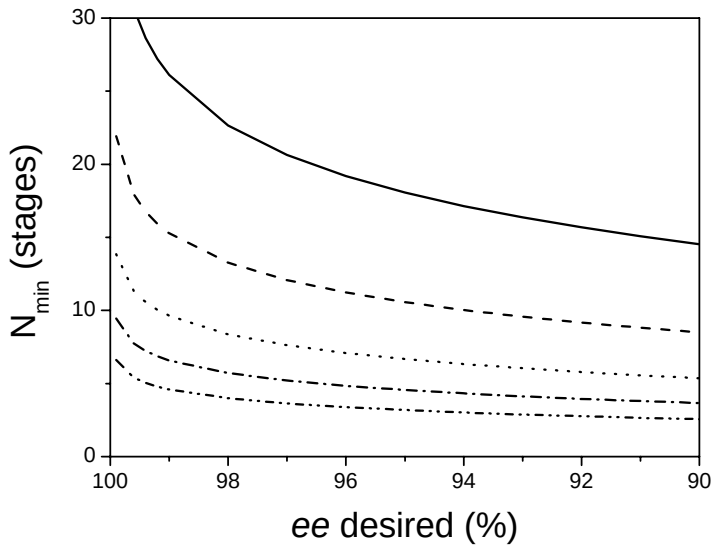

Figure 1.38. Minimum number of stages required for desired *ee* (symmetric operation: $ee_R = ee_S$), calculated with Eq.1.18. Lines: (—): α = 1.5; (---): α = 2; (…): α = 3; (-.-.): α = 5; (-..-..): α = 10.

In a real process, part of the recovered product is removed from the process for downstream processing. Therefore, the Fenske equation may provide a good estimate, but the actual number of stages will be higher[176]. To model an equilibrium multistage process,

at each of the stages, all appropriate equilibrium relations (e.g. Eqs. 1.9, 1.11, and 1.15 for both enantiomers) should be solved simultaneously with the component mass balances. The stages are coupled by the component mass balances.

1.5.3 Dynamic Extraction Processes

In the previous subsection, only equilibrium extraction processes were considered. In reality, the equilibrium approach is not always valid and more complex non-equilibrium approaches may be needed. Dynamic modeling for prediction and optimization of extraction processes involves macro level modeling (i.e. residence time distribution, interfacial area, and continuous phase determination) and volume element level modeling involving equilibrium and rate analyses[177]. There is ample literature available about transport phenomena[115] and equipment for LLE[112], and macroscopic reactor modeling is in general well established[153,178,179]. On volume element level, however, discussions on the locus of reaction (at the interface, or in one or both liquids) [143] are still ongoing. This indicates that kinetic modeling of liquid-liquid processes is not straight forward, and in this subsection kinetic modeling on volume element level is emphasized.

In the introduction of this section, a dynamical physical liquid-liquid extraction stage was considered. Here the discussion is expanded to systems with chemical reaction(s). After derivation of the relevant flux equations, this section is concluded by a short discussion on reactor modeling and techniques available for determining hydrodynamic characteristics of the extraction equipment.

Mass transfer with interfacial reaction

When a chemical reaction is involved in the extraction system, several mechanisms for the mass transfer and reaction are possible, depending on the solubilities of the reactants. In case the solutes in the feed are completely insoluble in the extract (organic) phase, and the extractant is insoluble in the feed (aqueous) phase, the reaction is confined to the interface. This type of extraction mechanism is widely applied in metal extraction chemistry[147,169], and for the extraction of penicillin G[180,181]. The interfacial reaction mechanism is displayed in Figure 1.36 for an anion exchange extraction. In a dynamic interfacial reaction process, mass transfer and reaction are serial steps. In this type of process with three steps (transport of reactants to the interface, reaction at the interface and transport of products from the interface) basically four regimes are distinguishable[182], ranging from very slow reaction where the chemical reaction is completely limiting the overall rate of conversion (Figure

1.39a), to instantaneous reaction at the interface (Figure 1.39d), where the rate is completely determined by the rate of mass transfer to the interface.

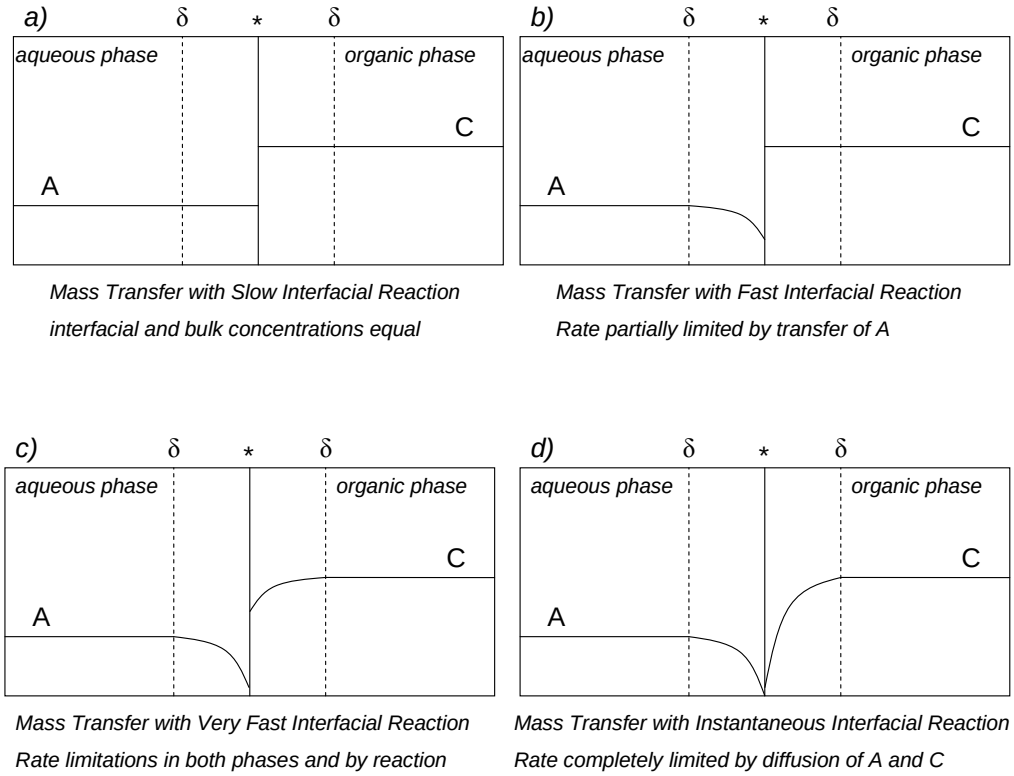

Figure 1.39. Qualitative concentration profiles of the reactants near the interface for different regimes in Mass Transfer with Interfacial Reaction (A + C → AC)[182].

In the situation where the reaction is limiting the overall rate, the intrinsic kinetics may be determined in terms of elementary reaction steps at the interface (adsorption on the interface, reaction at the interface, and desorption from the interface[147]). The elementary steps that describe the interfacial reaction of A and C in Figure 1.36 are given in Scheme. 1.1.

Scheme 1.1. Elementary reaction steps for interfacial reaction between A and C (see Fig. 1.36).

$$XC_{org} \underset{k_{-1}}{\overset{k_1}{\rightleftharpoons}} C^+_{ads} + X^-_{aq}$$

$$C^+_{ads} + A^-_{aq} \underset{k_{-2}}{\overset{k_2}{\rightleftharpoons}} AC_{ads}$$

$$AC_{ads} \underset{k_{-3}}{\overset{k_3}{\rightleftharpoons}} AC_{org}$$

The design equations for this case do not contain any diffusion terms, but only bulk concentrations and interfacial reaction rate equations. When the reaction is fast to instantaneous, depletion of one or more reactants at the interface is observed and the overall rate of transport is described by diffusion to and from the interface. In the intermediate regimes, both mass transfer and reaction govern the overall rate of the process. In the mass transfer limited regime, the chemical reaction is treated as a boundary condition in the design equations[183]. Typically, a diffusion limited interfacial process is described by Maxwell-Stefan equations for multicomponent diffusion[147,184]. A detailed discussion about Maxwell-Stefan diffusion is beyond the scope of this introduction. For further reading the book by Wesselingh and Krishna[184] is suggested.

Mass transfer with homogeneous reaction

When either the extractant is soluble in the aqueous phase, or the solutes are soluble in the organic phase, reaction may occur in one or both phases, and mass transfer and reaction are parallel processes. In aqueous/organic biphasic extractive systems, several situations have been reported.

When the solutes are soluble in the organic phase, and the extractant is insoluble in the aqueous phase, the locus of reaction is generally assumed to be the organic phase. This situation is reported for extractions of lactic acid[185] and acetic acid[186] using lipophilic tertiary amines in organic diluents, and also for the enantioselective extraction of aqueous amines and amino alcohols using a crown ether dissolved in toluene[46].

When the solutes are insoluble in the organic solvent, but the extractant is somewhat soluble in the aqueous phase, the reaction is assumed to take place in the aqueous phase. In metal extractions using phosphoric acid derivatives (for example di-(2-ethylhexyl)phosphoric acid, D2EHPA) or hydroxyoximes, complexation in the aqueous phase is suggested[143,187,188].

If the solutes are soluble in the organic phase and the extractant in the aqueous phase, reactions in both phases may be suggested. This situation occurs rarely[97,189-192].

In processes with homogeneous reaction(s), the reaction kinetics are coupled to the transport equations[183]. For two phase gas-liquid systems with mass transfer and reaction in parallel, ample literature on quantitative overall rates is available[153,193,194]. Although many industrial liquid-liquid processes involve homogeneous reaction in either one or both of the liquid phases[194,195], the use of regime analysis for the quantitative description of overall rates in liquid-liquid systems with homogeneous reaction is much less developed than for gas-liquid systems.

Several LLE-studies make use of the concept of regime analysis[175,196,197]. The routine for regime analysis as proposed by Doraiswamy and Sharma[194] should be used with care in LLE systems. Generally, it is assumed that resistance in the non-reactive phase is negligible. This is not so obvious for liquid-liquid processes and not always valid[46]. Further complicating factors for regime analysis are the usual (desired) reversibility of the reaction in (E)LLE and dissociation and/or protonation phenomena in the aqueous phase.

With mass transfer and chemical reaction(s) in parallel, the flux equation (Eq.1.11) needs to be modified with so called enhancement factors. For an ELLE system with enantiomers A and B transferring from the aqueous phase to the organic phase and homogeneous organic phase complexation with the extractant, the following relations hold:

$$J_A = \left(\frac{1}{k_{L,aq} E_{A,aq}} + \frac{1}{m_A k_{L,org} E_{A,org}} \right)^{-1} \left([A]_{aq} - \frac{[A]_{org}}{m_A} \right) \qquad (1.27a)$$

$$J_B = \left(\frac{1}{k_{L,aq} E_{B,aq}} + \frac{1}{m_B k_{L,org} E_{B,org}} \right)^{-1} \left([B]_{aq} - \frac{[B]_{org}}{m_B} \right) \qquad (1.27b)$$

The enhancement factors $E_{i,k}$ are added to describe the effect of the chemical reaction(s) on the rate of mass transfer and are regime-dependent[153]. In general, enhancement factors are defined as the ratio of the flux with parallel chemical reaction and the flux in absence of chemical reaction (at equal driving force).

$$E_A = \frac{J_{A,chem}}{J_{A,phys}} \tag{1.28}$$

The enhancement factors are depending on the relative rates of the chemical reaction and the mass transfer. In case of very slow reactions, compared to mass transfer, the overall rate is only determined by the reaction kinetics. The enhancement factor is then equal to unity. When the reaction is fast compared to mass transfer, the overall rate is enhanced[153] and the enhancement factor is larger than unity. The Hatta concept is generally applied to determine whether a reaction is slow or fast compared to mass transfer[153]. For reaction between A and C of order p and q in the organic phase, the Hatta number is defined as:

$$Ha_{A+C} = \frac{\sqrt{\frac{2}{p+1} D_A k_{pq} [A^*]_{org}^{p-1} [C]_{org}^{q}}}{k_{L,org}} \tag{1.29}$$

Here, D_A is the diffusivity of A in the organic phase.

For Ha < 0.2, the reaction is very slow compared to mass transport. In case 2 < Ha << $E_{A\infty}$, the reaction is fast and when Ha > $E_{A\infty}$, the reaction is instantaneous[153]. The asymptotic enhancement factor $E_{A\infty}$, for the reversible reaction between A and C where p = q = 1 is defined as[153]:

$$E_{A\infty,A+C} = 1 + \frac{D_A}{D_{AC}} \frac{K_{AC}[C]_{org}}{1 + \frac{D_{AC}}{D_C} K_{AC}[A^*]_{org}} \tag{1.30}$$

Figure 1.40 provides qualitative concentration profiles near the interface for several simplified situations with irreversible organic phase reaction A + B → P, where no dissociation or protonation is considered. For reversible reactions, the concentration profiles become more complex. Determination of the enhancement factor for mass transfer in the intermediate regimes for reversible reactions is not straightforward and beyond the scope of this introduction. Several workers have developed approximate and numerical solutions to describe the rate of enhanced mass transfer for situations of fast and instantaneous reversible chemical reactions[159,198-205].

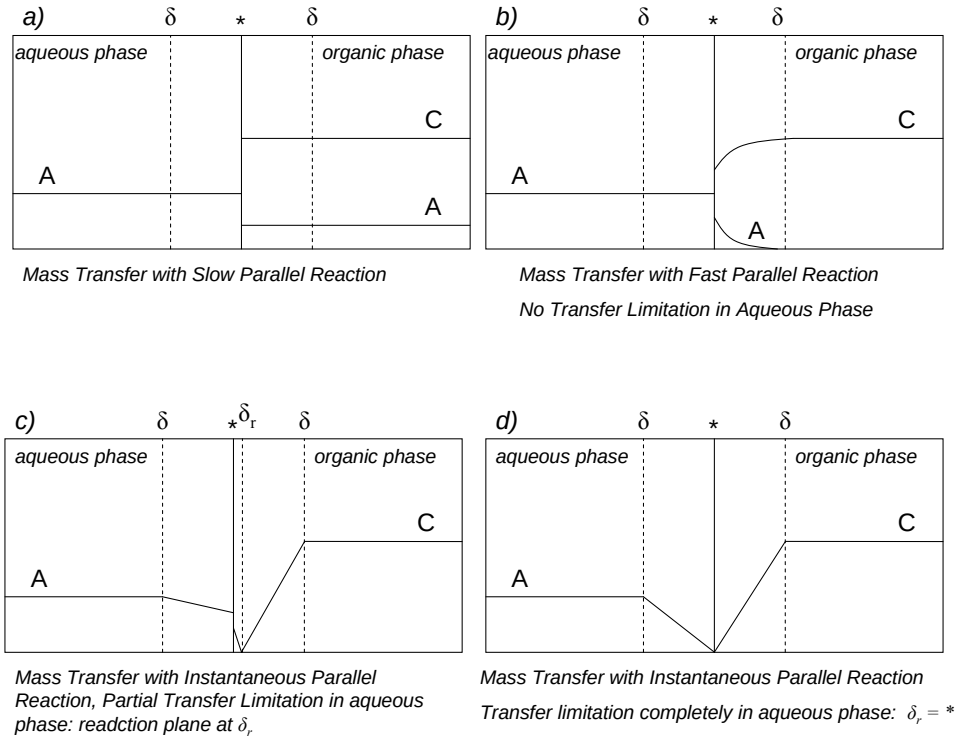

Figure 1.40. Qualitative concentration profiles of the reactants near the interface for different regimes of mass transfer and irreversible reaction in parallel (A + C → AC)

Determination of the intrinsic kinetics of multiphase reactions

When investigating interphase mass transfer, the mass transfer rate models should be used in combination with a proper reactor model. For determination of the mass transfer rate, proper equipment should be selected. Typically, studies on non-equilibrium liquid-liquid processes involve identification and estimation of the important resistances to mass transport. Several types of equipment are available for this purpose[206]. Studies using a Lewis type of stirred cell (Figure 1.41)[207] are by far the most abundant to determine the intrinsic rate(s) of the chemical reaction(s) involved in the process. The cell contains two liquid phases that are stirred independently. A horizontal baffle may be applied to create a system with a known interfacial area and well known hydrodynamic characteristics.

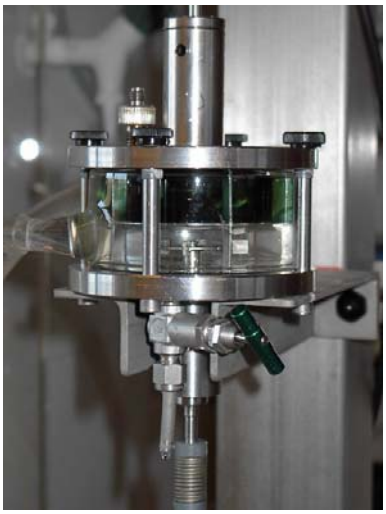

Figure 1.41. Picture of Lewis Cell.

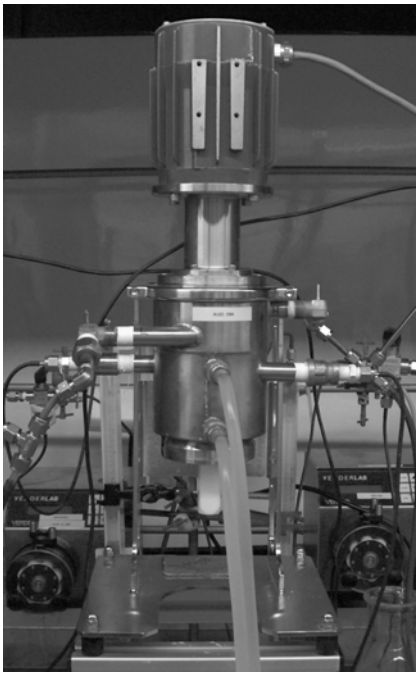

Figure 1.42. Picture of CINC V02.

Subsequently the experimentally determined kinetic constants are input in studies to identify and optimize the performance of the process equipment of choice (in this study a CINC V02, Figure 1.42). Hereto, the hydrodynamics, such as the interfacial area[208], the mixing behavior[177] and the phase behavior[209] should be investigated. A typical procedure for setting up a reactor model involves a study on the residence time distributions to determine whether the extractor is best described by a (series of) mixed tank(s) or by a plug flow reactor with axial dispersion[179]. Residence time distribution behavior can be examined by applying either a tracer pulse or step in the feed of the extractor and measuring how the composition in the outflow of the extractor responses[179]. Several techniques have been reported in literature on interfacial area determination. The interfacial area can either be determined by direct methods such as imaging[210] or indirect methods such as UV permeability[211] or chemical reaction[208,212]. In aqueous-organic two phase systems, determination of the continuous phase is traditionally done by measuring the conductivity of the dispersion[213,214], but recently a dye-tracer technique using laser-induced fluorescence has been reported[215].

1.6 Aim of the research and outline of the thesis

Over the past four decades, the knowledge on enantioselective liquid-liquid extraction (ELLE) has grown gradually. However the step towards commercialization appears to be hindered by the enormous gap between exploratory science in the laboratory and application on larger scale in continuous equipment. CCS technology is compact, flexible and appears a promising device to bridge this gap.

In an approach to bridge this gap, at the company DSM a study was done using CCS equipment for separation of racemic DNB-amino acids using cinchona-based chiral extractants[216]. In the DSM-project, two CCS units were applied in a mode where one CCS continuously extracts DNB-amino acid from the aqueous feed into the organic extract phase. The second CCS continuously back-extracted the extracted DNB-amino acids into a second aqueous phase. A flow sheet of this type of setup is given in Figure 1.43.

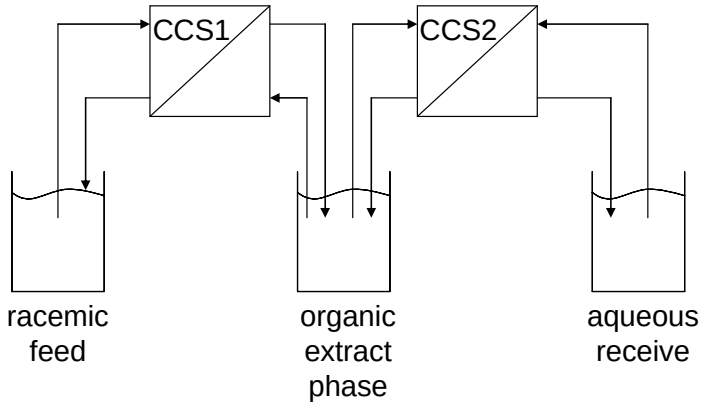

Figure 1.43. Schematic representation of the setup as applied at DSM[216].

In the DSM-approach low extractant concentrations compared to the racemate concentration were used at varying equipment settings. The results showed that the concept of ELLE has the potential to be competitive with technologies as chiral simulated bed chromatography (see section 1.2). The main conclusions were that for full separation of racemates into single enantiomers the setup as displayed in Figure 1.43 is not satisfactory as the enantiomeric excess deteriorates in time, and an engineering study on continuous flow modes would be needed. Moreover, for other racemate classes, other extractants should be developed.

These two conclusions resulted in a research project at the University of Groningen. In the department of Organic Chemistry development of new extractants for other racemate classes is aimed at. This thesis describes the work carried out in the Chemical Engineering department on continuous ELLE. The aim of the work described in this thesis is to determine the potential of CCS equipment for performing ELLE in a continuous mode without deterioration of the enantiomeric excess. For this purpose, two attractive ELLE systems were selected for engineering studies. The first involves the extraction of a racemic amino-acid derivative (3,5-dinitrobenzoyl-(*R*),(*S*)-leucine) using a cinchona alkaloid extractant (also used in the DSM-project), the second the separation of a primary amine derivative (phenylglycinol) with a bis-naphthyl phosphoric acid derivative (newly developed by Bas Verkuijl in the Organic Chemistry department of the University of Groningen).

Both systems are explored in batch setups and the effect of process variables on extraction performance is studied. Subsequently, the experimental results are modeled using equilibrium models to gain (better) understanding of the extraction systems. The ELLE of the DNB-Leu/cinchona alkaloid system is also studied in a single CCS device and in a cascade of countercurrently operated CCS devices including a back-extraction step to explore the potential of using ELLE in CCS-equipment.

In the first part of this thesis (Chapters 2-3) the effect of process variables on the equilibrium performance of the two ELLE systems in batch reactors will be provided. The ELLE of 3,5-dinitrobenzoyl-(*R*),(*S*)-leucine using a cinchona alkaloid extractant is described in Chapter 2. An extraction mechanism will be proposed and the experimental data will be modeled using an equilibrium model. Chapter 3 describes the study on the ELLE of phenylglycinol (PGL) using a new bis-naphthyl phosphoric acid derivative as extractant developed by Bas Verkuijl (Feringa Group, RUG). The effect of temperature on the selectivity will be investigated and a temperature dependent single stage equilibrium model developed, validated and used for optimization of a single stage equilibrium process.

Chapters 4 and 5 deal with the experimental determination of important chemical reactor engineering features of the CCS equipment. Determination of the liquid-liquid interfacial area of the CINC V02 is described in Chapter 4, using a chemical reaction method. Chapter 5 describes experimental studies in the CCS to gain insight in the drop size distribution in the (annular) mixing zone, the residence time distribution (RTD) of both liquid phases, the liquid hold-up of both phases and the phase behavior (disperse versus continuous) as a function of process variables. Several water-organic solvent combinations (i.e. water - toluene, heptane, octanol, dichloromethane, dichloroethane, and chloroform) are studied.

In the last part of the thesis (Chapters 6-7) studies on the continuous ELLE of 3,5-dinitrobenzoyl-(*R*),(*S*)-leucine in CCS equipment are reported. Chapter 6 describes experiments in a single CCS to indicate the potential of CCS devices for both extraction

and back-extraction. The results are compared with the equilibrium model derived in chapter 2 to check the applicability of the model for the continuous extraction in the CCS.

Chapter 7 describes an experimental and modeling study on the ELLE of 3,5-dinitrobenzoyl-R,S-leucine using a cascade of seven CCS devices, six for a countercurrent multistage extraction step and one for the backextraction. With a multistage model including the system parameters derived in Chapter 2, the optimum process conditions and configuration for a cascade of 6 CINC V02's to obtain one of the enantiomers in a 99% *ee* are determined. The experimental studies are used for verification of the model and to demonstration that continuous ELLE is possible without deterioration of the enantiomeric excess or yield.

1.7 Nomenclature

a	Constant in Debye- Hückel law
ads	Adsorbed at the interface
aq	Aqueous phase, subscript
A	A-enantiomer
A	interfacial area
b	Constant in Debye-Hückel law
B	B-enantiomer
C	Complexant, host, or extractant
D	Distribution, (-)
D	Diffusion coefficient, m^2/s
E	Extract stream
$E_{i,k}$	Enhancement factor for component i in phase k
Ef	Extraction factor, (-)
F	Flow, m^3/s
ΔG	Gibbs free energy change
Ha	Hatta number, (-)
int	intrinsic
int	interface
I	Ionic strength, (mol/L)
J	Flux, $mol/(m^2s)$
k	Index for phases, aq and org
k	Rate coefficient, various dimensions
K	Equilibrium constant, various dimensions
L	Liquid
N	Number of stages
op	operational

org	Organic phase, subscript
p	Reaction order of A
q	Reaction order of B
R	R-enantiomer
R	Raffinate stream
R	Gas constant, 8.314 J/(mol K)
S	S-enantiomer
T	Temperature, K
V	Volume, m^3
x	fraction (-)
z	electron valence, (-)

symbols and Greek letters

[]	concentrations, mol/L
*	interfacial concentrations
ε	extraction efficiency (-)
α	selectivity, (-)
β	constant in Debye- Hückel law
γ	activity coefficient, (-)
δ	film layer thickness according to film model, m

1.8 References

[1]. Bauer, K.; Falk, H.; Schlogl, K. *Monatshefte für Chemie* **1968,** *99*, 2186-&.

[2]. Bowman, N. S.; Mccloud, G. T.; Schweitz, G. K. *J. Am. Chem. Soc.* **1968,** *90*, 3848-3852.

[3]. Romano, S. J.; Wells, K. H.; Rothbart, H. L.; Rieman, W. *Talanta* **1969,** *16*, 581-590.

[4]. Schweitz, G. K.; Supernaw, I. R.; Bowman, N. S. *J. Inorg. Nucl. Chem.* **1968,** *30*, 1885-1890.

[5]. Bernstein, G. J.; Grosvenor, D. E.; Lenc, J. F.; Levitz, N. M. *Nucl. Technol.* **1973,** *20*, 200-202.

[6]. Leonard, R. A.; Bernstein, G. J.; Ziegler, A. A.; Pelto, R. H. Annular centrifugal contactors for solvent extraction. Separation Science and Technology 15[4], 925-943. 1980.

[7]. Meikrantz, D. H.; Macaluso, L. L.; Sams, H. W.; Schardin, C. H.; Federici, A. G. US Patent 5,762,800, Jun 9, 1998.

[8]. Breuer, M.; Ditrich, K.; Habicher, T.; Hauer, B.; Kesseler, M.; Sturmer, R.; Zelinski, T. *Angew. Chem. Int. Ed.* **2004,** *43*, 788-824.

[9]. Rouhi, A. M. *Chem. Eng. News* **2003,** *81*, 45-55.

[10]. Eliel, E. L.; Wilen, S. H. *Stereochemistry of Organic Compounds;* 1994.
[11]. Sheldon, R. A. *Chirotechnology; industrial synthesis of optically active compounds;* Marcel Dekker, Inc.: New York, 1993.
[12]. Pasteur, L. *Comptes rendus hebdomadaires des séances de l'Académie des sciences* **1848,** *26*, 535-539.
[13]. Ehrlich, P. *British Medical Journal* **1913,** *2(2746)*, 353-359.
[14]. Duursma, A. Asymmetric catalysis with chiral monodentate phosphoramidite ligands. University of Groningen, Groningen, The Netherlands, 2004.
[15]. Mulzer, J. Basic Principles of Asymmetric Synthesis. In *Comprehensive Asymmetric Catalysis*, Jacobsen, E. N., Pfaltz, A., Yamamoto, H., Eds.; Springer: Berlin, 1999; pp 33-97.
[16]. Collins, A. N.; Sheldrake, G. N.; Crosby, J. *Chirality in Industry II;* John Wiley & sons Ltd.: Chichester, 1997.
[17]. Waites, M. J. *Industrial Microbiology;* Blackwell Science: Oxford, 2001.
[18]. Reschke, M.; Schugerl, K. *Chemie Ingenieur Technik* **1984,** *56*, 141.
[19]. Cascaval, D.; Oniscu, C.; Galaction, A. I. *Biochemical Engineering Journal* **2001,** *7*, 171-176.
[20]. Jacobsen, E. N.; Pfaltz, A.; Yamamoto, H. *Comprehensive Asymmetric Catalysis;* Springer: Berlin, 1999; Vol. 1.
[21]. Faber, K. *Biotransformations in Organic Chemistry;* fourth edition ed.; Springer: Berlin, 2000.
[22]. Maier, N. M.; Franco, P.; Lindner, W. *Journal of Chromatography A* **2001,** *906*, 3-33.
[23]. Faigl, F.; Fogassy, E.; Nogradi, M.; Palovics, E.; Schindler, J. *Tetrahedron-Asymmetry* **2008,** *19*, 519-536.
[24]. Fogassy, E.; Nogradi, M.; Kozma, D.; Egri, G.; Palovics, E.; Kiss, V. *Organic & Biomolecular Chemistry* **2006,** *4*, 3011-3030.
[25]. Vries, T.; Wynberg, H.; van Echten, E.; Koek, J.; ten Hoeve, W.; Kellogg, R. M.; Broxterman, Q. B.; Minnaard, A.; Kaptein, B.; van der Sluis, S.; Hulshof, L.; Kooistra, J. *Angew. Chem. Int. Ed.* **1998,** *37*, 2349-2354.
[26]. Bruggink, A. Rational Design in Resolutions. In *Chirality in Industry II*, Collins, A. N., Sheldrake, G. N., Crosby, J., Eds.; John Wiley & sons Ltd.: Chichester, 1997; pp 81-98.
[27]. Steensma, M.; Kuipers, N. J. M.; de Haan, A. B.; Kwant, G. *Chirality* **2006,** *18*, 314-328.
[28]. Crosby, J. *Tetrahedron* **1991,** *47*, 4789-4846.
[29]. Davankov, V. A. *Journal of Chromatography A* **1994,** *666*, 55-76.
[30]. Gubitz, G.; Schmid, M. G. *Journal of Chromatography A* **1997,** *792*, 179-225.
[31]. Ahuja, S. *Chiral Separations: Application and technology;* ACS: Washington, 1997.
[32]. Subramanian, G. *Chiral separaration techniques: A practical approach;* Wiley-VCH: Weinheim, 2001.
[33]. Toda, F. *Enantiomer separation: Fundamentals and practical methods;* Kluwer Academic publishers: Dordrecht, 2004.
[34]. Gübitz, G.; Schmid, M. G. *Chiral Separations;* Humana Press: Totowa (NJ), 2004.
[35]. Francotte, E.; Leutert, T.; La Vecchia, L.; Ossola, F.; Richert, P.; Schmidt, A. *Chirality* **2002,** *14*, 313-317.

[36]. Gavioli, E.; Maier, N. M.; Minguillon, C.; Lindner, W. *Anal. Chem.* **2004,** *76*, 5837-5848.
[37]. Zenoni, G.; Quattrini, F.; Mazzotti, M.; Fuganti, C.; Morbidelli, M. *Flavour and Fragrance Journal* **2002,** *17*, 195-202.
[38]. Afonso, C. A. M.; Crespo, J. G. *Angew. Chem. Int. Ed.* **2004,** *43*, 5293-5295.
[39]. Baragana, B.; Blackburn, A. G.; Breccia, P.; Davis, A. P.; de Mendoza, J.; Padron-Carrillo, J. M.; Prados, P.; Riedner, J.; de Vries, J. G. *Chemistry-A European Journal* **2002,** *8*, 2931-2936.
[40]. Keurentjes, J. T. F.; Nabuurs, L. J. W. M.; Vegter, E. A. *J. Membr. Sci.* **1996,** *113*, 351-360.
[41]. Maximini, A.; Chmiel, H.; Holdik, H.; Maier, N. W. *J. Membr. Sci.* **2006,** *276*, 221-231.
[42]. Viegas, R. M. C.; Afonso, C. A. M.; Crespo, J. G.; Coelhoso, I. M. *Sep. Purif. Technol.* **2007,** *53*, 224-234.
[43]. Koska, J.; Haynes, C. A. *Chem. Eng. Sci.* **2001,** *56*, 5853-5864.
[44]. Pickering, P. J.; Chaudhuri, J. B. *Chem. Eng. Sci.* **1997,** *52*, 377-386.
[45]. Steensma, M.; Kuipers, N. J.; de Haan, A. B.; Kwant, G. *J. Chem. Technol. Biotechnol.* **2006,** *81*, 588-597.
[46]. Steensma, M.; Kuipers, N. J. M.; de Haan, A. B.; Kwant, G. *Chem. Eng. Sci.* **2007,** *62*, 1395-1407.
[47]. Steensma, M.; Kuipers, N. J. M.; de Haan, A. B.; Kwant, G. *Chem. Eng. Proc.* **2007,** *46*, 996-1005.
[48]. Lo, T. C.; Baird, M. H. I.; Hanson, C. *Handbook of Solvent Extraction;* Reprint ed.; Krieger Publishing Company: Malabar, USA, 1991.
[49]. Treybal, R. E. *Liquid Extraction, 2nd ed.;* second edition ed.; McGraw-Hill: New York, 1963.
[50]. Pirkle, W. H.; Pochapsky, T. C. *Chemical Reviews* **1989,** *89*, 347-362.
[51]. Maier, N. M.; Schefzick, S.; Lombardo, G. M.; Feliz, M.; Rissanen, K.; Lindner, W.; Lipkowitz, K. B. *J. Am. Chem. Soc.* **2002,** *124*, 8611-8629.
[52]. Zhang, X. X.; Bradshaw, J. S.; Izatt, R. M. *Chemical Reviews* **1997,** *97*, 3313-3361.
[53]. Davankov, V. A. *Chirality* **1997,** *9*, 99-102.
[54]. Koska, J.; Mui, C.; Haynes, C. A. *Chem. Eng. Sci.* **2001,** *56*, 29-41.
[55]. Kyba, E. B.; Koga, J.; Sousa, L. R.; Siegel, M. G.; Cram, D. J. *J. Am. Chem. Soc.* **1973,** *95*, 2692-2693.
[56]. Lingenfelter, D. S.; Helgeson, R. C.; Cram, D. J. *J. Org. Chem.* **1981,** *46*, 393-406.
[57]. Newcomb, M.; Toner, J. L.; Helgeson, R. C.; Cram, D. J. *J. Am. Chem. Soc.* **1979,** *101*, 4941-4947.
[58]. Peacock, S. C.; Domeier, L. A.; Gaeta, F. C. A.; Helgeson, R. C.; Timko, J. M.; Cram, D. J. *J. Am. Chem. Soc.* **1978,** *100*, 8190-8202.
[59]. Breccia, P.; Van Gool, M.; Perez-Fernandez, R.; Martin-Santamaria, S.; Gago, F.; Prados, P.; de Mendoza, J. C. *J. Am. Chem. Soc.* **2003,** *125*, 8270-8284.
[60]. Galan, A.; Andreu, D.; Echavarren, A. M.; Prados, P.; de Mendoza, J. *J. Am. Chem. Soc.* **1992,** *114*, 1511-1512.
[61]. Verkuijl, B. J. V. Personal Communication

[62]. Overdevest, P. E. M.; van der Padt, A.; Keurentjes, J. T. F.; van't Riet, K. *Colloids and Surfaces A-Physicochemical and Engineering Aspects* **2000,** *163*, 209-224.
[63]. Pickering, P. J.; Chaudhuri, J. B. *Chirality* **1999,** *11*, 241-248.
[64]. Takeuchi, T.; Horikawa, R.; Tanimura, T. *Anal. Chem.* **1984,** *56*, 1152-1155.
[65]. Tan, B.; Luo, G. S.; Wang, H. D. *Tetrahedron-Asymmetry* **2006,** *17*, 883-891.
[66]. Tan, B.; Luo, G. S.; Wang, J. D. *Sep. Purif. Technol.* **2007,** *53*, 330-336.
[67]. Tan, B.; Luo, G. S.; Qi, X.; Wang, J. D. *Sep. Purif. Technol.* **2006,** *49*, 186-191.
[68]. Andrisano, V.; Gottarelli, G.; Masiero, S.; Heijne, E. H.; Pieraccini, S.; Spada, G. P. *Angew. Chem. Int. Ed.* **1999,** *38*, 2386-2388.
[69]. Dzygiel, P.; Monti, C.; Piarulli, U.; Gennari, C. *Organic & Biomolecular Chemistry* **2007,** *5*, 3464-3471.
[70]. Dzygiel, P.; Reeve, T. B.; Piarulli, U.; Krupicka, M.; Tvaroska, I.; Gennari, C. *European Journal of Organic Chemistry* **2008,** 1253-1264.
[71]. Kellner, K. H.; Blasch, A.; Chmiel, H.; Lämmerhofer, M.; Lindner, W. *Chirality* **1997,** *9*, 268-273.
[72]. Lindner, W.; Lämmerhofer, M.; Maier, N. M. EP 0912563, 1997.
[73]. Reeve, T. B.; Cros, J. P.; Gennari, C.; Piarulli, U.; de Vries, J. G. *Angew. Chem. Int. Ed.* **2006,** *45*, 2449-2453.
[74]. Tsukube, H.; Uenishi, J.; Kanatani, T.; Itoh, H.; Yonemitsu, O. *Chemical Communications* **1996,** 477-478.
[75]. Tsukube, H.; Shinoda, S.; Uenishi, J.; Kanatani, T.; Itoh, H.; Shiode, M.; Iwachido, T.; Yonemitsu, O. *Inorg. Chem.* **1998,** *37*, 1585-1591.
[76]. Stryer, L. *Biochemistry;* 4th edition ed.; Freeman: New York, 1995.
[77]. Pursell, M. R.; Mendes-Tatsis, M. A.; Stuckey, D. C. *Biotechnol. Bioeng.* **2003,** *82*, 533-542.
[78]. Naemura, K.; Matsunaga, K.; Fuji, J.; Ogasahara, K.; Nishikawa, Y.; Hirose, K.; Tobe, Y. *Anal. Sci.* **1998,** *14*, 175-182.
[79]. Naemura, K.; Nishioka, K.; Ogasahara, K.; Nishikawa, Y.; Hirose, K.; Tobe, Y. *Tetrahedron-Asymmetry* **1998,** *9*, 563-574.
[80]. Abe, Y.; Shoji, T.; Kobayashi, M.; Qing, W.; Asai, N.; Nishizawa, H. *Chem. Pharm. Bull.* **1995,** *43*, 262-265.
[81]. Abe, Y.; Shoji, T.; Fukui, S.; Sasamoto, M.; Nishizawa, H. *Chem. Pharm. Bull.* **1996,** *44*, 1521-1524.
[82]. Prelog, V.; Stojanac, Z.; Kovacevic, K. *Helv. Chim. Acta* **1982,** *65*, 377-384.
[83]. Tang, L.; Choi, S.; Nandhakumar, R.; Park, H.; Chung, H.; Chin, J.; Kim, K. *The Journal of Organic Chemistry* **2008,** *73*, 5996-5999.
[84]. Steensma, M. Chiral separation of amino-alcohols and amines by fractional reactive extraction. University of Twente, The Netherlands, 2005.
[85]. Ohki, A.; Miyashita, R.; Naka, K.; Maeda, S. *Bull. Chem. Soc. Jpn.* **1991,** *64*, 2714-2719.
[86]. Jiao, F. P.; Chen, X. Q.; Hu, W. G.; Ning, F. R.; Huang, K. L. *Chemical Papers* **2007,** *61*, 326-328.
[87]. Tang, K.; Chen, Y.; Huang, K.; Liu, J. *Tetrahedron-Asymmetry* **2007,** *18*, 2399-2408.
[88]. Nishizawa, H.; Tahara, K.; Hayashida, A.; Abe, Y. *Anal. Sci.* **1993,** *9*, 611-615.
[89]. Colera, M.; Costero, A. M.; Gavina, P.; Gil, S. *Tetrahedron: Asymmetry* **2005,** *16*, 2673-2679.

[90]. Nazarenko, A. Y.; Huszthy, P.; Bradshaw, J. S.; Lamb, J. D.; Izatt, R. M. *J. Inclusion Phenom.* **1994,** *20*, 13-22.
[91]. Moore, S. S.; Tarnowski, T. L.; Newcomb, M.; Cram, D. J. *J. Am. Chem. Soc.* **1977,** *99*, 6398-6405.
[92]. von Zeiewsky, A.; Belser, P.; Hayoz, P.; Dux, R.; Hua, X.; Suckling, A.; Stoeckli-Evans, H. *Coord. Chem. Rev.* **1994,** *132*, 75-85.
[93]. Barton, J. K. *Science* **1986,** *233*, 727-734.
[94]. Lacour, J.; Goujon-Ginglinger, C.; Torche-Haldimann, S.; Jodry, J. J. *Angew. Chem. Int. Ed.* **2000,** *39*, 3695-3697.
[95]. Tsurubou, S. *Anal. Chim. Acta* **1988,** *215*, 119-129.
[96]. Tsurubou, S. *Anal. Sci.* **1991,** *7*, 45-48.
[97]. Mhaskar, R. D.; Sharma, M. M. *Chem. Eng. Sci.* **1975,** *30*, 811-818.
[98]. Lindner, W.; Lämmerhofer, M. Eur. Pat. Appl. No. 96 109 072.7, 1996.
[99]. Caner, H.; Biedermann, P. U.; Agranat, I. *Chirality* **2003,** *15*, 637-645.
[100]. Dijkstra, G. D. H.; Kellogg, R. M.; Wynberg, H.; Svendsen, J. S.; Marko, I.; Sharpless, K. B. *J. Am. Chem. Soc.* **1989,** *111*, 8069-8076.
[101]. Dijkstra, G. D. H.; Kellogg, R. M.; Wynberg, H. *J. Org. Chem.* **1990,** *55*, 6121-6131.
[102]. Uccello-Barretta, G.; Balzano, F.; Quintavalli, C.; Salvadori, P. *J. Org. Chem.* **2000,** *65*, 3596-3602.
[103]. Daintree, L. S.; Kordikowski, A.; York, P. *Advanced Drug Delivery Reviews* **2008,** *60*, 351-372.
[104]. Keszei, S.; Simandi, B.; Szekely, E.; Fogassy, E.; Sawinsky, J.; Kemeny, S. *Tetrahedron-Asymmetry* **1999,** *10*, 1275-1281.
[105]. Bauza, R.; Rios, A.; Valcarcel, M. *Anal. Chim. Acta* **1999,** *391*, 253-256.
[106]. Kmecz, I.; Simandi, B.; Balint, J.; Szekeley, E.; Fogassy, E.; Kemeny, S. *Chirality* **2001,** *13*, 568-570.
[107]. Kmecz, I.; Simandi, B.; Szekely, E.; Lovasz, J.; Fogassy, E. *Chirality* **2007,** *19*, 430-433.
[108]. Simandi, B.; Keszei, S.; Fogassy, E.; Sawinsky, J. *J. Org. Chem.* **1997,** *62*, 4390-4394.
[109]. Bauza, R.; Rios, A.; Valcarcel, M. *Anal. Chim. Acta* **2001,** *450*, 1-11.
[110]. Bauza, R.; Rios, A.; Valcarcel, M. *Sep. Sci. Technol.* **2004,** *39*, 459-478.
[111]. Szekely, E.; Simandi, B.; Fogassy, E.; Kemeny, S.; Kmecz, I. *Chirality* **2003,** *15*, 783-786.
[112]. Godfrey, J. C.; Slater, M. J. *Liquid-Liquid Extraction Equipment;* John Wiley & Sons: New York, 1994.
[113]. Lo, T. C. Commercial Liquid-Liquid Extraction Equipment. In *Handbook of Separation Techiques for Chemical Engineers*, 3rd ed.; Schweitzer, P. A., Ed.; McGraw-Hill: New York, 1996.
[114]. Hines, A. L.; Maddox, R. N. *Mass Transfer; Fundamentals & Applications;* 1985: New Jersey, 1985.
[115]. Laddha, G. S.; Degaleesan, T. E. *Transport Phenomena in Liquid Extraction;* Tata McGraw-Hill: New Delhi, 1976.
[116]. Blass, E. Centrifugal Extractors. In *Liquid-Liquid Extraction Equipment*, Godfrey, J. C., Slater, M. J., Eds.; John Wiley & Sons, Ltd: Chichester, 1994; pp 531-568.

[117]. Hafez, M. Centrifugal Extractors. In *Handbook of Solvent Extraction*, Lo, T. C., Baird, M. H. C., Hanson, C., Eds.; Krieger Publishing Company: Malabar, 1991; pp 459-474.
[118]. Robbins, L. A.; Cusack, R. W. Liquid-liquid extraction operations and equipment. In *Perry's Chemical Engineers' Handbook*, 7th ed.; Perry, R. H., Green, D. W., Eds.; McGraw-Hill: New York, 1999.
[119]. Müller, E.; Berger, E.; Blass, E.; Sluyts, D. Liquid-Liquid Extraction. In *Uhlmann's Processes and Process Engingeering Vol. 1: Separation Processes*, Wiley-VCH: Weinheim, 2004.
[120]. Podbielniak, W. J. US Patent 2,044,996, 1936.
[121]. Verrall, M. S. Partition in the pharmaceutical industry. In *Science and Practice of Liquid-Liquid Extraction*, Thornton, J. D., Ed.; Clarendon Press: Oxford, 1994; pp 194-308.
[122]. Leonard, R. A.; Pelto, R. H.; Ziegler, A. A.; Bernstein, G. J. Flow over circular weirs in a centrifugal field. Canadian Journal of Chemical Engineering 58[4], 531-534. 1980.
[123]. Leonard, R. A. *Sep. Sci. Technol.* **1988,** *23*, 1473-1487.
[124]. Meikrantz, D. H. 4,959,158, Sep 25, 1990.
[125]. Webster D.S.; Jennings, A. S.; Kishbaugh, A. S.; Bethmann, H. K. *Performance of Centrifugal Mixer Settler in the Reprocessing of Nuclear Fuel*;DP-MS-67-71; Savannah River Laboratory: 67.
[126]. Zhou, J.; Duan, W. H.; Zhou, X. Z.; Zhang, C. Q. *Hydrometallurgy* **2007,** *85*, 154-162.
[127]. Zhou, X. Z.; Zhou, J. Z.; Zhang, C. Q.; Yu, W. D. *Sep. Sci. Technol.* **1997,** *32*, 2705-2713.
[128]. Ruffer, N.; Heidersdorf, U.; Kretzers, I.; Sprenger, G. A.; Raeven, L.; Takors, R. *Bioprocess and Biosystems Engineering* **2004,** *26*, 239-248.
[129]. Zhu, J. Q.; Chen, J.; Li, C. Y.; Fei, W. Y. *Sep. Purif. Technol.* **2007,** *56*, 237-240.
[130]. Xu, J. Q.; Duan, W. H.; Zhou, X. Z.; Zhou, H. Z. *J. Hazard. Mater.* **2006,** *131*, 98-102.
[131]. Kulprathipanja, S. *reactive separation process;* Taylor & Francis: New York, 2002.
[132]. Stanckiewicz, A.; Moulijn, J. A. *Re-Engineering the chemical processing plant; Process Intensification;* Marcel Dekker, Inc: New York, 2004.
[133]. King, C. J. *Separation Processes;* second ed.; McGraw-Hill: New York, 1980.
[134]. Danesi, P. R. Supported Liquid Membranes. In *Developments in Solvent Extraction*, Alegret, S., Ed.; Ellis Horwood: Chichester, 1988; pp 159-165.
[135]. Kraai, G. N.; van Zwol, F.; Schuur, B.; Heeres, H. J.; de Vries, J. G. *Angew. Chem.* **2008,** *120*, 3969-3972.
[136]. Vedantam, S.; Joshi, J. B. *Chemical Engineering Research & Design* **2006,** *84*, 522-542.
[137]. Klasson, K. T.; Taylor, P. A.; Walker, J. F.; Jones, S. A.; Cummins, R. L.; Richardson, S. A. *Sep. Sci. Technol.* **2005,** *40*, 453-462.
[138]. Meikrantz, D. H.; Meikrantz, S. B.; Macaluso, L. L. *Chem. Eng. Commun.* **2001,** *188*, 115-127.
[139]. Meikrantz, D. H.; Macaluso, L. L.; Flim, W. D.; Heald, C. J.; Mendoza, G.; Meikrantz, S. B. *Chem. Eng. Commun.* **2002,** *189*, 1629-1639.

[140]. Deshmukh, S. S.; Vedantam, S.; Joshi, J. B.; Koganti, S. B. *Ind. Eng. Chem. Res.* **2007,** *46*, 8343-8354.
[141]. Wardle, K. E.; Allen, T. R.; Anderson, M. H.; Swaney, R. E. *AIChE J.* **2008,** *54*, 74-85.
[142]. Batey, W. Nuclear Fuel Reprocessing using Solvent Extraction. In *Science and Practice of Liquid-Liquid Extraction*, Thornton, J. D., Ed.; Clarendon: Oxford, 1992; pp 102-193.
[143]. Cox, M. Liquid-Liquid Extraction in hydrometallurgy. In *Science and Practice of Liquid-Liquid Extraction*, Thornton, J. D., Ed.; Clarendon: Oxford, 1992; pp 1-101.
[144]. Kertes, A. S.; King, C. J. *Biotechnol. Bioeng.* **1986,** *28*, 269-282.
[145]. King, C. J. *Chemtech* **1992,** *22*, 285-291.
[146]. Baniel, A. M.; Blumberg, R.; Hajdu, K. 4,275,234, 1981.
[147]. Bart, H. J. *Reactive Extraction;* 18 ed.; Springer Verlag: Berlin, 2001.
[148]. Cusack, R. W.; Fremeaux, P. *Chemical Engineering* **1991,** *98*, 132-138.
[149]. Hanson, C. *Recent Advances in Liquid-Liquid Extraction;* Pergamon Press Ltd.: 1971.
[150]. Thornton, J. D. *Science and Practice of Liquid-Liquid Extraction;* Clarendon: Oxford, 1992; Vol. 1 and 2 (two volumes).
[151]. Steiner, L.; Hartland, S. Unsteady-state extraction. In *Handbook of Solvent Extraction*, Lo, T. C., Baird, M. H. I., Hanson, C., Eds.; Krieger Publishing Company: Malabar, 1991; pp 249-264.
[152]. Pratt, H. R. C. Computation of stagewise and differential contactors: plug flow. In *Handbook of Solvent Extraction*, Lo, T. C., Baird, M. H. I., Hanson, C., Eds.; Krieger Publishing Company: Malabar, 1991; pp 151-198.
[153]. Westerterp, K. R.; van Swaaij, W. P. M.; Beenackers, A. A. C. M. *Chemical Reactor Design and Operation;* Wiley: Chichester, 1987.
[154]. Sawistowski, H. Physical Aspects of Liquid-Liquid Extraction. In *Mass Transfer with Chemical Reaction in Multiphase Systems*, Alper, E., Ed.; Martinus Nijhoff Publishers: The Hague, 1983; pp 613-635.
[155]. Javed, K. H. Mass Transfer Coefficients, Interfacial Effects, and Surface Renewal. In *Science and Practice of Liquid-Liquid Extraction*, Thornton, J. D., Ed.; Clarendon Press: Oxford, 1992.
[156]. Lewis, W. K.; Whitman, W. G. *Industrial and Engineering Chemistry* **1924,** *16*, 1215-1220.
[157]. Higbie, R. *Transactions of the American Institute of Chemical Engineers* **1935,** *31*, 365-388.
[158]. Danckwerts, P. V. *Industrial and Engineering Chemistry* **1951,** *43*, 1460-1467.
[159]. Huang, C. J.; Kuo, C. H. *AIChE J.* **1965,** *11*, 901-910.
[160]. Bakierowska, A. M.; Trzeszczynski, J. *Fluid Phase Equilib.* **2003,** *213*, 139-146.
[161]. Schwartzenbach, R. P.; Gschwend, P. M.; Imboden, D. M. *Environmental Organic Chemistry;* Wiley: New York, 1993.
[162]. Baldascini, H. G. Bioreaction Engingeering for the Kinetic Resolution of Racemic Epoxides by Epoxide Hydrolase. University of Groningen, Groningen, The Netherlands, 2004.

[163]. Steiner, L. Computational Procedures for Column Simulation and Design. In *Liquid-Liquid Extraction Equipment*, Godfrey, J. C., Slater, M. J., Eds.; John Wiley & Sons: Chichester, 1994; pp 115-136.
[164]. Hartland, S. *Counter-Current Extraction;* Pergamon Press Ltd.: Oxford, 1970.
[165]. Robinson, R. A.; Stokes, R. H. *Electrolyte Solutions, Dover Ed.;* Dover edition ed.; Dover: New York, 2002.
[166]. Cusack, R. W.; Fremeaux, P.; Glatz, D. *Chemical Engineering* **1991,** *98*, 66-76.
[167]. Prochazka, J.; Heyberger, A.; Bizek, V.; Kousova, M.; Volaufova, E. *Ind. Eng. Chem. Res.* **1994,** *33*, 1565-1573.
[168]. Tamada, J. A.; King, C. J. *Ind. Eng. Chem. Res.* **1990,** *29*, 1327-1333.
[169]. Cox, M.; Flett, D. S. Metal Extractant Chemistry. In *Handbook of Solvent Extraction*, Reprint Edition ed.; Lo, T. C., Baird, M. H. I., Hanson, C., Eds.; Krieger Publishing Company: Malabar, 1991; pp 53-89.
[170]. Lämmerhofer, M.; Lindner, W. Chiral Seprations by Capillary Electrophoresis Using Cinchona Alkaloid Derivatives as Chiral Counter-Ions. In *Chiral Separations*, Gübitz, G., Schmid, M. G., Eds.; Humana Press: Totowa (NJ), 2004; pp 323-342.
[171]. Jones, R. A. *Quaternary Ammonium Salts: Their use in Phase-Transfer Catalysis;* Academic Press: London, 2001.
[172]. Maruoka, K. *Org. Process Res. Dev.* **2008,** *12*, 679-697.
[173]. Robbins, L. A. Liquid-Liquid Extraction. In *Handbook of Separation Techniques for Chemical Engineers*, 3rd edition ed.; Schweitzer, P. A., Ed.; McGraw-Hill: New York, 1997; pp 1-417-1-447.
[174]. Tamada, J. A.; King, C. J. *Ind. Eng. Chem. Res.* **1990,** *29*, 1333-1338.
[175]. Wasewar, K. L.; Heesink, A. B. M.; Versteeg, G. F.; Pangarkar, V. G. *Chem. Eng. Sci.* **2004,** *59*, 2315-2320.
[176]. Pratt, H. R. C. *Countercurrent Separation Processes;* Elsevier: Amsterdam, 1967.
[177]. Tavlarides, L. L. *Chem. Eng. Commun.* **1981,** *8*, 133-164.
[178]. Levenspiel, O. *Chemical Reaction Engingeering;* third ed.; John Wiley & Sons: New York, 1999.
[179]. Scott Fogler, H. *Elements of Chemical Reaction Engineering;* third edition ed.; Prentice Hall: Upper Saddle River, 1999.
[180]. Lee, S. C. *AIChE J.* **2004,** *50*, 119-126.
[181]. Reschke, M.; Schugerl, K. *Chemical Engineering Journal and the Biochemical Engineering Journal* **1984,** *29*, B25-B29.
[182]. Kirk, R. E.; Othmer, D. F.; Mark, H. F. Liquid Liquid Extraction. In *Kirk-Othmer Encyclopedia of Chemical Technology Vol.9*, 3rd edition ed.; Kirk, R. E., Othmer, D. F., Mark, H. F., Eds.; Wiley: New York, 1980.
[183]. Skelland, A. H. P. Interphase Mass Transfer. In *Science and Practice of Liquid-Liquid Extraction*, Thornton, J. D., Ed.; Clarendon Press: Oxford, 1992; pp 40-156.
[184]. Wesselingh, J. A.; Krishna, R. *Mass Transfer in Multicomponent Mixtures;* Delft University Press: Delft, 2000.
[185]. Wasewar, K. L.; Pangarkar, V. G.; Heesink, A. B. M.; Versteeg, G. F. *Chem. Eng. Sci.* **2003,** *58*, 3385-3393.
[186]. Ziegenfuss, H.; Maurer, G. *Fluid Phase Equilib.* **1994,** *102*, 211-255.

[187]. Hanson, C.; Hughes, M. A.; Marsland, J. G. Mass Transfer wiht Chemical Reaction in Liquid-Liquid systems. In *Proceedings of the International Solvent Extraction Conference, ISEC 1974, Lyon, France*, Thornton, J. D., Naylor, A., McKay, H. A. C., Jeffreys, G. V., Eds.; Society of Chemical Industry: London, 1974; pp 2401-2414.
[188]. Hughes, M. A.; Rod, V. *Faraday Discussions of the Chemical Society* **1984,** *77*, 75-84.
[189]. Asai, S.; Konishi, Y.; Yamaguchi, H. *Industrial & Engineering Chemistry Fundamentals* **1986,** *25*, 452-455.
[190]. Rod, V. *Collect. Czech. Chem. Commun.* **1973,** *38*, 3228-3235.
[191]. Rod, V. *The Chemical Engineering Journal* **1974,** *7*, 137-140.
[192]. Sharma, M. M. Extraction with Reaction. In *Handbook of Solvent Extraction*, Reprint Edition ed.; Lo, T. C., Baird, M. H. I., Hanson, C., Eds.; Krieger Publishing Company: Malabar, 1991; pp 37-52.
[193]. Danckwerts, P. V. *Gas-Liquid Reactions;* McGraw-Hill: New York, 1970.
[194]. Doraiswamy, L. K.; Sharma, M. M. *Heterogeneous reactions: analysis, examples, and reactor design; Vol 2: fluid-fluid-solid reactions;* Wiley: New York, 1984.
[195]. Cornils, B.; Herrmann, W. A.; Horváth, I. T.; Leitner, W.; Mecking, S.; Olivier-Bourbigou, H.; Vogt, D. *Multiphase Homogeneous Catalysis;* Wiley-VCH Verlag GmbH & Co. KGaA: Weinheim, 2005.
[196]. Nikhade, B. P.; Moulijn, J. A.; Pangarkar, V. G. *J. Chem. Technol. Biotechnol.* **2004,** *79*, 1155-1161.
[197]. Wasewar, K. L.; Heesink, A. B. M.; Versteeg, G. F.; Pangarkar, V. G. *J. Biotechnol.* **2002,** *97*, 59-68.
[198]. Cornelisse, R.; Beenackers, A. A. C. M.; Vanbeckum, F. P. H.; Vanswaaij, W. P. M. *Chem. Eng. Sci.* **1980,** *35*, 1245-1260.
[199]. Decoursey, W. J.; Thring, R. W. *Chem. Eng. Sci.* **1989,** *44*, 1715-1721.
[200]. Ferreira, F. C.; Peeva, L. G.; Livingston, A. G. *Chem. Eng. Sci.* **2005,** *60*, 1029-1042.
[201]. Hoorn, J. A. A.; Versteeg, G. F. *AIChE J.* **2006,** *52*, 2551-2564.
[202]. Olander, D. R. *AIChE J.* **1960,** *6*, 233-239.
[203]. Onda, K.; Sada, E.; KOBAYASH.T; Fujine, M. *Chem. Eng. Sci.* **1970,** *25*, 753-&.
[204]. Versteeg, G. F.; Kuipers, J. A. M.; Vanbeckum, F. P. H.; Vanswaaij, W. P. M. *Chem. Eng. Sci.* **1989,** *44*, 2295-2310.
[205]. Winkelman, J. G. M.; Brodsky, S. J.; Beenackers, A. A. C. M. *Chem. Eng. Sci.* **1992,** *47*, 485-489.
[206]. Hanna, G. J.; Noble, R. D. *Chemical Reviews* **1985,** *85*, 583-598.
[207]. Lewis, J. B. *Chem. Eng. Sci.* **1954,** *3*, 248-259.
[208]. van Woezik, B. A. A.; Westerterp, K. R. *Chem. Eng. Proc.* **2000,** *39*, 299-314.
[209]. Davies, G. A. Mixing and coalescence phenomena in liquid-liquid systems. In *Science and Practice of Liquid-Liquid Extraction*, Thornton, J. D., Ed.; Clarendon Press: Oxford, 1992; pp 244-342.
[210]. Tavlarides, L. L.; Stamatoudis, M. The analysis of interphase reactions and mass transfer in liquid-liquid dispersions. In *Advances in Chemical Engineering Vol. 11*, Drew, T. B., Cokelet, G. R., Hoopes, J. W., Vermeulen, T., Eds.; Academic Press: New York, 1981; pp 199-273.
[211]. Watarai, H.; Cunningham, L.; Freiser, H. *Anal. Chem.* **1982,** *54*, 2390-2392.

[212]. Sharma, M. M.; Danckwerts, P. V. *British Chemical Engineering* **1970,** *15*, 522-&.
[213]. Clarke, S. I.; Sawistowski, H. *Transactions of the Institution of Chemical Engineers* **1978,** *56*, 50-55.
[214]. Selker, A. H.; Sleicher, C. A. *Can. J. Chem. Eng.* **1965,** *43*, 298-&.
[215]. Liu, L.; Matar, O. K.; de Ortiz, E. S. P.; Hewitt, G. F. *Chem. Eng. Sci.* **2005,** *60*, 85-94.
[216]. Hallett, A. J.; Kwant, G. J.; de Vries, J. G. *Chemistry European Journal,* accepted for publication.

Chapter 2

Equilibrium Studies on Enantioselective Liquid-Liquid Amino Acid Extraction using a Cinchona Alkaloid Extractant

Boelo Schuur, Jozef G.M. Winkelman, Hero J. Heeres

this chapter is accepted for publication in

Industrial and Engineering Chemistry Research

Abstract

The enantioselective extraction of aqueous 3,5-dinitrobenzoyl-(*R*),(*S*)-leucine ($A_{R,S}$) by a cinchona alkaloid extractant (C) in 1,2-dichloroethane was studied at room temperature (294 K) in a batch system for a range of intake concentrations (10^{-4}-10^{-3} mol/L) and pH values (3.8-6.6). The experimental data were described by a reactive extraction model with a homogeneous organic phase reaction of $A_{R,S}$ with C. Important parameters of this model were determined experimentally. The acid dissociation constant, K_a, of $A_{R,S}$ was $(1.92\pm0.07)\times10^{-4}$ mol/L. The physical distribution coefficient of $A_{R,S}$ between the organic and aqueous phase was 8.04±0.39. The equilibrium constants of the organic phase complexation reaction were $(9.31\pm0.76)\times10^{4}$ L/mol and $(2.71\pm0.76)\times10^{4}$ L/mol for the S- and R-enantiomer, respectively. With these parameters an optimum performance factor, PF, of 0.19 was predicted. The PF was independent of the pH provided that pH >> pK_a. The model was verified experimentally with excellent results (±7.9%).

Keywords:

enantioselectivity; liquid-liquid extraction; equilibrium stage; 3,5-dinitrobenzoyl-(*R*),(*S*)-leucine; cinchona alkaloid

2.1 Introduction

The demand for enantiopure compounds is growing rapidly.[1] Especially in the fragrance, pharmaceutical and food industries a clear tendency towards the production of enantiopure compounds exists as both enantiomers often show different bioactivity in the human body.[2] The most common technique for obtaining enantiopure compounds on a commercial scale is classical resolution by crystallization.[3] This technique is not always applicable and interest for other methods such as enantioselective synthesis or racemic synthesis followed by enantioseparation is growing. Among other techniques, such as racemic synthesis followed by separation using liquid membranes[4] or chromatographic techniques[5], racemic synthesis and subsequent separation of enantiomers by liquid-liquid extraction is considered a very promising technique.[6-10] However, to the best of our knowledge, processes making use of this technique have not been commercialized. Compared to other methods, such as chiral liquid chromatography[11] and chiral capillary electrophoresis,[12] liquid-liquid extraction is expected to be cheaper and easier to scale up to commercial scale. The process requires an enantioselective extractant dissolved in the extract phase which reacts with the solute in the feed. Although ample literature is available for reactive extraction, only a few studies provide fundamental insights in the reaction engineering mechanisms.[13-18]

Chiral cinchona alkaloid extractants, patented by Lindner and Lämmerhofer,[19] have shown to be good extractants for enantiopurification of amino acids and amino acid derivatives. Research on the molecular aspects of the enantioselective extractions by cinchona alkaloids has been reported by Kellner *et al.*[20] This has provided valuable information on the complexation mechanism between cinchona alkaloids and 3,5-dinitrobenzoyl-(*R*),(*S*)-leucine ($A_{R,S}$, Figure 2.1 left) on a molecular level.[21] However, process studies combining experimental studies and mathematical modeling to predict and optimize the extraction performance of this system have not been reported.

The aims of this study are to determine the effects of process conditions, such as the concentrations, volume ratio and aqueous pH, on the enantioselective extraction of $A_{R,S}$ and to optimize the extraction process by equilibrium modeling. This information is essential input for further development of this system, especially for the design of a continuous extraction process in dedicated equipment such as integrated mixer-settler devices. A cinchona alkaloid extractant was chosen as this family of compounds is known to be very versatile for (substituted)- amino-acids.[20] O-(1-t-butylcarbamoyl)-11-octadecylsulfinyl-10,11-dihydro-quinine (further referred to as C, Figure 2.1 right) was selected as the model extractant for its favorable selectivity as compared to other cinchona

alkaloids.[22] 1,2-dichloroethane was selected as the solvent of choice as it gives high enantioselectivity.

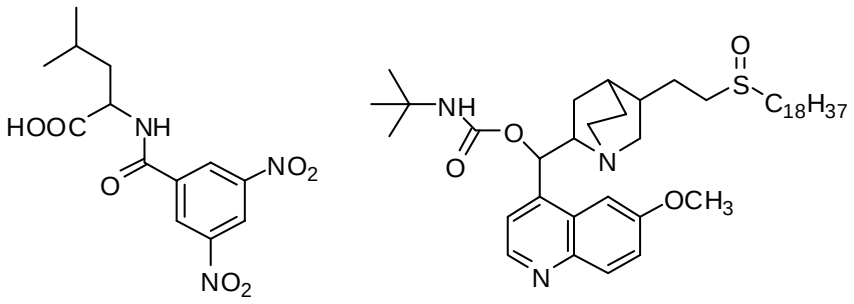

Figure 2.1. Chemical structures of the solute $A_{R,S}$ (left) and the extractant C (right).

2.2 Experimental

2.2.1 Chemicals

Purified water was obtained by reverse osmosis followed by distillation. 1,2-Dichloroethane (99.8%) was obtained from Sigma-Aldrich, potassium dihydrogen phosphate (*pa*), di-sodium hydrogen phosphate dodecahydrate (*pa*) and triethylamine (99%) from Merck, glacial acetic acid from Acros, methanol (AR) and acetonitrille from Labscan. O-(1-t-butylcarbamoyl)-11-octadecylsulfinyl-10,11-dihydro-quinine (C), 3,5-dinitrobenzoyl-(*R*),(*S*)-leucine ($A_{R,S}$), 3,5-dinitrobenzoyl-(*R*)-leucine (A_R) and 3,5-dinitrobenzoyl-(*S*)-leucine (A_S) were kindly provided by DSM Research.

2.2.2 Procedures

All experiments in this study were performed in batch at a temperature of 294 K.

2.2.2.1 The acid dissociation constant of $A_{R,S}$

The acid dissociation constant of $A_{R,S}$ was determined by measuring the pH of aqueous solutions with $A_{R,S}$ concentrations in the range of $(0.1\text{-}3.0)\times10^{-4}$ mol/L. The solutions were

obtained by dilution of a stock solution with water in 100 mL flasks. The pH of each solution was measured after stirring several minutes to ensure homogeneity.

2.2.2.2 The distribution coefficient of $A_{d,l}$

Experiments to determine the distribution coefficient of $A_{R,S}$ over the aqueous and 1,2-dichloroethane phases were carried out in 150 mL flasks. To 100 mL of aqueous $A_{R,S}$ solutions with a concentrations in the range of $(1.0\text{-}3.4)\times10^{-4}$ mol/L, typically 10 to 15 mL 1,2-dichloroethane was added. The biphasic systems were stirred vigorously for 12 h, after which the phases were allowed to settle. The pH of the aqueous phase was measured and its composition was analyzed by HPLC. The organic phase concentration of $A_{R,S}$ was determined from a mass balance for $A_{R,S}$ over both phases. A similar series of experiments with buffered solutions was performed to investigate the influence of the pH on the distribution.

2.2.2.3 Reactive liquid-liquid extraction of A_R, A_S and $A_{R,S}$

Reactive extraction experiments were carried out with the pure enantiomers, A_R and A_S, to obtain the equilibrium constants of the organic phase complexation reaction. A subsequent series with racemic mixtures, $A_{R,S}$, was performed to verify the extraction mechanism and the proposed model with its parameters. In all experiments, phosphate buffers were used to set the desired pH.

In a typical reactive extraction experiment for parameter estimation, about 5 mL of a pH-buffered 4×10^{-4} mol/L A_R or A_S solution was mixed in a 20 mL flask for 2 h with 1–10 mL of a $(1.0\text{-}4.0)\times10^{-4}$ mol/L solution of C in 1,2-dichloroethane. After 2 h the phases were allowed to settle, after which the pH of the aqueous phase was measured and its composition was analyzed by HPLC.

In experiments with the racemate, $A_{R,S}$, the aqueous phase pH was buffered at 6.58 and a aqueous racemate concentration of 1×10^{-3} mol/L was applied. To 5 mL of the aqueous solution, 10 mL of a $(0.2\text{-}1.0)\times10^{-3}$ mol/L solution of C in 1,2-dichloroethane was added. The composition of the aqueous phase was determined as described above.

2.2.3 Analytical procedures

The concentrations of the enantiomers, A_R and A_S, in the aqueous phase were determined by HPLC using an Agilent LC 1100 series apparatus, equipped with an Astec Chirobiotic T column (now Supelco, Sigma-Aldrich). An UV detector operated at 270 nm was applied. The eluent was a 3:1 (v/v) mixture of acetonitrile and methanol, to which 0.25% (vol) triethyl amine and 0.25% (vol) acetic acid were added. The flow rate was set at 1 mL per minute. Before injecting the aqueous phase samples to the column, 0.10 mL of the samples was diluted with 1.0 mL eluent and filtered over a syringe filter with pore size 0.45 μm (Waters Chrom). Quantitative analysis (+/- 3%) was enabled by using calibration curves. The pH of the aqueous phase was measured using an Inolab pH 730 pH-meter equipped with a SenTix 81 probe (both probe and meter from WTW, Germany).

2.2.4 Modeling software and optimization

Parameter fitting for all parameters was done using a nonlinear least squares method (lsqnonlin) provided by the software package Matlab (Mathworks). The reported confidence intervals of the parameter values are 95% confidence limits.

2.3 Theory and reactive extraction modeling

2.3.1 Theory of enantioselective extraction

For optimization of a reactive extraction process knowledge of the extraction mechanism is required. In aqueous-organic biphasic extraction systems, the reaction may take place in either the organic phase, the aqueous phase or at the interface. For metal extractions[23,24] the locus of the reaction is usually assumed to be the interface. This is rationalized by the often poor solubility of the polar solutes in the organic phase and the poor solubility of the extractant in the aqueous phase. This extraction mechanism, also known as interfacial complexation was also reported for the enantioselective solvent extraction of the ligand exchange type.[13,14]

The extraction of $A_{R,S}$ by C is of the ligand addition type[25], where C reacts with the neutral forms of A_R or A_S. In general, such reactions occur either at the interface or in one of the phases. However, in this case the extractant, C, is highly hydrophobic which excludes the possibility that the reaction takes place in the aqueous phase. Depending on

the solubility of $A_{R,S}$ in the organic phase, the complexation reaction will either be limited to the interface or may take place in the organic phase. The more hydrophobic amino acids and derivatives are known to distribute over the aqueous and organic phases.[17,25] Therefore we have applied the homogeneous organic phase ligand addition mechanism here. Further in this paper we will validate this mechanism for the system under study. The model is analogous to the one developed by Steensma *et al.*[25], and is also commonly used in organic acid extractions.[26-28]. The homogeneous organic phase ligand addition mechanism is depicted in Figure 2.2.

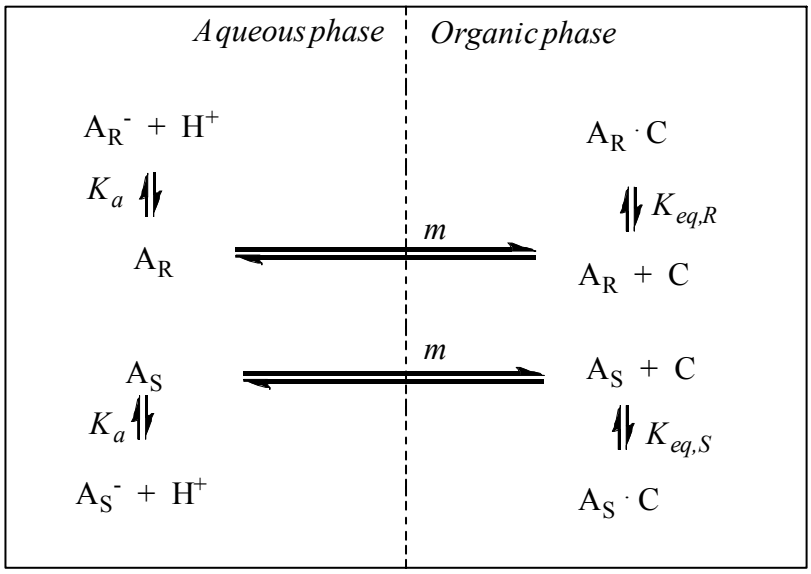

Figure 2.2. Homogeneous organic phase ligand addition extraction mechanism of $A_{R,S}$.

2.3.2 Model equations

The extraction system displayed in Figure 2.2 may be modeled by a series of coupled equilibrium relations and component balances:
- aqueous phase acid dissociation equilibria

$$K_a = \left(\frac{(\gamma_{H^+})(\gamma_{A_R^-})}{(\gamma_{A_R})} \frac{[H^+][A_R^-]}{[A_R]} \right)_{aq} \qquad (2.1a)$$

$$K_a = \left(\frac{(\gamma_{H^+})(\gamma_{A_S^-})}{(\gamma_{A_S})} \frac{[H^+][A_S^-]}{[A_S]} \right)_{aq} \tag{2.1b}$$

- distribution equilibria between the aqueous and organic phases

$$m = \frac{[A_R]_{org}}{[A_R]_{aq}} \tag{2.2a}$$

$$m = \frac{[A_S]_{org}}{[A_S]_{aq}} \tag{2.2b}$$

- organic phase complexation equilibria

$$K_{eq,R} = \left(\frac{[A_R C]}{[A_R][C]} \right)_{org} \tag{2.3}$$

$$K_{eq,S} = \left(\frac{[A_S C]}{[A_S][C]} \right)_{org} \tag{2.4}$$

- component balances for the enantiomers, A_R and A_S, and the extractant, C

$$V_{aq}[A_R]_{aq,0} = V_{aq}\left([A_R]_{aq} + [A_R^-]_{aq}\right) + V_{org}\left([A_R]_{org} + [A_R C]_{org}\right) \tag{2.5}$$

$$V_{aq}[A_S]_{aq,0} = V_{aq}\left([A_S]_{aq} + [A_S^-]_{aq}\right) + V_{org}\left([A_S]_{org} + [A_S C]_{org}\right) \tag{2.6}$$

$$V_{org}[C]_{org,0} = V_{org}\left([C]_{org} + [A_R C]_{org} + [A_S C]_{org}\right) \tag{2.7}$$

The concentration of the undissociated $A_{R,S}$ enantiomers is very low in our studies, and therefore their activity coefficients in eq. 2.1 are assumed to be 1. For the ionic species, non-ideality was taken into account because buffered solutions are used to control the pH. The ionic activities were obtained from the Debye-Hückel law[29] [30].

$$^{10}\log(\gamma_i) = \frac{-Az_i^2 I^{1/2}}{1 + BI^{1/2}} \qquad (2.8)$$

The values of the constants A and B for aqueous sodium chloride solutions at 25ºC [30] have been used as an approximation, A=0.5115 and B=1.316. The ionic strength in eq. 2.8 is calculated according to: [30]

$$I = \frac{1}{2}\sum_i z_i^2 c_i \qquad (2.9)$$

2.4 Results and discussion

To model the extraction process with homogeneous organic phase complexation, the values of important physical parameters are needed. These were determined experimentally and the results are provided in the following sub-sections. Next, we will discuss the validation of the model presented above, and the optimization of the extraction process.

2.4.1 The acid dissociation constant K_a

Due to the low solubility of $A_{R,S}$ the calculation of K_a from titration curves gave large errors Therefore, the K_a of $A_{R,S}$ was determined by measuring the pH of dilute unbuffered solutions. The $A_{R,S}$ concentration was always small, $(0.1\text{-}3.0)\times10^{-4}$ mol/L, therefore ion activity corrections could be neglected. The acid dissociation constant was calculated as $(1.92\pm0.07)\times10^{-4}$ mol/L by minimizing the differences between the experimental and calculated $[H^+]$ data, see Figure 2.3. The estimated K_a of $A_{R,S}$ is in good agreement with the reported acidities of organic acids with comparable chemical structures.[31]

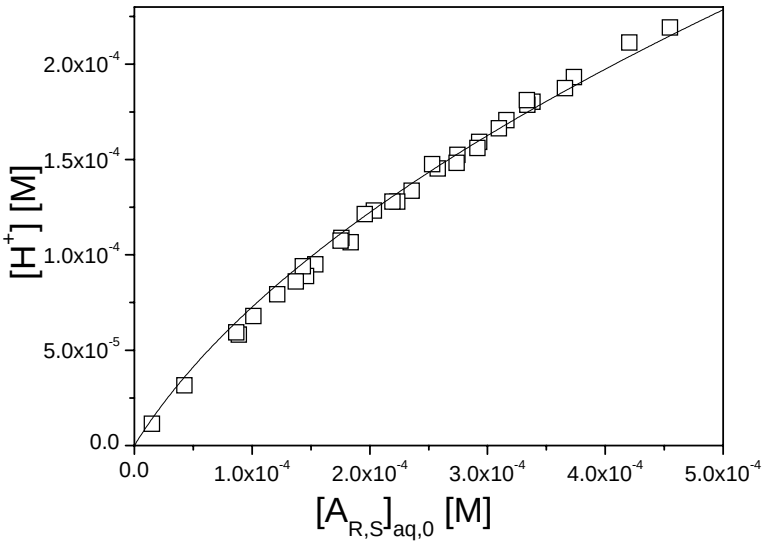

Figure 2.3. $[H^+]$ vs $[A_{R,S}]_0$. Symbols: experimental. Line: calculated with K_a = 1.92×10^{-4} mol/L.

2.4.2 The distribution coefficient *m*

The distribution coefficient *m* was determined using physical extraction experiments as described in section 2.2.2.2 In absence of a pH-buffer, and for pH<5, $[A^-_{R,S}] = [H^+] = 10^{-pH}$. The total aqueous phase amino acid concentration was obtained from the HPLC measurements. These data, together with the $A_{R,S}$ intake concentration, allowed the determination of the undissociated amounts of amino acid in both phases, $[A_{R,S}]_{aq}$ and $[A_{R,S}]_{org}$. The results are shown in Figure 2.4. Apparently, within the concentration range applied here, $[A_{R,S}]_{org}$ is proportional to $[A_{R,S}]_{aq}$ with a constant distribution coefficient. From linear regression, the distribution coefficient *m*, according to eq. 2.2, was obtained as 8.04±0.39. The amino-acid is considerably better soluble in the organic phase than the aqueous phase, which is not surprising considering the presence of the highly hydrophobic aromatic ring and the C_4-carbon group in the compound, see Figure 2.1.

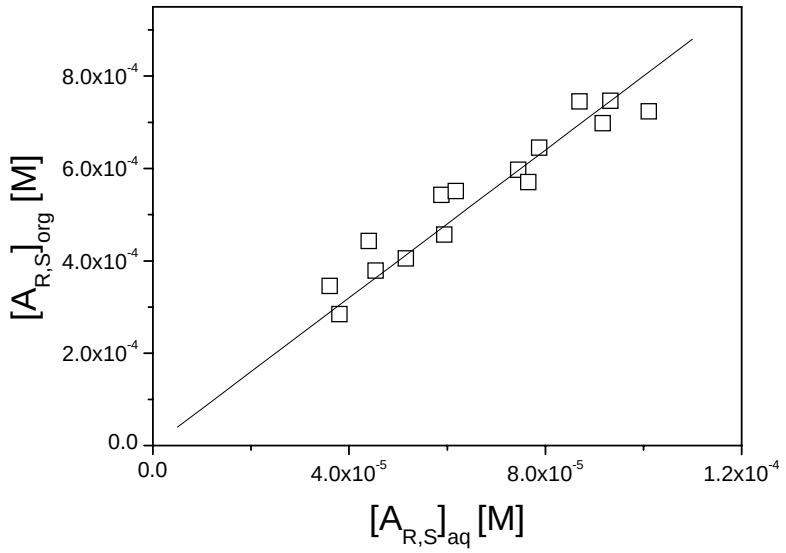

Figure 2.4. Equilibrium concentrations $[A_{R,S}]_{org}$ vs $[A_{R,S}]_{aq}$. Symbols: experimental. Line: linear correlation with m = 8.04.

2.4.3 The complexation equilibrium constants $K_{eq,R}$ and $K_{eq,S}$

Several methods, i.e. ^{1}H-NMR, UV-vis spectrometry, IR spectrometry were investigated for direct, independent measurement of the organic phase complexation equilibria. However, in all measurements the extractant-enantiomer complexes, $A_{R,S}C$, could not be distinguished clearly from the uncomplexed compound, C. The equilibrium constants were therefore determined using reactive extraction experiments with the pure enantiomers, A_R and A_S, as described in section 2.2.2.3.

For A_R, an optimum value of $K_{eq,R}$ was obtained by minimizing the differences between the experimental and calculated values of the total aqueous phase A_R-concentration, $[A_R]_{aq} + [A_R^-]_{aq}$, over all experiments. The experimental values of $[A_R]_{aq} + [A_R^-]_{aq}$ were obtained from HPLC analysis, while the calculated values were obtained from simultaneously solving the model equations 2.1-2.9. In this way, an optimum

value for $K_{eq,R}$ was found of (2.71±0.76)×10^4 L/mol. A parity plot of the total aqueous phase A_R-concentration, $[A_R]_{aq} + [A_R^-]_{aq}$, is shown in Figure 2.5.

A similar procedure using the experiments with the pure S-enantiomer resulted in a $K_{eq,S}$ value of (9.31±0.76)×10^4 L/mol. For this case, the calculated and experimental values of the total aqueous concentration of A_S, $[A_S]_{aq} + [A_S^-]_{aq}$, are shown in Figure 2.6.

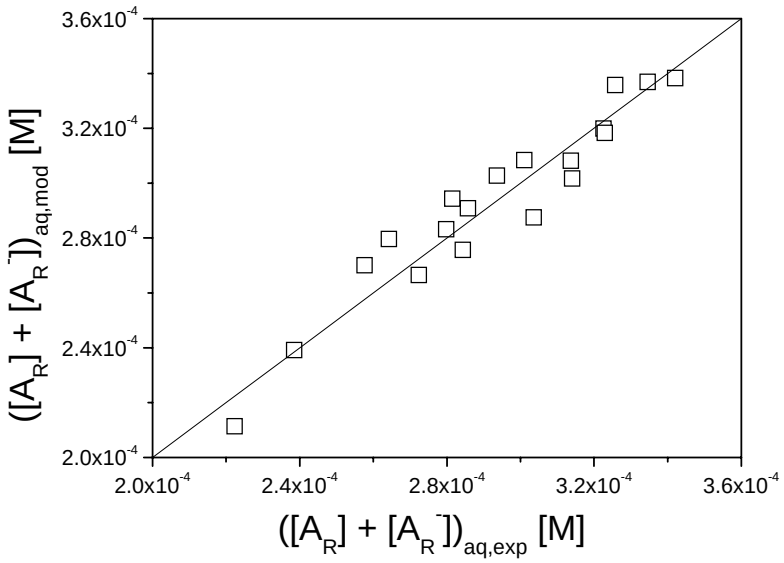

Figure 2.5. Parity plot for reactive extraction with enantiopure A_R .

For a number of reactive extractions known to proceed according to the homogeneous complexation model, Steensma *et al.*[15] reported equilibrium complexation constants ranging from a few hundred to 1.5×10^5 L/mol. The equilibrium constants obtained here for the $A_{R,S}$ extraction by C are at the high end of this range. The intrinsic selectivity of the system, defined as the ratio of the equilibrium complexation constants, is obtained here as $K_{eq,S}/K_{eq,R}$ = 3.43. This value is well in line with those reported by Maximini *et al.*[4] for a comparable system (DNB-R-S-leu with a related cinchona alkaloid extractant) and at the high end of the values reported in the literature.[13,15,18,32]

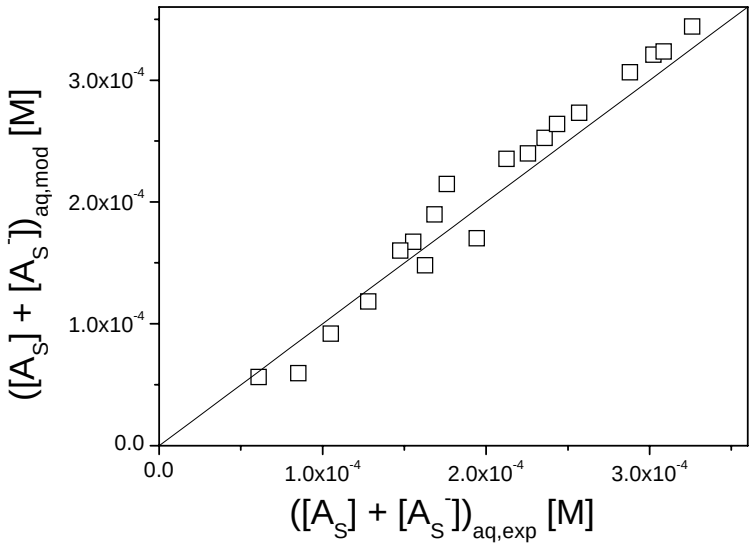

Figure 2.6. Parity plot for reactive extraction with enantiopure A_S.

Based on predictions using the Fenske equation for total reflux conditions,[33] with this selectivity about 9 theoretical equilibrium stages are sufficient to fully separate the two enantiomers with enantiomeric excess of at least 99% in both phases. Here, the Fenske equation for a countercurrent separation of DNB-R,S-leu is defined as:

$$N_{\min} = \frac{\ln\left[\dfrac{x_{S,e}/\left(1-x_{S,e}\right)}{x_{S,r}/\left(1-x_{S,r}\right)}\right]}{\ln\left(\alpha\right)} \qquad (2.10)$$

x_e is the fraction of the feed that ends up in the extract, x_r is the fraction that ends up in the raffinate and α is the selectivity ($K_{eq,S}/K_{eq,R}$). With this equation, an indication of the minimum number of stages required for any given separation may be predicted, provided that the selectivity and desired purity are known.

2.4.4 Model validation

In cases where the extractant is insoluble in the aqueous phase, two important reactive extraction models have been reported in the literature, the interfacial reaction model and the homogeneous organic phase reaction model.[17] The main difference between both models is the locus of the chemical reaction between substrate and extractant and is among other factors determined by the charge of the substrate. In the current system, either the undissociated $A_{R,S}$ or its anion may be involved in the reaction. In case the anion is the reacting species, the complexation reaction is expected to take place solely at the interface, because ion transfer from the aqueous into the organic phase is not facile. If the undissociated forms of $A_{R,S}$ are the reactive species, the location of the reaction is either the organic or the aqueous phase, depending on the partitioning of $A_{R,S}$ between both phases.

To discriminate between both models, experimental studies on the effect of the pH on the distribution of $A_{R,S}$ over the aqueous and organic phase in the presence and absence of the extractant were performed. First, a number of physical extraction experiments with A_R were performed at different pH values. The overall distribution, D_R, was determined for each experiment. Here D_R is defined as the ratio of the total amounts of A_R in the organic and aqueous phases:

$$D_R = \frac{[A_R]_{org} + [A_R C]_{org}}{[A_R]_{aq} + [A_R^-]_{aq}} \qquad (2.11)$$

A comparison of the experimental values with the model predictions of D_R is shown in Figure 2.7. Evidently, D_R is a function of the pH, with low pH values leading to higher values for D_R. To understand the results, the Henderson-Hasselbalch equation[34] is illustrative:

$$pH = pK_a + {}^{10}\log\frac{[A_R^-]_{aq}}{[A_R]_{aq}} \qquad (2.12)$$

This equation predicts that for pH << pK_a the predominant compound in solution is the undissociated form A_R. This species is expected to be better soluble in the organic phase than the aqueous phase (*vide infra*), leading to higher values of D_R.

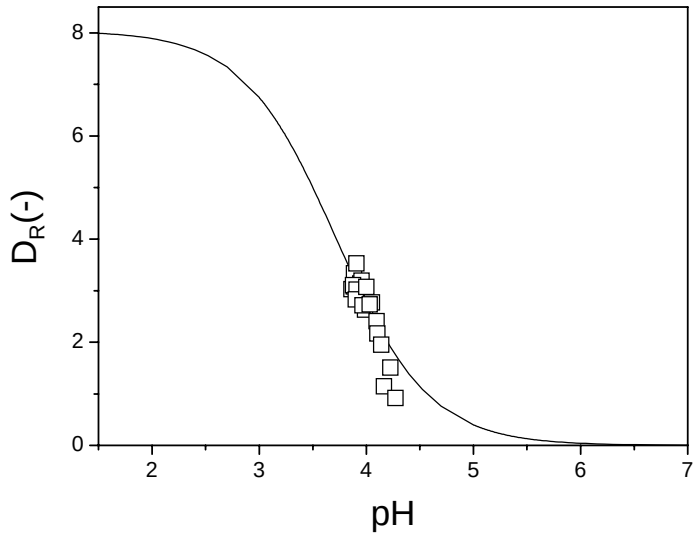

Figure 2.7. Overall distribution D_R vs pH. Symbols: experimental. Line: model prediction.

A second series of reactive experiments was carried out with A_R using extractant C. The effect of the $[C]_{org,0}$ on D_R is shown in Figure 2.8. The slope of the plot of the D_R versus the $[C]_{org,0}$ is a clear function of the aqueous phase pH. At higher pH values, the slope is considerably reduced. Thus, the effect of the extractant concentration on the D_R is reduced at higher pH values. This clearly indicates that the undissociated form of A_R is the reactive species and not the anion. If the latter would be involved, larger effects of the extractant concentration on the distribution of A_R are expected at high pH values. Similar observations were also observed for experiments with the pure S-enantiomer. All experimental observations are in line with the homogeneous organic phase ligand addition mechanism as depicted in Figure 2.2.

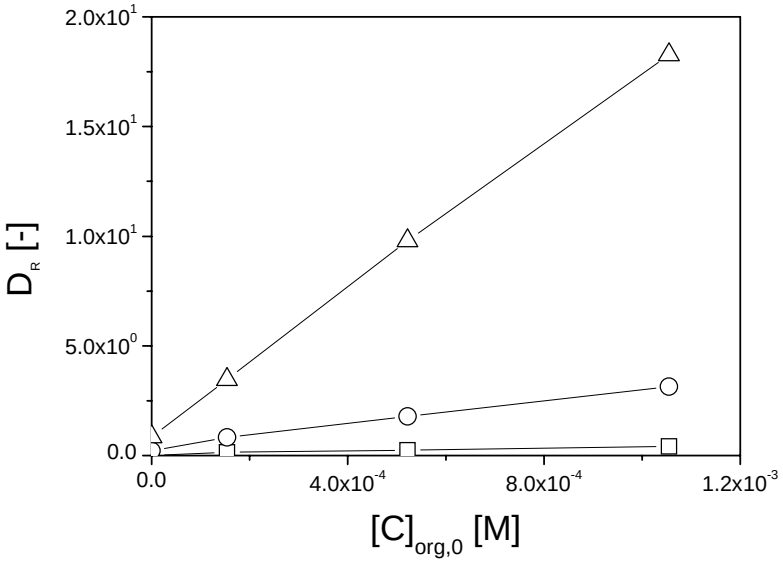

Figure 2.8. Overall distribution D_R vs $[C]_{org,0}$. Symbols: experimental, -Δ-: pH=3.8, -○-: pH=4.9 and -□-: pH=6.1.

2.4.5 Experimental validation of the homogeneous extraction model

The extraction model for the reactive extraction of $A_{R,S}$ with C was tested experimentally by performing 8 reactive extraction experiments with racemic $A_{R,S}$ mixtures and various extractant concentrations as described in section 2.2.2.3. The results of these experiments are compared graphically with the model predictions in Figure 2.9, where the yields are shown. Here, the yield of an enantiomer is defined as the fraction of the aqueous feed that ends up in the organic extract phase:

$$Y_R = \frac{[A_R]_{org} + [A_R C]_{org}}{[A_R]_{aq,0}} \frac{V_{org}}{V_{aq}} \tag{2.13a}$$

$$Y_S = \frac{[A_S]_{org} + [A_S C]_{org}}{[A_S]_{aq,0}} \frac{V_{org}}{V_{aq}} \tag{2.13b}$$

The agreement between the modeled and experimental data is good, as shown by a mean absolute relative error of 7.9%. Thus, it may be concluded that the extraction model developed in this paper is applicable to predict the performance of the reactive extractions of racemic $A_{R,S}$ with C.

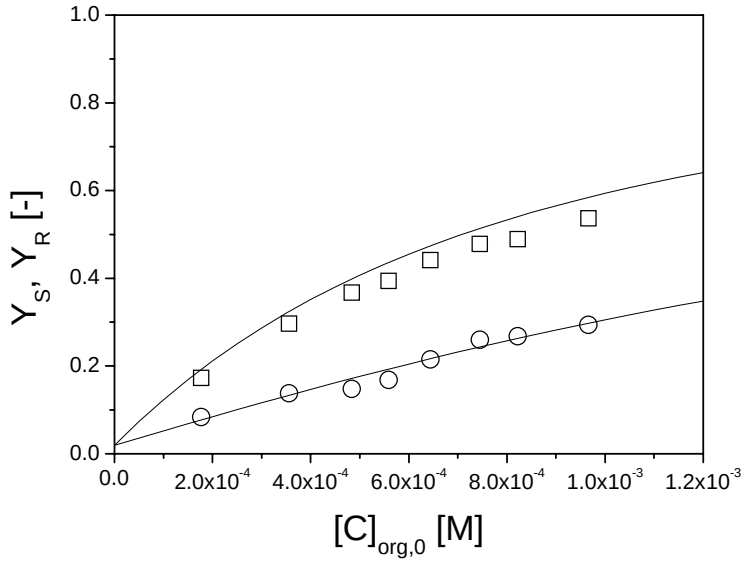

Figure 2.9. The extraction yields of both enantiomers vs $[C]_{org,0}$ with racemic $A_{R,S}$ intake. Symbols: experimental, ○: Y_R, □: Y_S. Lines: model predictions.

2.4.6 Optimization of the reactive extraction of $A_{R,S}$ with C using the performance factor

In chiral chemistry and engineering, the enantiomeric excess (*ee*) is used as a measure of the enantioselectivity of a process. For the system described here, the reaction takes place in the organic phase and the extractant C is selective towards the S-enantiomer. Therefore the *ee* in the organic phase is defined as the excess of A_S in that phase. Similarly, an *ee* in the aqueous phase was defined:

$$ee_{org} = \frac{[A_S]_{org,\text{all forms}} - [A_R]_{org,\text{all forms}}}{[A_S]_{org,\text{all forms}} + [A_R]_{org,\text{all forms}}} \qquad (2.14a)$$

$$ee_{aq} = \frac{[A_R]_{aq,\text{all forms}} - [A_S]_{aq,\text{all forms}}}{[A_R]_{aq,\text{all forms}} + [A_S]_{aq,\text{all forms}}} \tag{2.14b}$$

Requirements for a good enantioselective extraction process are not only a high *ee* of the desired enantiomer but also a high yield. Koska and Haynes[13] combined the yield and *ee* in the performance factor, *PF*. The *PF* is a very useful tool to optimize an enantioselective extraction process and is defined as:

$$PF = ee_{org} Y_S \tag{2.15}$$

The model described in section 2.3 with the parameters obtained in section 2.4 is used to optimize the enantioselective reactive extraction process in terms of the *PF*. In Figure 2.10, the *PF* is plotted as function of the extractant intake concentration for several pH-values. The volumetric phase ratio, the ion activity and the amino acid intake concentration are equal for all cases.

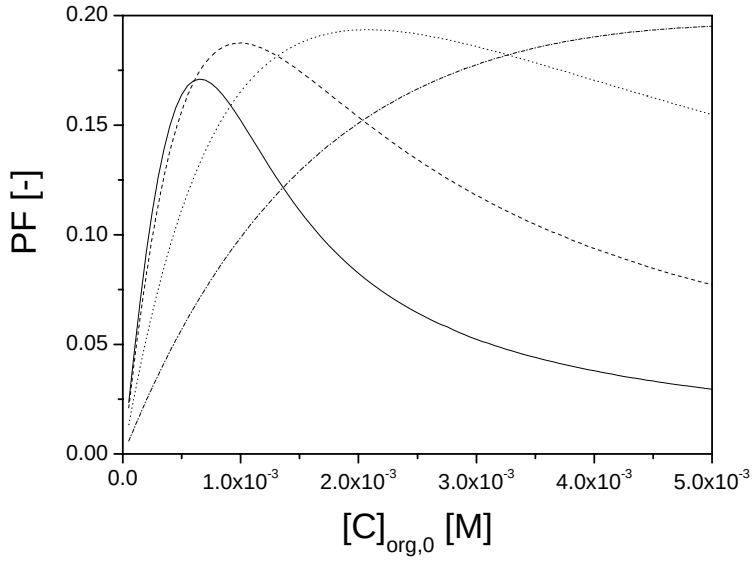

Figure 2.10. Calculated *PF* values vs $[C]_{org,0}$. Conditions: $[A_{R,S}]_{aq,0}$ = 1 × 10^{-3} mol/L, V_{org}/V_{aq} = 1, $\gamma_+ = \gamma_- = 0.757$. Lines: —: pH=5.5, ---: pH=6.0, …: pH=6.5, -.-.-: pH=7.0.

The *PF* for each pH exhibits a clear maximum. Both the maximum value of the *PF* and the position of the maximum are dependant on the pH. The observation of a maximum PF is the result of two opposing effects, *i.e.* the yield and the *ee*. At very low extractant concentrations, the yield is very low, resulting in a low *PF*. An increase in the extractant concentration will increase the yield and *PF*. However, at some point, the extractant is present in excess with respect to the desired enantiomer and the undesired enantiomer will also be extracted in considerable amounts. This will lead to a significant drop in the *ee* and a reduction of the *PF*. An illustration of the effects of *ee* and yield as a function of the intake concentration of the extractant is depicted in Figure 2.11 for an aqueous phase pH of 6.5.

Figure 2.10 furthermore illustrates that at pH > 6, the maximum *PF* becomes nearly independent of the pH. Thus, under conditions where pH >> pK_a the maximum value of *PF* is independent of the pH and has a value of 0.19.

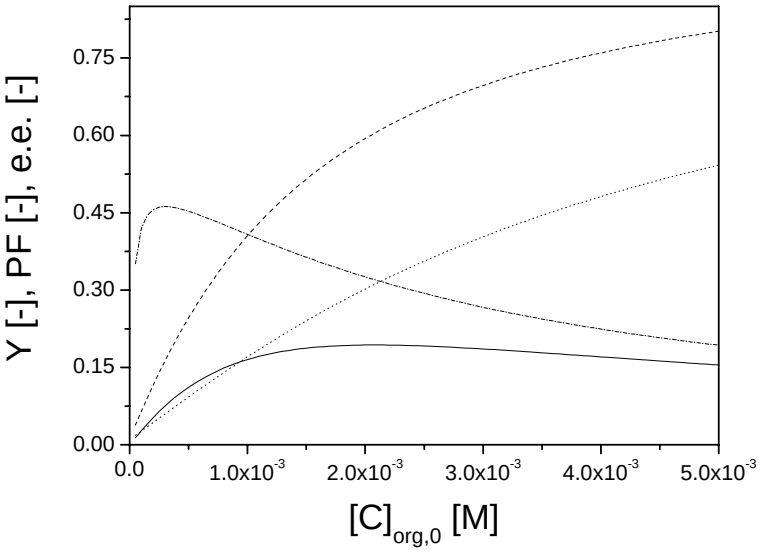

Figure 2.11. Calculated results vs $[C]_{org,0}$. Conditions pH = 6.5, $[A_{R,S}]_{aq,0}$ = 1 × 10^{-3} mol/L, V_{org}/V_{aq} = 1, $\gamma_+ = \gamma_- = 0.757$. Lines: —: *PF*, ---: Y_S, …: Y_R, -.-.-: ee_{org}.

The Figure 2.12 shows the *PF* as function of $[C]_{org,0}$ (mol/L) for different values of $[A_{R,S}]_{aq,0}$. The figure illustrates that, at least for pH = 6.5 (>> pK_a), the optimum value of the *PF* is independent on the concentration of $A_{R,S}$. This is due to the low concentration of undissociated $A_{R,S}$ species at these high pH values, almost completely excluding physical phase transfer of $A_{R,S}$. At the observed maxima, the ratio of species present in the organic phase is constant, thus for higher intakes of $A_{R,S}$, the required amount of extractant at the maximum *PF* is also higher.

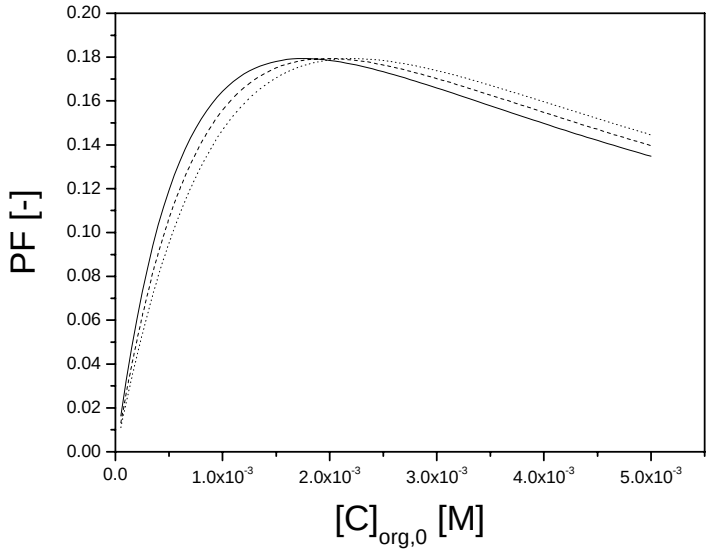

Figure 2.12. Calculated *PF* values vs $[C]_{org,0}$. Conditions: pH = 6.5, V_{org}/V_{aq} = 1, $\gamma_+ = \gamma_-$ = 0.757. Lines: —: $[A_{R,S}]_{aq,0}$ =5·10^{-4} mol/L, ---: $[A_{R,S}]_{aq,0}$ =1.0 × 10^{-3} mol/L, …: $[A_{R,S}]_{aq,0}$ =1.5 × 10^{-3} mol/L.

2.5. Conclusions

The enantioselective reactive extraction of $A_{R,S}$ by a cinchona alkaloid extractant, C, has been investigated. Experimental data indicate that the reactive extraction process proceeds according to a homogeneous complexation model and involves reaction of the undissociated form of the amino acid derivative and the extractant in the organic phase. The experimental data were modeled according to this extraction model and excellent agreement between the model and experimental data (±7.9%) was observed.

The performance of the extraction process was evaluated using the performance factor, *PF*. The model predicts a maximum value for *PF* of 0.19, in line with experimental values (0.20). This indicates that a high *ee* in combination with a high yield is not possible in a single equilibrium step and that multistage extraction will be required for full separation of the racemate $A_{R,S}$.

2.6 Nomenclature

a	activity (mol L^{-1})
A	constant in Debye-Hückel law, ($L^{1/2}mol^{-1/2}$)
$A_{R,S}$	3,5-dinitrobenzoyl-R,S-leucine (solute)
B	constant in Debye-Hückel law, ($L^{1/2}mol^{-1/2}$)
C	cinchona alkaloid extractant
D	overall distribution, (-)
DNB-R,S-leu	3,5-dinitrobenzoyl-d,l-leucine (solute)
ee	enantiomeric excess, (-)
I	ionic strength (mol L^{-1})
K_a	acid dissociation constant of $A_{R,S}$, (mol/L)
K_{eq}	equilibrium constant of the organic phase reaction between $A_{R,S}$ and C, (L/mol)
m	distribution coefficient of undissociated $A_{R,S}$, (-)
N	number of equilibrium stages
PF	performance factor, (-)
T	temperature, (K)
V	volume, (L)
Y	yield, (-)
z	ion valence, (-)
[ ] square brackets	concentration, (mol/L)

greek letters

α	(enantio)selectivity, (-)
γ	activity coefficient, (-)

subscripts

0	initial or feed
a	acidity
aq	aqueous
eq	equilibrium
min	minimum
org	organic
R	R-enantiomer
S	S-enantiomer

Acknowledgements

The authors thank Joelle Flour and Andy Hallett of DSM Research kindly for the syntheses of the enantioselective extractant, DNB-R,S-leu, DNB-R-leu and DNB-S-leu. DSM and Organon are acknowledged for their financial support through the Separation Technology programme of NWO (Netherlands Scientific Organisation).

2.7 References:

[1]. Rouhi, A. M. *Chem. Eng. News* **2003,** *81*, 45-55.
[2]. Sheldon, R. A. *Chirotechnology; industrial synthesis of optically active compounds;* Marcel Dekker, Inc.: New York, 1993.
[3]. Bruggink, A. Rational Design in Resolutions. In *Chirality in Industry II*, Collins, A. N., Sheldrake, G. N., Crosby, J., Eds.; John Wiley & sons Ltd.: Chichester, 1997; pp 81-98.
[4]. Maximini, A.; Chmiel, H.; Holdik, H.; Maier, N. W. *J. Membr. Sci.* **2006,** *276*, 221-231.
[5]. Gavioli, E.; Maier, N. M.; Minguillon, C.; Lindner, W. *Anal. Chem.* **2004,** *76*, 5837-5848.
[6]. Abe, Y.; Shoji, T.; Fukui, S.; Sasamoto, M.; Nishizawa, H. *Chem. Pharm. Bull.* **1996,** *44*, 1521-1524.
[7]. Lacour, J.; Goujon-Ginglinger, C.; Torche-Haldimann, S.; Jodry, J. J. *Angew. Chem. Int. Ed.* **2000,** *39*, 3695-3697.
[8]. Prelog, V.; Stojanac, Z.; Kovacevic, K. *Helv. Chim. Acta* **1982,** *65*, 377-384.
[9]. Tsukube, H.; Shinoda, S.; Uenishi, J.; Kanatani, T.; Itoh, H.; Shiode, M.; Iwachido, T.; Yonemitsu, O. *Inorg. Chem.* **1998,** *37*, 1585-1591.

[10]. Ohki, A.; Miyashita, R.; Naka, K.; Maeda, S. *Bull. Chem. Soc. Jpn.* **1991,** *64*, 2714-2719.
[11]. Davankov, V. A. *Journal of Chromatography A* **1994,** *666*, 55-76.
[12]. Gubitz, G.; Schmid, M. G. *Journal of Chromatography A* **1997,** *792*, 179-225.
[13]. Koska, J.; Haynes, C. A. *Chem. Eng. Sci.* **2001,** *56*, 5853-5864.
[14]. Pickering, P. J.; Chaudhuri, J. B. *Chem. Eng. Sci.* **1997,** *52*, 377-386.
[15]. Steensma, M.; Kuipers, N. J.; de Haan, A. B.; Kwant, G. *J. Chem. Technol. Biotechnol.* **2006,** *81*, 588-597.
[16]. Takeuchi, T.; Horikawa, R.; Tanimura, T. *Anal. Chem.* **1984,** *56*, 1152-1155.
[17]. Tan, B.; Luo, G. S.; Qi, X.; Wang, J. D. *Sep. Purif. Technol.* **2006,** *49*, 186-191.
[18]. Viegas, R. M. C.; Afonso, C. A. M.; Crespo, J. G.; Coelhoso, I. M. *Sep. Purif. Technol.* **2007,** *53*, 224-234.
[19]. Lindner, W.; Lämmerhofer, M. Eur. Pat. Appl. No. 96 109 072.7, 1996.
[20]. Kellner, K. H.; Blasch, A.; Chmiel, H.; Lämmerhofer, M.; Lindner, W. *Chirality* **1997,** *9*, 268-273.
[21]. Maier, N. M.; Schefzick, S.; Lombardo, G. M.; Feliz, M.; Rissanen, K.; Lindner, W.; Lipkowitz, K. B. *J. Am. Chem. Soc.* **2002,** *124*, 8611-8629.
[22]. Hallett, A. J.; Kwant, G.; de Vries, J. G. *Journal of Organic Chemistry,* accepted for publication.
[23]. Cox, M. Liquid-Liquid Extraction in hydrometallurgy. In *Science and Practice of Liquid-Liquid Extraction*, Thornton, J. D., Ed.; Clarendon: Oxford, 1992; pp 1-101.
[24]. Bart, H. J. *Reactive Extraction;* 18 ed.; Springer Verlag: Berlin, 2001.
[25]. Steensma, M.; Kuipers, N. J. M.; de Haan, A. B.; Kwant, G. *Chem. Eng. Sci.* **2007,** *62*, 1395-1407.
[26]. Prochazka, J.; Heyberger, A.; Bizek, V.; Kousova, M.; Volaufova, E. *Ind. Eng. Chem. Res.* **1994,** *33*, 1565-1573.
[27]. Wasewar, K. L.; Heesink, A. B. M.; Versteeg, G. F.; Pangarkar, V. G. *J. Biotechnol.* **2002,** *97*, 59-68.
[28]. Ziegenfuss, H.; Maurer, G. *Fluid Phase Equilib.* **1994,** *102*, 211-255.
[29]. Atkins, P. W. *Physical Chemistry;* 5th edition ed.; Oxford University Press: Oxford, 1994.
[30]. Robinson, R. A.; Stokes, R. H. *Electrolyte Solutions;* Dover edition ed.; Dover: New York, 2002.
[31]. Kortüm, G.; Vogel, W.; Andrussow, K. *Dissociation constants of organic acids in aqueous solution;* Butterworths: London, 1961.
[32]. Abe, Y.; Shoji, T.; Kobayashi, M.; Qing, W.; Asai, N.; Nishizawa, H. *Chem. Pharm. Bull.* **1995,** *43*, 262-265.
[33]. Pratt, H. R. C. *Countercurrent Separation Processes;* Elsevier: Amsterdam, 1967.
[34]. Stryer, L. *Biochemistry;* 4th edition ed.; Freeman: New York, 1995.

Chapter 3

Experimental and Modeling Studies on the Enantioselective Liquid-Liquid Extraction of (*R),(S)*-Phenylglycinol using a Bis(Naphthyl)Phosphoric Acid derivative as extractant

Boelo Schuur, Jeroen Bokhove, Bas J.V. Verkuijl, Johannes G. de Vries, Ben L. Feringa, Hero J. Heeres

To be submitted

Abstract

The enantioselective liquid-liquid equilibrium extraction of (R),(S)-phenylglycinol ($PGL_{R,S}$) was studied experimentally using 3,3'-(3,5-bis(trifluoromethyl)phenyl)-2,2'-diyl hydrogenphosphate-1,1'-binaphthyl (P) as extractant in dichloromethane (DCM). Batch experiments with variable volume ratios (V_{org}/V_{aq} = 0.5 - 1) were performed in the temperature range 279-303 K and pH ranges of 1 - 8.5 and concentration ranges of $2.5 \cdot 10^{-4}$ - $1.0 \cdot 10^{-3}$ mol/L for both extractant and solute. The equilibrium extraction process was modeled using a homogeneous organic phase reaction model. The model parameters Kb (aqueous basicity), m (physical partition coefficient) and the equilibrium constants of the complexation reaction between $PGL_{R,S}$ with P (Kcq) for both enantiomers were estimated as function of temperature. The Kcq values were very high (> 10^{10} L/mol) and decreased with increasing temperature. The intrinsic enantioselectivity of the system was 1.72 at 303 K and 1.89 at 279 K. The optimum conditions for a single equilibrium stage with $1 \cdot 10^{-3}$ mol/L $PGL_{R,S}$ in the feed were modeled and found to be $5.5 \cdot 10^{-4}$ mol/L extractant, a phase ratio of 1, a pH of 3, and a temperature of 280 K. The optimum performance factor was 0.1, indicating that multistage operation is needed to obtain both high ee and yields.

3.1 Introduction

In the last decades, the share of enantiopure drugs on the market has grown dramatically[1]. The main driver for this development is the difference in bioactivity of the individual enantiomers[2]. For instance, (*S*),(*S*)-ethambutol is tuberculostatic, while (*R*),(*R*)-ethambutol causes blindness[3].

Racemic synthesis followed by racemate separation is often the method of choice[2-5] for obtaining enantiopure products. The traditional resolution approach using diastereomeric crystallization[6-8] has proven to be a very suitable technique. However, the methodology is not always applicable, involves solids handling[9] and therefore alternatives have been explored. Typical examples are chiral chromatography and electrophoresis, originally developed for analytical purposes[10-12]. However, chiral separations using these techniques on industrial scale are still scarce. Enantioseparation[13,14] using liquid membranes is also a promising alternative, however fouling issues and low transport rates through membranes are serious issues and need to be resolved.

Enantioseparation using liquid-liquid extraction (ELLE) is an interesting alternative for chromatographic and membrane separations. It involves a chiral extractant (host) that is usually dissolved in the organic phase. Key element in ELLE is enantiomeric recognition between the substrate and the host[15]. This requires a minimum of two functional groups in the guest. Most reported ELLE-studies deal with enantioseparation of amino acids and amino acid derivatives[16-27] and amino alcohols[9,28-35], both having at least two functionalities. Recently, a new extractant, 3,3'-(3,5-bis(trifluoromethyl) phenyl)-2,2'-diyl hydrogenphosphate-1,1'-binaphthyl (P, Figure 3.1, left) was synthesized in our research institute[36]. The extractant shows unprecedented chiral recognition for a range of benzylic primary amines bearing no other functional groups. We here report an in depth experimental and equilibrium modeling study on the reactive extraction characteristics of this novel extractant. Phenylglycinol ($PGL_{R,S}$, Figure 3.1, right) was selected as model substrate as it showed better performance than un-substituted primary amines[36]. Exploratory experiments also showed that dichloromethane (DCM) was the solvent of choice and this solvent was applied throughout this study. All essential parameters of the model, i.e. the complexation constants between P and both enantiomers of PGL, the partitioning coefficient and the basicity of PGL were determined as a function of the temperature. With this information, equilibrium stage performance was optimized.

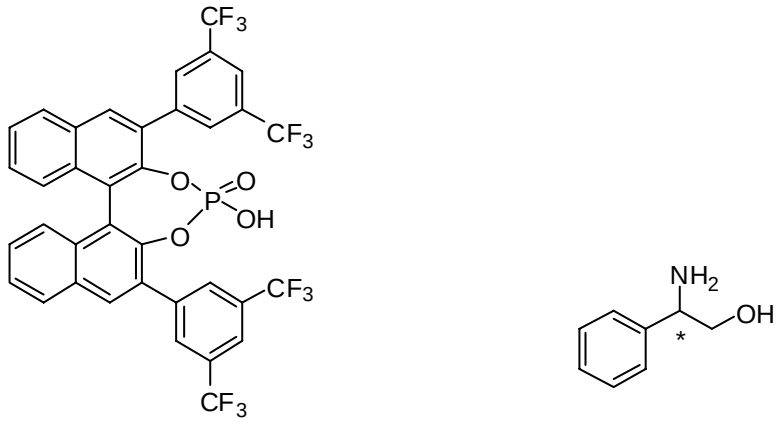

Figure 3.1. Structures of extractant P (left) and substrate PGL (right)

3.2 Experimental

3.2.1 Chemicals

The extractant P was synthesized by a procedure described by Verkuijl *et al* [36]. (*R*)-phenylglycinol (98%, PGL_R) and (*S*)-phenylglycinol (98%, PGL_S) were purchased from Sigma-Aldrich. Racemic (*R*),(*S*)-phenylglycinol (98%, $PGL_{R,S}$) and dichloromethane (DCM) were purchased from Acros. Potassium dihydrogen phosphate (*pa*), di-sodium hydrogen phosphate dodecahydrate (*pa*), glacial acetic acid, hydrogen chloride (37%), potassium chloride (*pa*) and sodium acetate trihydrate (*pa*) were obtained from Merck. All experiments were performed with double distilled water.

3.2.2 Experimental procedures

Estimation of the basicity constant (K_b) of PGL

To estimate the temperature dependent basicity constant (K_b) of PGL, the pH of diluted $PGL_{R,S}$ solutions was measured while heating the well stirred solutions at a rate of 1 K/min. Two experiments were performed with different $PGL_{R,S}$ concentrations ($3 \cdot 10^{-5}$ mol/L and $11 \cdot 10^{-5}$ mol/L) in the temperature range of 295 K < T < 335 K under an inert atmosphere to avoid disturbance by CO_2.

Physical extraction experiments

Physical extraction experiments were performed with DCM as organic phase and buffered (0.1 mol/L phosphate buffer, pH 10) aqueous $PGL_{R,S}$-solutions to determine the temperature dependent partitioning behavior of non-dissociated PGL. The pH of 10 was selected to ensure that all PGL was in its neutral, non-dissociated form. In all experiments the total liquid volume was 15 mL, the volume ratio $\phi = V_{org} / V_{aq}$ was varied between 0.19 - 2.61, the temperature between 279 - 303 K, and the initial PGL concentration between $9 \cdot 10^{-4}$ - $14 \cdot 10^{-3}$ mol/L. The two phase systems were stirred vigorously for 12 h, after which the phases were allowed to settle. Samples were taken from the aqueous phase and analyzed by HPLC. The organic phase concentrations were calculated using the overall mass balance.

Reactive extraction experiments

Reactive extraction experiments were performed using aqueous solutions of enantiopure PGL_q (q = R or S) and solutions of P in DCM at varying temperatures (279-303 K), volume ratio (V_{org}/V_{aq} = 0.5 - 1) and initial concentrations ($2.5 \cdot 10^{-4}$ to $1 \cdot 10^{-3}$ mol/L PGL_q and $3 \cdot 10^{-4}$ to $8 \cdot 10^{-4}$ mol/L P). The pH was kept constant at 3.2 (0.1 mol/L acetate buffer). The biphasic systems were stirred vigorously for 3 h to ensure equilibrium. Samples were taken from the aqueous phase and analyzed by HPLC. The organic phase concentrations were calculated by using the overall mass balance.
For model verification, experiments with enantiopure PGL_R and PGL_S were performed at the conditions described above, except for the pH, which was varied from 1 to 8.5 (using a 0.1 mol/L HCl/KCl buffer for pH < 3, a 0.1 mol/L acetate buffer for 3 < pH < 5, and a 0.1 mol/L phosphate buffer for pH > 5).

3.2.3 Analytical procedures

Samples (10 µL) from the aqueous phase were analyzed using reverse phase HPLC using 0.100 mol/L perchloric acid as eluent with a flow rate of 0.5 mL/min. Before injection, the samples were filtered over a PTFE syringe filter with pore size 0.45 µm (Waters Chrom). The equipment consisted of Shimadzu CC-20AD pumps, a Crownpak CR(+) chiral column (Diacel, Japan) equipped with guard column and a SPD-M20A diode array detector. Detection was done at 204 nm UV-light. Quantitative analysis (accuracy 2%) was performed using calibration curves.

The pH-measurements were performed using an Inolab pH 730 pH-meter equipped with a Sentix 81 Probe.

3.2.4 Modeling software and optimization

Parameter fitting was performed using a nonlinear least squares method (lsqnonlin) provided by the software package Matlab (Mathworks). 95% Confidence intervals are reported for the parameters. The model correlation parameters used are R^2 and the mean relative error (MRE).

3.3 Theory

3.3.1 Theory of enantioselective extraction

Enantioselective extractions were first reported in the late 1960's[37-40]. Since then, numerous studies have been published, most of them exploring the origin of the enantioselectivity on a molecular level[16,25,26,34,41-46]. The enantioselectivity of the process may be expressed as the operational selectivity[9]. For the current system, the S-enantiomer is preferentially extracted and the operational selectivity is defined as:

$$\alpha_{op} = \frac{D_{PGL_S}}{D_{PGL_R}} \qquad (3.1)$$

Here, the distributions *D* are defined as the ratios of the total concentration of all PGL species in the organic phase over the total concentrations in the aqueous phase[9]. For PGL_S, the distribution is defined as:

$$D_{PGL_S} = \frac{[PGL_s]_{org}^{all\ forms}}{[PGL_S]_{aq}^{all\ forms}} \tag{3.2}$$

The operational selectivity as defined in Eq. 3.1 is not a system property, but is a function of the experimental conditions. To gain insights in the potential of an ELLE system, the intrinsic selectivity is a better measure. It is defined as the ratio of the actual complexation constants[31]:

$$\alpha_{\text{int}} = \frac{K_{cS}}{K_{cR}} \tag{3.3}$$

The higher the intrinsic selectivity, the easier it is to obtain both enantiomers in high enantiopurity. An appropriate measure for operational performance is the performance factor (*PF*) [17]. For the current extraction system, *PF* is defined as:

$$PF_S = ee_{org} Y_{S,org} \tag{3.4a}$$

$$PF_R = ee_{aq} Y_{R,aq} \tag{3.4b}$$

Here, the *ee* is defined as:

$$ee = \frac{\left|[PGL_S]_k - [PGL_R]_k\right|}{[PGL_S]_k + [PGL_R]_k} \qquad (k = aq, org) \tag{3.5}$$

The yields are defined as the fraction of the enantiomer in the feed that ends up in the desired phase (i.e. the organic phase for the S-enantiomer and the aqueous phase for the R-enantiomer):

$$Y_{S,org} = \frac{V_{org}[PGL_S]_{org}^{all\ forms}}{V_{aq}[PGL_S]_{aq,init}^{all\ forms}} \tag{3.6a}$$

$$Y_{R,aq} = \frac{[PGL_R]_{aq}^{all\ forms}}{[PGL_R]_{aq,init}^{all\ forms}} \tag{3.6b}$$

In an ideal extraction process where the enantiomers are completely separated, both the PF_S and the PF_R are 1.

3.3.2 Enantioselective liquid-liquid extraction models

Reactive liquid-liquid extractions are generally modeled using either the interfacial extraction model or the homogeneous organic phase model. Discrimination between the two models is not straight forward. After many years of debate, it is now generally accepted that reactive metal extractions by lipophilic phosphoric acid derivatives occur through the interfacial extraction mechanism[47]. In the literature on reactive extractions of organic acids, however, still ambiguity exists. Bart[48] describes acid extraction with tri-octyl amine (TOA) as an interfacial process, whereas others[49,50] use a homogeneous organic phase complexation model. This ambiguity is also observed in the enantioselective extraction literature. For instance, Takeuchi *et al* [21] described the extraction of several amino acids by a copper(II)hydroxyproline complex with a homogeneous organic phase complexation reaction, whereas Pickering and Chaudhuri[19] described the extraction of phenylalanine with the same extractant with the interfacial reaction model.

In this study a lipophilic phosphoric acid derivative is used as extractant. Similar to the models used for metal extractions using lipophilic phosphoric acid derivatives[48], an interfacial complexation mechanism may be proposed (Figure 3.2, left). However, as the neutral form of PGL is highly soluble in DCM (*vide infra*)[31], a homogeneous organic phase complexation (Figure 3.2, right) is more likely to apply and has been used in this study. The homogeneous extraction model (Figure 3.2, right) consists of six equilibrium relations (three for each enantiomer) and mass balances for three components (PGL_q with q = R,S, and extractant P). The aqueous phase equilibrium constant is given by:

$$K_b = \frac{\gamma_{PGL_qH^+}[PGL_qH^+]_{aq}\gamma_{OH^-}[OH^-]_{aq}}{[PGL_q]_{aq}} \tag{3.7}$$

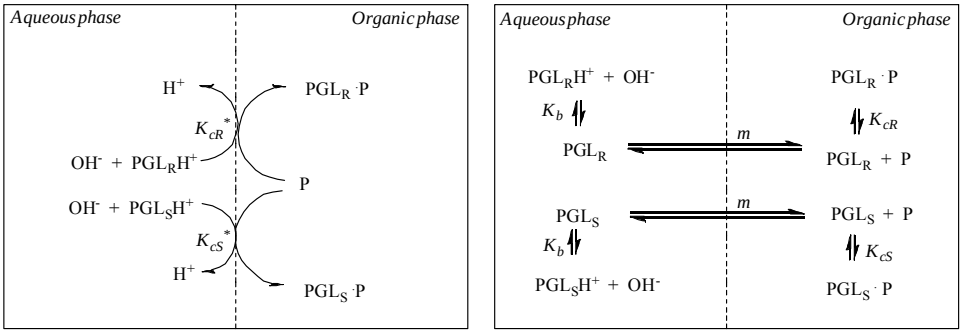

Figure 3.2. Possible extraction mechanisms for ELLE of $PGL_{R,S}$ using P. The interfacial reaction is depicted on the left and homogeneous organic phase reaction on the right.

The γ's in Eq. 3.7 represent the activity coefficients for ionic species in water. In case the aqueous phase ionic strength exceeds 10^{-3} mol/L, non-ideality phase should be taken into account[51]. The ionic strength is calculated using Eq. 3.8.

$$I = \frac{1}{2}\sum_i z_i^2 c_i \tag{3.8}$$

The activity coefficients were calculated using a Debye-Hückel law (Eq.3.9)[51].

$$^{10}\log(\gamma_i) = \frac{-Az_i^2 I^{1/2}}{1 + BI^{1/2}} \tag{3.9}$$

The values of the constants A and B for aqueous sodium chloride solutions at 25ºC have been used as an approximation (A = 0.5115 and B = 1.316)[51]. In PGL-extraction experiments using pH-buffers, the aqueous ionic strength was much higher than 10^{-3} mol/L and the ion activity coefficients were calculated using Eq. 3.9.
The homogeneous complexation constant for each enantiomer is defined as:

$$K_{cq} = \frac{[PGL_q P]_{org}}{[P]_{org}[PGL_q]_{org}} \tag{3.10}$$

Partitioning of PGL between the organic and aqueous phase is given by the following equilibrium relation:

$$m = \frac{[PGL_q]_{org}}{[PGL_q]_{aq}} \tag{3.11}$$

The mass balance for P for the total system is given by:

$$[P]_{org,init} = [P]_{org} + [PGL_R P]_{org} + [PGL_S P]_{org} \tag{3.12}$$

The mass balances for both enantiomers PGL_q for the total system read:

$$\begin{aligned} &V_{aq}[PGL_q]_{aq,init} = \\ &V_{aq}\left([PGL_q]_{aq} + [PGL_q H^+]_{aq}\right) + V_{org}\left([PGL_q]_{org} + [PGL_q P]_{org}\right) \end{aligned} \tag{3.13}$$

When the pH and ionic strength of the solution are fixed, as is the case with buffered solutions, the nine unknown concentrations may be solved simultaneously.

3.4 Results and Discussion

Equilibrium modeling of the extraction process using the homogeneous reaction model requires knowledge of the values of the parameters K_b, m and the organic phase complexation constants K_{cq}. For the system under study, these were determined experimentally one-by-one using a systematic approach, instead of defining the extraction equilibrium in terms of the overall equilibrium.

3.4.1 Estimation of the temperature dependent basicity constant

The value of K_b for PGL at various temperatures was determined by measuring the pH of diluted aqueous solutions of $PGL_{R,S}$ ($[PGL_{R,S}]_{init} = 3 \cdot 10^{-5}$ and $11 \cdot 10^{-5}$ mol/L) under an inert atmosphere from 295 to 335 K. At these ideal conditions ($c << 10^{-3}$ mol/L), the K_b may be determined from the experimentally observed $[OH^-]$ and the intake of PGL_{RS} (Eq. 3.14). The K_b may be related to the standard enthalpy and entropy of reaction using Eq. 3.14 [52]:

$$\ln(K_b) = \ln\left(\frac{[OH^-]}{[PGL_{R,S}]_{init} - [OH^-]}\right) = \frac{-\Delta H_b^{\theta}}{R \cdot T} + \frac{\Delta S_b^{\theta}}{R} \qquad (3.14)$$

By fitting Eq. 3.14 to the experimental data, the standard enthalpy and entropy of the protonation equilibrium were estimated to be $(-9.54 \pm 0.09) \cdot 10^4$ J/mol and at $(-4.29 \pm 0.03) \cdot 10^2$ J/(mol K), respectively. The correlation between experimental data and model was excellent. This is clearly illustrated by the parity plot provided in Figure 3.3 and the value of the mean relative error (MRE) of only 3%. The value of K_b at room temperature ($3.53 \cdot 10^{-6}$ mol/L) is well in agreement with the value reported in the literature[53].

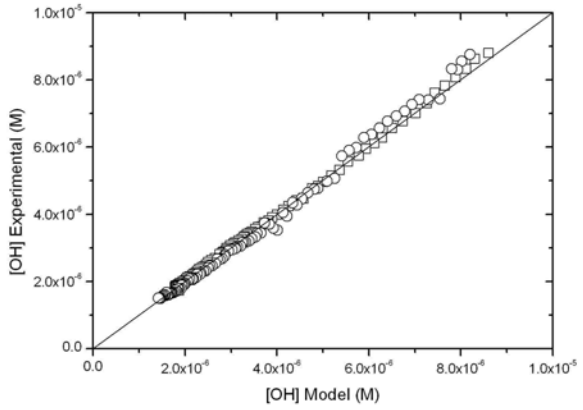

Figure 3.3. Parity plot for modeled and experimental [OH^-] Symbols: □: $[PGL_{R,S}]_{init} = 3 \cdot 10^{-5}$ mol/L, ○: $[PGL_{R,S}]_{init} = 11 \cdot 10^{-5}$ mol/L.

3.4.2 Estimation of the temperature dependent partitioning coefficient (*m*) of PGL

The physical partitioning of undissociated $PGL_{R,S}$ over the aqueous and DCM-phases (in the absence of extractant) was studied at 279- 303 K using the procedure described in section 3.2.2. The value of *m* was calculated using Eq. 3.15. This equation is obtained by rearranging Eq. 3.13 with [P] and the concentration un-dissociated $PGL_{R,S}$ set to zero and combining this modified equation with Eq. 3.11.

$$[PGL_{R,S}]_{aq} = \frac{[PGL_{R,S}]_{aq,init}}{1 + \phi \cdot m} \qquad (3.15)$$

Here, the ϕ is the volume ratio V_{org}/V_{aq}, and $[PGL_{R,S}]_{aq}$ the experimentally determined value of the two enantiomers in the aqueous phase The value of *m* was fitted to the experimental data using Eq. 3.15 for the various temperatures. The temperature dependency of *m* was quantified an empirical relation as given in Eq. 3.16.

$$m = a_1 \cdot (T - 273)^2 + a_2 \cdot (T - 273) + a_3 \qquad (3.16)$$

The estimated values of the coefficients a_i are given in Table 3.1. and a parity plot for experimental and modelled data is provided in Figure 3.4.

Table 3.1. Estimated coefficients for Eq. 3.20.

Coefficient	**value**
a_1 [1/K^2]	$(-1.33 \pm 0.49) \cdot 10^{-3}$
a_2 [1/K]	$(5.82 \pm 1.63) \cdot 10^{-2}$
a_3 [-]	$(1.28 \pm 1.24) \cdot 10^{-1}$

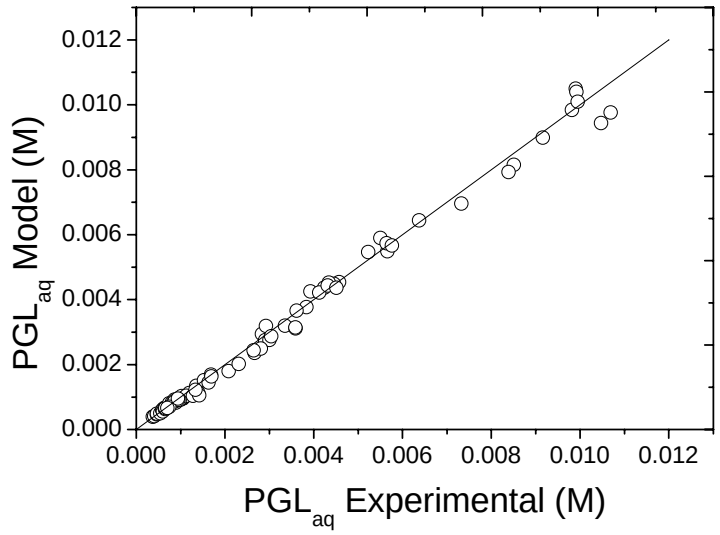

Figure 3.4. Parity plot of the experimental and modeled data using Eq. 3.15.

Agreement between modeled and experimental data is good as is evident from the parity plot in Fig 3.4 and the values for the MRE (5%) and R^2 (0.998). At 298 K the value of *m* is 0.73, which is a slightly higher the value of 0.6 reported in the literature [31]. Thus, it can be concluded that the solubility of $PGL_{R,S}$ in DCM is only slightly lower than in water and this justifies our choice to apply the homogeneous model to describe the process.

3.4.3 Estimation of the equilibrium constants of complexation (K_{cq})

Reactive experiments to estimate the equilibrium constants of complexation were performed at 279 - 303 K by the procedure described in section 3.2.2. The experimentally determined aqueous phase PGL_q concentrations at equilibrium were used to determine the values for K_{cq}. The estimated values of the equilibrium constants at 294 K are $(1.57\pm0.17)\cdot10^9$ for K_{cS} and $(8.75\pm1.12)\cdot10^8$ for K_{cR}. A good correlation between model prediction and experimental data was observed (Figure 3.5), confirmed by the values for R^2 (0.997) and the MRE (6.8%).

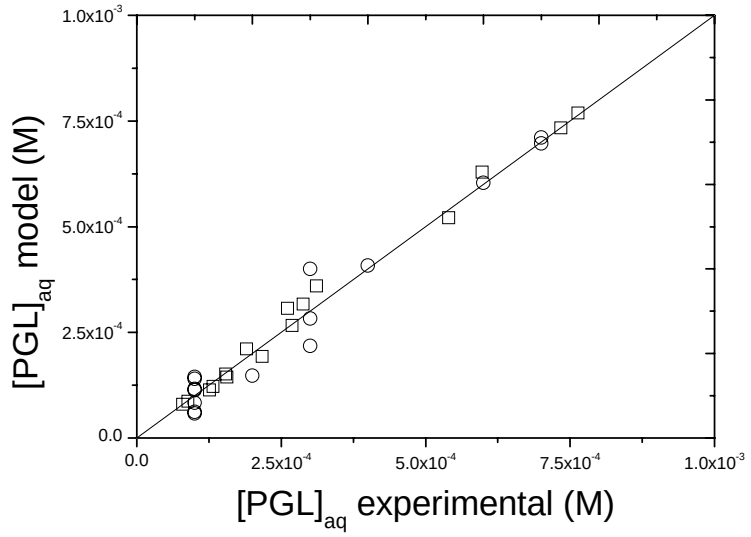

Figure 3.5. Parity between extraction model and experimental data (T = 294 K). Symbols: □: PGL_R, ○: PGL_S.

The effect of the temperature on the equilibrium constants was quantified using Eq. 3.21.

$$\ln(K) = -\frac{\Delta H^{\theta}}{R \cdot T} + \frac{\Delta S^{\theta}}{R} \qquad (3.21)$$

The experimental values for the equilibrium constants obtained at 279, 283, 288, 294, 298, and 303 K were modeled using Eq. 3.21 to obtain the values of ΔH^{θ} and ΔS^{θ}. The values are given in Table 3.2. A Van 't Hoff plot [52] is given in Figure 3.6. It shows that the slopes of the lines for both enantiomers are essentially similar, indicating that the effect of temperature on the intrinsic selectivity (Eq. 3.3) is small. The intrinsic selectivity increases slightly from 1.72 at 303 K to 1.89 at 279 K. An increase in the selectivity at lower temperature is frequently observed for enantioselective liquid-liquid extractions[31,43] .

Table 3.2. Thermodynamic constants of the complexation reaction of P with PGL_q

	ΔH^{θ} *[10^5 J/mol]*	ΔS^{θ} *[10^2 J/(mol K)]*
PGL_S	-1.78 ± 0.017	-4.28 ± 0.39
PGL_R	-1.75 ± 0.017	-4.23 ± 0.42

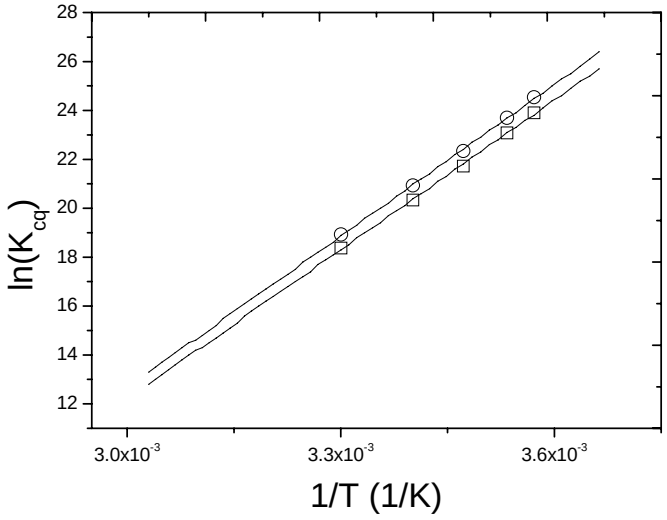

Figure 3.6. Van 't Hoff plot for the complexation reaction of P with PGL_q (Eq. 3.21). □: PGL_R, ○: PGL_S.

3.4.4 Model validation

A series of enantioselective extraction experiments were performed to validate the model over a broad pH range (1-8.5). The temperature was set at 294 K, initial values for P and PGL_q were $7 \cdot 10^{-4}$ mol/L and $1 \cdot 10^{-3}$ mol/L, respectively. In Figure 7. the experimental aqueous PGL_q concentrations are compared with the model predictions using Eqs. 3.7, 3.10-3.13. It may be concluded that the model is valid over a broad pH range, confirmed by R^2 values of 0.991 for PGL_S and 0.988 for PGL_R.

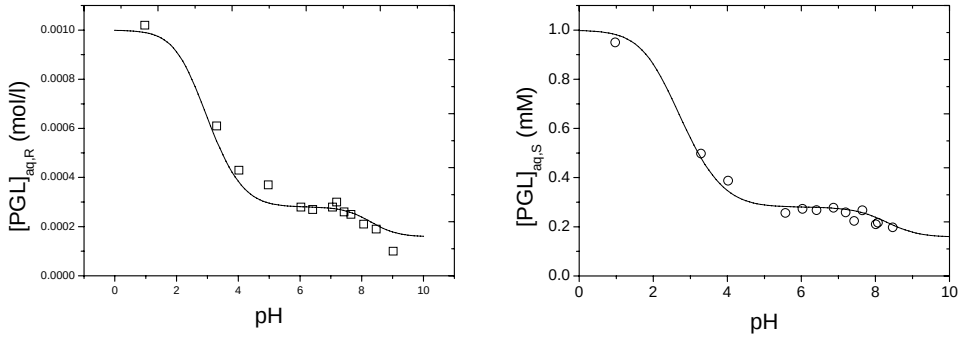

Figure 3.7. Model validation for a broad pH range. Left figure: PGL_R, right figure: PGL_S. In both figures $[P]_{org,init} = 7 \cdot 10^{-4}$ mol/L and $[PGL_q]_{aq,init} = 1 \cdot 10^{-3}$ mol/L. Lines are model predictions, squares are experimental points

3.5 Optimization of the performance of a single equilibrium stage

In this section, the homogeneous equilibrium model is used to determine the optimum conditions for a single equilibrium stage. Hereto, the *PF* as defined in Eq. 3.4 is used. The *PF* is the product of the *ee* and the yield, two important factors in enantioselective liquid-liquid extraction.

The effect of the pH on the reactive extraction process was modeled at 280 K, $[PGL_{R,S}]_{aq,init} = 1.0 \cdot 10^{-3}$ mol/L, $\phi = 1$ and $[P]_{org,init} = 1.0 \cdot 10^{-3}$ mol/L. The effects on the ee_{org} and yield are given in Figure 8, and for the *PF* in Figure 3.9 (left, solid line). The *PF* shows a clear

maximum of 0.1 at a pH of about 2. This is the resulting of two opposing effects, the ee_{org} decreases and the yield increases at higher pH's (Figure 3.8).

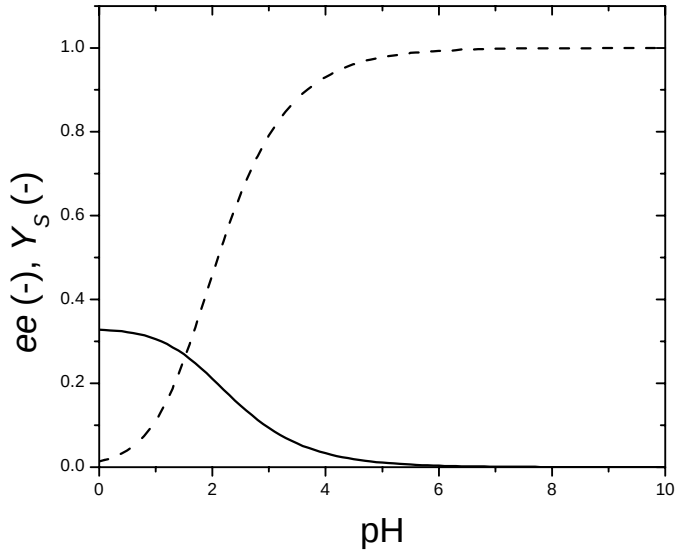

Figure 3.8. ee_{org} (—) and Y_S (--) at 280 K and varying pH. $[PGL_{R,S}]_{aq,init}$ = $1.0 \cdot 10^{-3}$ mol/L, $\phi = 1$, $[P]_{org,init}$ = $1.0 \cdot 10^{-3}$ mol/L.

At higher pH values, the yield of the S-enantiomer increases due to a higher aqueous phase equilibrium concentration of the neutral form of PGL_q. However, not only the yield of the desired S-enantiomer increases but also that of the undesired R-enantiomer. As a result, the ee_{org} drops at increasing pH and is even zero at a pH exceeding 7. It can be concluded that at pH values higher than 7 and a host P to $PGL_{R,S}$ ratio of 1, both enantiomers are transferred to the organic phase and complexed to the host.

The effect of the host to PGL ratio was modeled by lowering the host concentration at a constant $[PGL_{R,S}]_{aq,init}$ ($1.0 \cdot 10^{-3}$ mol/L). The results are given in Figure 3.9. At a ratio below 1, the profiles are more complicated than for a ratio of 1. To gain insights on the effects of the host to PGL ratio, it is illustrative to consider the effects on both the ee_{org} and the Y_s separately (see Figure 3.10). For a ratio of host to PGL ratio of 0.7, the effect of the pH on the ee_{org} and Y_s is similar to that observed for a ratio of 1, i.e. the ee_{org} decreases and the yield increases. Thus, both enantiomers are extracted with a preference for the desired S enantiomer. In the pH region between 5 and 7, both the ee_{org} and the Y_s remain constant and

as a result the PF is also constant. This is because all host is occupied in this region. At a pH near the pK_b, the yield again increases and the ee_{org} drops. In this region physical partitioning of undissociated PGL becomes significant.

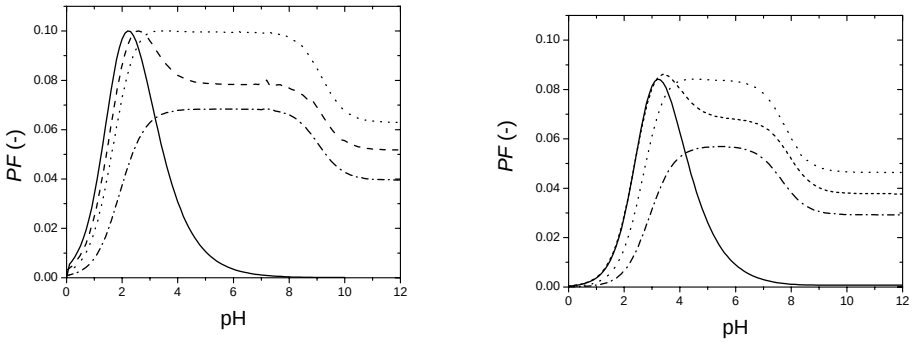

Figure 9. *PF* at 280 K (left) and 303 K (right) for various host concentrations. $[PGL_{R,S}]_{aq,init}$ = $1.0 \cdot 10^{-3}$ mol/L, $\phi = 1$. Lines: solid: $[P]_{org,init}$ = $1.0 \cdot 10^{-3}$ mol/L, dashed: $[P]_{org,init}$ = $7.0 \cdot 10^{-4}$ mol/L, dotted: $[P]_{org,init}$ = $5.0 \cdot 10^{-4}$ mol/L, dash dotted: $[P]_{org,init}$ = $2.0 \cdot 10^{-4}$ mol/L

Similar trends in the *PF* as a function of the pH were observed when working at lower host to PGL ratio's (Figure 3.9). Thus, by reducing the host to PGL ratio, the pH window for enantioselective extraction is larger, However, the yields are lower than when using a ratio of 1.

The profiles of the *PF* as a function of the pH and the host to PGL ratio at 303 K closely resemble those at 280 K (Figure 3.10, right). The maximum *PF* is though lower, which is due to the lower intrinsic selectivity at higher temperatures (*vide supra*).

Thus, it can be concluded that the highest *PF* values are found at a pH below 5, that the host to PGL ratio has an effect on the maximum *PF* and that the temperature also plays a role. Therefore, the *PF* at two low pH values (3 and 5), with a large spread in host to PGL ratio's (0.1 - 2) at three temperatures (280, 290, 300 K) was modeled and the results are given in Figure 3.11. All PF curves show clear maxima. The highest PF of 0.1 was found at 280 K at a host to PGL ratio of 0.5. This value was obtained at both a pH of 3 and 5. However, it appears advantageous to perform the reactive extraction at a pH of 3 as the PF gradients at this pH are less steep than observed for pH is 5. Thus, slight variations in the pH when working at a pH of 3 are less detrimental for the PF than when working at a pH of 5.

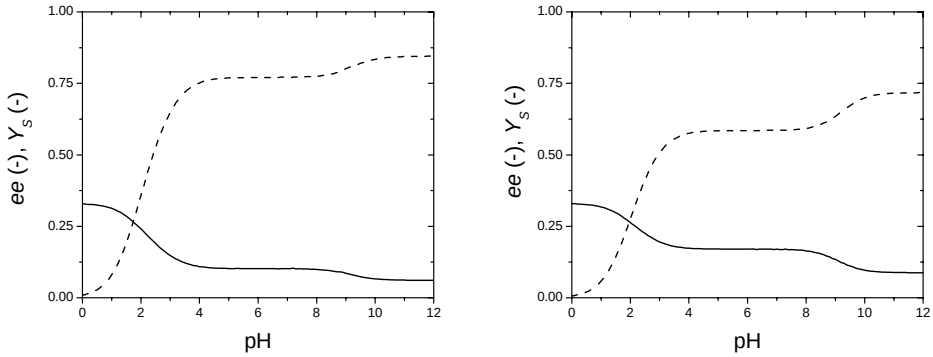

Figure 3.10. ee_{org} (—) and Y_S (--) at 280 K and varying pH. $[PGL_{R,S}]_{aq,init}$ = $1.0 \cdot 10^{-3}$ mol/L, $\phi = 1$. Left: $[P]_{org,init}$ = $0.7 \cdot 10^{-3}$ mol/L. Right: $[P]_{org,init}$ = $0.5 \cdot 10^{-3}$ mol/L

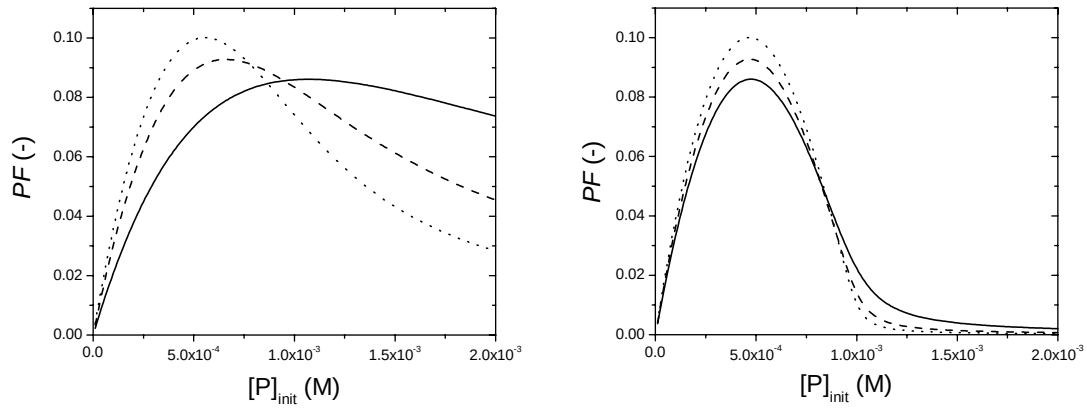

Figure 3.11. *PF* as a function of the extractant P concentration. $[PGL_{R,S}]_{aq,init}$ = $1.0 \cdot 10^{-3}$ mol/L, $\phi = 1$. Left figure: pH = 3, right figure: pH = 5. Lines: dotted: 280 K, dashed: 290 K, solid: 300 K.

The highest modeled value of the PF was 0.10. With this value, it is clear that both a high *ee* and yield are not possible in a single equilibrium step. Therefore a multistage extraction process will be required when full separation of the racemate is pursued.

3.6. Conclusions

The equilibrium enantioselective reactive extraction of $PGL_{R,S}$ by extractant P was investigated gain insights in the effect of process variables on the yield and ee_{org}. The reactive extraction process was assumed to proceed via the homogeneous reaction model, rationalized by the high solubility of PGL in the organic phase. Important model parameters like the K_b, m and the equilibrium complexation constant of both enantiomers were determined using a systematic approach. The equilibrium constants for complexation were high and typically in the order of 10^8-10^{10} L/mol. The intrinsic selectivity was 1.89 at 280 K and 1.72 at 303 K. The performance of the extraction process was modeled using the performance factor, *PF*. The model predicts a maximum value for *PF* of 0.10 at 280 K. This indicates that a high *ee* in combination with a high yield is not possible in a single equilibrium step and that multistage extraction will be required for full separation of $PGL_{R,S}$.

3.7 Nomenclature

a_i	coefficients in Eq. 16 (i= 1-3)
A	constant in Debye-Hückel law, [-]
B	constant in Debye-Hückel law, [-]
c	concentration
D	distribution [-]
ee	enantiomeric excess [-]
ΔH^θ	standard enthalpy of reaction [J/mol]
I	ionic strength [mol/L]
K	equilibrium constant [various dimensions]
m	partitioning ratio [-]
P	the extractant: 3,3'-(3,5-bis(trifluoromethyl) phenyl)-2,2'-diyl hydrogenphosphate-1,1'-binaphthyl
PGL	phenylglycinol
R	gas constant, 8.3144 [J/(mol K)]
ΔS^θ	standard entropy of reaction [J/(mol K)]

T	Temperature [K]
V	volume [m^3]
Y	yield [mol/mol]
z	ion valence [-]

greek letters

α	selectivity
γ	activity coefficient [-]
ϕ	volume ratio [-]

subscripts

aq	aqueous phase
b	basicity
c	complexation
i	index for ions
init	initial
int	intrinsic
k	index for phases
op	operational
org	organic phase
q	index for enantiomers, R and S
R	R-enantiomer
S	S-enantiomer

superscripts

all forms	all forms, i.e. protonated and neutral forms in the aqueous phase, and complexated and noncomplexated in the organic phase
*	interfacial

3.8 References

[1]. Rouhi, A. M. *Chem. Eng. News* **2003,** *81*, 45-55.
[2]. Sheldon, R. A. *Chirotechnology; industrial synthesis of optically active compounds;* Marcel Dekker, Inc.: New York, 1993.
[3]. Crosby, J. *Tetrahedron* **1991,** *47*, 4789-4846.
[4]. Breuer, M.; Ditrich, K.; Habicher, T.; Hauer, B.; Kesseler, M.; Sturmer, R.; Zelinski, T. *Angew. Chem. Int. Ed.* **2004,** *43*, 788-824.
[5]. Collins, A. N.; Sheldrake, G. N.; Crosby, J. *Chirality in Industry II;* John Wiley & sons Ltd.: Chichester, 1997.

[6]. Bruggink, A. Rational Design in Resolutions. In *Chirality in Industry II*, Collins, A. N., Sheldrake, G. N., Crosby, J., Eds.; John Wiley & sons Ltd.: Chichester, 1997; pp 81-98.
[7]. Faigl, F.; Fogassy, E.; Nogradi, M.; Palovics, E.; Schindler, J. *Tetrahedron-Asymmetry* **2008,** *19*, 519-536.
[8]. Fogassy, E.; Nogradi, M.; Kozma, D.; Egri, G.; Palovics, E.; Kiss, V. *Organic & Biomolecular Chemistry* **2006,** *4*, 3011-3030.
[9]. Steensma, M.; Kuipers, N. J. M.; de Haan, A. B.; Kwant, G. *Chirality* **2006,** *18*, 314-328.
[10]. Francotte, E.; Leutert, T.; La Vecchia, L.; Ossola, F.; Richert, P.; Schmidt, A. *Chirality* **2002,** *14*, 313-317.
[11]. Gavioli, E.; Maier, N. M.; Minguillon, C.; Lindner, W. *Anal. Chem.* **2004,** *76*, 5837-5848.
[12]. Zenoni, G.; Quattrini, F.; Mazzotti, M.; Fuganti, C.; Morbidelli, M. *Flavour and Fragrance Journal* **2002,** *17*, 195-202.
[13]. Keurentjes, J. T. F.; Nabuurs, L. J. W. M.; Vegter, E. A. *J. Membr. Sci.* **1996,** *113*, 351-360.
[14]. Maximini, A.; Chmiel, H.; Holdik, H.; Maier, N. W. *J. Membr. Sci.* **2006,** *276*, 221-231.
[15]. Pirkle, W. H.; Pochapsky, T. C. *Chemical Reviews* **1989,** *89*, 347-362.
[16]. Andrisano, V.; Gottarelli, G.; Masiero, S.; Heijne, E. H.; Pieraccini, S.; Spada, G. P. *Angew. Chem. Int. Ed.* **1999,** *38*, 2386-2388.
[17]. Koska, J.; Haynes, C. A. *Chem. Eng. Sci.* **2001,** *56*, 5853-5864.
[18]. Koska, J.; Mui, C.; Haynes, C. A. *Chem. Eng. Sci.* **2001,** *56*, 29-41.
[19]. Pickering, P. J.; Chaudhuri, J. B. *Chem. Eng. Sci.* **1997,** *52*, 377-386.
[20]. Pickering, P. J.; Chaudhuri, J. B. *Chirality* **1999,** *11*, 241-248.
[21]. Takeuchi, T.; Horikawa, R.; Tanimura, T. *Anal. Chem.* **1984,** *56*, 1152-1155.
[22]. Tan, B.; Luo, G. S.; Qi, X.; Wang, J. D. *Sep. Purif. Technol.* **2006,** *49*, 186-191.
[23]. Tan, B.; Luo, G. S.; Wang, H. D. *Tetrahedron-Asymmetry* **2006,** *17*, 883-891.
[24]. Tan, B.; Luo, G. S.; Wang, J. D. *Sep. Purif. Technol.* **2007,** *53*, 330-336.
[25]. Kellner, K. H.; Blasch, A.; Chmiel, H.; Lämmerhofer, M.; Lindner, W. *Chirality* **1997,** *9*, 268-273.
[26]. Breccia, P.; Van Gool, M.; Perez-Fernandez, R.; Martin-Santamaria, S.; Gago, F.; Prados, P.; de Mendoza, J. C. *J. Am. Chem. Soc.* **2003,** *125*, 8270-8284.
[27]. Galan, A.; Andreu, D.; Echavarren, A. M.; Prados, P.; de Mendoza, J. *J. Am. Chem. Soc.* **1992,** *114*, 1511-1512.
[28]. Abe, Y.; Shoji, T.; Kobayashi, M.; Qing, W.; Asai, N.; Nishizawa, H. *Chem. Pharm. Bull.* **1995,** *43*, 262-265.
[29]. Abe, Y.; Shoji, T.; Fukui, S.; Sasamoto, M.; Nishizawa, H. *Chem. Pharm. Bull.* **1996,** *44*, 1521-1524.
[30]. Prelog, V.; Stojanac, Z.; Kovacevic, K. *Helv. Chim. Acta* **1982,** *65*, 377-384.
[31]. Steensma, M.; Kuipers, N. J.; de Haan, A. B.; Kwant, G. *J. Chem. Technol. Biotechnol.* **2006,** *81*, 588-597.
[32]. Steensma, M.; Kuipers, N. J. M.; de Haan, A. B.; Kwant, G. *Chem. Eng. Sci.* **2007,** *62*, 1395-1407.
[33]. Steensma, M.; Kuipers, N. J. M.; de Haan, A. B.; Kwant, G. *Chem. Eng. Proc.* **2007,** *46*, 996-1005.

[34]. Tang, L.; Choi, S.; Nandhakumar, R.; Park, H.; Chung, H.; Chin, J.; Kim, K. *The Journal of Organic Chemistry* **2008,** *73*, 5996-5999.
[35]. Viegas, R. M. C.; Afonso, C. A. M.; Crespo, J. G.; Coelhoso, I. M. *Sep. Purif. Technol.* **2007,** *53*, 224-234.
[36]. Verkuijl, B. J. V.; Browne, W. R.; Feringa, B. L. *Chirality,* accepted for publication.
[37]. Bauer, K.; Falk, H.; Schlogl, K. *Monatshefte für Chemie* **1968,** *99*, 2186-&.
[38]. Bowman, N. S.; Mccloud, G. T.; Schweitz, G. K. *J. Am. Chem. Soc.* **1968,** *90*, 3848-3852.
[39]. Romano, S. J.; Wells, K. H.; Rothbart, H. L.; Rieman, W. *Talanta* **1969,** *16*, 581-590.
[40]. Schweitz, G. K.; Supernaw, I. R.; Bowman, N. S. *J. Inorg. Nucl. Chem.* **1968,** *30*, 1885-1890.
[41]. Dzygiel, P.; Monti, C.; Piarulli, U.; Gennari, C. *Organic & Biomolecular Chemistry* **2007,** *5*, 3464-3471.
[42]. Lacour, J.; Goujon-Ginglinger, C.; Torche-Haldimann, S.; Jodry, J. J. *Angew. Chem. Int. Ed.* **2000,** *39*, 3695-3697.
[43]. Peacock, S. C.; Domeier, L. A.; Gaeta, F. C. A.; Helgeson, R. C.; Timko, J. M.; Cram, D. J. *J. Am. Chem. Soc.* **1978,** *100*, 8190-8202.
[44]. Reeve, T. B.; Cros, J. P.; Gennari, C.; Piarulli, U.; de Vries, J. G. *Angew. Chem. Int. Ed.* **2006,** *45*, 2449-2453.
[45]. Tsukube, H.; Shinoda, S.; Uenishi, J.; Kanatani, T.; Itoh, H.; Shiode, M.; Iwachido, T.; Yonemitsu, O. *Inorg. Chem.* **1998,** *37*, 1585-1591.
[46]. Tsurubou, S. *Anal. Sci.* **1991,** *7*, 45-48.
[47]. Cox, M. Liquid-Liquid Extraction in hydrometallurgy. In *Science and Practice of Liquid-Liquid Extraction*, Thornton, J. D., Ed.; Clarendon: Oxford, 1992; pp 1-101.
[48]. Bart, H. J. *Reactive Extraction;* 18 ed.; Springer Verlag: Berlin, 2001.
[49]. Nikhade, B. P.; Moulijn, J. A.; Pangarkar, V. G. *J. Chem. Technol. Biotechnol.* **2004,** *79*, 1155-1161.
[50]. Wasewar, K. L.; Heesink, A. B. M.; Versteeg, G. F.; Pangarkar, V. G. *J. Chem. Technol. Biotechnol.* **2002,** *77*, 1068-1075.
[51]. Robinson, R. A.; Stokes, R. H. *Electrolyte Solutions, Dover Ed.;* Dover edition ed.; Dover: New York, 2002.
[52]. Atkins, P. W. *Physical Chemistry;* 5th edition ed.; Oxford University Press: Oxford, 1994.
[53]. Hein, Fr.; Meier, F. Z. Anorg. Allg. Chem. 1970, 376, 296-302.

Chapter 4

Determination of the interfacial area of a continuous integrated mixer/separator (CINC) using a chemical reaction method

Boelo Schuur, Wiebe J. Jansma, Jozef G. Winkelman, Hero J. Heeres

This chapter was published:
Chemical Engineering & Processing 2008, 47, 1484-1491

Abstract

The effect of the liquid flow rates (18-100 mL/min) and rotor frequency (30-60 Hz) on the interfacial area of a liquid – liquid system in a CINC-V02 continuous integrated mixer/separator have been studied using a chemical reaction method. Typical specific interfacial areas were in the range of $3.2 \cdot 10^2$ to $1.3 \cdot 10^4$ m^2 per m^3 liquid volume, which is comparable with those for a continuously stirred tank reactor (CSTR). A pronounced maximum in the interfacial area with respect to the rotor frequency was found at about 45 Hz. The interfacial area increased considerably at higher aqueous phase flow rates whereas the organic phase flow rate had no significant effect. The experimental data were modelled using a linear empirical model. Good agreement between experiments and model was observed.

4.1. Introduction

Process intensification is a powerful concept to replace large, energy intensive equipment or processes with smaller plants that combine multiple operations in single, highly integrated devices[1]. Examples are reactive distillation[2] and reactive extraction[2]. For the latter, the integration of reaction and separation is not only advantageous with respect to energy and investments costs but also to the efficiency and/or the selectivity of the extraction process[3-5].

A very attractive device to integrate chemical reaction and separation is the CINC integrated mixer/separator[6]. The CINC basically consists of a rotating hollow centrifuge in a static housing (Figure 4.1). The liquid(s) enter the device in the annular zone between the static wall and the rotating centrifuge, where they are intensely mixed. Next, they are transferred into the centrifuge where separation occurs by the action of centrifugal forces[7]. The centrifugal forces can be as high as 900 g, allowing excellent phase separation even when the densities of the phases differ only slightly. A cutaway view of the CINC is depicted in Figure 4.1.

The CINC device was initially developed for oil spill clean up. Further applications were developed in the field of liquid-liquid separation and extraction (e.g. metal extractions)[2]. The equipment is available in different sizes and may be operated in a wide volumetric flow window (10^{-5} - 50 m^3 /h). When required, a number of CINC's may be interconnected for multistage operation.

The CINC device is potentially very attractive for the integration of reaction and separation. To the best of our knowledge the device has not been applied for this application yet.

We have recently demonstrated the application of the CINC for the continuous biphasic enzyme catalyzed (*Rhizomucor miehei* lipase) esterification of oleic acid with n-butanol in a heptane/water mixture[7]. Oleic acid conversions of up to 70% were obtained when operating at full recycle of the aqueous, enzyme containing, stream and partial recycle of the organic stream. We have also studied racemate separation in the CINC-V02 using reactive liquid-liquid extraction with chiral extractants. Racemate separation is of pivotal importance for the fine chemical and pharmaceutical industry. Very promising results were obtained for the enantioselective extraction of 3,5-dinitrobenzoyl-(*R*),(*S*)-leucine (DNB-R,S-leu) using a cinchona alkaloid extractant. A non-optimized

enantiomeric excess (*ee*) of 52% in the organic phase at 35% yield was obtained in once through operation[8,9].

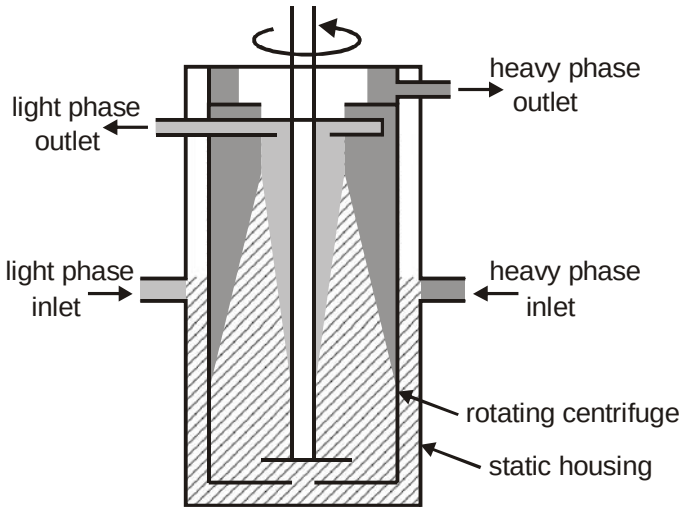

Figure 4.1. Cutaway view of the CINC, hatched: dispersion, darker gray: heavy phase, lighter gray: light phase.

Optimization of these novel applications in the CINC as well as existing applications in the field of solvent separation require detailed scientific knowledge about the hydrodynamics in the devices like liquid flow patterns, liquid hold-ups in the various zones and the liquid-liquid interfacial area.

Here we report experimental results on the interfacial area in the CINC as a function of process conditions (flow rates and rotational speed of the centrifuge). The interfacial area can be determined both by direct measurements (imaging)[10] and indirect methods such as UV permeability measurements[11] and a liquid-liquid biphasic chemical reaction[12]. Since imaging and permeability measurements are not possible in the CINC because of its steel walls, in this study the reaction between n-butyl formate and sodium hydroxide[12] was used for determination of the total interfacial area.

4.2 Experimental Section

4.2.1 Chemicals

NaOH pellets, 0.100 M HCl (Titrisol) and n-butanol were obtained from Merck, n-butyl formate was obtained from Aldrich, aceton (AR) from Labscan Ltd, n-octane from Janssen Chimica and N_2 (>99.99%) from Hoek Loos . Reverse osmosis water was applied to prepare the NaOH and HCl solutions.

4.2.2 Experimental set-up

All experiments were carried out under a nitrogen atmosphere in a CINC V-02 (a table top version with a maximum total throughput of 2 L min^{-1} ($3.3 \cdot 10^{-5}$ $m^3.s^{-1}$) and maximum rotational frequency of 100 Hz) made from Hastelloy and equipped with a heating/cooling jacket. The reaction temperature was kept under 300 K (typically 295-298K) by cooling with water. Both liquids were transferred to the reactor using Verder VL1000 Control peristaltic tube pumps equipped with double pump heads (1.6 x 1.6 x 8R). All supply and receive vessels were made out of glass and kept under a nitrogen atmosphere. The aqueous in- and outlet streams and the cooling water in- and outlet streams were equipped with temperature sensors (CMA, Amsterdam) connected with a PC via a CoachLab II interface (CMA, Amsterdam). Aqueous and organic phase inlet flows, as well as the cooling water flow were measured with flowmeters. A schematic representation of the setup is provided in Figure 4.2.

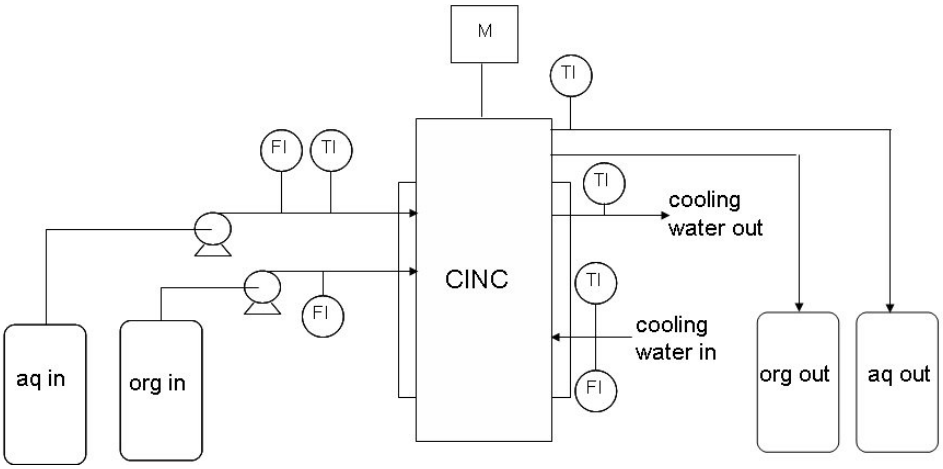

Figure 4.2. Schematic representation of the experimental setup.

4.2.3 Experimental procedure

The NaOH-solutions were made by dissolving NaOH pellets in RO-water. n-Butyl formate was used as received. Prior to the experiments, the supply and receive vessels were flushed with nitrogen gas (three times) and subsequently the solutions were bubbled with nitrogen at least four hours to ensure the system was free of CO_2. The cooling water rate was set at 1.1 L min^{-1} and the temperature measurement was started. After one hour a nitrogen atmosphere was applied to the CINC, and the pump of the aqueous solution and the centrifuge were started. When the reactor was filled with the aqueous solution and water appeared from the aqueous phase outlet, the organic phase pump was started. As soon as the organic phase reactor outlet started running, samples were collected every 2 minutes during 20 minutes. The flow rates were registered at regular time intervals. After 20 minutes, the measurements were stopped.

4.2.4. Analytical procedures

Organic phase samples were analyzed by GC-FID using a HP 5890 series II plus GC apparatus equipped with an HP-5 column (30 m length, 0.25 mm diameter and 0.25 μm film thickness) and an HP 7673 GC-SF injector. The GC measurements were carried out

isothermally at a column temperature of 60°C, injection and detection temperatures were 250°C. Samples for analysis were made by mixing 0.08 g of the organic phase with 1.00 g of a 0.2 % wt octane solution in acetone.

4.2.5. Model development

The operating variables of interest are the flow rates of both phases and the rate of rotation of the centrifuge. The significance of these variables on the variance of the total interfacial area was analysed statistically using Design Expert 7 sofware (Stat-Ease). The total interfacial area was modeled for this purpose using a standard expression as given in equation 4.1:

$$y = b_0 + \sum_{i=1}^{3} b_i x_i + \sum_{i=1}^{3} \sum_{j=i}^{3} b_{ij} x_i x_j \qquad (4.1)$$

The operating variables N, F_{aq} and F_{org} are represented by the indices 1-3. The regression coefficients were obtained by statistical analyses of the data. Significance of factors was determined by their *p* value in the ANOVA analyses. A factor was considered significant if the *p* value was lower than 0.05, meaning that the probability of noise causing the correlation between a factor and the response is lower than 0.05. Insignificant factors were eliminated using backward elimination. The significant factors were used to fit a linear model to the data.

4.3 Theory

The selected reaction to determine the total interfacial area in the CINC device is represented in Figure 4.3. The saponification of butyl formate is irreversible and first order in butyl formate and in the hydroxide-ion. The reaction takes place in the aqueous phase and butyl formate has to transfer from the butyl formate phase to the aqueous phase to react (Figure 4.4).

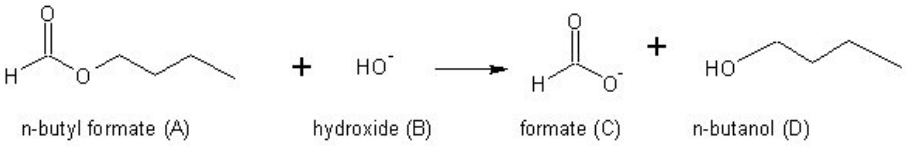

Figure 4.3. Saponification of n-butyl formate using hydroxide.

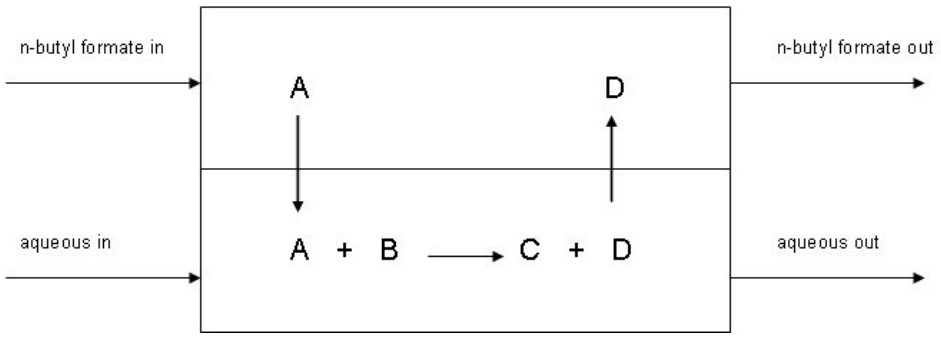

Figure 4.4. Representation of the biphasic reaction applied in this study.

The total interfacial area may be determined from the amount of A transferring from the organic phase to the aqueous phase. This quantity may be obtained from a mass balance of compound B in the aqueous phase. When assuming that the liquid phases are fully backmixed[13], the mass balance of compound B in the aqueous phase is given by:

$$V_R \varepsilon_{aq} \frac{dC_{B,aq}}{dt} = \phi_{v,aq,in} C_{B,aq,in} - \phi_{v,aq,out} C_{B,aq,out} + R_B \varepsilon_{aq} V_R \qquad (4.2)$$

The reaction rate of B is correlated to the flux of A by the following relation:

$$R_B \varepsilon_{aq} V_R = -J_A A_{tot} \qquad (4.3)$$

Combination of Eqs. 2 and 3 and when operating at steady state conditions, Eq. 4.2 simplifies to:

$$J_A A_{tot} = \phi_{v,aq,in} C_{B,aq,in} - \phi_{v,aq,out} C_{B,aq,out} \quad (4.4)$$

According to the film theory, the flux of A through the interface is given by[14]:

$$J_A = k_{L,aq} C^*_{A,aq} E_A \quad (4.5)$$

Here $C_{A,eq}^*$ is the interfacial concentration of A ($C^*_{A,aq} = mC_{A,org}$) and E_A is the enhancement factor for mass transfer. E_A is a function of the regime of mass transfer, for which information may be obtained using the Hatta number[14]. For irreversible reactions of a 1,1 stoichiometry, the Hatta number is given by:

$$Ha = \frac{\sqrt{k_{1,1} C_{B,aq} D_A}}{k_{L,aq}} \quad (4.6)$$

In case Ha is smaller than 0.3, the reaction takes place in the slow regime and E_A is equal to 1. In the fast regime ($2 < Ha << E_{A\infty}$), Eq. 4.7 is valid:

$$E_A = Ha = \frac{\sqrt{k_{1,1} C_{B,aq} D_A}}{k_{L,aq}} \quad (4.7)$$

Here $E_{A\infty}$ is the instantaneous enhancement factor, which is defined as:

$$E_{A\infty} = 1 + \frac{D_B C_B}{D_A m_A C^*_{A,org}} \quad (4.8)$$

In the instantaneous regime ($Ha > E_{A\infty}$), E_A equals $E_{A\infty}$.

In case the reaction takes place in the fast regime (Eq. 4.7), the flux is not a function of the unknown mass transfer coefficient (see Eq. 4.5). In this regime, the liquid-liquid interfacial area may be determined using Eq. 4.3, provided that the physico-chemical parameters such as the rate constant and the diffusivities are known.

When using this approach, the following considerations should be taken into account. Transport limitations in the organic phase should be avoided to simplify the equations. For this purpose, pure n-butyl formate (A) is applied. The interfacial concentration of A may thus be written as:

$$C^{*}_{A,aq} = m_A C_{A,org} \tag{4.9}$$

Diffusion limitation of B in the aqueous phase should be avoided, which holds if the concentration of B is very large compared to the concentration A in the aqueous phase. In addition, when using a large excess of B, the reaction can be considered as a pseudo-first order reaction in A. This considerably simplifies the equations. Furthermore, the concentration of product should remain low to avoid dilution of the organic phase and the possible introduction of mass transfer resistance in the organic phase. For this purpose, the conversion of B was kept always below 0.15[12]. Here, the conversion of B is defined as:

$$X_B = \frac{C_{B,aq,in} - C_{B,aq,out}}{C_{B,aq,in}} = \frac{\phi_{v,aq}}{\phi_{v,org}} \frac{C_{D,org}}{C_{B,aq,in}} \tag{4.10}$$

When these requirements are met, the interfacial area follows from Eqs. 4.4-4.7 and 4.9:

$$A_{tot} = \frac{\phi_{v,aq,in} C_{B,aq,in} - \phi_{v,aq,out} C_{B,aq,out}}{m_A C_{A,org} \sqrt{k_{1,1} C_{B,aq,out} D_A}} \tag{4.11}$$

4.4. Physico-chemical parameters

The ionic strength of the aqueous phase is calculated using Eq. 4.12. Here, it is assumed that the system is completely free of CO_2:

$$I = \frac{1}{2}\left(C_{Na^+} z^2_{Na^+} + C_{OH^-} z^2_{OH^-} + C_{HCOO^-} z^2_{HCOO^-}\right) \tag{4.12}$$

$HCOO^-$ and OH^- are related by the reaction stoichiometry and therefore Eq. 4.12 simplifies to:

$$I = \frac{1}{2}\left(C_{Na^+} z^2_{Na^+} + C_{OH^-} z^2_{OH^-}\right)_{aq,in} \tag{4.13}$$

The viscosity of the aqueous NaOH solution is related to the viscosity of pure water by using the correlation of Onda *et al.* [15]:

$$\mu_{aq} = \mu_w\left(1 + 0.177I + 0.0527I^2\right) \tag{4.14}$$

The viscosity of water is calculated using[12]:

$$\log(\mu_w) = \frac{1.3271(293.15 - T) - 0.001053(T - 293.15)^2}{T - 168.15} - 3 \tag{4.15}$$

The diffusion coefficient of butyl formate ester in the aqueous phase is a function of temperature and the concentration of sodium hydroxide in the aqueous phase. The Wilke-Chang method[16] is used to estimate the diffusion coefficient of butyl formate in water (Eq. 4.16). The diffusion coefficient of butyl formate in an aqueous solution of sodium hydroxide[15] is subsequently correlated to the diffusion coefficient in water using Eq. 4.17.

$$D_{A,w} = 2.67 \cdot 10^{-15} \frac{T}{\mu_w} \tag{4.16}$$

$$D_{A,aq} = \frac{D_{A,w}}{1 + 0.118413I + 0.0217124I^2} \tag{4.17}$$

The pseudo-first order reaction rate constant is given by[12]:

$$k_{1,1} = 9.02 \cdot 10^7 e^{-\left(\frac{36.2 \cdot 10^6}{RT} + 0.33I\right)} \tag{4.18}$$

The second term in the exponent of this equation accounts for the effect of the ionic strength of the aqueous phase on the reaction rate.

From their experimental results van Woezik *et al.*[11] obtained the value of the parameter group $m_A\sqrt{k_{11}D_A}$ as

$$m_A\sqrt{k_{11}D_A} = e^{\left(-2.05 - \frac{3350}{T} - 0.65I\right)} \tag{4.19}$$

From this, the partition coefficient, m_A, was calculated using the reaction rate constant and diffusivity given above.

4.5. Results and Discussion

4.5.1 Determination of the total interfacial area in the reactor

The model reaction (Figure 4.3) was carried out in the CINC using various flow rates and rotational speeds of the centrifuge (Table 4.1). The conversion profiles of OH^- (B) for a typical experiment are depicted in Figure 4.5. The conversion of OH^- was calculated by determination of the concentration D in the organic phase using GC-FID (see Eq. 4.10). A typical conversion profile is provided in Figure 4.5. Only after the organic phase reactor outlet started running the conversion measurements were started. The measurement that was taken before steady-state was achieved shows a higher conversion than in steady-state. This is due to the start-up procedure, in which the organic hold up has to build up towards steady-state, causing the residence time being longer than the residence time in steady-state.

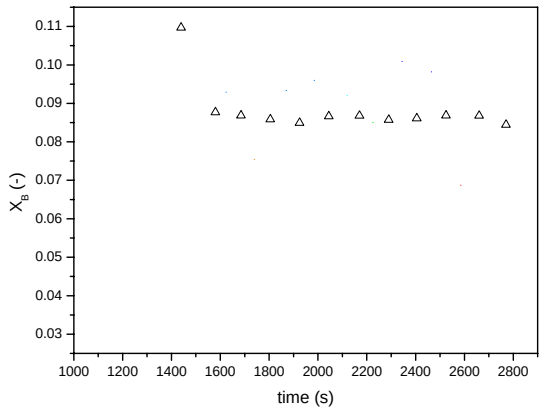

Figure 4.5. Conversion of B in time.

Table 4.1. Overview of experimental conditions and results.

Exp.	F_{org} (mL/min)	F_{aq} (mL/min)	N (Hz)	T (K)	$C_{B,in}$ (kmol/m3)	X_B (-)	A $(m^2)^a$
1	36	29	30	295	5.64	$3.60 \cdot 10^{-2}$	0.11
2	35	29	30	295	5.64	$1.75 \cdot 10^{-2}$	0.057
3	36	29	40	296	8.86	$5.49 \cdot 10^{-2}$	1.51
4	33	28	40	296	8.81	$5.53 \cdot 10^{-2}$	1.44
5	71	24	60	297	7.37	$1.28 \cdot 10^{-2}$	0.12
6	72	18	60	298	7.65	$4.66 \cdot 10^{-2}$	0.33
7	31	30	60	296	7.82	$2.46 \cdot 10^{-2}$	0.38
8	34	30	60	296	7.82	$1.83 \cdot 10^{-2}$	0.29
9	52	48	60	296	7.56	$3.35 \cdot 10^{-2}$	0.68
10	41	48	60	298	7.10	$4.67 \cdot 10^{-2}$	0.62
11	100	75	60	294	7.35	$1.11 \cdot 10^{-1}$	2.41
12	45	49	60	300	8.49	$9.65 \cdot 10^{-3}$	0.18

a. The total interfacial area was calculated using Eq. 4.11 .

4.5.2 Quantification of the effect of process variables on interfacial area

To quantify the effect of the process variables on the interfacial area, the total interfacial area was modeled as described in section 4.2.5. After elimination of the insignificant factors, the following model was fitted to the data:

$$A_{\text{mod}} = -11.14 + 0.612N - 0.0685F_{aq} - 6.76 \cdot 10^{-3} N^2 + 1.1 \cdot 10^{-3} F_{aq}^2 \quad (4.20)$$

Remarkably, factors including the variable F_{org} were insignificant, therefore this variable is not included in the model. A parity plot of the experimental and modeled data is provided in Figure 4.6. Agreement is good ($R^2 = 0.9775$) implying that the total interfacial area is a strong function of the aqueous flowrate and the rate of rotation of the centrifuge.

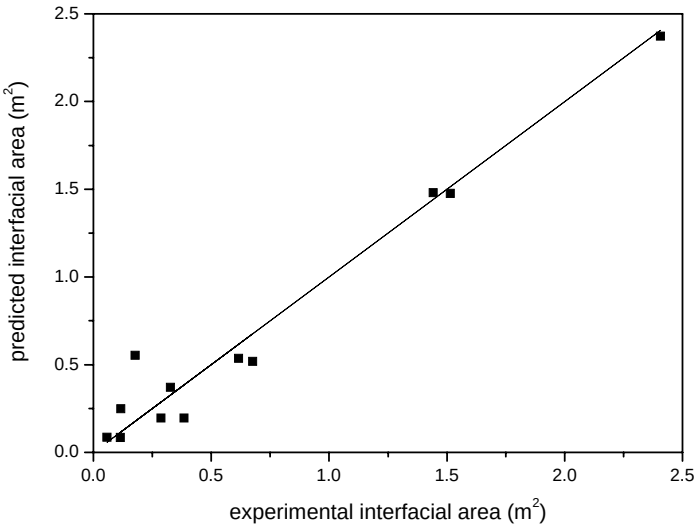

Figure 4.6. Parity plot of the experimental and modeled interfacial area.

4.5.3 Effect of the operating variables on the total interfacial area

In Figure 4.7, the effect of the rotational speed of the centrifuge on the interfacial are is provided. The interfacial area shows a clear maximum at 40-50 Hz and is reduced considerably at lower and higher centrifugal speeds. To explain this pronounced effect, the mechanisms of both mixing and separation in the CINC devices should be considered. The observed total interfacial area is expected to be a function of the extent of mixing in the annular zone, affecting the average drop size, and the droplet settling velocity in the centrifuge zone, that will determine the volume of the dispersed phase in the centrifugal zone.

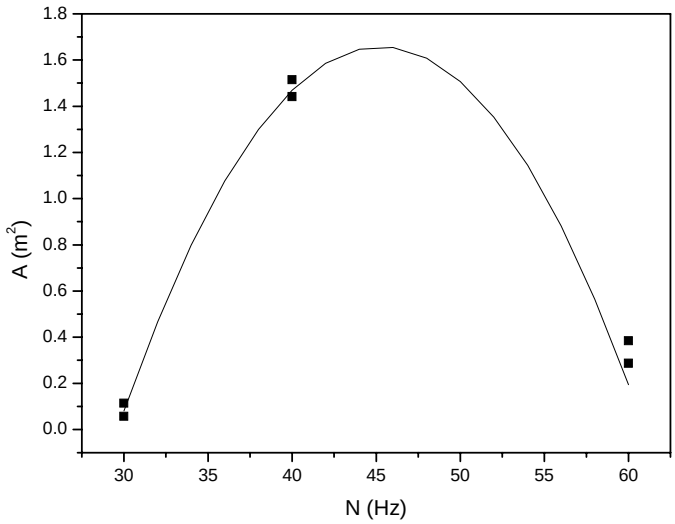

Figure 4.7. The total interfacial area versus the rate of rotation of the centrifuge at constant aqueous flowrate of 30 mL/min. Dots: experimental, line: Eq. 4.20.

The extent of mixing in the annular zone is expected to be intensified at increasing rate of rotation. This will result in a lowering of the average drop size in the dispersion and an increase in the interfacial area. However, we clearly see that this explanation only holds for rotor speeds below 40-50 Hz. Apparently, another mechanism is operative, which leads to a reduction in the interfacial area when further increasing the rotor speed. This effect is likely related to the dynamics in the centrifugal zone. Three different zones are distinguishable in the centrifuge, one with the lighter of the two liquid phases, one with the heavier phase and a dispersed zone (Figure 4.8). Besides the annular zone, the latter zone also contributes to the interfacial area in the CINC. The volumes of the various zones in the centrifuge are expected to be a function of the rate of rotation.

.

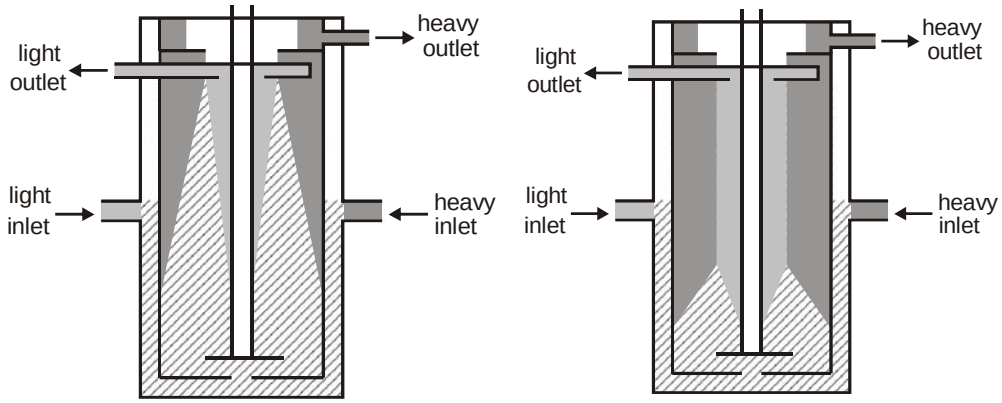

Figure 4.8. Cross-sectional view on the CINC for a low (left) and a fast rotational speed (right) of the centrifuge. Hatched: dispersion, darker gray: heavy phase, lighter gray: light phase

To gain insights in the volumes of the individual zones in the centrifuge, the settling velocity of individual drops will be considered. For centrifugal settlers such as in the CINC, the settling velocity is given by equation 4.21[17].

$$v_{S,CINC} = \frac{d_d^2(\rho_d - \rho_c)\varpi^2 r}{18\mu_c} \tag{4.21}$$

The settling velocity is thus proportional to the difference in density and the angular acceleration, and proportional to the squared drop diameter. Due to the proportionality of the settling velocity with the angular momentum, we can expect that the volume of the dispersed phase in the centrifuge will be reduced considerably at high rotational speeds. This reduction in the volume of the dispersed phase at increasing rotational speeds most likely accounts for the observed reduction in total interfacial area at higher rotor speeds. Apparently, in the range below 40-45 Hz, reduction of the average drop size at increasing rotational speeds leading to higher interfacial areas has more impact than a reduction of the volume of the dispersed zone in the centrifuge.

The effect of the aqueous flowrate on the interfacial area is best visualized by plotting the total interfacial area at constant rate of rotation of the centrifuge versus the flowrate of the aqueous phase. A typical example is given in Figure 4.9.

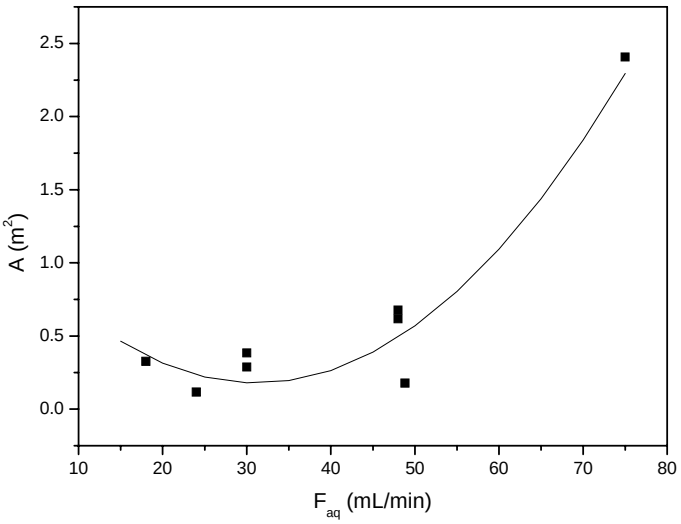

Figure 4.9. Total interfacial area versus the aqueous flowrate at constant rate of rotation of 60 Hz. Dots: experimental, line: Eq. 4.20.

The total interfacial area increases strongly at higher aqueous flowrates. The maximum experimentally observed total interfacial area was 2.41 m^2 at an aqueous flowrate of 75 mL min^{-1}. This effect is best explained by considering the amount of dispersed phase in the centrifugal zone. (Figure 4.8). At higher liquid velocities in the centrifuge, an increase in the volume of the dispersed zone and thus the interfacial is expected. Further enlargement of the interfacial area by further increasing the aqueous liquid flow rate is limited by the separation capacity. At too high flowrates, quantitative separation of the two immiscible liquids is not possible.

It was experimentally observed that the organic flowrate has no significant effect on the total interfacial area. This observation suggests that the organic phase is the continuous phase and the water phase the dispersed phase. Further experiments with a modified CINC-V02, including electrodes to measure the conductivity, are in progress to confirm this statement.

4.5.4 Determination of the specific interfacial area

For comparability, the interfacial area of a liquid-liquid system is commonly expressed in terms of specific interfacial area (m^2/m^3 reactor volume or m^2/m^3 dispersion). For the CINC, the volume of the dispersion is not known quantitatively. However, information on the liquid hold-up as well as the geometrical volume of the reactor is available. Therefore, the specific interfacial area is expressed per m^3 total liquid volume in the reactor. The total liquid holdup has been determined experimentally at $1.8 \cdot 10^{-4}$ m^3, essentially independent of the liquid throughputs. On the basis of these data and the experimentally determined total interfacial area (A), the specific interfacial areas as a function of process conditions are determined (Table 4.2).

Table 4.2. Experimentally determined specific interfacial areas as a function of process conditions.

Exp.	A (m^2)	a_L (m^2/m^3 total liquid volume)
1	0.11	$6.3 \cdot 10^2$
2	0.057	$3.2 \cdot 10^2$
3	1.51	$8.4 \cdot 10^3$
4	1.44	$8.0 \cdot 10^3$
5	0.12	$6.4 \cdot 10^2$
6	0.33	$1.8 \cdot 10^3$
7	0.38	$2.1 \cdot 10^3$
8	0.29	$1.6 \cdot 10^3$
9	0.68	$3.8 \cdot 10^3$
10	0.62	$3.4 \cdot 10^3$
11	2.41	$1.3 \cdot 10^4$
12	0.18	$9.9 \cdot 10^2$

The specific interfacial area in the CINC ranged from $3.2 \cdot 10^2$ to $1.3 \cdot 10^4$ m^2 per m^3 liquid volume, which is comparable to those reported for CSTR's[12,18] and much larger than, for example a spray or packed column[19] or a type of impinging jet reactor[20,21].

4.5.5 Validity of reaction regime

The calculation of the total interfacial area is only justified in case the reaction takes place in the fast regime, thus $2 < Ha < E_{A\infty}$. Calculation of the Hatta number is though, not possible, because the mass transfer coefficient $k_{L,A,aq}$ is not known for the CINC. Therefore the guidelines presented by Trambouze, Van Landeghem and Wauquier[22] for mass transfer coefficients in liquid-liquid systems were used to estimate the range for the values of the mass transfer coefficients of A in the CINC.

For diffusion coefficients ranging from $D_{min} = 1 \cdot 10^{-9}$ to $D_{max} = 5 \cdot 10^{-9}$ m^2/s, the liquid mass transfer coefficient typically has values between $k_{L,min} = 5 \cdot 10^{-5}$ to $k_{L,max} = 5 \cdot 10^{-4}$ m/s. However, the diffusivity of butyl formate ester in concentrated sodium hydroxide solutions is much lower and in the order of 10^{-11} m^2/s, and therefore typical mass transfer coefficients are also expected to be much less than $5 \cdot 10^{-5}$ to $5 \cdot 10^{-4}$ m/s. An estimation of the range of $k_{L,A,aq}$ values is obtained using Eq. 4.22 and a D_A of 10^{-11}:

$$\frac{D_A}{D_{\max}} \cdot k_{L,\min} < k_{L,A,aq} < \frac{D_A}{D_{\min}} \cdot k_{L,\max} \qquad (4.22)$$

With the range of $k_{L,A,aq}$ values available, the Hatta numbers may be calculated using Eq. 4.6. For all experiments, the minimum and maximum value for Hatta and $E_{A\infty}$ are listed in Table 4.3. It may be concluded that all reactions were performed in the fast regime ($2 < Ha < E_{A\infty}$) and that the relation $E_A = Ha$ was valid.

Table 4.3. The minimum and maximum Hatta number and $E_{A\infty}$ values for each experiment

Exp.	Ha_{min} (-)	Ha_{max}(-)	$E_{A\infty}$ (-)
1	6.5	323	381
2	6.5	325	402
3	7.6	382	2016
4	7.6	380	1971
5	7.5	373	1055
6	7.6	381	1063
7	7.4	371	1315
8	7.5	375	1338
9	7.3	366	1108
10	7.4	369	827
11	6.9	343	761
12	7.9	395	1127

4.6. Conclusions

The specific interfacial area in the CINC V02 integrated mixer/separator was determined as a function of process variables using the chemical reaction method. The liquid flowrates were varied from 18 to 100 mL min^{-1} each, the rotor frequency from 30 to 60 Hz. The experimentally determined specific interfacial area was found to vary from $3.2 \cdot 10^2$ to $1.3 \cdot 10^4$ m^2 per m^3 liquid volume, which is comparable with the specific interfacial area in a CSTR. The effects of the process conditions on the interfacial area were quantified using statistical methods and agreement between model and experiments was very satisfactorily.

The rate of rotation of the centrifuge and the flowrate of the aqueous phase both have significant effects on the specific interfacial area. However, the specific interfacial area was independent of the organic flow rate, suggesting that the organic phase is the continuous phase and the aqueous phase is the dispersed phase in the CINC device. The interfacial area showed a clear maximum (2.41 m^2) at intermediate rate of rotation of the centrifuge (40 - 50 Hz), which was ascribed to several opposing effects in the centrifuge and annular zone.

The results described here will be valuable input for subsequent modeling and optimization studies for classical CINC applications like liquid-liquid separation as well as new and exiting applications in the field of combined reaction and separation.

Acknowledgement

The research was financially supported by: the Dutch Foundation for Scientific Research (NWO) through the Separation Technology program in cooperation with DSM and Organon.

4.7 Nomenclature

a	specific interfacial area, m^2m^{-3}
A_{tot}	total interfacial area
C	concentration, $kmol \cdot m^{-3}$
d	drop diameter, m
D	diffusion coefficient, $m^2 \cdot s^{-1}$
E_A	enhancement factor
$E_{A\infty}$	asymptotic enhancement factor

E_{act}	energy of activation, J $kmol^{-1}$
F	volumetric flowrate, mL min^{-1}
g	gravitational constant, m s^{-2}
Ha	Hatta number
I	ionic strength, kmol m^{-3}
J	molar flux, $kmol \cdot m^{-2} \cdot sec^{-1}$
k	mass transfer coefficient, $m \cdot s^{-1}$
$k_{1,1}$	rate of the reaction, $m^3 \bullet kmol^{-1} \bullet s^{-1}$
k_I	ionic strength reaction rate constant, $m^3 kmol^{-1}$
k_∞	preexponential constant, $m^3 \bullet kmol^{-1} \bullet s^{-1}$
m	partition coefficient
N	rate of rotation, Hz
R	rate of production, kmol s^{-1}
R	gas constant = 8315 J $kmol^{-1} K^{-1}$
T	temperature, K
V	volume, m^3
X	conversion
z	charge of ion
v_S	settling velocity, m s^{-1}

Greek letters

ε	volume fraction of total reactor volume, m^3 m^{-3}
μ	viscosity, N s m^{-2}
ρ	density, kg m^{-3}
φ_v	volumetric flowrate, m^3 s^{-1}
ω	angular velocity, rad s^{-1}

Superscripts

*	interfacial

Subscripts

aq	aqueous phase
A	component A, i.e. n-butyl formate
B	component B, i.e. ionic hydroxide
c	continuous phase
d	dispersed phase
G	geometrical
in	inlet
L	liquid

min	minimum value
max	maximum value
org	organic phase
out	outlet
R	reactor
w	water

4.8 References

[1]. Stanckiewicz, A.; Moulijn, J. A. *Re-Engineering the chemical processing plant; Process Intensification;* Marcel Dekker, Inc: New York, 2004.

[2]. Kenig, E. Y.; Gorak, A.; Bart, H. J. Reactive Separations in Fluid Systems. In *Re-Engingeering the Chemical Processing Plant; Process Intensification*, Stanckiewicz, A., Moulijn, J. A., Eds.; Marcel Dekker, Inc.: New York, 2004; pp 309-378.

[3]. Godfrey, J. C.; Slater, M. J. *Liquid-Liquid Extraction Equipment;* John Wiley & Sons: New York, 1994.

[4]. Hanson, C. *Recent Advances in Liquid-Liquid Extraction;* Pergamon Press Ltd.: 1971.

[5]. Thornton, J. D. *Science and Practice of Liquid-Liquid Extraction;* Clarendon: Oxford, 1992; Vol. 1 and 2 (two volumes).

[6]. Meikrantz, D. H.; Macaluso, L. L.; Sams, H. W.; Schardin, C. H.; Federici, A. G. US Patent 5,762,800, Jun 9, 1998.

[7]. Kraai, G. N.; van Zwol, F.; Schuur, B.; Heeres, H. J.; de Vries, J. G. *Angew. Chem. Int. Ed.* **2008,** *47*, 3905-3908.

[8]. Schuur, B.; Winkelman, J. G. M.; Heeres, H. J. Continuous enantioselective extraction of amino acids in a highly intensified centrifugal extractor. *proceedings of the International Solvent Extraction Conference ISEC 2008, Tucson, USA,* in press.

[9]. Schuur, B.; Floure, J.; Hallett, A. J.; Winkelman, J. G. M.; de Vries, J. G.; Heeres, H. J. *Org. Process Res. Dev.* **2008,** *12*, 950-955.

[10]. Tavlarides, L. L.; Stamatoudis, M. The analysis of interphase reactions and mass transfer in liquid-liquid dispersions. In *Advances in Chemical Engineering Vol. 11*, Drew, T. B., Cokelet, G. R., Hoopes, J. W., Vermeulen, T., Eds.; Academic Press: New York, 1981; pp 199-273.

[11]. Watarai, H.; Cunningham, L.; Freiser, H. *Anal. Chem.* **1982,** *54*, 2390-2392.

[12]. van Woezik, B. A. A.; Westerterp, K. R. *Chem. Eng. Proc.* **2000,** *39*, 299-314.

[13]. Schuur, B.; Kraai, G. N.; Winkelman, J. G. M.; Heeres, H. J.

[14]. Westerterp, K. R.; van Swaaij, W. P. M.; Beenackers, A. A. C. M. *Chemical Reactor Design and Operation;* Wiley: Chichester, 1987.

[15]. Onda, K.; Takenchi, H.; Fujine, M.; Takanashi, Y. *J. Chem. Eng. Jpn.* **1975,** *8*, 30-34.
[16]. Wilke, C. R.; Chang, P. *AIChE J.* **1955,** *1*, 264-270.
[17]. Perry, R. H.; Green, D. W.; Maloney, J. O. *Perry's Chemical Engineers' Handbook;* 7th ed.; McGraw-Hill: New York, 1997.
[18]. Santiago, M. D.; Trambouz, P. *Chem. Eng. Sci.* **1971,** *26*, 29-38.
[19]. Puranik, S. A.; Sharma, M. M. *Chem. Eng. Sci.* **1970,** *25*, 257-&.
[20]. Dehkordi, A. M. *AIChE J.* **2002,** *48*, 2230-2239.
[21]. Dehkordi, A. M. *Ind. Eng. Chem. Res.* **2002,** *41*, 4085-4093.
[22]. Trambouze, P.; Landeghem, H. v.; Wauquier, J. P. *Chemical Reactors;* Editions Technip: Paris, 1988.

Chapter 5

Hydrodynamic Studies in a Centrifugal Contactor Separator; Liquid Hold-up, Residence Time Distribution, Phase behavior and Drop Size Distributions

Boelo Schuur; Gerard N. Kraai; Jozef G. M. Winkelman; Hero J. Heeres*

to be submitted

Abstract

Liquid hold-up, residence time distributions (RTD), drop size distributions and conductivity measurements to determine the continuous phase were carried for various L-L systems in a centrifugal contactor separator (CCS) of the type CINC V02. The total liquid hold-up of both liquid phases were determined for water-heptane (293 K < T < 318 K). The aqueous hold-up at various flow rates ($10 < F_{aq} = F_{org} < 50$ mL/min) increased from 118 at low flow rates to 122 mL at the highest flow rate, the heptane hold up from 41 to 55 mL. The hold-ups in the centrifuge alone were determined at 294 K for four binary systems, water - heptane, water - toluene, water - 1-octanol and water - dichloroethane and were shown to be essentially independent of the rotor frequency and flow rates. The RTD of the liquid phases was studied at 294 K for several aqueous-organic solvent combinations (heptane, toluene, 1-octanol, and dichloroethane). At all experimentally tested configurations (low mix/high mix option, flow rates and rotational frequencies (30-60 Hz)) the macro-mixing pattern of both phases was close to plug flow. Drop size distribution measurements using a FBRM probe for various solvent combinations showed that the Sauter mean drop sizes of the dispersed phase are between 30 and 600 micron. Phase inversion was observed for several solvent combinations (e.g. water - 1-octanol, water - dichloromethane and water - dichloroethane) and was found to be perfectly reversible.

Keywords: Process Intensification, Centrifugal Contactor Separator, Hydrodynamics, Residence Time Distribution, Phase Inversion, Drop Size Distribution

5.1. Introduction

Process intensification (PI) is a powerful concept to replace large, energy intensive equipment or processes with smaller plants that combine multiple operations in single, highly integrated devices[1]. Typical separations that may be integrated with reactions in a single device are distillation[2], chromatography, adsorption or extraction[3,4]. For the latter, the integration of reaction and separation is not only advantageous with respect to energy and investments costs but also for the efficiency and/or the selectivity of the extraction process [5-7].

A very attractive device to integrate chemical reaction and separation for liquid-liquid systems is the Centrifugal Contactor Separator (CCS). The CCS has been developed at the Argonne National Laboratory in the USA. An improved version was patented under the trade name CINC by Costner Industries Nevada Corporation[8]. The CINC basically consists of a rotating hollow centrifuge in a static house. The liquid(s) enter the device in the annular zone between the static wall and the rotating centrifuge, where they are intensely mixed. Subsequently, they are transferred into the centrifuge where separation occurs by the action of centrifugal forces. A low mix configuration may be used to avoid direct contact of the entering liquids with the centrifuge. Also, one of the liquids can be introduced directly into the centrifuge through the bottom plate of the device. These different configurations are depicted in Figure 5.1.

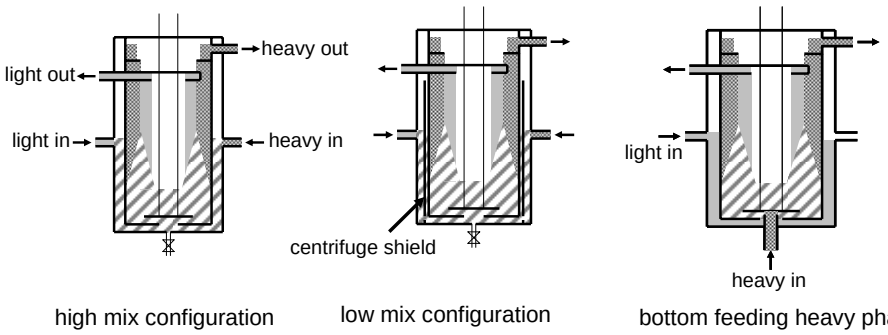

Figure 5.1. Sketch of the CINC in different operation modes. Left: high mix, middle: low mix with shielded centrifuge, right: heavy phase fed directly in centrifuge through bottom. Hatched: dispersion. Darker gray: heavy phase. Lighter gray: light phase.

The CCS was initially developed for clean up of nuclear waste[9]. Applications such as oil-water separation and liquid-liquid extraction were claimed in a patent issued by Meikrantz[8]. Open source literature in which the CCS is used for combined chemical

reaction and integrated separation is scarce and only devoted to reactive extractions[10-13]. With the recent attention for process intensification and integration[1,2,4], we started our investigations in the PI field using the CCS for continuous biphasic (bio)catalysis[14] and enantioselective liquid-liquid extraction[15].

For reactor modeling purposes, detailed information is required on hydrodynamic properties such as the liquid hold-ups, (specific) interfacial areas, mixing and phase behavior. Although the use of CCS equipment has been reported extensively[16], only a few studies on the hydrodynamics of CCS equipment have been published. Schuur *et al.* described the interfacial area in the CINC[17], and Wardle *et al.* studied the free surface flow to describe the flow pattern in the annular zone[18]. Here we present the results of hydrodynamic studies in a typical CCS device, the CINC V02. This table-top device has a geometric volume of 322 mL and may be operated at a maximum throughput of 1.9 L/min. Valuable information to be used as input for reactor modeling studies as well as fundamental insights in the functioning of the apparatus was obtained.

5.2. Experimental

5.2.1 Chemicals

Water, purified by reverse osmosis, was applied for all experiments. 1,2-Dichloroethane (99%), and 1-octanol (98%) were obtained from Sigma-Aldrich, potassium dihydrogen phosphate (*pa*) and di-sodium hydrogen phosphate dodecahydrate (*pa*) from Merck, n-heptane (99%) and acetophenenone (99%) from Acros, chloroform from Labscan ltd, sodium chloride (99.9%) from Akzo Nobel and dichloromethane (99.95%) and toluene (99.7%) from Chemproha. 3,5-Dinitrobenzoyl-(*R*),(*S*)-leucine and O-(1-t-butylcarbamoyl)-11-octadecylsulfinyl-10,11-dihydro-quinine were kindly provided by DSM Research.

5.2.2. Equipment and procedures

5.2.2.1 Hold-up

The liquid hold-up determinations were carried out in a stainless steel CINC V02 obtained from CINC Industries (Carson City, Nevada USA). The V02 is a Table top version with a maximum total throughput of 1.9 L min^{-1} (3.2×10^{-5} m^3s^{-1}) and maximum rotational frequency of 100 Hz. Both liquids were transferred to the reactor using Verder VL1000

Control peristaltic tube pumps equipped with double pump heads (1.6 × 1.6 × 8R). The supply and receive vessels were made of glass. The total liquid hold-ups of both phases in the system were determined using 4 Mettler PM4000 balances connected to a PC. The mass of the supply and receive vessels were monitored using Labview® software (National Instruments). The experiments were performed at 293 < T < 318 K in the low-mix configuration (see Figure 5.1, middle). A measurement was initiated by starting the rotor and the pump of the heavier of the two liquids. After the heavy phase outlet started running, the light phase pump was started. The total hold-ups were obtained from weight measurements of the supply and receive vessels. By subtracting the steady-state hold-up in the tubes from the measured values, the actual hold-up in the device could be determined.

The hold-ups in the centrifuge were determined by performing an experiment with the selected solvent combination. After four average residence times of both phases, steady state was ensured[15]. For determination of the residence time, a total liquid hold-up of 180 mL was assumed (*vide infra*)[15]. Then, the pumps were shut down and the annular volume was drained by opening the valve in the bottom of the annular zone. Subsequently, the centrifuge was stopped and the remaining liquid in the device (centrifuge) was removed. The volumes of both phases were determined using a measuring cylinder. Measurements were performed for all three configurations (Figure 1).

5.2.2.2 RTD

The RTD measurements were carried out with the device described above except that the aqueous reactor inlet and outlet were equipped with conductivity cells (Vernier) connected to a PC via a Coachlab II (CMA) interface. The organic phase inlet and outlet were equipped with 2 S8D31D UV LED's (Roithner-lasertechnik) and monitored using UVB-sensors (Vernier). The RTD curves were determined for 4 different CCS configurations. In the standard configuration (high mix), the liquids enter on the sides as depicted on the left in Figure 5.1 and are in direct contact with the rotating centrifuge. In the "low mix" configuration, the rotating centrifuge is shielded for the entering liquids, see Figure 5.1 middle. In the other two configurations, either the aqueous phase or the organic phase is fed via a tube through the bottom hole directly into the centrifuge, see Figure 5.1 right. Feeding to the CINC was started and the device was allowed to reach steady state (four average residence times, *vide infra*). The RTD curves were determined at 294 K by measuring the response to a step in the inlet. Flow rates were varied from 20 to 50 mL/min per phase, the rotational frequency from 30 to 60 Hz. For the aqueous phase, NaCl (typically 15 g/L) was used as the tracer. For the organic phase acetophenone (typically 0.3-2 vol%, depending on the solvent) was used. The step responses were measured every 0.33 s using UV absorbance (organic phase) and conductivity (aqueous phase).

5.2.2.3 Drop size distributions

For determination of the drop size distributions a CS50 equipped with a Perspex window purchased from CINC Solutions (Doetinchem, The Netherlands) was used. The internal geometry of the CS50 is identical to that of the CINC V02. The drop size distributions were determined with Lasentec® S400A focused beam reflectance measurement (FBRM) equipment with a PI 14/206 probe (Mettler Toledo). The tip of the probe was positioned between the vanes of the high mix bottom plate under an angle of 45°, pointing into the direction of the flow, see Figure 5.2.

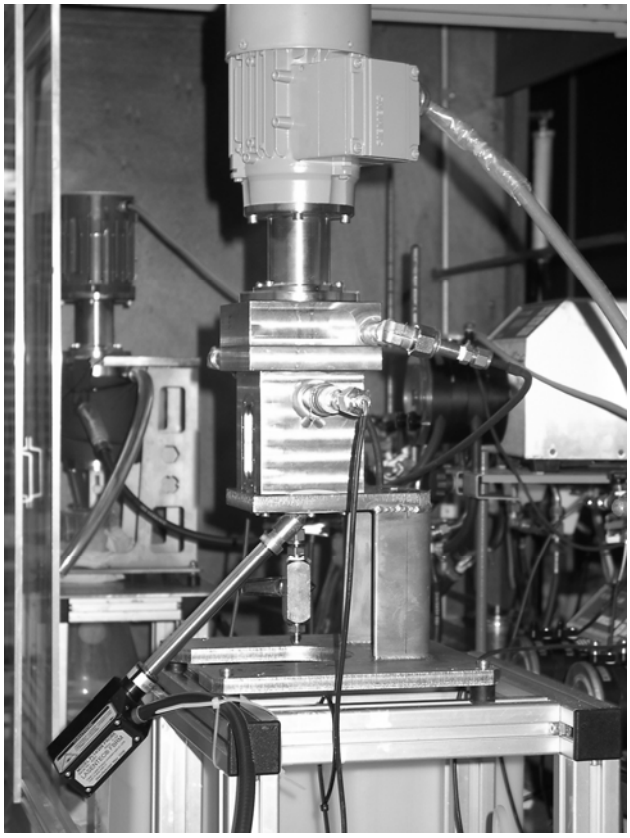

Figure 5.2. Photograph of the CS50 showing the position of the tip of the FBRM probe in the bottom plate.

The FBRM uses laser light to measure the reflectance of drops and converts this to chord size distributions. The chord size distribution were corrected to actual droplet size distributions by applying a correction factor. For perfectly round droplets and assuming that the system is intensely mixed [19], the average droplet size is 79% of the average chord size. Measurements were done at 294 K at steady-state, flow rates were varied from 10 to 50 mL/min per phase, and the rotational frequency from 30 to 50 Hz.

5.2.2.4 Conductivity measurements to determine the continuous phase

A modified CS50 with a Perspex window was used for determination of the continuous and dispersed phase. The Perspex window was equipped with copper electrodes. An electronic circuit with a 10V potential was connected to the two lowest copper electrodes and a 10kΩ resistance in series. The partial resistance over the liquid in the annular zone of the CCS was measured using a voltmeter connected to a PC via a Coachlab II interface (CMA). The experiments were carried out at 294 K at steady-state, flow rates were varied from 20 to 80 mL/min per phase, and the rotational frequency from 30 to 50 Hz.

5.3. Theory

5.3.1 Residence Time Distribution Functions

The residence time distribution (RTD) gives valuable information on the overall flow pattern of each liquid phase in the CCS. The CCS may be spatially separated into three distinct zones. The liquids enter the device in the annular zone, where intense mixing occurs. In the centrifuge, both phases are settled. Subsequently, the liquids pass through a set of collector ring channels in the upper part of the device. The overall RTD of the CCS will be determined by the flow pattern in each of these zones.

Experimentally, the response of the system to a step disturbance in the feed was measured at both the entrance and the exit of the CCS. These concentration profiles were normalized to obtain an F-curve (Eq. 5.1).

$$F(t) = \frac{C(t)}{C_{step}} \tag{5.1}$$

The F-curves were modeled using an empirical relation (Eq. 5.2).

$$F(t) = \frac{e^{pt^q}}{e^{pt^q} + ue^{vt^w}} \tag{5.2}$$

The F-curves were transformed to E-curves using Eq. 5.3.

$$E(t) = \frac{dF(t)}{dt} \tag{5.3}$$

The E(t)-curves were corrected for inlet effects using deconvolution to obtain the E-curve of the CCS, E_{CCS} (Eq. 5.4)

$$E_{out}(\tau) = \int_0^t E_{in}(t)\, E_{CCS}(t-\tau)dt \tag{5.4}$$

With the RTD curves of the CCS available, the mean residence time and the hold up of the phase in the CCS were determined using Eq. 5.5 and 5.6.

$$t_m = \int_0^\infty tE_{CCS}\, dt \tag{5.5}$$

$$V_k = t_m F_k \qquad (k = aq, org) \tag{5.6}$$

The empirically modeled RTD curves of the CCS were compared with the tanks-in-series model. Hereto, the model parameter N (number of stages) was calculated from the maximum value of the E_{CCS} curves using[20]:

$$E_{CCS,\max} = \frac{N(N-1)^{N-1}}{t_m(N-1)!}e^{-(N-1)} \tag{5.7}$$

5.3.2 Drop Size Distributions in L-L systems

A key parameter for the modeling of L-L reactors is the specific interfacial area, defined as[21]:

$$a = \frac{6\varepsilon}{\overline{d_{vs}}} \tag{5.8}$$

Here, ε is the fraction of the dispersed phase and $\overline{d_{vs}}$ is the Sauter mean drop size, defined as[19]:

$$\overline{d}_{vs} = \frac{\sum_{1}^{N} n_i d_i^3}{\sum_{1}^{N} n_i d_i^2} \tag{5.9}$$

5.3.3 Phase behavior in L-L systems (dispersed versus continuous)

Experimental data on the phase behavior e.g. which phase is the continuous and which the dispersed phase and the occurrence of phase inversions are not available for CCS devices. For stirred tank reactors, the phase with the highest hold-up is usually the continuous phase[22,23]. The organic phase hold-up ($\varepsilon = V_{org}/V_{tot}$) at which phase inversion occurs is a function of the physical properties of the fluids and the power input. There is usually an ambivalent region present where both phases can be continuous[22,23]. This region is usually caused by variations in the startup procedure[24]. Liu *et al.* recently demonstrated that the ambivalence region becomes smaller when increasing the power input. At high stirring speeds ambivalence may even be absent[25].

5.4. Results and Discussion

All results discussed are obtained in the low flow regime of the equipment (< 0.1 L/min total flow). The maximum total throughput in the CINC is 1.9 L/min. For the applications of our interest (e.g. biphasic catalysis and other reactive separations), however, typically relatively low flow rates (< 100 mL/min total flow) are applied to allow for sufficient

residence times to achieve good conversions. All systems described here are aqueous - organic biphasic systems.

5.4.1 Determination of the liquid Hold-ups

The total liquid hold-up ($V_{L,\,tot.} = V_{org} + V_{aq}$) in the device as well as the individual liquid holds-ups in the centrifuge ($V_{aq,CENTR}$ and $V_{org,CENTR}$) and annular zone (V_{ANN}) were determined using two different experimental methods. The $V_{L.tot}$ was determined for a heptane-water system, the $V_{aq,CENTR}$ and $V_{org,CENTR}$ for a broader range of water-organic solvent combinations.

5.4.1.1 Total liquid hold-up for heptane-water system

The liquid hold-up of both the organic and the aqueous phase in the complete device were determined for heptane-water at $293 < T < 318$ K in the low mix configuration (Figure 5.1, middle) by weight measurement of the supply and receive vessels. By continuous monitoring the weights of the supply vessels, the mass flow into the system was determined and by monitoring the weights of the receive vessels the mass flow out of the system was determined. Combining both measurements gives the total liquid hold-up. The flow rates were varied from 10 mL/min each to 50 mL/min each and the rotational frequency was varied from 30 to 60 Hz. At 30 Hz and a flow rate of 10 mL/min for each phase, the total water hold-up (119 mL) was considerably higher than the total heptane hold-up (41 mL). The flow rate only has a small effect on the hold-ups and for instance, when increasing the flow rate to 50 mL/min for each phase, the total water hold-up in the system increased slightly from 119 to 123 mL and that of heptane from 41 to 55 mL.

This remarkable small effect of the flow rates on the liquid hold-up can be rationalised by taking a closer look at the hold-up in the annular zone and the distribution of the liquids in the centrifuge.

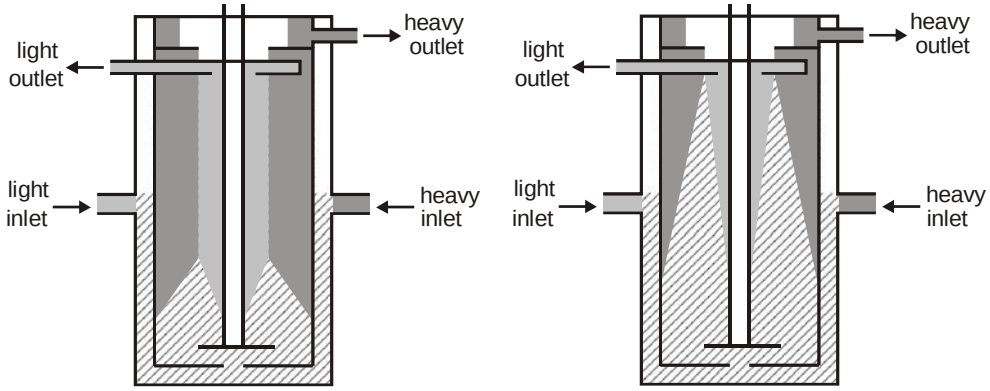

Figure 5.3. Schematical representations of the CCS for different conditions. Right: high flow rates,. Left: low flow rates. Dark grey: heavy phase only, light grey: light phase only, hatched: dispersed zone.

In the high-mix configuration using the CS50 with a transparant window, it was determined visually that the total hold-up of both phases in the annular zone was independent on the flow rates in the investigated range. Apparently, the vanes at the bottom plate cause a centrifugal pump force into the centrifuge that is at low flow rates stronger than the supply. As a result, the liquid level is under these conditions constant at the level just enough to feed the centrifuge.

In Figure 5.3 the predicted liquid distribution in the centrifuge is provided as a function of the flow rates. The profile at our experimental conditions (below 50 mL/min for each phase) is likely best described by the left representation. This is rationalized by considering the flooding limit of the device, which is known to be about 1900 mL/min. Thus, it is likely that below 100 mL/min total flow the phases are separated quickly after entering the centrifuge. As a result, the liquid hold ups in the centrifuge are expected to be relatively independent of the flow rates when working at low flow rates.

5.4.1.2 Liquid hold-up in the centrifuge for several solvent systems

To check the reasoning above, the liquid hold-up of both phases in the centrifuge ($V_{aq,CENTR}$ and $V_{org,CENTR}$) was determined for a number of aqueous-organic solvent systems with heptane, toluene, DCE, DCM, chloroform and octanol as the organic solvents. The hold-ups in the centrifuge were determined for both the high mix and low mix configurations (the centrifuge hold-up was found to be independent on the configuration). An experiment

in the CINC was initiated with the pre-determined settings and allowed to reach steady state. Subsequently, the pumps were stopped and the liquids in the annular volume were purged. Then the centrifuge was stopped and the liquids in the centrifuge were collected and measured. The results for all measurements are given in Table 5.1.

Table 5.1. Measured V_{CENTR} for various aqueous-organic systems[a]

Organic solvent	$V_{aq,CENTR}$ ***(mL)***	$V_{org,CENTR}$ ***(mL)***	$V_{total,\ CENTR}$ ***(mL)***
heptane[b]	120-130	40 - 50	165 - 175
octanol[b]	100 - 110	60 - 70	165 - 175
toluene[b]	90 - 100	70 - 80	165 - 175
DCE[c]	80 - 90	80 - 90	165 - 175
DCM[c]	70 - 80	90 - 100	165 - 175
chloroform[c]	65 - 75	90 - 100	165 - 175

[a] V_{CENTR} was determined at 294 K and found independent of the rotational frequencies
[b] organic phase lighter than water
[c] organic phase heavier than water

The total centrifugal volume was rather constant and always between 165 and 175 mL. The geometrical volume is 322 mL, thus in steady-state operation about half the geometrical volume is occupied by liquid. It thus appears that the $V_{tot,CENTR}$ is independent on operational conditions (at least for $F_{tot} \leq 100$ mL/min). This is most likely due to the quick separation in the centrifuge at these conditions (*vide supra*).
The $V_{aq,CENTR}$ and $V_{org,CENTR}$ for all solvent combinations cover a broad range (Table 5.1). The $V_{org,CENTR}$ is a function of the density, with lower density solvents leading to lower liquid hold-ups.

For the heptane-water system the $V_{L,\ tot}$ was 120-130 mL for the aqueous phase and 41-55 mL for the heptane phase. In combination with the data for the V_{centr} (Table 5.1), this allows for calculation of the liquid hold-up in the annular zone ($V_{t,\ ann.}$) By using this approach, the under these low flow conditions ($F_{tot} \leq 100$ mL/min) the liquid hold-up in the annular zone was low, i.e. approximately 10 mL. This was confirmed by visual observations using the CINC equipped with the transparent Perspex window. The liquid level in the annular zone was always just above the bottom of the centrifuge.

5.4.2 Residence Time Distribution

RTD-functions were determined experimentally at 294 K for the solvent combinations water/toluene, water/heptane, water/DCE, and water/octanol by measuring the response of a step input. A typical response is displayed in Figure 5.4.

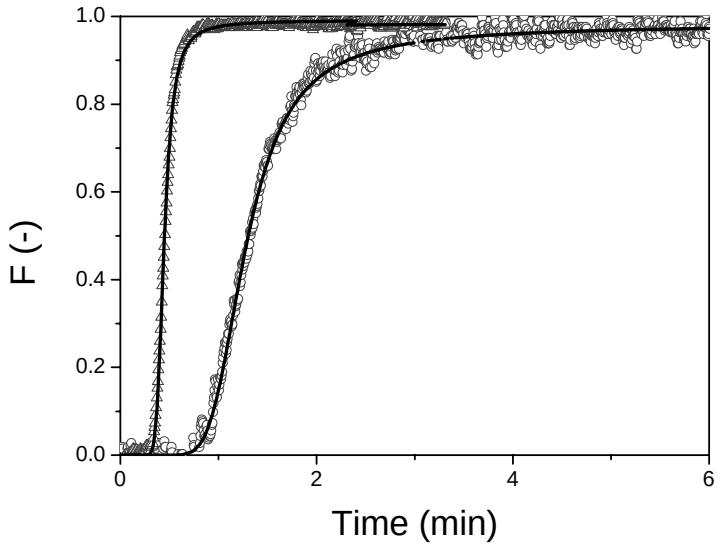

Figure 5.4. RTD-step response of toluene phase in toluene-water system, conditions: F_{org} = F_{aq}= 50 mL/min, υ = 30 Hz, high mix configuration (Figure 5.1, left). Symbols: inlet: Δ, outlet: ○. Lines are model curves.

The steepness of the experimental F-curve shows good resemblance with plug flow behavior. The curve shows, however, too much tailing to allow fitting of the full profile to the tanks in series model. The tailing is likely due to laminar flow in the collector rings, and should be disregarded when describing the mixing behavior of the zones of interest in the CCS (annular and centrifuge). To compare the maximum steepness of the F-curve with the tanks in series model, an empirical relation (Eq. 5. 2) was fit to the experimental curve. The RTD of the inlet of the step input was eliminated by numerical deconvolution. The number of tanks in series representing the mixing pattern was determined from the maximum of the normalized E-curves by using an analytical expression, Eq. 5. 7. As a typical example, the F-curves in Figure 5.4 was best represented by N = 11.

The RTD was analyzed for a number of solvent combinations (water- toluene, water-heptane, water-octanol, and water-DCE, and for the 3 configurations shown in Figure 5.1. Responses to step inputs were measured at varying rotational frequency and flow rates. The conditions for each experiment are listed in Table 5.2.

Table 5.2. Overview of RTD experimental conditions in aqueous-organic biphasic experiments

Organic solvent	*Configuration*	F_{aq} *(mL/min)*	F_{org} *(mL/min)*	*υ [Hz]*
heptane	low mix	10 - 50	10 - 50	30 - 60
toluene	low mix	30	30	40 - 60
	high mix	20 - 50	20 - 50	30 - 60
	aq bottom fed	30	30	40 - 60
	org bottom fed	30	30	40 - 60
1-octanol	high mix	20 - 50	20 - 50	30
DCE	high mix	20 - 50	20 - 50	30

For all solvents, configurations and experimental settings, the parameter N was always 8 or higher for both phases. It can therefore be concluded that the overall flow pattern in the CCS is plug flow alike for both phases.
It was also clearly shown that the overall flow pattern is not affected when changing the position of the feed, i.e. either directly into the centrifuge or in the annular zone. Thus, it can be concluded that the overall RTD pattern is heavily dominated by the centrifuge. This may be rationalized by considering that the liquid hold-up of the centrifuge is large (ca. 170 mL) compared to that of the annulary zone (ca. 10 mL), see previous section for details.

The total liquid hold-ups of the aqueous phase and organic phase may also be determined from RTD curves and the flow rates (Eq. 5. 6). The hold-ups obtained this way were in reasonable agreement with those determined independently as described in section 4.1. For example, for heptane-water under identical conditions (30 Hz, $F_{aq} = F_{org} = 40$ mL/min, low mix) the V_{aq} was 108 mL according to RTD measurements versus 120 mL for the flow experiments and the V_{org} was 60 mL for RTD versus 55 mL for the flow measurements.

5.4.3 Drop Size Distribution

The drop size distribution of the dispersed phase in the annular zone was determined at a fixed temperature (294 K) at various process conditions (solvent combination, flow rates, rotational frequency, solute(s)) using FBRM technology. For three aqueous-organic solvent

systems (heptane, toluene and DCE) the drop size distributions were studied. With the thus obtained drop size distribution, the specific interfacial area was calculated, assuming that the hold-up ratio of the liquid phases is equal to the flow ratio, which appears to be reasonable for well mixed reactors[26]. First, the effect of the flow rate ratio (F_{org}/Faq) is discussed for the system water - DCE, then the effect of rotational frequency and adding a solute to the DCE is discussed. The system heptane-water was used for an investigation on the effect of the flow rates. The subsection is concluded with a comparison of various systems.

5.4.3.1 Effect of the flow ratio on the mean drop size

For the system of pure DCE - water, the effect of the flow ratio on the drop size distribution was studied at 30 Hz. Starting at equal flow rates of 50 mL/min, the DCE flow was step wise reduced. After every reduction the system was allowed to attain steady-state. After several measurements in steady-state, the DCE flow was reduced further. The DCE flow was thus reduced to 20 mL/min and then increased again stepwise to 50 mL/min. Figure 5.5 displays the $\overline{d_{vs}}$ at a decreasing DCE flow rate. The $\overline{d_{vs}}$ increased gradually with decreasing DCE flow until 29 mL/min. At 29 mL/min (corresponding to a flow ratio F_{org}/F_{aq} = 0.58) the Sauter mean drop size suddenly increases dramatically. This increase is due to phase inversion (*vide infra*). When increasing again, the same point of inversion was found, and the drop size distributions were similar as before. The dramatic change in drop sizes when the phases were inverted was also reported by Van Woezik and Westerterp[27] for the system of butyl formate and sodium hydroxide.

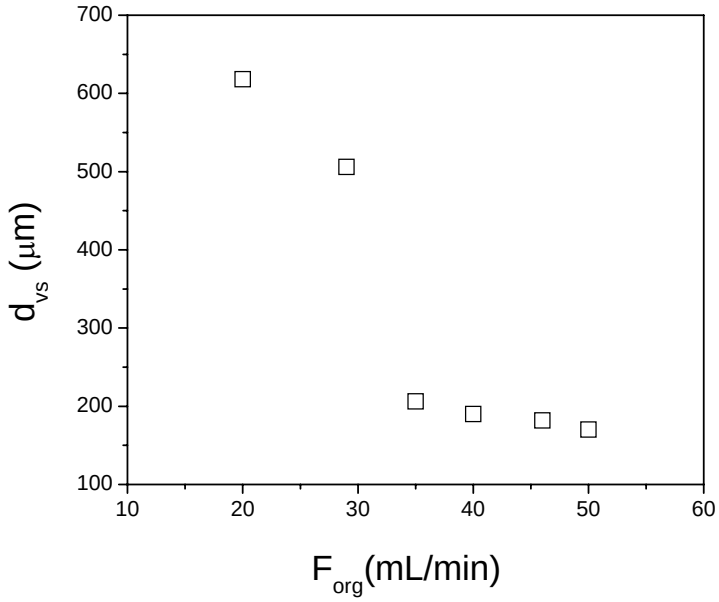

Figure 5.5. Sauter mean drop size for pure DCE and prue water at increasing organic flow rate, F_{aq} = 50 mL/min, υ = 30 Hz.

5.4.3.2 Effect of rotational frequency on the specific interfacial area

With the pure water-DCE system, the effect of the rotational frequency could not be measured, due to air bubbles that were struck in the dispersion above 30 Hz, disturbing the measurements. Therefore, a typical solvent combination that was used in a previous study on enantioselective liquid-liquid extraction of 3,5-dinitrobenzoyl-(*R*),(*S*)-Leucine (DNB-leu)[15] was used to study the effect of the rotational frequency. In this system the aqueous phase contains phosphate buffer and DNB-leu and DCE contains a cinchona alkaloid extractant (C). Figure 5.6. shows the drop size distributions for this system at different rotational frequencies.

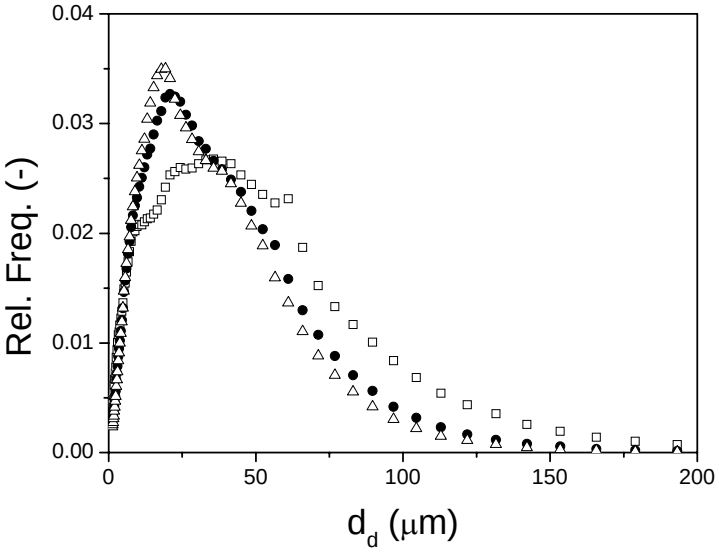

Figure 5.6. Drop size distributions at various rotational frequencies for DCE-water system containing $1 \cdot 10^{-3}$ mol/L DNB-leu (aq) and $3 \cdot 10^{-4}$ mol/L C (org). Flow rates: 50 mL/min water phase and 50 mL/min DCE phase. Symbols: Δ = 50 Hz, ● = 40 Hz, □ = 30 Hz.

Figure 5.6 shows that with increasing rotational frequency the number of small drops increases and the number of large drops decreases due to the increased shear stress.

From the experimental drop size distributions the Sauter mean drop size and the specific interfacial area were calculated using Eqs. 5.9 and 5.10. The resulting interfacial areas are displayed in Figure 5.7 for the DCE-water system with solutes DNB-leu and C at a series of rotational frequencies. With pure DCE and water only a single value at 30 Hz could be obtained because at higher rotational frequency air bubbles disturbed the measurements. The specific annular interfacial area is about a factor 2 smaller when the solutes are not present. Probably the solutes cause the interfacial tension to decrease, as there is a positive correlation between $\overline{d_{vs}}$ and the interfacial tension[22].

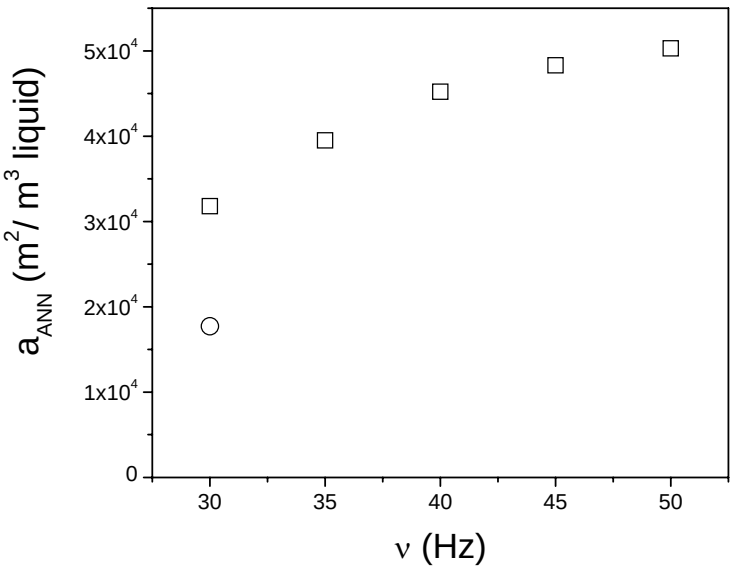

Figure 5.7. Specific interfacial area in the annular zone for the system DCE-water at 50 mL/min for both flows. Symbols: ○ pure DCE and water , □: DCE and water with the solutes DNB-leu and C.

The specific interfacial area in the annular zone is very large compared to the values of 10^2 - 10^4 $m^2/(m^3$ liquid) typically observed in stirred tank reactors [27,28] due to the small mean bubble size, as discussed above. The increase in specific interfacial area with increasing rotational frequency levels off as a result of a balance between break-up of larger drops and coalescence of smaller drops. Probably, above a certain rotational frequency the drop size distribution is not a function any more of the rotational frequency as the rates of break-up and coalescence converge. This could unfortunately not be tested, as above 50 Hz, air bubbles were struck in the dispersion, disturbing the measurements.

5.4.3.3 Comparison of different systems at 30 Hz

In Figure 5.8. the $\overline{d_{vs}}$ is displayed for several systems that were investigated, including the organic solvent toluene with several solutes and DCE with and without the solutes as above. When acetophenone is present in toluene, the $\overline{d_{vs}}$ is larger than for the pure

solvents. Apparently, acetophenone causes a small increase in interfacial tension. Addition of the phosphate buffer salts or sodium chloride in concentrations of up to 0.15 mol/L did not affect the $\overline{d_{vs}}$ significantly. Addition of DNB-leu to the toluene-water system, however, causes a dramatic reduction in the $\overline{d_{vs}}$. These observations seem to indicate that also in the DCE-water system DNB-leu causes the reduction in $\overline{d_{vs}}$ and not the compound C.

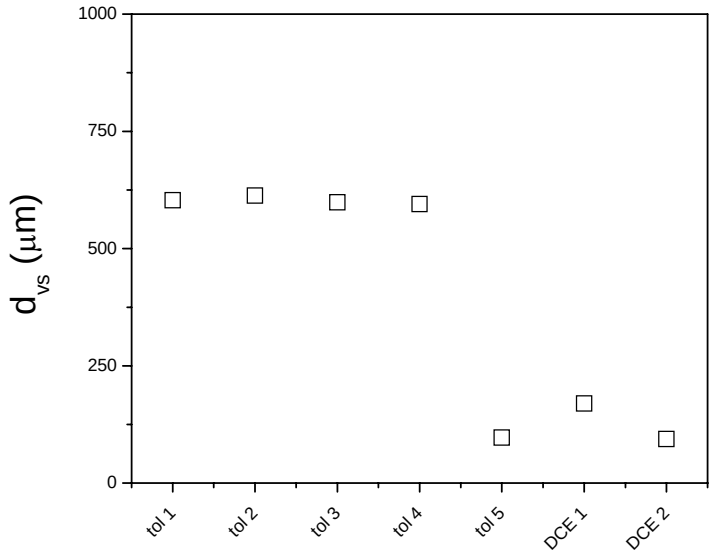

Figure 5.8. Sauter mean drop size for toluene-water and DCE-water systems at equal flows of 50 mL/min and 30 Hz. Tol 1 = pure toluene and pure water, tol 2 = toluene with 0.5% (vol) acetophenone, tol 3 and tol 4 = 0.1mol/L NaCl and phoshpate buffer, respectively in the aqeuous phase and pure toluene. Tol 5 and DCE 2 contain DNB-leu. DCE 1 is pure DCE and pure water.

5.4.3.4 Effect of flow rates

The system heptane - water with several solutes present, used in a previous study on enzymatic biphasic catalysis [14], was used for investigating the effect of the flow rates at 40 Hz. The results are displayed in Figure 5.9

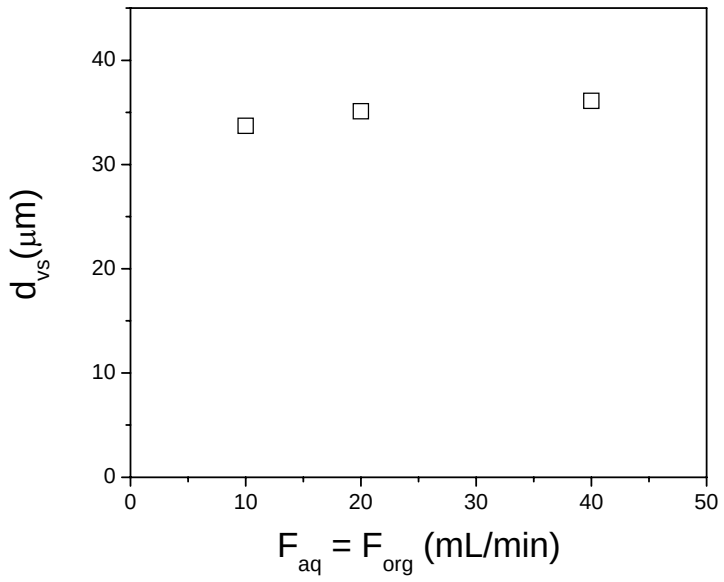

Figure 5.9. Sauter mean drop size for heptane-water with solutes butanol, oleic acid and phosphate buffer at equal flows and 40 Hz.

With the heptane - water system including the solutes butanol and oleic acid, the maximum specific annular interfacial area was calculated as $8.91 \cdot 10^4$ $m^2/(m^3$ liquid). This is almost 6 times higher than the upper values reported for stirred tanks[27,28]. Due to this very high specific interfacial area in the annular mixing zone, the overall specific interfacial area over the complete CCS is comparable to that of a stirred tank, eventhough the flow pattern in the centrifuge resembles plug flow.

5.4.4 Phase Behavior

For a number of aqueous - organic biphasic systems (water with DCE, DCM, chloroform, octanol, heptane and toluene) the continuous phase was determined at 294 K and varying flow rates and rotational frequencies using conductivity measurements as described in section 5.2.

In the case of toluene-water, toluene was the continuous phase over the entire operating window ($0.25 < R = F_{org}/F_{aq} < 4$, and $30 < \upsilon < 50$), while n-heptane and chloroform were

always disperse. For DCM, DCE and 1-octanol phase inversion was observed in the operating window. At high values of R, the organic phase was continuous whereas the opposite was observed at low values of R. It was also found that the phase inversion was a function of the rotational frequency. Figure 5.10 shows the R-lines at which the phase inversions were observed, it is assumed that in the low flow range of operation (F_{tot} < 100 mL/min) the flow ratio at which phase inversion takes place is not affected by the total flow rate.

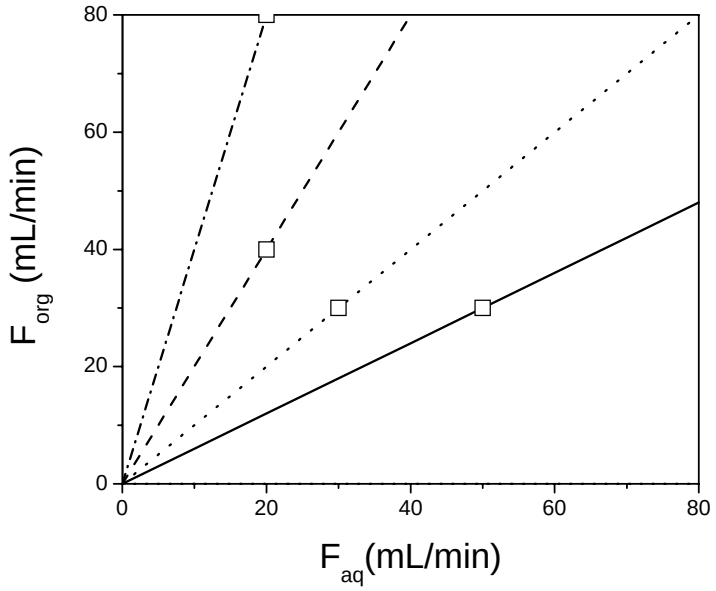

Figure 5.10. Phase inversion lines: (—): DCE 30 Hz, (…): DCM 50 Hz, (---): 1-octanol 50 Hz, (-.-): DCM 30 Hz. Symbols: experimental.

For 1-octanol at 30 Hz, no inversion was observed and the aqueous phase was continuous over the entire operating window, while at 50 Hz, at 20 mL/min aqueous flow and 1-octanol flows ≥ 40 mL/min, the octanol phase was continuous. For DCM at 30 Hz, only at R = 4 (F_{org} = 80, F_{aq} = 20 mL/min) DCM became the continuous phase, while at 50 Hz, DCM was continuous already above R = 2 (F_{org} = 40, F_{aq} = 20 mL/min). Thus, inversion from a continuous aqueous phase to a continuous organic phase is easier at higher rotational frequency, i.e. higher power input. This observation is in line with the results of Liu *et al.*[25], who found that the ambivalence region becomes smaller at increasing power input. Thus, at a low power input, the ambivalence region is large and when starting with the

aqueous phase as continuous phase, the fraction hold-up of the organic phase should become very high before phase inversion is observed. At a high power input, the ratio at which the inversion is observed is much lower. In the case of 1-octanol, the inversion point at 30 Hz even falls outside the operating window, while at 50 Hz phase inversion is observed at R = 2. For DCM, both at 30 and at 50 Hz, phase inversion is observed, and in line with the argumentation the inversion at 30 Hz takes place at a higher flow ratio than at 50 Hz.

Numerous correlations have been proposed for prediction of the hold-up fraction organic phase at which phase inversion should be observed[22]. Often they are verified only for a limited number of systems and conditions in stirred tanks. Frequently used relations are those proposed by Luhring and Sawistowski. They proposed for inversion from a continuous aqueous phase to a continuous organic phase[22]:

$$\varepsilon_{org,IO} = 0.160 + 6.0 \cdot 10^{-5} We_I \tag{5.10}$$

And for inversions from a continuous organic phase to a continuous aqueous phase[22]:

$$\varepsilon_{org,IA} = 0.470 + 2.0 \cdot 10^{-5} We_I \tag{5.11}$$

The impeller Weber number in these equations is defined as[22]:

$$We_I = \frac{\rho_c \nu^2 d_I^3}{\sigma} \tag{5.12}$$

The Eqs. 5.10 and 5.11 were developed for impeller systems. To test their applicability the CCS used here, we considered the inversion from a continuous aqueous to a continuous organic phase at a constant rotational frequency of 30 Hz for various organic components. For these cases, according to Eq. 5.10, the inversion hold-up should be proportional to $1/\sigma$. Table 5.3 lists literature values of the interfacial tensions for the tested solvents and the experimentally observed phase inversion flow ratios.

Table 5.3
Interfacial tension of water-organic solvent systems at 20°C and observed inversion flow ratios R = F_{org}/F_{aq} at 30 Hz.

organic solvent	*reference*	*σ [mN/m]*	*inversion flow ratio, R*
heptane	[29]	51.4	> 4
toluene[a]	[30]	36.1	< 0.25
DCM	[31]	27	4
DCE	[32]	23	0.58
chloroform[a]	[30]	23	> 4
1-octanol	[33]	8.19	> 4

[a]values reported at 25°C

If a modified form of Eq. 5.10 would be applicable for phase inversion to the organic phase, at an increasing R, the inversions for the various solvents should take place in the order: heptane, toluene, DCM, DCE, chloroform, 1-octanol. It follows from Table 5.3, that this order is not followed for the tested solvents and that applicability of the relation is not likely.

Recently, a simple prediction rule was proposed by Yeo *et al.*[34]:

$$\frac{\varepsilon_{org}}{1-\varepsilon_{org}} = \frac{\overline{d_{vs\ O/A}}}{\overline{d_{vs\ A/O}}} \tag{5.14}$$

Here, O/A means a continuous aqueous phase and A/O means a continuous organic phase. In the derivation of this simple prediction rule, it was assumed that the only interactions of importance are the liquid-liquid interactions and interactions with the reactor wall and/or the stirrer could be neglected. For the system DCE-water, a perfectly reversible inversion was observed at a flow ratio R = 0.58. Assuming a hold-up ratio equal to the flow ratio, valid for well mixed systems[26], this flow ratio corresponds to an organic phase hold-up fraction of 0.37. The experimentally obtained Sauter mean drop sizes around the inversion point were for a continuous organic phase 206 micron, and for a continuous aqueous phase 506 micron (see Figure 5.9). According to Eq. 5.14 with these Sauter mean drop sizes, the organic phase hold-up at the phase inversion should be 0.71, about twice the value experimentally obtained. This relation is thus not applicable either. The reason might be that in the annular zone between the bottom of the rotating centrifuge and the bottom plate of the vessel, the contact area of the liquids with the steel of the reactor is much higher than

in conventional mixed tanks and the assumption that interactions with the reactor wall are negligible are perhaps not valid.

5.5. Conclusions

Combined studies on liquid hold-ups, RTD, drop size distribution and phase behavior have provided valuable insight in the hydrodynamic characteristics of the CINC V02 under various conditions. Within the experimental window, the total liquid hold-ups are constant. In steady-state, the CCS contains in total about 180 mL liquid, of which 170 mL is situated in the centrifuge and only 10 mL in the annular zone. The geometrical volume is 322 mL, thus about half the geometrical volume is occupied by liquid. RTD-behavior of both phases was typically plug flow alike, which could be attributed to the large fraction of the hold-up in the centrifuge. The specific interfacial area in the annular mixing zone as determined by the FBRM measurements was up to 6 times as high as reported for stirred tanks.

Phase inversion was observed for several aqueous- organic solvent combinations. The experimental relations originally proposed for describing phase inversions in stirred tanks were checked on applicability for describing the CCS. However, none of the relations was found applicable. Expansion of the set of solvents and accurate phase inversion measurements at a range of conditions using Lasentec® FBRM equipment is suggested for quantification of the phase inversion. Also, dynamic modeling using population balances may bring a solution to the problem[35,36].

5.6 Nomenclature

a	specific interfacial area per volume dispersion, [m^2/m^3 liquid]
d	diameter, [m]
$\overline{d_{vs}}$	Sauter mean drop size, [m]
DCE	1,2-dichloroethane
DCM	dichloromethane
E	residence time distribution function, [-]
f	relative frequency, [-]
F	flow, [mL/min]
F	cumulative residence time distribution function, [-]
N	number of tanks in series, [-]
p	fit parameter in empirical RTD-function, [-]
q	fit parameter in empirical RTD-function, [-]

t	time [min]
t	fit parameter in empirical RTD-function, [-]
u	fit parameter in empirical RTD-function, [-]
v	fit parameter in empirical RTD-function, [-]
V	Volume (hold-up), [mL]
w	fit parameter in empirical RTD-function, [-]

greek letters

ε	hold-up fraction, [-]
υ	rotational frequency, [Hz]
τ	average residence time, [min]
Ω	resistance, [Ohm]
ρ	density, [kg/m^3]
σ	interfacial tension, [$mN/m = 10^{-3} kg/s^2$]
θ	reduced time [-]

subscripts

ANN	annular zone
CENTR	centrifuge
aq	aqueous phase
i	index for drop size classes
I	impeller
IA	inversion towards continuous aqueous phase
IO	inversion towards continuous organic phase
k	index for phases
max	maximum
org	organic phase

Acknowledgements

Gerard Kwant, Iris Verschuren and Karla Danen of DSM are acknowledged for helpful discussions. John Janssen is acknowledged for assisting with the Lasentec® FBRM equipment. DSM and Schering-Plough are acknowledged for their financial support through the Separation Technology program of the Netherlands Scientific Organization (NWO).

5.7 References

[1]. Stanckiewicz, A.; Moulijn, J. A. *Re-Engineering the chemical processing plant; Process Intensification;* Marcel Dekker, Inc: New York, 2004.

[2]. Harmsen, G. J. *Chem. Eng. Proc.* **2007,** *46*, 774-780.

[3]. Kulprathipanja, S. *reactive separation process;* Taylor & Francis: New York, 2002.

[4]. Schmidt-Traub, H.; Gorak, A. *Integrated Reaction and Separation Operations;* Springer: Berlin, 2006.

[5]. Godfrey, J. C.; Slater, M. J. *Liquid-Liquid Extraction Equipment;* John Wiley & Sons: New York, 1994.

[6]. Hanson, C. *Recent Advances in Liquid-Liquid Extraction;* Pergamon Press Ltd.: 1971.

[7]. Thornton, J. D. *Science and Practice of Liquid-Liquid Extraction;* Clarendon: Oxford, 1992; Vol. 1 and 2 (two volumes).

[8]. Meikrantz, D. H.; Macaluso, L. L.; Sams, H. W.; Schardin, C. H.; Federici, A. G. US Patent 5,762,800, Jun 9, 1998.

[9]. Bernstein, G. J.; Grosvenor, D. E.; Lenc, J. F.; Levitz, N. M. *Nucl. Technol.* **1973,** *20*, 200-202.

[10]. Ruffer, N.; Heidersdorf, U.; Kretzers, I.; Sprenger, G. A.; Raeven, L.; Takors, R. *Bioprocess and Biosystems Engineering* **2004,** *26*, 239-248.

[11]. Zhou, J.; Duan, W. H.; Zhou, X. Z.; Zhang, C. Q. *Hydrometallurgy* **2007,** *85*, 154-162.

[12]. Zhou, X. Z.; Zhou, J. Z.; Zhang, C. Q.; Yu, W. D. *Sep. Sci. Technol.* **1997,** *32*, 2705-2713.

[13]. Zhu, J. Q.; Chen, J.; Li, C. Y.; Fei, W. Y. *Sep. Purif. Technol.* **2007,** *56*, 237-240.

[14]. Kraai, G. N.; van Zwol, F.; Schuur, B.; Heeres, H. J.; de Vries, J. G. *Angew. Chem. Int. Ed.* **2008,** *47*, 3905-3908.

[15]. Schuur, B.; Floure, J.; Hallett, A. J.; Winkelman, J. G. M.; de Vries, J. G.; Heeres, H. J. *Org. Process Res. Dev.* **2008,** *12*, 950-955.

[16]. Vedantam, S.; Joshi, J. B. *Chemical Engineering Research & Design* **2006,** *84*, 522-542.

[17]. Schuur, B.; Jansma, W. J.; Winkelman, J. G. M.; Heeres, H. J. *Chemical Engineering and Processing: Process Intensification* **2008,** *47*, 1484-1491.

[18]. Wardle, K. E.; Allen, T. R.; Anderson, M. H.; Swaney, R. E. *AIChE J.* **2008,** *54*, 74-85.

[19]. Michaelides, E. E. *Particles, Bubbles and Drops;* World Scientific: New Jersey, 2006.

[20]. Levenspiel, O. *Chemical Reaction Engingeering;* third ed.; John Wiley & Sons: New York, 1999.

[21]. Westerterp, K. R.; van Swaaij, W. P. M.; Beenackers, A. A. C. M. *Chemical Reactor Design and Operation;* Wiley: Chichester, 1987.

[22]. Davies, G. A. Mixing and coalescence phenomena in liquid-liquid systems. In *Science and Practice of Liquid-Liquid Extraction*, Thornton, J. D., Ed.; Clarendon Press: Oxford, 1992; pp 244-342.
[23]. Sawistowski, H. Physical Aspects of Liquid-Liquid Extraction. In *Mass Transfer with Chemical Reaction in Multiphase Systems*, Alper, E., Ed.; Martinus Nijhoff Publishers: The Hague, 1983; pp 613-635.
[24]. Godfrey, J. C.; Hanson, C. Liquid-liquid systems. In *Handbook of Multiphase Systems*, Hetsroni, G., Ed.; Hemisphere Publishing Corporation: Washington, 1982.
[25]. Liu, L.; Matar, O. K.; de Ortiz, E. S. P.; Hewitt, G. F. *Chem. Eng. Sci.* **2005,** *60*, 85-94.
[26]. Godfrey, J. C. Mixers. In *Liquid-Liquid Extraction Equipment*, Godfrey, J. C., Slater, M. J., Eds.; John Wiley & Sons: Chichester, 1994; pp 363-409.
[27]. van Woezik, B. A. A.; Westerterp, K. R. *Chem. Eng. Proc.* **2000,** *39*, 299-314.
[28]. Santiago, M. D.; Trambouz, P. *Chem. Eng. Sci.* **1971,** *26*, 29-38.
[29]. Zeppieri, S.; Rodriguez, J.; Lopez de Ramos, A. L. *Journal of Chemical & Engineering Data* **2001,** *46*, 1086-1088.
[30]. Terent'eva, N. A.; Cherednichenko, G. I.; Nikulichev, Y. *Chemistry and Technology of Fuels and Oils* **1989,** *25*, 404-406.
[31]. Malzert, A.; Boury, F.; Saulnier, P.; Ivanova, T.; Pana∩otov, I.; Benoœt, J. P.; Proust, J. E. *J. Colloid Interface Sci.* **2003,** *259*, 398-407.
[32]. Sakka, T.; Tanaka, K.; Shibata, Y.; Ogata, Y. H. *Journal of Electroanalytical Chemistry* **2006,** *591*, 168-174.
[33]. Gunde, R.; Kumar, A.; Lehnert-Batar, S.; Maeder, R.; Windhab, E. J. *J. Colloid Interface Sci.* **2001,** *244*, 113-122.
[34]. Yeo, L. Y.; Matar, O. K.; Perez de Ortiz, E. S.; Hewitt, G. F. *Chem. Eng. Sci.* **2002,** *57*, 1069-1072.
[35]. Vaessen, G. E. J.; Visschers, M.; Stein, H. N. *Langmuir* **1996,** *12*, 875-882.
[36]. Yeo, L. Y.; Matar, O. K.; Perez de Ortiz, E. S.; Hewitt, G. F. *Chem. Eng. Sci.* **2002,** *57*, 3505-3520.

Chapter 6

Continuous Chiral Separation of Amino Acid Derivatives by Enantioselective Liquid-Liquid Extraction in Centrifugal Contactor Separators

Boelo Schuur, Joelle Floure, Andy Hallett, Jozef G.M. Winkelman,

Johannes G. de Vries, Hero J. Heeres

This chapter was published:

Organic Process Research & Development 2008, 12, 950-955

part of the results were published in:

Proceedings of ISEC 2008 Vol. II, 979-984

Abstract

The continuous enantioselective liquid-liquid extraction of aqueous 3,5-dinitrobenzoyl-(*R*),(*S*)-leucine (DNB-R,S-leu) by a cinchona alkaloid extractant (C) in 1,2-dichloroethane using a Centrifugal Contact Separator (CCS) was studied at 294K. Typical concentrations were in the order of 1mM for both DNB-R,S-leu and C. The best results were found at a pH of 6, with 61% yield for DNB-S-leu and an enantiomeric excess of 34%. Back extraction studies at different pH values showed that the host can be recovered efficiently in a single CCS, provided that pH > 9. Experimental studies indicate that the CCS behaves as an equilibrium extraction stage, even at total throughputs exceeding 50% of the equipment capacity (1.9 L min^{-1}). A previously developed equilibrium stage extraction model was successfully applied to describe the data for both the extraction and the back-extraction experiments.

Keywords:

continuous liquid-liquid extraction; CINC V02 centrifugal contactor separator; process intensification; enantioselectivity; 3,5-dinitrobenzoyl-(*R*),(*S*)-leucine; cinchona alkaloid

6.1 Introduction

The growing demand for enantiopure compounds[1] is evoking the development of new competitive technologies.[2-4] A promising technique is enantioseparation by liquid-liquid extraction.[5] Although a number of studies have shown the potential of this technique,[5-22] translations into processes for industrial practice are scarce.[16] To the best of our knowledge, processes making use of enantioselective liquid-liquid extraction have not been commercialized yet. In the pharmaceutical and fine chemical industries, batch processing in multi-purpose batch reactors and separators is state of the art. Although highly flexible, batch operation has a number of inherent drawbacks such as batch to batch product variation when multiple batches are required, relatively large equipment sizes and limited process control options.[23] The development of continuous, highly intensified processes is a major research topic in the field.[24]

The centrifugal contact separator (CCS) is an example of a compact continuous flow device that seems ideally suited for continuous operation in the pharmaceutical and fine chemical industry. A CCS combines efficient mixing of two immiscible liquids with fast phase separation. An example of such a CCS is the CINC device.[25] It is available in sizes with maximum liquid throughput ranging from 1.9 L min^{-1} to 757 L min^{-1}. The device was originally invented for oil-water separation.[26] We recently demonstrated that the device can also be used for process intensification by combining continuous biphasic (bio)catalytic reactions and separation.[27] The V02 is the smallest, table-top scaled version with a maximum total throughput of 1.9 L min^{-1}. Due to large centrifugal forces (up to 900 g), the apparatus is very compact but still capable of separating two immiscible liquids efficiently, even when their densities differ only 10 kg m^{-3}. The CINC basically consists of a rotating hollow centrifuge in a static housing, see Figure 6.1. The liquid(s) enter the device in the annular zone between the static wall and the rotating centrifuge, where they are intensely mixed. Next, they are transferred into the centrifuge where separation occurs by the centrifugal forces.

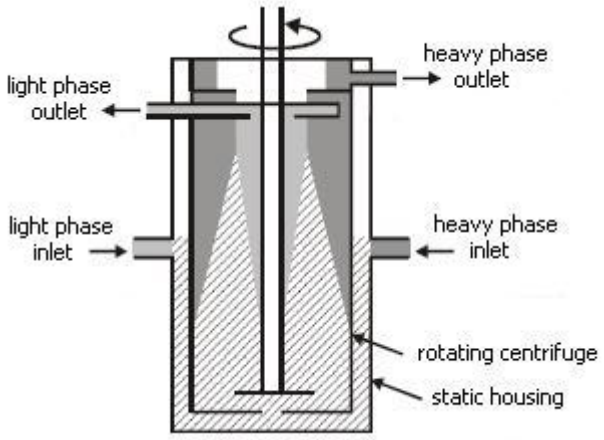

Figure 6.1. Sketch of the CINC, hatched: dispersion, darker gray: heavy phase, lighter gray: light phase

To investigate the potential of the CINC for continuous enantioselective liquid-liquid extraction and subsequent back-extraction of the host (extractant), we studied the enantioselective extraction of aqueous 3,5-dinitrobenzoyl-(*R*),(*S*)-leucine (DNB-R,S-leu, see Figure 6.2, left) using O-(1-t-butylcarbamoyl)-11-octadecylsulfinyl-10,11-dihydro-quinine (C, see Figure 6.2, right) as the host. This system was selected from the open literature for its promising selectivity.[28,29] In earlier studies in batch equipment, the effect of the operating variables such as concentrations, volume ratio and pH on the extraction and back-extraction performance was quantified and an equilibrium model was formulated.[30] In this contribution, reactive extraction experiments in the CCS will be reported. The experimental data are modeled using the previously developed equilibrium model.

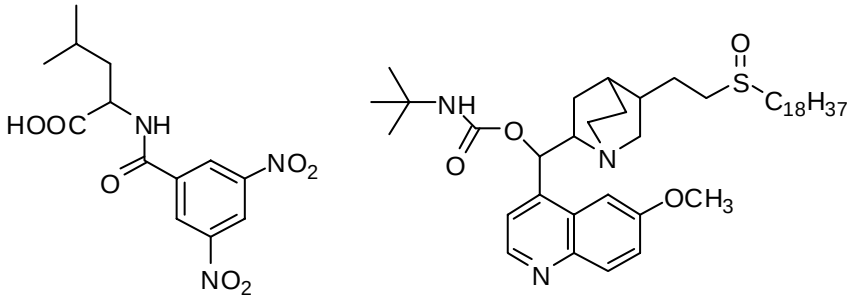

Figure 6.2. Chemical structures of DNB-R,S-leu (left) and extractant C (right)

6.2 Results and discussion

Proof of principle for enantioselective extraction in the CINC V02.

To prove the suitability of the CINC for enantioselective extraction, an experiment was performed with flow rates of 30 mL min^{-1} for both phases and a rotational frequency of 50 Hz. Initially, the CINC was fed with pure 1,2-dichloroethane as organic solvent and a buffered aqueous solution of racemic DNB-R,S-leu (1 mM). After several minutes steady-state was achieved (Figure 6.3). Subsequently, the organic feed was switched from pure 1,2-dichloroethane to a 0.5 mM CA solution in 1,2-dichloroethane.

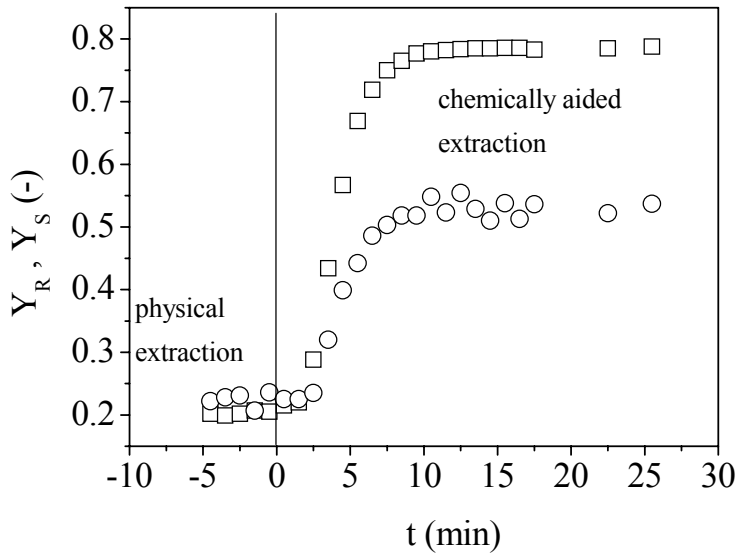

Figure 6.3. Extraction yield profiles. $F_{aq} = F_{org}$ = 30 mL min^{-1}, N = 50 Hz, pH = 5.12, $c_{DNB\text{-}R,S\text{-}leu,aq,0}$ = 1 mM, $c_{C,org,0}$ = 0.5 mM. Symbols □: Y_S, ○: Y_R.

As expected, the enantiomeric excess (*ee*) is negligible when applying 1,2-dichloroethane without host (t < 0). At t > 0, the extraction yields of both enantiomers increase dramatically due to the complexation with CA in the organic phase. Steady-state operation is achieved in less than 10 minutes. With a total liquid hold-up in the CCS of 180 mL and a total throughput of 60 mL min^{-1}, this corresponds with just over three average residence times. The steady-state yield of DNB-S-leu is 0.78 and that of DNB-R-leu is 0.53. Here, the yields are defined as:

$$Y_i = \frac{F_{org}}{F_{aq}} \frac{c_{i,org,tot}}{c_{i,aq,in}} \qquad [i = R,S] \qquad (6.1)$$

Furthermore, it is clear that the host has a preference for the L-enantiomer, leading to an organic phase *ee* of 19%. The *ee* in the aqueous phase is 37%. This experiment clearly illustrates the suitability of the CINC device for enantioselective liquid-liquid extraction.

Table 6.1. Experimental data for continuous extractions in the CINC[a]

Exp.	$c_{DNB\text{-}R,S\text{-}leu,aq,0}$ *(mM)*	$c_{C,org,0}$ *(mM)*	*pH*	F_{aq} *(mL min^{-1})*	F_{org} *(mL min^{-1})*	Y_R *(-)*	Y_S *(-)*	ee_{org}	ee_{aq}
1	1.01	0.326	5.74	26.0	32.5	0.29	0.57	33	25
2	0.995	0.274	5.73	26.0	34.1	0.29	0.49	26	16
3[b]	1.01	0.274	5.76	25.7	37.7	0.25	0.52	35	22
4[c]	1.00	0.478	5.94	29.0	30.2	0.28	0.57	34	25
5[d]	0.994	0.478	5.96	46.8	50.2	0.22	0.51	40	23
6	1.16	1.068	6.03	30.0	30.0	0.30	0.61	34	28
7	0.992	0.286	5.73	200	200	0.20	0.35	28	11
8	0.992	0.286	5.73	300	300	0.17	0.33	32	11
9	0.993	0.287	5.73	400	400	0.18	0.34	31	11
10	0.993	0.287	5.73	500	500	0.17	0.36	36	13

[a] 294 K, rotational frequency 50 Hz, ionic strength 0.11 M. [b] rotational frequency 40 Hz. [c] ionic strength 0.10 M. [d] ionic strength 0.13M

Influence of flow rates and the rotational frequency.

Experiments with different liquid flow rates were conducted to investigate the effects on the steady-state yields of the enantiomers (experiments 7-10, Table 6.1). The yield is essentially independent of the flow rates (Figure 6.4). This implies that the chemical composition of the outlet streams is at equilibrium for all experiments. The liquid residence time at the highest flow rate is about 12 seconds, meaning that the time needed for chemical and physical equilibrium to establish is very short. This conclusion is strengthened by comparison of experiments 2 and 3 (Table 6.1). These experiments were carried out at different rotational frequencies but otherwise comparable conditions. The results are very similar. From this it can be concluded that differences in hydrodynamic conditions (e.g. mass transfer coefficients and liquid hold-up) by changing the rotational frequency do not

affect the yields. This again justifies the statement that the overall rate of the complexation reactions is very fast and that the outlet streams are at chemical equilibrium.

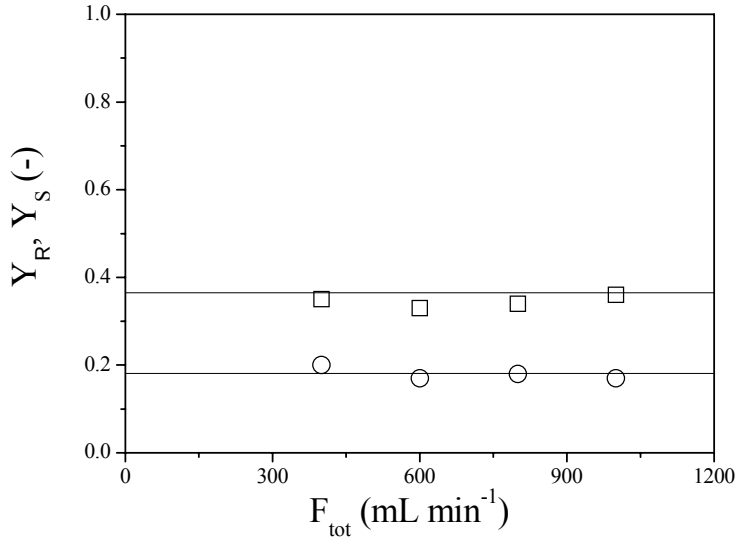

Figure 6.4. Extraction yields at different flow rates. N = 50 Hz, pH = 5.73, $c_{DNB\text{-}R,S\text{-}leu,aq,0}$ = 1 mM, $c_{C,org,0}$ = 0.3 mM, $F_{aq} = F_{org}$. Symbols: □ = Y_S, ○ = Y_R, lines are equilibrium model predictions.[30]

Equilibrium stage modeling of the continuous extraction experiments in the CCS.

We have previously developed an equilibrium model for the enantioselective extraction of DNB-R,S-leu with C based on batch experiments.[30] The model was validated at 294 K for concentrations up to 3 mM and 3.5 < pH < 11. The model is based on a homogeneous extraction mechanism (Scheme 1).[15] Here, complexation between host and enantiomer takes place in the organic phase. The values for the parameters in the model were determined earlier in our group[30] and are given in Table 6.2.

The experimental data in Table 6.1 were modeled using the equilibrium model. The correlation between the model predictions and the experimental data is depicted in Figure 6.5. The mean absolute relative error between model prediction and experiments is 11.5%. It may thus be concluded that the equilibrium model is very well suited to predict the CCS extraction performance and that chemical equilibrium was achieved in all

experiments, even those with total flow rates as high as 1L/min, corresponding to residence times as low as 5.5 seconds.

Scheme 6.1. Extraction model for DNB-R,S-leu by C

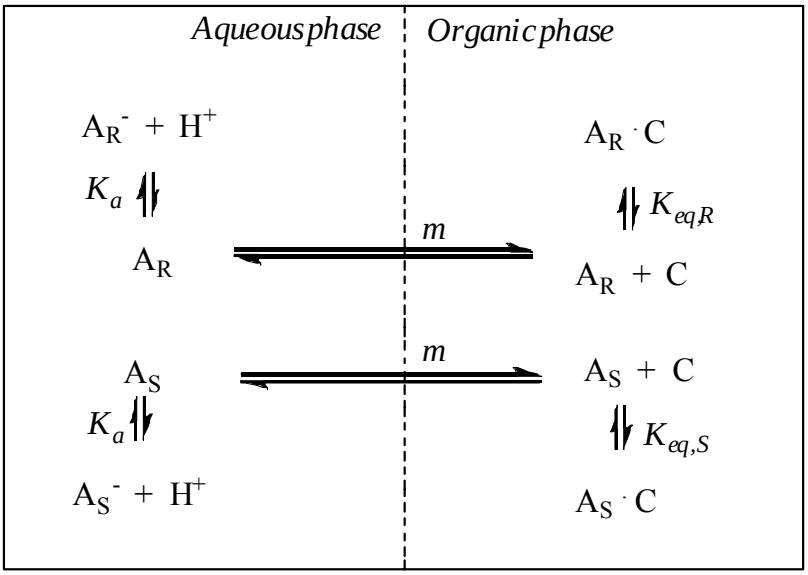

Table 6.2. Parameters of the equilibrium model

parameter	definition[a]	value	dimensions
K_a	$\frac{\gamma^2[H^+]_{aq}[DNB-leu^-]_{aq}}{[DNB-leu]_{aq}}$	1.92×10^{-4}	mol L^{-1}
m	$\frac{[DNB-leu]_{org}}{[DNB-leu]_{aq}}$	8.04	-
$K_{eq,R}$	$\frac{[C\cdot DNB-R-leu]_{org}}{[C]_{org}[DNB-R-leu]_{org}}$	2.71×10^{4}	L mol^{-1}
$K_{eq,S}$	$\frac{[C\cdot DNB-S-leu]_{org}}{[C]_{org}[DNB-S-leu]_{org}}$	9.31×10^{4}	L mol^{-1}

[a] The definitions of the parameters K_a and m are valid for both enantiomers

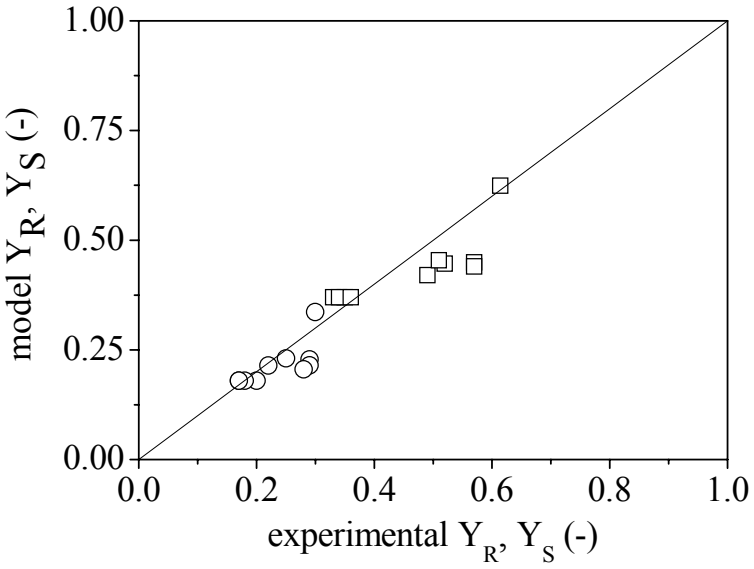

Figure 6.5. Parity plot of the experimental and modeled yields. □: Y_S, ○: Y_R.

With the use of the model, the observed experimental trends (Table 6.1) may be rationalized. Experiments 4 and 5 have comparable conditions (i.e. flow ratio, intake concentrations, pH), except for the ionic strength in the aqueous phase. The ionic strength in experiment 4 is 0.10 mol L^{-1} compared to 0.13 mol L^{-1} in experiment 5. The higher yields in experiment 5 are a direct result of the lower ion activities due to the higher buffer concentration. This comparison shows that the ionic strength has a profound effect on the extraction process.

The equilibrium extraction model may also be used to determine the optimum experimental conditions for the extraction process. For this purpose, the performance factor *PF* is very helpful. The *PF* is determined as the product of the organic phase *ee* and the yield of the preferred enantiomer:[8]

$$PF = Y_S ee_{org} \tag{6.2}$$

With the yield ranging from 0 to 1 and the *ee* from 0 to 100%, the *PF* ranges from 0 to 100%. The equilibrium extraction model was used to determine the optimum *PF*. The highest *PF* value was 19% at experimental conditions as given for experiment 6 (Table

6.1). The experimental Y_S and Y_R for experiment 6 were 0.61 and 0.30 respectively, leading to an organic phase *ee* of 34%. The experimental *PF* according to Eq. 6.2 is 21%, which is in good agreement with the model prediction.

Optimization of the back-extraction using model predictions.

The equilibrium model may also be used to optimize the efficiency of the back-extraction process. In the back-extraction, organic streams containing the host- DNB-R,S-leu complexes are brought in contact with an aqueous buffer to back-extract the DNB-R,S-leu and hereby recover the host solution. Particularly for expensive host compounds, efficient host recovery is of major importance. If the back-extraction has a high efficiency, the organic host solution may be returned to the extraction stage without further treatment. The efficiency of the back-extraction is expressed in yield terms. The yields in the back-extraction step are defined as:

$$Y_{B,i} = \frac{F_{aq}}{F_{org}} \frac{c_{i,aq,tot}}{c_{i,org,in}} \qquad [i = R,S] \qquad (6.3)$$

The equilibrium model predicts that the back extraction efficiency is very sensitive to the pH of the aqueous phase. With increasing pH, the equilibrium in the aqueous phase shifts towards the dissociated form of the amino acid derivative, leading to higher back-extraction yields (Scheme 6.1). This is demonstrated in Figure 6.6 for a model simulation at a high host concentration (3 mM), a flow ratio F_{org}/F_{aq} of 3.3, inlet concentrations of both enantiomers of 0.5 mM and an aqueous phase ionic strength of 0.12 M. Clearly, at pH > 9 the model predicts that the back-extraction of both enantiomers is quantitative in a single equilibrium stage.

A number of experiments were carried out in the CCS using an organic phase containing racemic DNB-R,S-leu and the host (0.9 mM DNB-R,S-leu, 0.3 mM C) and an aqueous phase with a buffer of appropriate concentration, typically I > 0.1 M (F_{org}/F_{aq} = 1.06, 59 mL min^{-1} total flow). The back-extraction yields at different pH values of the aqueous phase were measured to verify the model predictions. The experimental results and the model predictions are compared in Figure 6.7. Agreement between model and experiment is good. Thus, it can be concluded that the back extraction of the organic phase may be conveniently carried out using an aqueous solution with pH > 9. Hereafter, the recovered host solution can be recycled without further treatment for a new extraction step.

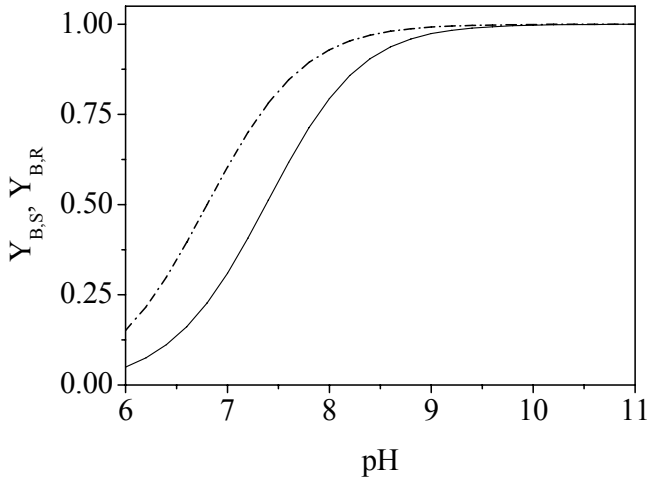

Figure 6.6. Predicted back-extraction yields as function of aqueous phase pH at constant ionic strength of 0.12 M. Organic phase input concentrations are 0.5 mM for both enantiomers and 3 mM for the host, F_{org}/F_{aq} = 3.3. solid line: $Y_{B,S}$, dashed line: $Y_{B,R}$.

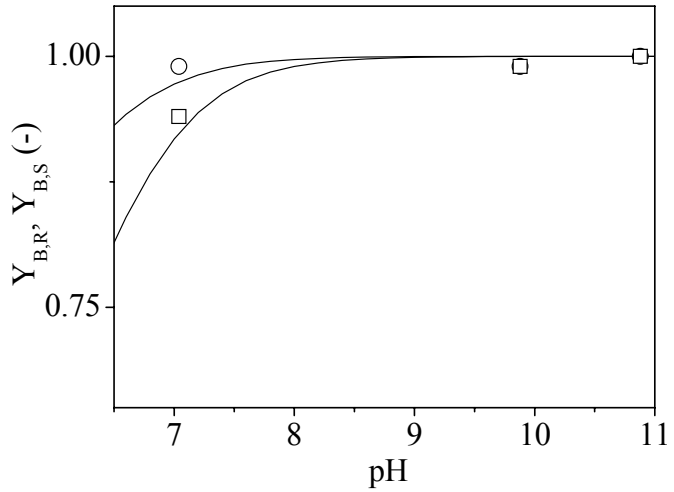

Figure 6.7. Back-extraction yields at an ionic strength of 0.2 M, R = 1.06, and organic phase intakes of racemate and host of 0.9 and 0.3 mM, respectively. Lines are model predictions. Symbols: □ : $Y_{B,S}$, ○ : $Y_{B,R}$.

6.3 Conclusions and outlook

In this paper, the proof of principle for the application of CCS equipment for the continuous separation of racemates is provided. The concept was demonstrated for a model system composed of a racemic mixture of protected amino acids (DNB-R,S-leu) with a chiral cinchona alkaloid host. Under optimum conditions, the ee_{org} was 34% and the S-enantiomer yield, Y_S was 0.61, leading to a *PF* of 21%. It was shown that the application of a single CCS for the back extraction is sufficient for efficient recovery of the host, provided that pH > 9. Experiments and subsequent modeling activities indicate that both the extraction and the back-extraction step in the CCS may be modeled as an equilibrium extraction stage. This statement was proven for total flow rates up to the flooding limit of the equipment at 1.8 L/min. Full separation of the enantiomers (ee_{org} and ee_{aq} > 0.99; *PF* > 98%) in a single extraction stage is not possible with the DNB-R,S-leu/C system. Multistage countercurrent extraction with a cascade of CCS's is envisaged to achieve this objective. A schematic representation of the proposed countercurrent process with a single back-extraction step for efficient host recycle in the extract phase is depicted in Figure 6.8.

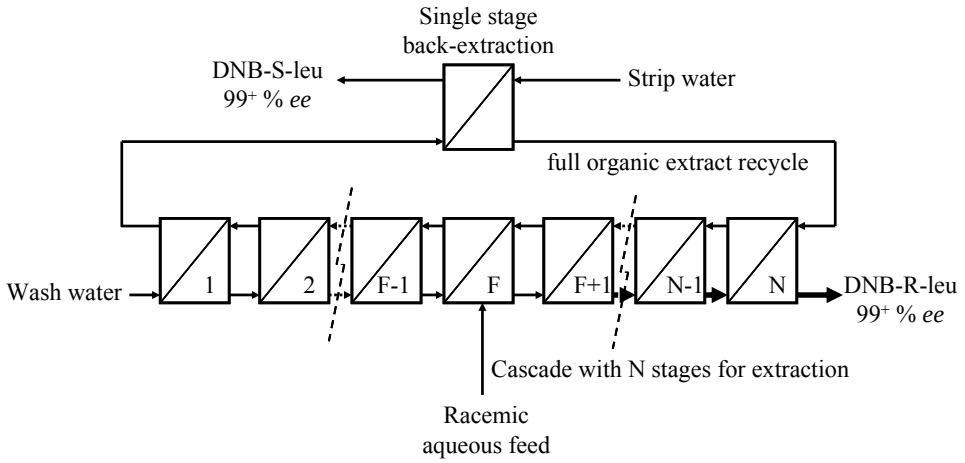

Figure 6.8. Schematical representation of a countercurrent setup of N CCS's for chiral separation with full recycle of the extract stream

Considering the operational limits of the bench-scale CCS (up to 1 L min^{-1} was verified experimentally in this study, equipment capacity 1.9 L min^{-1}) and the solubility of the

species to be separated, a typical separation capacity of 10 kg racemate per week should be possible. Further scale up may easily be achieved by application of larger (commercially available) CCS equipment.

6.4 Experimental

6.4.1 Chemicals

Water was obtained by reverse osmosis followed by deionisation using a deionisation apparatus from Labconco, 1,2-dichloroethane (99%) from Sigma-Aldrich, potassium dihydrogen phosphate (*pa*), di-sodium hydrogen phosphate dodecahydrate (*pa*) and triethyl amine (99%) from Merck, glacial acetic acid from Acros, methanol (AR) and acetonitrille from Labscan.

O-(1-t-butylcarbamoyl)-11-octadecylsulfinyl-10,11-dihydro-quinine, 3,5-dinitrobenzoyl-(*R*),(*S*)-leucine, 3,5-dinitrobenzoyl-(*R*)-leucine and 3,5-dinitrobenzoyl-(*S*)-leucine were kindly provided by DSM Research.

6.4.2 Experimental setup

All experiments were carried out in a CINC V02 (a table top version with a maximum total throughput of 1.9 L min^{-1} (3.2×10^{-5} m^3s^{-1}) and maximum rotational frequency of 100 Hz) made from Hastelloy and equipped with a heating/cooling jacket. Both liquids were transferred to the reactor using Verder VL1000 Control peristaltic tube pumps equipped with double pump heads (1.6 × 1.6 × 8R). Glass supply and receive vessels were used. Cooling the jacket with tap water enabled a constant temperature of 294 K, this was monitored using temperature sensors (CMA, Amsterdam) connected with a PC via a CoachLab II interface (CMA, Amsterdam).

6.4.3 Experimental procedures

Typical extraction experiments were started after calibration of the pumps by feeding the CINC with 1,2-dichloroethane (the heavier of the two liquids) and starting the centrifuge. When the reactor was filled with the heavy phase and the heavy phase outlet started running, the pump of the buffered aqueous DNB-R,S-leu solution (the light phase) was started. After achieving steady-state operation, the feed of heavy phase was switched from pure 1,2-dichloroethane to a C solution in 1,2-dichloroethane, hereby switching from pure

physical distribution of DNB-R,S-leu over the phases to an enantioselective reactive liquid-liquid extraction. After achieving steady-state in the enantioselective process, the experiments were continued for several minutes. Samples for analysis were taken from the aqueous phase at regular time intervals, starting directly after the aqueous reactor outlet had started running.

Back-extraction experiments were performed similarly, but now the DNB-R,S-leu and the C were fed as solution in 1,2-dichloroethane. After the heavy phase exit started running, the aqueous feed, containing a phosphate buffer to set the pH was started. Samples for analysis were taken from the aqueous phase.

6.4.4 Analytical procedures

The concentrations of the DNB-leu enantiomers in the aqueous phase were determined with an accuracy of 3% by HPLC using an Agilent LC 1100 series apparatus, equipped with an Astec Chirobiotic T column (now Supelco, Sigma-Aldrich). Detection was done using 270 nm UV light. The eluent was a 3:1 (v/v) mixture of acetonitrille and methanol, to which 0.25% (vol) triethyl amine and 0.25% (vol) acetic acid were added. The flow rate was set at 1 mL per minute. Before injecting the aqueous phase samples to the column, 0.10 mL of the samples was diluted with 1.0 mL eluent and filtered over a syringe filter with pore size 0.45 μm (Waters Chrom). Quantitative analysis was enabled using calibration curves.

6.5 Nomenclature

c	concentration, (M = mol L^{-1})
C	cinchona alkaloid (extractant), see Figure 2
DNB-R,S-leu	3,5-dinitrobenzoyl-(*R*),(*S*)-leucine, see Figure 2
ee	enantiomeric excess, (-)
F	Flow, (mL min^{-1})
I	ionic strength (M)
K	equilibrium constant, various dimensions
m	partition coefficient, (-)
N	rotational frequency, (Hz)
PF	performance factor, (%)
T	temperature, (K)
Y	yield, (-)

γ	activity coefficient for ionic species, determined using $^{10}\log(\gamma_i) = \frac{-0.5115 z_i^2 I^{1/2}}{1+1.316 I^{1/2}}$

subscripts

0	initial or feed
a	acidity
aq	aqueous
B	back-extraction
eq	equilibrium
i	index
org	organic
R	R-enantiomer
S	S-enantiomer
tot	total

Acknowledgements

Gerard Kwant (DSM) is acknowledged for helpful discussions. DSM and Organon are acknowledged for their financial support through the Separation Technology program of NWO (Netherlands Scientific Organization). Joelle Floure and Andrew Hallett thank the European Commission for financial support as part of the Marie Curie Research Training Network "Enantioselective Recognition: Towards the Separation of Racemates" HPRN-CT-2001-00182.

6.6 References

[1]. Rouhi, A. M. *Chem. Eng. News* **2003,** *81*, 45-55.
[2]. Ahuja, S. *Chiral Separations: Application and technology;* ACS: Washington, 1997.
[3]. Subramanian, G. *Chiral separaration techniques: A practical approach;* Wiley-VCH: Weinheim, 2001.
[4]. Toda, F. *Enantiomer separation: Fundamentals and practical methods;* Kluwer Academic publishers: Dordrecht, 2004.
[5]. Steensma, M.; Kuipers, N. J. M.; de Haan, A. B.; Kwant, G. *Chirality* **2006,** *18*, 314-328.

[6]. Abe, Y.; Shoji, T.; Kobayashi, M.; Qing, W.; Asai, N.; Nishizawa, H. *Chem. Pharm. Bull.* **1995,** *43*, 262-265.
[7]. Abe, Y.; Shoji, T.; Fukui, S.; Sasamoto, M.; Nishizawa, H. *Chem. Pharm. Bull.* **1996,** *44*, 1521-1524.
[8]. Koska, J.; Haynes, C. A. *Chem. Eng. Sci.* **2001,** *56*, 5853-5864.
[9]. Lacour, J.; Goujon-Ginglinger, C.; Torche-Haldimann, S.; Jodry, J. J. *Angew. Chem. Int. Ed.* **2000,** *39*, 3695-3697.
[10]. Ohki, A.; Miyashita, R.; Naka, K.; Maeda, S. *Bull. Chem. Soc. Jpn.* **1991,** *64*, 2714-2719.
[11]. Pickering, P. J.; Chaudhuri, J. B. *Chem. Eng. Sci.* **1997,** *52*, 377-386.
[12]. Prelog, V.; Stojanac, Z.; Kovacevic, K. *Helv. Chim. Acta* **1982,** *65*, 377-384.
[13]. Reeve, T. B.; Cros, J. P.; Gennari, C.; Piarulli, U.; de Vries, J. G. *Angew. Chem. Int. Ed.* **2006,** *45*, 2449-2453.
[14]. Steensma, M.; Kuipers, N. J.; de Haan, A. B.; Kwant, G. *J. Chem. Technol. Biotechnol.* **2006,** *81*, 588-597.
[15]. Steensma, M.; Kuipers, N. J. M.; de Haan, A. B.; Kwant, G. *Chem. Eng. Sci.* **2007,** *62*, 1395-1407.
[16]. Steensma, M.; Kuipers, N. J. M.; de Haan, A. B.; Kwant, G. *Chem. Eng. Proc.* **2007,** *46*, 996-1005.
[17]. Takeuchi, T.; Horikawa, R.; Tanimura, T. *Anal. Chem.* **1984,** *56*, 1152-1155.
[18]. Tan, B.; Luo, G. S.; Qi, X.; Wang, J. D. *Sep. Purif. Technol.* **2006,** *49*, 186-191.
[19]. Tan, B.; Luo, G. S.; Wang, H. D. *Tetrahedron-Asymmetry* **2006,** *17*, 883-891.
[20]. Tan, B.; Luo, G. S.; Wang, J. D. *Sep. Purif. Technol.* **2007,** *53*, 330-336.
[21]. Tsukube, H.; Shinoda, S.; Uenishi, J.; Kanatani, T.; Itoh, H.; Shiode, M.; Iwachido, T.; Yonemitsu, O. *Inorg. Chem.* **1998,** *37*, 1585-1591.
[22]. Viegas, R. M. C.; Afonso, C. A. M.; Crespo, J. G.; Coelhoso, I. M. *Sep. Purif. Technol.* **2007,** *53*, 224-234.
[23]. Anderson, N. G. *Org. Process Res. Dev.* **2001,** *5*, 613-621.
[24]. Stanckiewicz, A.; Moulijn, J. A. *Re-Engineering the chemical processing plant; Process Intensification;* Marcel Dekker, Inc: New York, 2004.
[25]. Meikrantz, D. H.; Macaluso, L. L.; Sams, H. W.; Schardin, C. H.; Federici, A. G. US Patent 5,762,800, Jun 9, 1998.
[26]. Meikrantz, D. H. 4,959,158, Sep 25, 1990.
[27]. Kraai, G. N.; van Zwol, F.; Schuur, B.; Heeres, H. J.; de Vries, J. G. *Angew. Chem. Int. Ed.* **2008,** *47*, 3905-3908.
[28]. Kellner, K. H.; Blasch, A.; Chmiel, H.; Lämmerhofer, M.; Lindner, W. *Chirality* **1997,** *9*, 268-273.
[29]. Lindner, W.; Lämmerhofer, M. Eur. Pat. Appl. No. 96 109 072.7, 1996.
[30]. Schuur, B.; Winkelman, J. G. M.; Heeres, H. J. *Ind. Eng. Chem. Res.,* accepted for publication.

Chapter 7

Experimental and modeling studies on the enantioseparation of 3,5-dinitrobenzoyl-(*R*),(*S*)-leucine by liquid-liquid extraction in a cascade of continuous centrifugal separators

Boelo Schuur, Jozef G.M. Winkelman, Johannes G. de Vries, Hero J. Heeres

submitted for publication in Chemical Engineering Science

Abstract

The enantioselective liquid-liquid extraction of aqueous 3,5-dinitrobenzoyl-(*R*),(*S*)-leucine ($A_{R,S}$) using O-(1-t-butylcarbamoyl)-11-octadecylsulfinyl-10,11-dihydro-quinine (a cinchona alkaloid) as extractant in 1,2-dichloroethane was studied experimentally in a countercurrently operated pilot scale cascade of six Centrifugal Contactor Separators (CCS) at 294 K. The extractant was efficiently recovered by back-extraction in a single CCS so that the cascade could run successfully for 10 h. The steady-state *ee* of A_R in the raffinate was 42% at a 99% yield, the A_S was obtained with high purity (98% *ee*) and a yield of 55% in the back-extraction raffinate. In total 2.23 g A_S was obtained in steady-state operation from 8.11 g racemate feed. Deterioration of the *ee* in time was not observed, demonstrating the robustness of the chemistry.

The experimental data was modeled using an equilibrium stage approach. The correlation between model and experiment was satisfactory. The model was applied to optimize the production of both enantiomers in > 97% *ee*. At zero reflux, 12 stages are required for 99% *ee* for both enantiomers. Application of a reflux allows a 25% reduction of the total liquid flow through the system by reduction of the wash feed as well as a reduction in the number of stages from 12 to 11. With a configuration of 12 CINC-V02's operating at an aqueous feed flow of 360 mL/min, the model predicts that 17.7 kg racemate per week may be separated into both enantiomers (99% *ee*) using only 60 g extractant.

keywords:

Enantioselective, Extraction, Multiphase reactors, Mathematical modeling, Optimization, Process intensification, Pilot Plant

7.1. Introduction

Due to more strict regulations for pharmaceutical products, the share of single enantiomer drugs has grown dramatically in the past decades[1]. The main driver for this development is a different bioactivity of the individual enantiomers[2]. This difference in bioactivity can have dramatic effects. (*S*),(*S*)-ethambutol for example is a very efficiently tuberculostatic, while (*R*),(*R*)-ethambutol causes blindness[3]. Various strategies have been developed for enantiopure productions, such as asymmetric catalysis[4] or fermentation[5]. Racemic production followed by enantioseparation is, however, used most abundantly. The separation is mostly done by classical resolution through diastereomeric crystallization[6]. Classical resolution is not always applicable and other techniques such as simulated moving bed chromatography[7,8], centrifugal partition chromatography[9], liquid membrane technology[10], and enantioselective liquid-liquid extraction (ELLE) are being explored for preparative enantioseparations. Due to the high costs of SMB and the limited transport rates in membrane processes, ELLE seems the most effective technology and the ease of scale-up makes it an interesting alternative.

Although the technique of enantioselective liquid-liquid extraction (ELLE) has already been reported in the 1960's[11-14], the number of publications has only grown significantly in the last decades.[15-22]. However, studies describing ELLE beyond the exploratory chemistry stage are scarce. The focus is mainly on development of suitable extractants for classes of racemates and further fine tuning of the selectivity, whereas typical chemical engineering studies for scale-up purposes are very limited. Only a few examples in the literature can be found where mathematical modeling is applied to describe enantioselective extractions[17,22-26] and to the best of our knowledge enantioselective extraction processes have not been commercialized yet.

ELLE is potentially a very attractive technology for commercial operation because it is very flexible in the chemistry, allows for the separation of a wide range of classes of organic compounds (i.e. amino acids and -derivatives, alcohols, amines and amino-alcohols have been reported[19,21,22,27,28]) and is relatively simple to scale-up.

Here, we report on the use of Centrifugal Contactor Separator (CCS) equipment for ELLE. In a CCS, two immiscible liquids are contacted very efficiently and are subsequently separated. Bench scale CINC V02 devices with maximum throughput of 1.9 L/min and a total liquid hold-up of 180 mL were applied (Figure 1). The CINC V02 may be regarded as a highly integrated process device combining liquid-liquid mixing and separation. In recent years, the concept of process intensification (PI) has become a popular tool to optimize all kinds of processes[29,30]. In PI, multiple unit operations are combined into single stage operations to improve energy efficiency, and shift equilibria[31].

Besides the excellent throughput/hold-up ratio, the mixing in the CINC V02 is intense, resulting in efficient mass transfer characteristics. Also the separative power allows for liquids differing only 10 kg/m^3 in density to be efficiently separated. For these beneficial properties, we selected the equipment to prove the continuous pilot scale enantioseparation using ELLE. Hereto, a cascade of CCS for ELLE was applied for the enantioseparation of a model system composed of a racemic aqueous *N*-protected amino acid and a suitable extractant dissolved in 1,2-dichloroethane. 3,5-Dinitrobenzoyl-(*R*),(*S*)-leucine ($A_{R,S}$, Figure 7.2 left) was selected as the model compound and the cinchona alkaloid O-(1-t-butylcarbamoyl)-11-octadecylsulfinyl-10,11-dihydro-quinine (C, Figure 7.2 right)[32] as the extractant. This extractant is versatile and can be used for separation of various *N*-protected amino acids such as $A_{R,S}$[16,33].

In previous studies[34,35], we reported a single stage equilibrium mode for the extraction of aqueous $A_{R,S}$ with C in 1,2-dichloroethane at 294K and demonstrated the applicability to continuous processing in CINC V02 equipment. Here, we demonstrate that continuous separation in a countercurrently operated cascade of 6 CINC V02's can be done with full back-extraction to recover the extractant in a single CCS, and that the developed model predicts the operation satisfactorily so that optimization necessary for scaling-up of the production is possible.

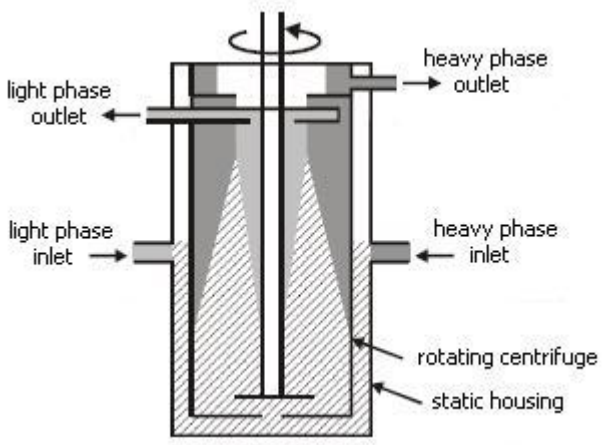

Figure 7.1. Sketch of the CCS, hatched: dispersion, darker gray: heavy phase, lighter gray: light phase.

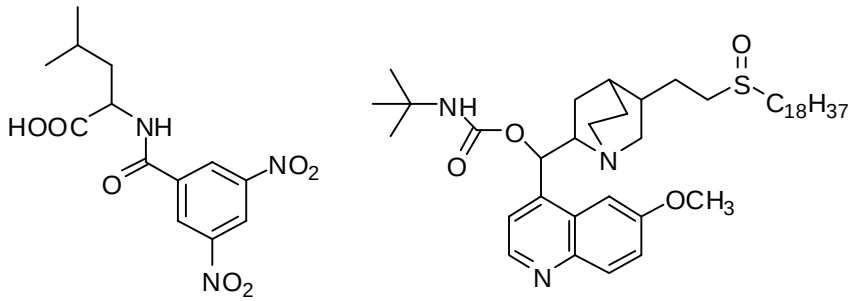

Figure 7.2. Chemical structures of $A_{R,S}$ (left) and cinchona alkaloid extractant C (right).

7.2. Multi-stage equilibrium ELLE model

A typical flow scheme of a cascade for the separation of racemic $A_{R,S}$ into the enantiomers A_R and A_S is depicted in Figure 7.3. The aqueous racemate is fed to the cascade at the feed stage, indicated with F. The stages F to N form the strip section, where A_S is predominantly extracted to the (organic) extract phase. The undesired co-extracted A_R is washed out of the extract stream with water in the stages 1 to F-1 (wash section). A_R leaves the cascade in $F_{out,1}$. The extracted A_S is washed out of the extract stream in the back-extraction stage and leaves the system in $F_{out,2}$. This can be done very efficiently with complete recovery of the extractant in the organic phase in a single stage, when the pH > 9[35]. When desired, part of the aqueous back-extraction outlet stream may be refluxed to the cascade[26].

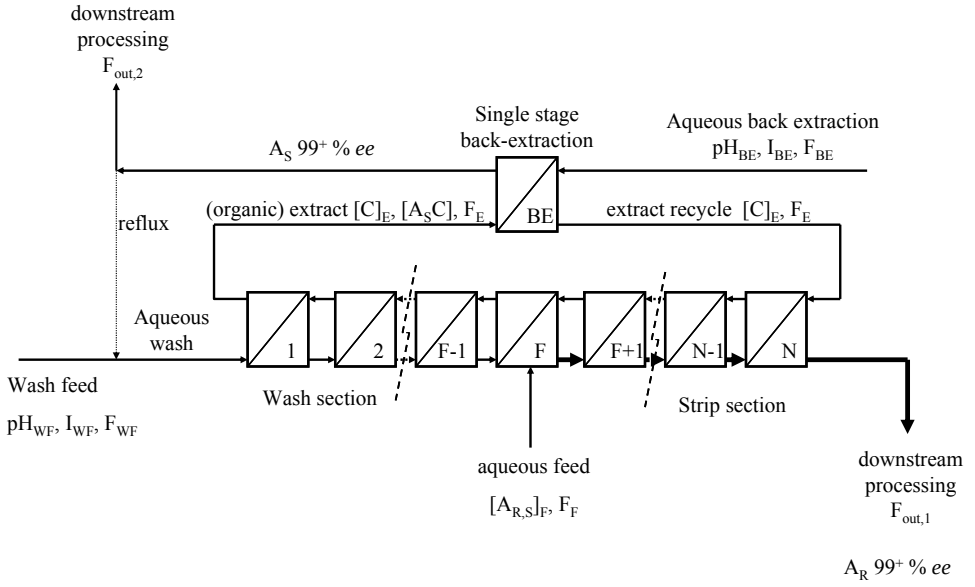

Figure 7.3. Cascade setup with single stage back-extraction and an optional reflux.

The stage relations in the cascade follow from Figure 7.4, in which a single stage from the cascade is displayed. The parameters are listed in Table 7.1.

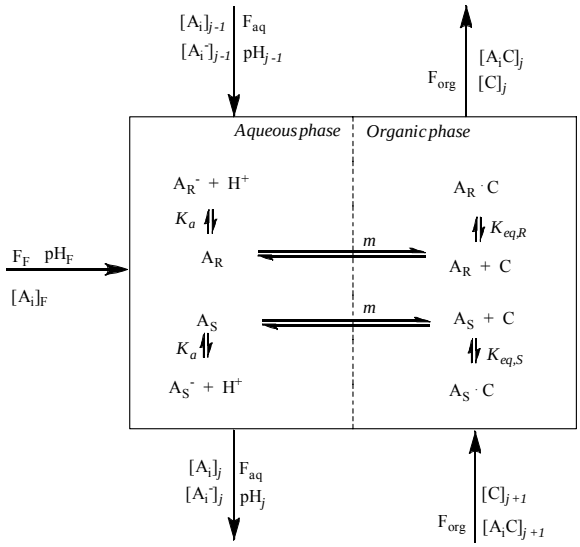

Figure 7.4. Single extraction stage. If j = F, then $F_F \neq 0$, else $F_F = 0$. i = R,S.

Table 7.1. Stage model parameters[34]

parameter	*definition*[a]	*value*	*dimensions*
K_a	$\frac{\gamma^2[H^+]_{aq}[A_i^-]_{aq}}{[A_i]_{aq}}$	$1.92 \cdot 10^{-4}$	mol/L
m	$\frac{[A_i]_{org}}{[A_i]_{aq}}$	8.04	-
$K_{eq,R}$	$\frac{[A_R \cdot C]_{org}}{[C]_{org}[A_R]_{org}}$	$2.71 \cdot 10^4$	L/mol
$K_{eq,S}$	$\frac{[A_S \cdot C]_{org}}{[C]_{org}[A_S]_{org}}$	$9.31 \cdot 10^4$	L/mol

For each of the stages $(j = 1 \cdots N, BE)$, the equilibrium relations are defined as

$$K_a = (\gamma_1{}^2 \frac{[H^+][A_i^-]}{[A_i]})_{aq,j}, \tag{7.1}$$

$$[A_i]_{org,j} = m[A_i]_{aq,j}, \tag{7.2}$$

and

$$K_{eq,i} = (\frac{[A_iC]}{[A_i][C]})_{org,j}, \tag{7.3}$$

where $(i = R, S)$.

The component balances for A_R, A_S and C for the extraction stages $(j = 1 \cdots N)$ are defined as

$$\begin{aligned} &F_{aq,j-1}([A_i]_{aq,j-1} + [A_i^-]_{aq,j-1}) + F_{org}([A_i]_{org,j+1} + \\ &[A_iC]_{org,j+1}) + F_{F,j}[A_i]_{F,j} \\ &= F_{aq,j}([A_i]_{aq,j} + [A_i^-]_{aq,j}) + F_{org}([A_i]_{org,j} + [A_iC]_{org,j}) \end{aligned}, \tag{7.4}$$

and

$$[C]_{org,j+1} + [A_iC]_{org,j+1} = [C]_{org,j} + [A_iC]_{org,j}. \tag{7.5}$$

For the back-extraction stage ($j = BE$), the component balances are defined as

$$\begin{aligned} F_{org}([A_i]_{org,1} + [A_iC]_{org,1}) = {} & F_{BE}([A_i]_{aq,BE} + [A_i^-]_{aq,BE}) \\ & + F_{org}([A_i]_{org,BE} + [A_iC]_{org,BE}) \end{aligned}, \tag{7.6}$$

and

$$[C]_{org,1} + [A_iC]_{org,1} = [C]_{org,BE} + [A_iC]_{org,BE}. \tag{7.7}$$

The overall component mass balances for the enantiomers A_i are defined as

$$F_F[A_i]_F^{tot} - \left(F_{out,1}[A_i]_{aq,N}^{tot} + F_{out,2}[A_i]_{aq,BE}^{tot}\right), \tag{7.8}$$

where

$$F_{out,1} = F_{WF} + F_R + F_F, \tag{7.9}$$

The reflux ratio is defined as

$$RR = \frac{F_R}{F_{out,2}} \tag{7.10}$$

The aqueous back-extraction outflow is divided in a stream $F_{out,2}$ leaving the system for downstream recovery of A_S, and a stream

$$F_R = \frac{RR}{1+RR} \cdot F_{BE}, \tag{7.11}$$

that is refluxed to the cascade. The wash flow and its composition are given as

$$F_W = F_{WF} + F_R, \tag{7.12}$$

and

$$[A_i]_W^{tot} = \frac{[A_i]_R^{tot} F_R}{F_R + F_{WF}}. \tag{7.13}$$

The model was solved using the software package Matlab®.

7.3. Experimental Methods

7.3.1. Materials

Water was obtained by deionization using a deionization apparatus from Labconco, 1,2-dichloroethane (99%) from Sigma-Aldrich, potassium dihydrogen phosphate (*pa*), di-sodium hydrogen phosphate dodecahydrate (*pa*) and triethyl amine (99%) from Merck, glacial acetic acid from Acros, methanol (AR) and acetonitrille from Labscan. The extractant O-(1-t-butylcarbamoyl)-11-octadecylsulfinyl-10,11-dihydro-quinine and 3,5-dinitrobenzoyl-(*R*),(*S*)-leucine were kindly provided by DSM Research.

7.3.2. Cascade configuration and operational settings

The experimental cascade consisted of 6 CCS's connected countercurrently for the extraction and a single CCS for the back-extraction (Figure 7.5). Reflux was not applied. The CCS's 2, 4 and 6 were equipped with a mantle and cooled with tap water to maintain isothermal operation at 294 K. The temperature in the raffinate stream was monitored for verification. All CCS's were operated at 40 Hz. With a simple prediction using the Fenske equation for full reflux [36]

$$N_{\min} = \frac{\ln\left[\dfrac{x_{S,E}/\left(1-x_{S,E}\right)}{x_{S,R}/\left(1-x_{S,R}\right)}\right]}{\ln\left(\alpha_{op}\right)}, \tag{7.14}$$

where the operational selectivity is defined as

$$\alpha_{op} = \frac{D_S}{D_R}, \tag{7.15}$$

it was predicted that with the available 6 CCS's for the cascade, full separation is impossible. Therefore, an asymmetrical operation was chosen to obtain only one of the enantiomers in high purity. A_S was selected arbitrarily, therefore the cascade was fed at stage 5, if A_R is to be obtained in high purity, the feed should enter at stage 2. The specifications of all streams in the process, i.e. W, F, E, and BE are listed in Table 7.2.

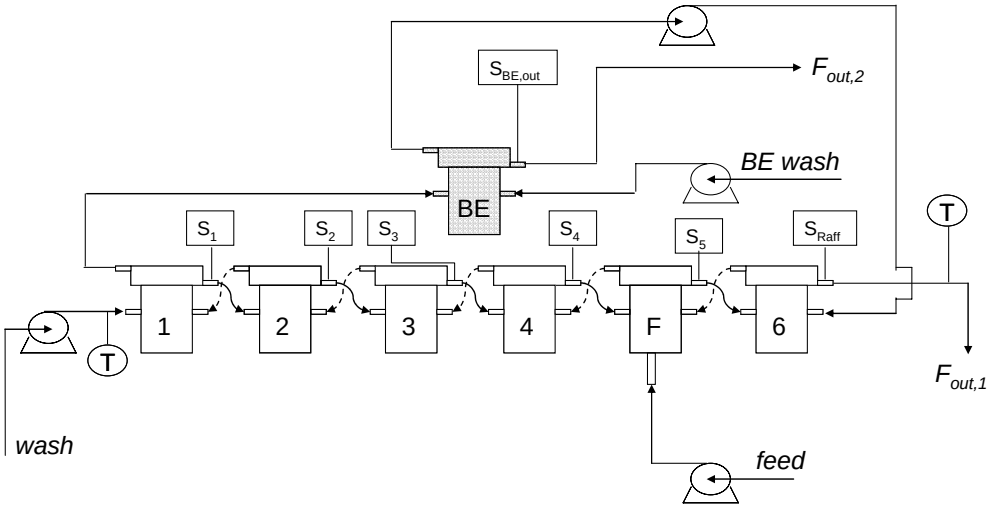

Figure 7.5. Experimental setup of 6 stage cascade with back-extraction stage. The feed CCS and back-extraction CCS are grey for clarity. Sampling points indicated with S_j (i = 1-5, Raff, and BE,out). Lines: Solid: aqueous streams, Dashed: organic streams.

Table 7.2. Experimental conditions for the cascade experiment with 6 CCS

variable	***Wash***	***Feed***	***Extract***	***Back-Extraction***
Flow rate (mL/min)	60.4	41.7	100	33.3
pH (-)	7.2	5.7[a]	n.a.	9.0
γ_1 (-)	0.82	0.79	n.a.	0.76
$[A_{R,S}]$ (10^{-3} mol/L)	0	1.5	0	0
[C] (10^{-3} mol/L)	0	0	4.3	0

[a] after mixing of wash and feed flows, the pH of the strip section becomes 6.2

7.3.3 Experimental procedures

Preparation of Solutions

To dissolve the $A_{R,S}$ more easily into the feed solution, the sodium salt of the amino acid derivative was made by mixing 5 g ($1.54 \cdot 10^{-2}$ mol) solutions of $A_{R,S}$ in 400 mL MeOH with an equimolar amount of sodium bicarbonate in 200 mL water. After mixing the solutions

the reactions started, as indicated by bubble formation. After one hour, no bubbles were formed anymore, indicating completion of the $Na^+A_{R,S}^-$ salt formation. The solvent mixture was evaporated using a rotary evaporator and the salt was dried under reduced pressure.

A total of 30 L feed solution ($1.5 \cdot 10^{-3}$ mol $A_{R,S}$ /L), 25 L back-extraction buffer solution and 50 L wash buffer solution were prepared. The extract solution was prepared in a 2L glass vessel by dissolving 4.25 g C ($5.85 \cdot 10^{-3}$ mol) in 1.35 L DCE.

Experimental details for a ELLE experiment in the cascade of 6 CCS's

The experiment was started up by starting the engines of all CCS's, opening the tap of the cooling water flow and starting the extract (organic phase) pump. After starting the extract pump, the CCS's are filled up in the order from 6 to 1 and finally the back-extraction CCS. After the recycle of the heavy extract phase was established the pumps of the lighter aqueous back-extraction and wash streams were started. When the wash flow reached the feed stage, the feed pump was started. As soon as the raffinate outlet started running, samples were taken, every 15 min during the first 2 hr. and afterward every 30 min from both the raffinate outlet and the aqueous back-extraction outlet to determine the concentrations $A_{R,S}$ using HPLC with a chiral stationary phase. Every hr. about 65 mL DCE was added in small portions to the extract storage vessel to compensate for the losses due to solubility of DCE in water (0.8% vol). Every 2 hr. samples were taken from the aqueous flows in between the stages and analysed by HPLC as described previously [35]. The experiment was run for 10 hr.

7.4. Results and Discussion

A 6 stage CCS cascade was run for 10 hours at 294 K to demonstrate that continuous enantioseparation of amino acid derivatives is possible in this type of equipment. The 4.25g C ($5.85 \cdot 10^{-3}$ mol) in the system was recycled fully in a single back-extraction step at pH 9.0. The racemic feed ($1.5 \cdot 10^{-3}$ mol/L, 0.52 g/L $Na^+A_{R,S}^-$) entered the cascade at stage 5. Enantiopure A_S was collected in the aqueous phase from the back-extraction CCS, the raffinate from the cascade contained excess of A_R. The concentrations in the exit and the back-extraction exit were measured every 15 min. during the first 2 h. and every 30 min. afterwards. At the sample points between the stages in the cascade, $[A_{R,S}]_{aq,tot}$ was measured every 2h. Figure 7.6 depicts the concentrations in the aqueous raffinate and back-extraction outlets. The raffinate outlet concentrations increase gradually during the first 4 hr (see Figure 7.6, left) After 4 hr. steady-state was established. This is more clearly illustrated by the concentration $[A_R]_{BEE}$, from initially higher values it drops to very low steady-state (see

Figure 7.6, right). The lines in Figure 7.6 correspond to model predictions. The experimental concentrations of A_R in both the raffinate and the back-extraction outlets appear to be in line with the model predictions. The concentration A_S in the raffinate outlet is lower than the model predicts and in the back-extraction outlet higher than the model predicts. This is caused by losses of DCE to the aqueous streams, causing the extractant concentration to be higher than intended. Every hr. 65 mL extra DCE was added to maintain a proper DCE-hold-up in the system. In general though, taking the higher extractant concentration into account, the model predicts the experimental results reasonably well.

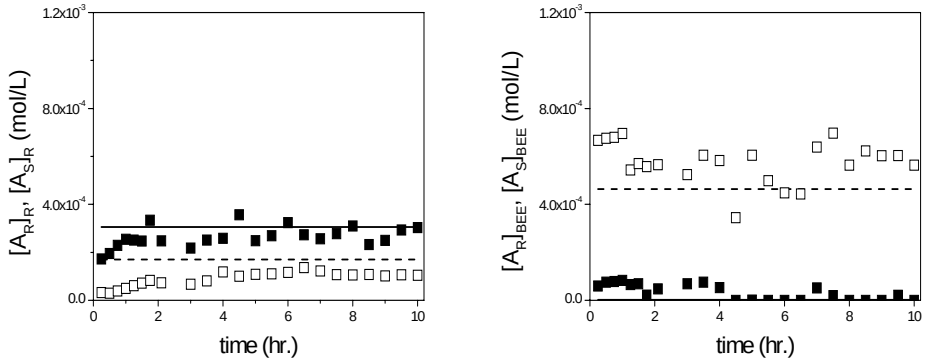

Figure 7.6. Left: $[A_R]_R$ and $[A_S]_R$, right: $[A_R]_{BEE}$ and $[A_S]_{BEE}$, open symbols $[A_S]$, closed symbols $[A_R]$, dashed lines: modeled $[A_S]$, solid lines: modeled $[A_R]$.

At steady-state, the average ee_S was 98% with a yield $Y_{S,BE}$ of 55%. The yield is defined as

$$Y_{S,BE} = \frac{[A_S]_{BE} F_{BE}}{[A_S]_F F_F}, \tag{7.16}$$

and the *ee* as

$$ee = \frac{|[A_S] - [A_R]|}{[A_S] + [A_R]}. \tag{7.17}$$

The ee_D in the raffinate was 42%, with raffinate yield $Y_{D,R}$ = 99%. The raffinate yield is defined as

$$Y_{D,R} = \frac{[A_D]_R (F_F + F_W)}{[A_D]_F F_F}. \qquad (7.18)$$

The asymmetric purity arises from the asymmetric operation (feed at stage 5).

The aqueous concentrations of A_i in the cascade, measured after 6, 8 and 10 hours, i.e. at steady-state, are depicted in Figure 7.7. It is clearly visible from Figure 7.7 that the model predicts the concentration profiles in the cascade well. For both enantiomers the general trend is followed, although the experimental concentration of A_S in the wash section of the cascade is high compared to the model prediction. The mean absolute relative error (MARE) between model prediction and experimental observation was 22%.

It follows from the constant cascade performance that no deterioration of the extractant activity was observed within 10 hr. The total extract phase hold-up in the system was 1.35 L, the flow rate was 100 mL/min, corresponding to almost 5 passes per hr. Thus after almost 50 passes of the extractant, the system performance was still stable. This indicates that with only a small amount of extractant, large amounts of racemates can be separated by continuous recycling of the extract in a single back-extraction CCS.

The experimental average steady-state ee_S was 98%, well in agreement with the 99% predicted by the model. With the observed concentrations and flow rates, during the steady state production lasting 6 hr, 2.23g enantiopure A_S was produced. This small amount was due to the low concentrations in the pilot experiment. When enough C is available, the production rate may be increased significantly, being limited only by the solubility of $Na^+A_{R,S}^-$ in water and by the flooding limit of the equipment.

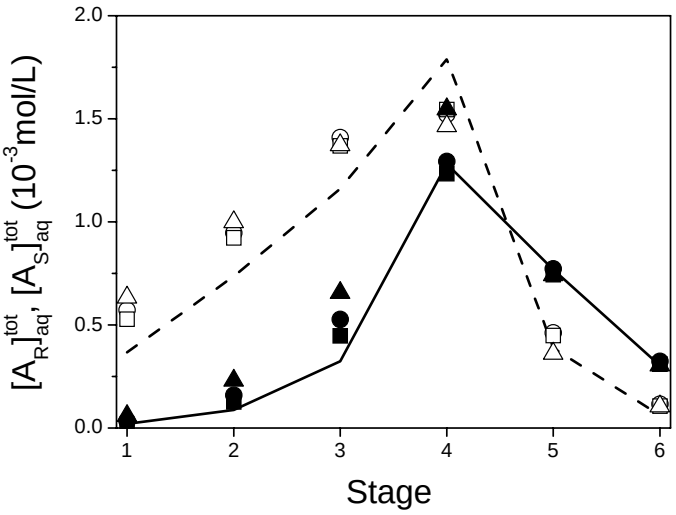

Figure 7.7. Aqueous phase concentrations in the cascade at steady state. Measurements after 6hr. (circles), 8hr. (squares), and 10hr. (triangles). Open symbols indicate $[A_S]^{tot}_{aq}$, closed symbols $[A_R]^{tot}_{aq}$, dashed and solid lines the model predictions for $[A_S]^{tot}_{aq}$ and $[A_R]^{tot}_{aq}$, respectively.

7.5. Cascade Optimization by equilibrium stage modeling

In the previous section we have shown experimentally that CCS equipment is suitable for countercurrent enantioselective extraction and that the equilibrium stage model is suitable to predict the performance of such a cascade. In this section we use the model to optimize the separation process. For a symmetrical separation with both high ee_R and ee_S, for example > 99%, or >97%, the aim of the optimization study is to find the minimum number of stages and a minimum wash feed to minimize downstream recovery effort. Hereto, first the minimum number of stages was determined under zero reflux conditions and subsequently the effect of applying reflux was studied.

Modeling of minimum number of stages required at zero reflux

The minimum number of stages was determined for both > 97% *ee* and > 99% *ee* (typical industrial purity requirements) using a direct search method applied to the equilibrium stage cascade model. All independent and dependent variables, as well as the parameters of the model are listed in Table 7.3. Full back-extraction in a single stage was assumed at $F_{BE} = F_E/3$ and at an appropriate pH_{BE}[35].

Table 7.3. Cascade model variables and parameters

independent variables	***parameters***	***dependent variables***[a]
$[A_i]_F$	K_a	$[A_i]^{aq}_j$, $[A_i^-]^{aq}_j$, $[A_i]^{org}_j$, $[A_i]_W$, $[A_i]_E$
$[C]_E$	m	$[A_iC]^{org}_j$
F_F, F_{WF}, F_E ,F_{BE}, F_R	$K_{eq,D}$	$[C]^{org}_j$
pH_{WF}, pH_S, pH_{BE}	$K_{eq,L}$	F_W
γ_{1WF}, γ_{1F}, γ_{1BE}		γ_{1W}, γ_{1S}
N, F, RR		

[a] *j* is the stage-index, ranging from 1 to N in the extraction or BE in the back-extraction

The variable $[A_{R,S}]_F$ was fixed at a typical concentration of $1 \cdot 10^{-3}$ mol/L, F_F at an arbitrary value of 100 mL/min. For γ_{1W} a fixed value of 0.82 was taken as this is corresponds to the lowest buffer concentration at which the pH can be kept constant. Here, the reflux ratio was fixed at RR = 0. In a subsequent section the influence of applying a reflux will be investigated.

The optimized settings for the two investigated cases are listed in Table 7.4. When the *ee* should be higher than 99%, a minimum of 12 stages was found, whereas for 97% *ee* a cascade of 9 stages was found to be sufficient. These values are about 1.5 times the predicted values by the Fenske equation for full reflux[36]. The difference in pH of the wash and the strip sections is explained by the effect of the dissociation equilibrium in the aqueous phase on the distribution of the enantiomers. In the wash section, the undesired enantiomer should be washed out of the (organic) extract stream[26,37]. By shifting the pH to a higher value, the distribution equilibrium of the enantiomers over the organic and aqueous phases is shifted towards the aqueous phase and the undesired enantiomer is washed out.

Table 7.4. Optimized settings for symmetrical separations with $[A_{R,S}]_F = 1 \cdot 10^{-3}$ mol/L, F_F = 100 mL/min and $\gamma_{1W} = 0.82$ and zero reflux (RR = 0)

variable	ee_S & $ee_{R>}$ *99% settings*	ee_S & $ee_{R>}$ *97% settings*
N	12	9
F	7	5
pH_w (-)	7.0	7.2
pH_s (-)	6.2	6.2
γ_{1S} (-)	0.79	0.79
$[C]_E$ (10^{-4} mol/L)	23	29
F_{WF} (mL/min)	85	85
F_E (mL/min)	240	220

Minimization of the exit flow rates using a reflux

Minimizing the exiting streams at constant feed results in more concentrated streams, which reduces the downstream recovery efforts. This can be achieved by applying a reflux[26]. By reintroducing A_S from the back-extraction aqueous exiting stream to the wash inlet of the cascade (see Figure 7.4), the holdup of A_S in the system increases. As a result, $[A_S]_{BE,out}$ increases and $F_{out,2}$ decreases. The resulting mol flow of A_S exiting the system is equal to the zero reflux operation, a prerequisite due to the mass balance over the entire system. In addition to the lowered $F_{out,2}$ also the excess of A_S in the wash section of the cascade is expected to increase, leading to a wash flow that can be decreased, while still obeying the enantiopurity constraint. As minimization criterion, the total outflow of aqueous streams from the system is taken. With the constraint of equal mass flow in and out of the system, this is defined as

$$F_{out,tot}^{\min} = \left(F_{out,1} + F_{out,2}\right)_{\min} = F_F + F_{WF} + F_{BE}\,. \qquad (7.19)$$

From Table 7.3 it follows that the total number of independent variables is 15, far too much to vary all in the optimization routine and still understand well the direction of the optimization. A direct search showed that, starting from the conditions in Table 7.4 for ee_R & ee_S > 99%, changing operational variables such as $[C]_E$ and F_E and the pH in the various sections have a very strong negative effect of the performance. The performance almost immediately drops to *ee*'s below the enantiopurity constraints, even when the number of

stages is increased significantly. Therefore, here, the effect of reflux on the enantiopurities is studied with all the settings fixed to the values in Table 7.4, except for F_{WF}. With the F_F and F_{BE} fixed, minimization of the total outflow of the system is basically reduced to a minimization of F_{WF}. To study the effect of the F_{WF} on the *ee*'s as function of RR, isoenantiomeric excess lines were calculated. The 99% isoenantiomeric excess lines are displayed in Figure 7.8.

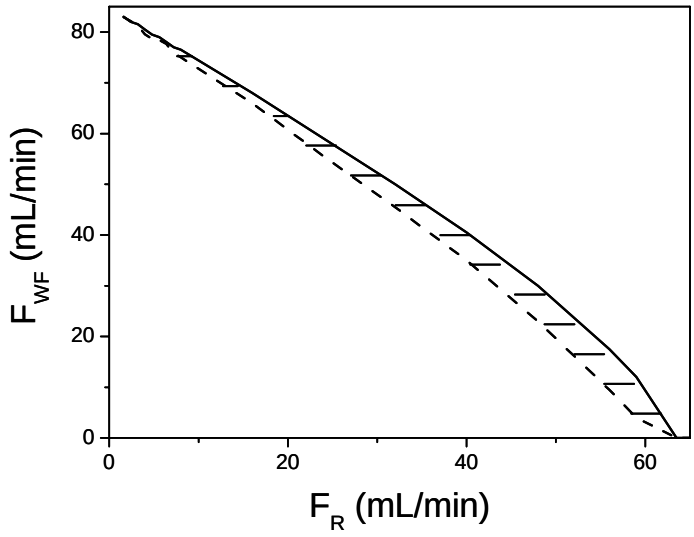

Figure 7.8. Effect of F_{WF} and F_R on the enantiomeric excess for 12 stage process, all other conditions as in Table 7.4. In the dashed region between the solid line (ee_R = 99%) and the dashed line (ee_S = 99%) both constraints are satisfied.

At constant F_R the ee_S increases with F_{WF}, whereas ee_R drops with increasing F_{WF}. The ee_S = 99% line thus gives the lower boundary and the ee_R = 99% the upper boundary of operation, the area in between the selected isoenantiomeric excess lines is the feasibility area. For example, at RR = 1, corresponding to F_R = 40, the system can only be operated with both ee_R and ee_S above 99% when $35 < F_{WF} < 41$. The optimum reflux ratio is 3.85, corresponding to a F_R of 63.5 mL/min as at this reflux ratio, the wash feed even may be completely eliminated.

Practical limitation

The found optimum, where $F_{WF} = 0$, at a reflux ratio of 3.85, implies that 79% of the back-extraction outlet stream is directly returned to the cascade in stage 1. However, the back-extraction is operated at pH 9 and the wash section of the cascade is operated at pH 7. A minimum buffer concentration is required for maintaining the pH at the desired value. This requirement causes that the concentration in the reflux stream cannot be made so low that simple addition of buffer salt can reduce the pH enough, while still working at the ionic strength desired in the wash section of the cascade. Therefore, 2 practical solutions may be applied. First, the buffer strength in the wash (and as a consequence, also in the strip) of the cascade may be increased. Secondly, a small stream of F_{WF} may be added. With the current cascade settings from Table 7.4, for ee_R & ee_S > 99%, the minimum F_{WF} for which the buffer salt constraint is satisfied is 19 mL/min (ratio $F_{WF}/F_F = 0.19$). This value was obtained at a reflux ratio of 2.33.

Reduction of stages under nonzero reflux

Figure 7.8 shows that there is still some flexibility in the operation range, thus the number of stages could possibly be reduced further. With a direct search it was found that indeed with 11 stages the constraints ee_R & ee_S > 99% can be satisfied, even for two configurations, with the feed at stage 4, and at stage 5, respectively. With 10 stages, no feasible operation region was found. The feasibility regime with respect to the F_{WF} and F_R for the 11 stage configuration with feed at stage 5 (the most flexible and economic of the two) and conditions otherwise equal to those in Table 7.4 is displayed in Figure 7.9 as the regions in between the isoenantiomeric excess lines. The line ee_R gives the maximum wash feed for which the constraint ee_R > 99% is satisfied and the line ee_S the minimum wash feed for which ee_S is satisfied. Operation is thus feasible for 40 mL/min < F_R < 64. The operational flexibility is, however, minimal as follows from Figure 7.9, and the risk of running off spec (either ee_R or ee_S below 99%) due to small offsets of pumps is high. Therefore, a much more robust process with 12 stages seems advisable.

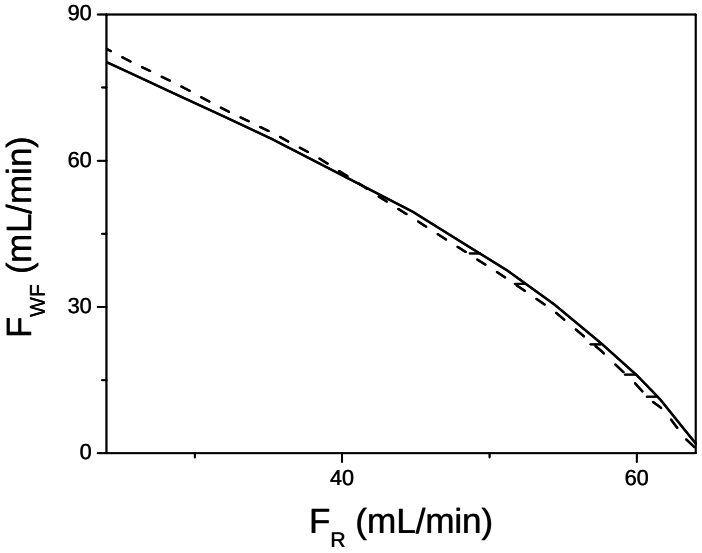

Figure 7.9. Isoenantiomeric excess lines for 11 stage cascade. Feed stage = stage 5, other conditions as in Table 7.4. In the dashed region between the solid line (ee_R = 99%) and the dashed line (ee_S = 99%) both constraints are satisfied.

7.6. Maximizing the $A_{R,S}$ throughput

The described optimization was performed with an arbitrary flow rate and $A_{R,S}$. Here, the maximum production rate in a cascade of CINC V02 devices is determined. The maximum production rate equals the loading per liter feed solvent times the volumetric throughput. In order to determine the highest possible production rate, the solubility and the flooding limit were determined, as these two factors determine how much $A_{R,S}$ per unit time can be produced. The solubility of $Na^+A_{R,S}^-$ in water was determined experimentally at (29 +/- 1)·10^{-3} mol/L. The maximum concentration in the cascade may reach up to 1.8 times the feed concentration (see for example Figure 7.7). To avoid precipitation of $A_{R,S}$, the maximum $A_{R,S}$ concentration that should be fed to the system is 15·10^{-3} mol/L.

The limiting flow rate was determined by flooding, as even at the flooding limit no deviation from equilibrium was observed. The flooding limit, and thus the operational limit for DCE/water was determined experimentally at 1.8 L/min. At the flooding limit, the F_F of a 12 stage cascade is 0.36 L/min. The maximum capacity of a cascade of CINC V-02's is

thus $5.4 \cdot 10^{-3}$ mol/min, corresponding to 1.76 g/min or 17.7 kg per week. Hereto, only about 60 g of the extractant is needed, due to the extremely low liquid hold-up in the CCS equipment and the efficient recycle.

7.7. Conclusions

It has been demonstrated that the separation of 3,5-dinitrobenzoyl-R,S-leucine, $A_{R,S}$, into its enantiomers can efficiently be done in CCS equipment by multistage countercurrent enantioselective extraction using a cinchona alkaloid extractant. The process was optimized using a mathematical model that was developed and experimentally verified with good results.

The zero reflux minimum number of stages for complete separation was determined at 12 and 9 for the constraints ee_R & ee_S > 99%, and ee_R & ee_S > 97%, respectively. These values at zero reflux are about 1.5 times the predicted values by the Fenske equation for full reflux[36].

To obtain 99% ee at both exits, the wash feed flow could completely be eliminated at a reflux ratio of 3.85. However, due to practical limitations, the optimum practical operation would be at a reflux ratio of 2.33 and a wash feed/racemate feed flow ratio of 0.19. By applying a reflux, it was also possible to reduce the number of stages to 11, but operational flexibility at 11 stages is extremely low and it seems wiser to use a more robust 12 stage process to avoid off spec products.

In the experimental verification, during a 6 hr. steady-state run with an average ee_S of 98% 2.23 g enantiopure A_S was produced, while no detoriation of the purity was observed at all. From this it can be concluded that the chemistry is very robust and can be applied very efficiently in longer lasting continuous separation processes. With a 12 stage cascade of CCS's of the type CINC V02 as much as 17.7 kg racemate per week can be separated using only about 60 g extractant.

7.8 Nomenclature

a	activity (mol/L)
A	constant in Debye-Hückel law, ($L^{1/2}mol^{-1/2}$)
$A_{R,S}$	3,5-dinitrobenzoyl-R,S-leucine (solute)
B	constant in Debye-Hückel law, ($L^{1/2}mol^{-1/2}$)
C	cinchona alkaloid extractant
D	overall distribution, (-)
ee	enantiomeric excess, (%)

F	flow (mL/min), feed stage
i	index for *R,S*
I	ionic strength (mol/L)
j	stage index
K_a	acid dissociation constant of $A_{R,S}$, (mol/L)
$K_{eq,i}$	equilibrium constant of the organic phase reaction between $A_{R,S}$ and C, (L/mol)
m	distribution coefficient of undissociated $A_{R,S}$, (-)
N	number of stages
PF	performance factor, (%)
T	temperature, (K)
V	volume, (L)
Y	yield, (-)
z	ion valance, (-)
[ ] square brackets	concentration, (mol/L)

greek letters

α	selectivity, (-)
γ	activity coefficient, (-)

subscripts

0	initial or feed
a	acidity
aq	aqueous
BE	back extraction inlet stream
BEE	back-extraction exit = BE - R
E	extract
F	feed
eq	equilibrium
i	index for *R,S*
j	stage index
max	maximum
min	minimum
org	organic
R	reflux
R	DNB-R-leu
S	strip
S	DNB-S-leu
tot	total, for concentrations: all forms

W	wash
WF	wash feed = W - R

Acknowledgements:

The authors acknowledge DSM Research kindly for providing the enantioselective extractant and DNB-R,S-leu. Dr. Gerard Kwant (DSM) and Prof. Hans Wesselingh are acknowledged for helpful discussions. DSM and Organon are acknowledged for their financial support through the Separation Technology programme of NWO (Netherlands Scientific Organisation).

7.9 References

[1]. Rouhi, A. M. *Chem. Eng. News* **2003,** *81*, 45-55.
[2]. Sheldon, R. A. *Chirotechnology; industrial synthesis of optically active compounds;* Marcel Dekker, Inc.: New York, 1993.
[3]. Crosby, J. *Tetrahedron* **1991,** *47*, 4789-4846.
[4]. Jacobsen, E. N.; Pfaltz, A.; Yamamoto, H. *Comprehensive Asymmetric Catalysis;* Springer: Berlin, 1999; Vol. 1.
[5]. Breuer, M.; Ditrich, K.; Habicher, T.; Hauer, B.; Kesseler, M.; Sturmer, R.; Zelinski, T. *Angew. Chem. Int. Ed.* **2004,** *43*, 788-824.
[6]. Bruggink, A. Rational Design in Resolutions. In *Chirality in Industry II*, Collins, A. N., Sheldrake, G. N., Crosby, J., Eds.; John Wiley & sons Ltd.: Chichester, 1997; pp 81-98.
[7]. Francotte, E.; Leutert, T.; La Vecchia, L.; Ossola, F.; Richert, P.; Schmidt, A. *Chirality* **2002,** *14*, 313-317.
[8]. Zenoni, G.; Quattrini, F.; Mazzotti, M.; Fuganti, C.; Morbidelli, M. *Flavour and Fragrance Journal* **2002,** *17*, 195-202.
[9]. Gavioli, E.; Maier, N. M.; Minguillon, C.; Lindner, W. *Anal. Chem.* **2004,** *76*, 5837-5848.
[10]. Maximini, A.; Chmiel, H.; Holdik, H.; Maier, N. W. *J. Membr. Sci.* **2006,** *276*, 221-231.
[11]. Bauer, K.; Falk, H.; Schlogl, K. *Monatshefte für Chemie* **1968,** *99*, 2186-&.
[12]. Bowman, N. S.; Mccloud, G. T.; Schweitz, G. K. *J. Am. Chem. Soc.* **1968,** *90*, 3848-3852.
[13]. Romano, S. J.; Wells, K. H.; Rothbart, H. L.; Rieman, W. *Talanta* **1969,** *16*, 581-590.
[14]. Schweitz, G. K.; Supernaw, I. R.; Bowman, N. S. *J. Inorg. Nucl. Chem.* **1968,** *30*, 1885-1890.
[15]. Abe, Y.; Shoji, T.; Kobayashi, M.; Qing, W.; Asai, N.; Nishizawa, H. *Chem. Pharm. Bull.* **1995,** *43*, 262-265.

[16]. Kellner, K. H.; Blasch, A.; Chmiel, H.; Lämmerhofer, M.; Lindner, W. *Chirality* **1997,** *9*, 268-273.
[17]. Pickering, P. J.; Chaudhuri, J. B. *Chem. Eng. Sci.* **1997,** *52*, 377-386.
[18]. Prelog, V.; Stojanac, Z.; Kovacevic, K. *Helv. Chim. Acta* **1982,** *65*, 377-384.
[19]. Steensma, M.; Kuipers, N. J. M.; de Haan, A. B.; Kwant, G. *Chirality* **2006,** *18*, 314-328.
[20]. Takeuchi, T.; Horikawa, R.; Tanimura, T. *Anal. Chem.* **1984,** *56*, 1152-1155.
[21]. Tan, B.; Luo, G. S.; Wang, H. D. *Tetrahedron-Asymmetry* **2006,** *17*, 883-891.
[22]. Viegas, R. M. C.; Afonso, C. A. M.; Crespo, J. G.; Coelhoso, I. M. *Sep. Purif. Technol.* **2007,** *53*, 224-234.
[23]. Koska, J.; Haynes, C. A. *Chem. Eng. Sci.* **2001,** *56*, 5853-5864.
[24]. Steensma, M.; Kuipers, N. J.; de Haan, A. B.; Kwant, G. *J. Chem. Technol. Biotechnol.* **2006,** *81*, 588-597.
[25]. Steensma, M.; Kuipers, N. J. M.; de Haan, A. B.; Kwant, G. *Chem. Eng. Sci.* **2007,** *62*, 1395-1407.
[26]. Steensma, M.; Kuipers, N. J. M.; de Haan, A. B.; Kwant, G. *Chem. Eng. Proc.* **2007,** *46*, 996-1005.
[27]. Ohki, A.; Miyashita, R.; Naka, K.; Maeda, S. *Bull. Chem. Soc. Jpn.* **1991,** *64*, 2714-2719.
[28]. Tan, B.; Luo, G. S.; Wang, J. D. *Sep. Purif. Technol.* **2007,** *53*, 330-336.
[29]. Schmidt-Traub, H.; Gorak, A. *Integrated Reaction and Separation Operations;* Springer: Berlin, 2006.
[30]. Stanckiewicz, A.; Moulijn, J. A. *Re-Engineering the chemical processing plant; Process Intensification;* Marcel Dekker, Inc: New York, 2004.
[31]. Kulprathipanja, S. *reactive separation process;* Taylor & Francis: New York, 2002.
[32]. Lindner, W.; Lämmerhofer, M. Eur. Pat. Appl. No. 96 109 072.7, 1996.
[33]. Hallett, A. J.; Kwant, G. J.; de Vries, J. G. *Chemistry European Journal,* accepted for publication.
[34]. Schuur, B.; Winkelman, J. G. M.; Heeres, H. J. *Ind. Eng. Chem. Res.,* accepted for publication.
[35]. Schuur, B.; Floure, J.; Hallett, A. J.; Winkelman, J. G. M.; de Vries, J. G.; Heeres, H. J. *Org. Process Res. Dev.* **2008,** *12*, 950-955.
[36]. Pratt, H. R. C. *Countercurrent Separation Processes;* Elsevier: Amsterdam, 1967.
[37]. Treybal, R. E. *Liquid Extraction, 2nd ed.;* second edition ed.; McGraw-Hill: New York, 1963.

Scientific résumé of Boelo Schuur

Peer reviewed journal publications

published

Continuous Chiral Separation of Amino Acid Derivatives by Enantioselective Liquid-Liquid Extraction in Continuous Contactor Separators
Boelo Schuur; Andrew J. Hallett; Joelle Floure; Jozef G. M. Winkelman; Johannes G. de Vries; Hero J. Heeres, *Organic Process Research & Development*, **2008**, 12, 950-955.

Determination of the interfacial area of a continuous integrated mixer/separator (CINC) using a chemical reaction method
Boelo Schuur; Wiebe J. Jansma; Jozef G. Winkelman; Hero J. Heeres, *Chemical Engineering and Processing*, **2008**, 47, 1484-1491.

Two-Phase (Bio) catalytic Reactions in a Table-Top Centrifugal Contactor Separator
Gerard N. Kraai; Floris van Zwol; Boelo Schuur; Hero J. Heeres; Johannes G. de Vries**,** *Angewandte Chemie International Edition*, **2008**, 47, 3905-3908.

A synthetic strategy for novel nonsymmetrical bola amphiphiles based on carbohydrates
Boelo Schuur; Anno Wagenaar; André Heeres; Hero J. Heeres, *Carbohydrate Research*, **2004**, 339, 1147-1153.

Equilibrium Studies on Enantioselective Liquid-Liquid Amino Acid Extraction using a Cinchona Alkaloid Extractant
Boelo Schuur; Jozef G. Winkelman; Hero J. Heeres, *Accepted for publication in Industrial and Engineering Chemistry Research*

submitted

Novel Highly Integrated Biodiesel Production Technology in a Centrifugal Contact Separator
Gerard N. Kraai; Boelo Schuur; Floris van Zwol; Henk H. van de Bovenkamp; Hero J. Heeres, *Submitted*.

Experimental and modeling studies on the enantioseparation of 3,5-dinitrobenzoyl-(*R*),(*S*)-leucine by liquid-liquid extraction in a cascade of continuous centrifugal separators
Boelo Schuur; Jozef G.M. Winkelman; Johannes G. de Vries; Hero J. Heeres, *submitted.*

Continuous Flow Separation of Amino Acid Derivative Enantiomers Using Liquid-Liquid Extraction in a Cascade of Centrifugal Contactor Separators.
Boelo Schuur; Andrew J. Hallett; Johannes G. de Vries; Hero J. Heeres, *submitted.*

Hydrodynamic Studies in a Centrifugal Contactor Separator; Liquid Hold-up, Residence Time Distribution, Phase behavior and Drop Size Distributions
Boelo Schuur; Gerard N. Kraai; Jozef G. M. Winkelman; Hero J. Heeres, *submitted.*

in preparation

Experimental and Modeling Studies on the Enantioselective Liquid-Liquid Extraction of (*R),(S)*-Phenylglycinol using a Bis(Naphtyl)Phosphoric Acid derivative as extractant
Boelo Schuur; Jeroen Bokhove; Bas J.V. Verkuijl; Johannes G. de Vries; Ben L. Feringa; Hero J. Heeres, *to be submitted*

Determination of Reaction Kinetics in Enantioselective Extraction using a Stirred Cell
Boelo Schuur; Jozef G. M. Winkelman; Hero J. Heeres, *in preparation*

Epoxidation, Hydroxylation, and Alkokylation of Jatropha oil
Louis Daniel; Agnes A. Ardiyanti; Boelo Schuur; Robert Manurung; Hero J. Heeres, in preparation, *in preparation.*

Exploration of Epoxidation routes for Jatropha Oil
Louis Daniel; Boelo Schuur; Robert Manurung; Hero J. Heeres, in preparation, *in preparation*.

Peer reviewed conference proceedings

Continuous enantioselective extraction of amino acids in a highly intensified centrifugal extractor
Boelo Schuur; Jozef G. Winkelman; Hero J. Heeres, *Proceedings of the International Solvent Extraction Conference ISEC,* **2008**, Vol II, 979-984.

Process Intensification. Continuous Two-Phase Catalytic Reactions in a Table-Top Centrifugal Contact Separator
Gerard N. Kraai; Boelo Schuur; Floris van Zwol; Robert Haak; Adriaan J. Minnaard; Ben L. Feringa; Hero J. Heeres; Johannes G. de Vries, *Proceedings of the 22nd conference of the Organic Reactions Catalysis Society,* **2008**, in press.

International conference proceedings

A Compact Integrated Mixer/Separator for Enantioselective Solvent Extraction
Boelo Schuur; Wiebe J. Jansma; Jozef G. Winkelman; Hero J. Heeres, *European Congress on Chemical Engineering*, **2007**, Copenhagen, Denmark.

Green Chemicals from Jatropha Oil
Agnes R. Ardiyanti; Boelo Schuur; Robert Manurung; Hero J. Heeres, *International Catalysis Engineering Symposium*, **2007**, Delft, The Netherlands.

Green Chemicals from Jatropha Curcas Oil
Agnes R. Ardiyanti; Boelo Schuur; Robert Manurung; Hero J. Heeres, *International Green Chemistry Conference,* **2006,** Kuala Lumpur, Malaysia.

Novel Biodiesel Production Technology using a Continuous Contactor Separator
Boelo Schuur; Floris van Zwol; Henk H. van de Bovenkamp; Gerard N. Kraai; Hero J. Heeres, submitted to *International Symposium on Chemical Reaction Engineering 20,* **2008**, 378-379, Kyoto, Japan.

Process Intensification using a Continuous Highly Integrated Reactor-Separator Device
Gerard N. Kraai; Boelo Schuur; Johannes G. de Vries; Hero J. Heeres, submitted to XVIII International Conference on Chemical Reactors, **2008**, Malta.

Dankwoord

Mijn vier jaar als AIO zit erop! Dat het werk ook echt af is in vier jaar en een paar weken, is niet het resultaat van slechts één man met een missie, maar is toe te schrijven aan de inzet en betrokkenheid van een groot aantal mensen. De laatste bladzijdes van dit proefschrift wil ik vullen met het bedanken van de betrokken personen.

Te beginnen bij Prof. dr. ir. Erik Heeres, eerste promotor. Erik, dank je wel voor het vertrouwen en enthousiasme dat je nu bijna 5 jaar geleden getoond hebt, waardoor ik toch weer ging geloven in een wetenschappelijk avontuur. Dat enthousiasme is een karaktereigenschap die ik nooit zal vergeten, want dat was wat mij in twijfelmomenten telkens weer een enorme impuls gaf. Fantastisch was je enorme inzet de laatste maanden, waardoor het gelukt is om het manuscript spoedig af te ronden, bedankt!
Prof. dr. Hans de Vries en Prof. dr. Ben Feringa, ook jullie bedankt voor het vertrouwen, waarmee ik 4 jaar geleden kon beginnen aan het avontuur. Hans, ook bedankt voor alle wetenschappelijke input en de mogelijkheden om bij DSM kennis op te doen.
Een bijzondere kracht was Dr. ir. Jos Winkelman. Jos, je trad voor de buitenwereld nooit op de voorgrond in het kader van mijn project, maar was naast Erik mijn belangrijkste steunpilaar. Dank voor al je bijdragen aan dit proefschrift, je scherpe analyses en de soms zeer snelle correcties wanneer er weer eens een deadline te halen was.
Naast deze begeleiders wil ik ook de beoordelingscommissie, bestaande uit Prof. dr. ir. André de Haan, Prof. ir. Jan Harmsen en Prof. dr. ir. Geert Versteeg bedanken voor het beoordelen van het manuscript.

Een groot deel van de experimenten was niet mogelijk zonder technische ondersteuning. Anne, Marcel, Erwin en Laurens bedankt voor jullie bijdrage. Naast techniek is analyse essentieel. Jan Henk, Peter, Hans vd V en Theadora bedankt. De afdeling vakdidactiek wordt bedankt voor het uitlenen van de contiburet, Pieter van Zandbergen voor het titratieprogramma. Karla, Iris, Andy, Joelle en Gerard Kwant van DSM bedankt voor jullie bijdragen. Prof. Hans Wesselingh bedankt dat ik langs mocht komen voor advies, mevrouw Wesselingh bedankt voor de hartelijkheid en de lekkere koffie. John Janssen en Mettler Toledo bedankt voor de metingen met de Lasentec apparatuur. Ton Wolterinck van Auxill Nederland bedankt voor het venster met elektrodes in de CS50 en de adviezen. Mitch St.George thank you for the interesting discussion on CCS equipment.

Niet alle experimenten beschreven in dit proefschrift heb ik zelf gedaan, in deze alinea wil ik de studenten die ik begeleid heb bedanken. Wiebe bedankt voor je werk, het heeft een

mooie bijdrage aan een internationaal congres, een wetenschappelijke publicatie en hoofdstuk 4 van dit proefschrift opgeleverd. Op z'n Gronings: kon minder! Jeroen, ook jij bedankt voor je uitstekende werk dat hoofdstuk 3 opleverde en hopelijk binnenkort een publicatie. Agnes, Louis en Floris, hoewel niet in dit proefschrift opgenomen, leverde (of gaat dat binnenkort doen) het werk van jullie gemiddeld meer dan 1 publicatie per student op. Dank jullie wel, niet alleen voor de publicaties maar ook voor alle gezellige momenten en interessante en leerzame discussies. Voor alle studenten geldt dat ik veel van jullie heb geleerd, ik hoop jullie ook van mij. Dat 60% van jullie AIO geworden is, is bijzonder voor techneuten en daar ben ik trots op! Succes bij jullie verdere (wetenschappelijke) stappen.

Mijn uitstapjes richting (organische) synthese en analyse leidden mij vaak richting gebouw 14 en 15. Adri, Wesley, Jaap, Tieme, Joost, Patrick, Chris, Hans de B en Niek bedankt voor jullie hulp. Bas, dank voor je hulp bij het kolommen, maar vooral ook voor alle discussies over ons project, je hulp bij de recovery van 'P7' en niet in het minst voor al onze buitenchemische activiteiten, o.a. in het kader van metaal en het Pieterpad.

Met het bedanken van Bas *et al*. van organisch ben ik aangekomen bij het interface tussen werk en gezelligheid. Dat interface bestaat ook bij de collegae techneuten. Gerard voorop door de gezamenlijke CINC-belangen, maar ook Jelle, Hans H, Marcel W (the French guy), Henk vd B, Nidal, Arjan en de laatste paar keren ook CB, Teddy (yesyes) en Agnes, bedankt voor de VriMiBo's. Buana, geen vrimibo's voor jou, maar wel bijna 4 jaar kamergenoot, bedankt voor het delen van je Matlab-expertise én, oh my en de glimlach bij (de niet zeldzame) mooie momenten. Het ga je goed!
Verder Franchesca G, Anant, Jasper, Poppy, Asaf, Zhang, Jaap B, Gerald, Farchad, Henky, Inge and Judy (it was fun in Copenhagen), Laura, Lidia, Sebastien, Asal, Marya en Francesco, Ton en Leon bedankt. Tenslotte buurman Ignacio, dank je voor de gezelligheid en de interessante discussies.

Nu volledig in de vrijetijdsfase beland: Lichting '96 (uitgebreide versie), bedankt voor alle mooie Hemelvaart en andere dagen waarop gefeest werd. Dat de Hemelvaart-traditie lang mag stand houden, Ronnie zorg dat je ook eens kan, je aanwezigheid wordt gewaardeerd!
Bijzondere LAW-selectie binnen de groep: de Pieterpadters: Ronald, BasS, BasV en Mark, laten we het helemaal aflopen!

Naast wandelen bood natuurlijk zwemmen en training geven bij de Golfbreker een welkome afwisseling op de chemie. Alle zwemmers bedankt, in het bijzonder de trainingsgroep Anique, Axel, Frank, Joost, Linda, Mark, Onno, Remco, Roos en Wendy. Daarnaast het eerste Golfbrekerteam op de NK: Jorinde, Wendy, Monique en Marlies en de

collega-trainers door de jaren heen: Marjan, Peter t S, Menno B, Anko, Jouke, Ramses, Frank, Gerben en Anne-Rogier.

Naast training geven was besturen een hobby, alle ACLO-bestuurders uit AB en DB van de jaren 2004-2007 bedankt voor de mooie vergaderuurtjes en de leuke borrels en andere gezellige activiteiten. DB ’05-’06 bedankt voor de leuke attenties. Jascha, bedankt dat je me overgehaald hebt een extra jaartje te zitten, ’t was bijzonder, kom je een keertje naar Eindhoven (er is toch nog steeds ACLO-wijn uit 19?? of 200?) Menno K: we moeten nog altijd een keertje tennissen. Dank ook aan mijn bestuursgenootjes bij De Golfbreker (Jessica, Marieke B, Marijke Oosterhuis en P) en de SIZ (Linda, Martin, Mischa, Rory Bob en Wiebke) voor de interessante discussies en de leuke avonden.

Het begon met samen zwemmen, maar onze band is sterk gegroeid de afgelopen jaren, dat het nog jaren mag duren, bedankt voor jullie vriendschap: Gert-Jan (Gertie), Marieke de R Peter S, Esther, Sander en Hester, Werner (von Strumpfenhofen dos Santos de Witt), Linda, Jasperien en de collegae Stroppen. Stroppen, jullie in ’t bijzonder, laten we nog vaak overleggen en wat mooi dat jullie paranimfen willen zijn. P, we gaan samen nog iets moois verzinnen.

Ook bedankt voor de mooie vriendschap door de (al vele) jaren: Niek, Anja, Marco, Sandra, Johan, Thérèse, Heijo. Rolf en Ina Neske, dank jullie wel voor alle hartelijkheid de afgelopen jaren. Rolf, jouw inmiddels oeroude kreet “kan niet bestaat niet en wil niet ligt op het kerkhof” heeft mijn karakter in belangrijke mate beïnvloed. Dank je wel voor de mentale vorming in mijn jeugd en al je inzet t.b.v. mijn mobiliteit in de afgelopen paar jaar.

Marijke Onneweer, dank je wel voor je gezelligheid en voor je inzet als Doro en ik weer eens allebei of samen een date hadden.

Ten slotte een woord van dank aan mijn familie.

Liebe Waltraud, liebe Gudrun, danke schön für alle Liebe, und für alle Aushilfe, es ist wunderbar was ihr Beiden so schafft!

Greetje en Ildreon, Frederik en Jolanda, Papa en Mama, bedankt dat jullie er altijd voor me waren. Het betekent veel voor me!

Dorothee en Quentin: dank jullie wel voor jullie liefde en alle uren die jullie afstonden ten behoeve van het onderzoek. Dat we samen gelukkig mogen blijven, in Eindhoven en waar ons het leven brengt.